A mobile measurement unit to measure road traffic emissions and air quality

M. Dal Maso[1], H.Wihersaari[1] and T. Rönkkö[2]

[1]Department of Physics, Tampere University of Technology, P.O. Box 692, 33101, Tampere, Finland

Keywords: atmospheric aerosols, measurement, urban aerosol, emissions.

In populated areas, the concentrations of harmful trace gases and aerosol particles may vary greatly even over short distances. To understand the causes of this variance, data at high spatial resolution is needed for different areas, and for the many types of emission sources that can be found (eg. Diesch et al., 2011; Gurney et al., 2012). Typically, atmospheric observation and monitoring data is obtained from stationary measurements with less than optimal spatial coverage of the area of interest.

Air pollution studies require simultaneous observation data on gas phase pollutants, aerosol mass and number concentration, and information on the meteorological conditions and solar irradiation. To produce such data, a measurement system consisting of several instruments is required, and it needs to be coupled with positioning information (Drewnick et al., 2012). To achieve this, we have constructed a mobile measurement unit that allows high-quality observations while simultaneously allowing easy transport and deployment of the whole observation setup. The main purposes of the unit are a) roadside observation campaign measurements near urban sources of air pollution emissions; b) easy transportation and deployment of a full measurement setup to emission laboratories; c) field observations of atmospheric trace gases and aerosols copupled with mobile chamber observations; and d) on-road chasing observations of vehicle emissions.

The mobile measurement unit was constructed by modifying an automatic-transmission Mercedez-Benz Sprinter van (2.0 m wide, 2.8 m high and 6.9 m long) to accommodate high-quality aerosol and trace gas observation setups. The modifications included a stable electronic power supply, consisting of an 100A supplementary generator powered by the van engine, a 180 Ah lithium battery, a current regulation system and a 24 V, 8000 W inverter-charger. The electronic system allows operation with both utility power and while driving, and allows switching between the the power supplies without powering down the setup. The battery capacity allows for operation for 6-8 hours without external power.

The back of the van was outfitted with floor railings for easy attachment of instruments and instrument racks. At the walls, we installed a modular system with railing-fitted shelves at configurable heights. 6 sealable openings for sample inlets (3 at the roof, 1 at each side and 1 in the back door) are available for use. 10 sample lines were installed (5 stainless steel lines and 5 teflon lines) to bring air samples from the car front for sampling during driving. The roof of the car is fitted with footwalks and racks for instrument installation, and a weather station and positioning unit (Airmar WX200) can be installed. The weather station provides GPS data at 10-Hz frequency, as well as temperature, barometric pressure, relative humidity, and apparent and true wind speed and direction.

A typical instrumentation setup of the mobile measurement unit consists of key trace gas (CO_2, SO_2, NO_x, O_3) monitors, fast-response aerosol number size distribution instruments (e.g. Dekati ELPI, TSI EEPS), aerosol number concentration instruments (e.g. CPC), nanosized aerosol detection instruments (Airmodus PSM), solar irradiation sensors, and diffusion charging –based aerosol sensors (Pegasor PPS-M). Aerosol processing systems, e.g. a potential aerosol mass (PAM) chamber can also be installed. Depending on the measurement target, a suitable dilution setup will also be installed.

In this presentation, we will present data obtained with the mobile measurement unit at stationary roadside conditions as well as observations wihile the laboratory is moving. We will show how mobile measurements can be applied to complement the existing air quality monitoring network, and also its uses in understanding the dynamics of emission transformation during dilution, atmospheric aging and photochemical processing.

Acknowledgements: The research presented here has been supported by the Academy of Finland.

Drewnick, F., *et al*: Design of a mobile aerosol research laboratory and data processing tools for effective stationary and mobile field measurements, Atmos. Meas. Tech., 5, 1443-1457, doi:10.5194/amt-5-1443-2012, 2012.

Diesch, J.-M., *et al*.: Variability of aerosol, gaseous pollutants and meteorological characteristics associated with changes in air mass origin at the SW Atlantic coast of Iberia, Atmos. Chem. Phys., 12, 3761-3782, doi:10.5194/acp-12-3761-2012, 2012.

Gurney, K. R., *et al*.: Quantification of fossil fuel CO2 emissions on the building/street scale for a large US city, Environ. Sci. Technol., 46, 12194–12202, 2012.

A polar nephelometer for laboratory and atmospheric aerosols

H. Horvath[1]

[1]University of Vienna, Faculty of Physics, Aerosol Physics and Environmental Physics, Vienna, 1090, Austria

Keywords: Scattering function, phase function, nephelometer, calibration

The angular scattering of aerosols is a valuable source of information. It is needed for all investigations of the propagation of light through and in an aerosol The volume scattering function, $\gamma(\theta)$, is defined as the flux of light, $d^2\Phi$, scattered in a given direction characterized by the scattering angle, θ, per solid angle $d\omega$, per incident flux density, *S*, and scattering volume *dV* ; see figure 1.

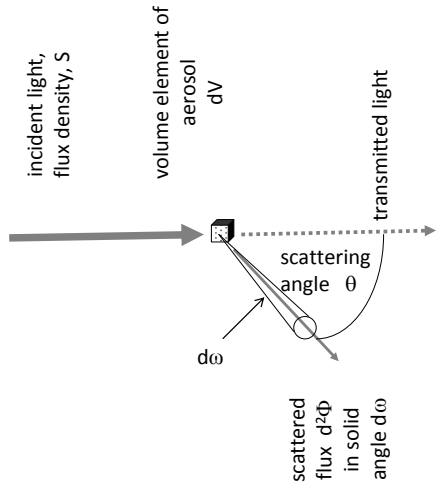

Figure 1. Definition of the volume scattering function and schematics of the polar nephelometer.

Using this definition as measuring principle a polar nephelometer has been designed: The illumination is achieved by a green solid state laser, the observation of the light flux $d^2\Phi$ is done with a photomultiplier, which receives it light via an optical fiber. The scattering volume is defined by the intersection of the laser beam with the cone of acceptance of the observation. Since the angle between the direction illumination and the direction of observation depends on the angle under which the scattering is measured, the scattering volume is proportional to $\frac{1}{|\sin\theta|}$. Multiplying the measured signal of the photomultiplier with $\sin\theta$ gives a value which is proportional to the volume scattering function. The calibration of the nephelometer can be done with Rayleigh scattering gases, normally with particle free air and carbon dioxide. The internal scattering of the nephelometer can be determined by filling the nephelometer with helium, the scattering coefficient can be neglected in first approximation (being 1.6% of the scattering of air).

The laser light is polarized, thus the signal measured by the photo detector is proportional to the scattering function for the direction of polarization relative to the observation plane. For consideration of the scattering of non polarized light, such as daylight, the laser beam passes through a $\frac{\lambda}{4}$ plate, creating a circular polarized light which can be considered as quasi-unpolarized. Alternately the direction of the polarization of the laser can be rotated by 90 degrees by inserting a thin optically active crystal in the laser beam, permitting the measurement of the volume scattering function of the aerosol for the two main direction of polarization.

Experimentally it is not possible to measure the scattered light at angles less than 5° and larger than 172°. If an integral quantity such as the total scattering coefficient or the back scattered fraction is to be obtained, it is necessary to estimate the scattering function in the missing angular range. This is possible by an extrapolation routine which accurate to $\pm 5\%$.

Figure 2 shows the measured phase function of a 0.5 µm latex aerosol for unpolarized light and the comparison with a Mie calculation.

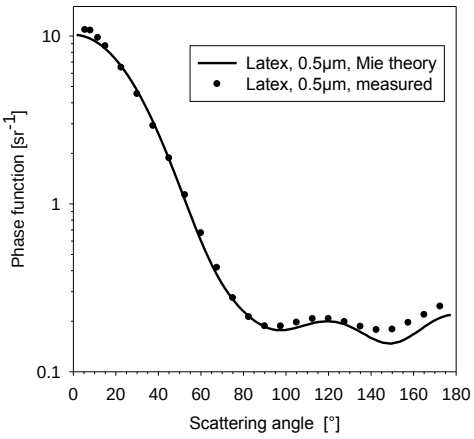

Fi ering

A simulation-based method for determining collision and evaporation rates from measured cluster distributions

O. Kupiainen-Määttä, H. Vehkamäki

Department of Physics, University of Helsinki, P.O. Box 64, FI-00014 University of Helsinki, Finland.

Keywords: particle formation, molecular clusters, data analysis, mass spectrometry

The instrumentation for studying the formation of secondary aerosol particles in the atmosphere has developed rapidly in recent years. High-resolution mass spectrometers (Junninen et al., 2010) now enable the detection and characterization of small electrically charged molecular clusters corresponding to the very first steps of particle formation. However, these measurements give information only on the concentrations of different cluster types but not on the dynamic processes governing their formation and growth.

The time evolution of a cluster population can be described by a set of differential equations (the birth-death equations) giving the time derivative of each cluster concentration based on collision and evaporation rates and external source and loss terms. The formation and growth of clusters can be simulated by integrating numerically these birth-death equations – given that the rate constants are known. In recent studies, cluster kinetics simulations using quantum chemistry–based evaporation rates have produced cluster distributions (Olenius et al., 2013) and formation rates (Almeida et al., 2013) that are in qualitative agreement with experiments. However, measurements and simulations have mostly remained two separate approaches for understanding cluster formation instead of truly complementing each other.

The present study introduces a new method for analysing experimental cluster distribution measurements using state-of-the-art kinetic modelling. The technique is applied here to negatively charged sulphuric acid–ammonia clusters, but it can be used for any set of clusters as no prior knowledge about the compounds is needed.

The central idea of the method is to perform simulations with different values of the rate coefficients, and compare the results with the experimental cluster concentrations in order to find values that reproduce the measurements as closely as possible. As there are tens of unknown rate constants even for a relatively small set of clusters, and as the cluster concentrations depend on them in a highly nonlinear way, the task of finding optimal values for the parameters is tackled by Markov chain Monte Carlo (MCMC).

The time evolution of the cluster concentrations is simulated by ACDC, a code that solves the birth-death equations taking into account all possible collision and evaporation processes as well as ion production and external losses. The rate constants are not taken from any theory as was done in our previous modelling studies (Olenius et al., 2013; Almeida et al., 2013) but are instead treated as free parameters that are varied by MCMC.

The data analysis method was first tested by applying it to simulated cluster distributions. In this case the "correct" values of the collision and evaporation rates are known, and we can examine how well the analysis of the cluster distributions reproduces these known values. It was found that a large fraction of the rate constants could be successfully determined from the analysis. More specifically, the method performed well for rate constants corresponding to rate-limiting steps on the formation pathway, while the less important rate constants could not be determined. In addition to the collision and evaporation rates, also the ion production rate and wall loss rate as well as fragmentation probabilities in the inlet of the mass spectrometer were treated as unknown parameters and their values could be successfully extracted from the analysis.

The new analysis method was also applied to the experimental cluster distributions measured at CLOUD (Olenius et al., 2013). The ammonia concentration was below the detection limit and thus unknown in many of the experiments, leading to uncertainties in the analysis, but some insight on the dynamics of the system was nevertheless obtained.

The new simulation-based method shows great potential as a powerful tool for analysing cluster distribution measurements.

This work was supported by the Vilho, Yrjö and Kalle Väisälä Foundation and the European Research Council (project ERC-StG 257360-MOCAPAF), and computer resources were provided by CSC – IT Center for Science Ltd.

Almeida, J., Schobesberger, S., Kürten, A., Ortega, I. K., Kupiainen-Määttä, O., et al. (2013). *Nature*, 502, 359-363.

Junninen, H., Ehn, M., Petäjä, T., Luosujärvi, L., Kotiaho, T., Kostiainen, R., Rohner, U., Gonin, M., Fuhrer, K., Kulmala, M., & Worsnop, D. R. (2010). *Atmospheric Measurement Techniques*, 3, 1039-1053.

Olenius, T., Schobesberger, S., Kupiainen-Määttä, O., Franchin, A., Junninen, H., Ortega, I. K., Kurtén, T., Loukonen, V., Worsnop, D. R., Kulmala, M., & Vehkamäki, H. (2013). *Faraday Discussions*, 165, 75-89.

A STUDY ON CARBONACEOUS PARTICLES OVER NORTHERN INDIA: SIMPLIFYING THE METHOD OF CALCULATATION OF FRACTAL DIMENSION

Sachin Gautam[1]

[1]National Physical Laboratory, Dr. K.S. Krishnan Marg, 110012, New Delhi, India

Keywords: fractal-like aggregates, fractal dimension, Indo-Gangetic Plain, atmospheric aerosols

Increasing urbanization, burning of fossil fuels along with vehicular emissions around the globe are a major source of aerosols which have very different morphological properties, generally exhibiting fractal like geometry, as compared to natural aerosols. Coupled with their complicated shapes it becomes computationally difficult to find the very basic parameter, fractal dimension, needed to quantify such aggregates.

The particle collection was done at Delhi and Kanpur in the Indo-Gangetic Plain (comprising of highly urbanized areas) in India to maximize percentage collection of carbonaceous aggregates. The individual particles were collected on Cu-TEM grids for individual particle morphology using High Resolution Transmission Electron Microscope (HRTEM). Further image analysis was done using ImageJ.

The particles collected exhibited fractal like morphology each composed of 110-150 spherical monomers, with radius varying from 25nm-50nm, exhibiting shapes varying from chain-like to aggregates coagulated into almost spherical shapes.

The empirical relation given by Lewis F. Richardson (which was reinstated by Mandelbrot, 1967) was used in the calculation of fractal dimension. Other recent studies have also used this empirical relation for its simplicity (Brown 1987; Bo-An Jang 2006).

$$L(r) = a*r^{(1-Df)}$$

where L(r) is the length of the aggregate taken along its periphery/perimeter, a is any positive constant, r is the length of the measuring scale or span and Df is the fractal dimension.

By knowing all the other parameters, value of fractal dimension is determined.

The perimeter of the aggregate profile was calculated using ImageJ using different measuring spans. A log-log plot of the above equation for a carbonaceous aggregate collected at Delhi is shown in Figure 1 along with the tabulated values, as shown in Table 1, of the log of the perimeter of the aggregate profile against log of measuring span.

The value of the fractal dimension for the same aggregate obtained from this method is 1.324 (1-slope, where slope is obtained from Figure 1).

The accuracy of the method increases as the number of measuring spans are increased to measure different perimeters. It gives satisfactory results within a percentage error of 5 when 4 to 5 different cases of measuring spans are used to measure perimeter of the profile.

Table 1. Computed log values of measuring span r and perimeter L(r) for an aggregate collected at Delhi

log(r)	log(L(r))
1.69	3.48
1.87	3.44
2	3.39
2.09	3.35

Figure 1. log-log plot of measuring span r against perimeter L(r) for the same aggregate.

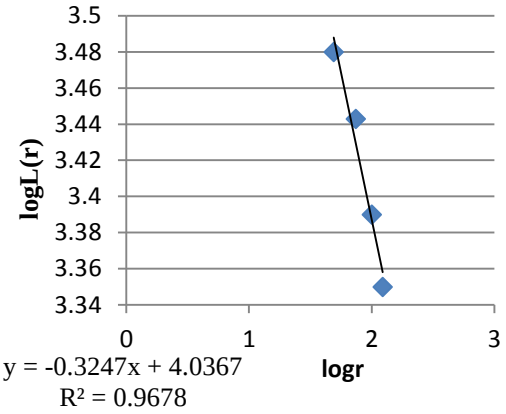

By making the calculations of fractal dimension less tedious it has become easier for us to understand the behavior of carbonaceous aerosols, their ageing mechanisms, their effects on human health and air quality as fractal dimension is a crucial parameter to quantify and characterize a carbonaceous aerosol.

This work was supported by the National Physical Laboratory, New Delhi, India.

Mandelbrot, B. B. How Long Is the Coast of Britain? Statistical Self-Similarity and Fractional Dimension, Science, New Series, Vol. 156, No. 3775 (May 5, 1967).

Brown, S. R. (1987). A note on the description of surface roughness using fractal dimension, Geophysical Research Letters. 14(11):1095-1098.

Bo-An Jang, Hyun-Sic Jang & Hyuck-Jin Park (2006): A new method for determination of joint roughness coefficient IAEG2006 Paper number 95.

A transportable Ice Nucleation Chamber for field measurement

J. Duplissy[1], Q. Nguyen[2], E.S. Thomson[3], V. Hemmilä[4], M. Kulmala[4], T. Petäjä[4], M. Sipilä[4], M. Bilde[2], E. Swietlicki[5] and Z.A. Kanji[6]

[1]Helsinki Institute of Physics, University of Helsinki, 00014, Helsinki, Finland
[2]Department of Chemistry and iNANO, Aarhus University, 8000 Aarhus, Denmark
[3]Department of Chemistry and Molecular Biology, Atmospheric Science, University of Gothenburg, 41296, Gothenburg, Sweden
[4]Department of Physics, University of Helsinki, 00014 Helsinki, Finland
[5]Department of Physics, Lund University, Box 118, 222 11 Lund, Sweden
[6]Institute for Atmospheric and Climate Sciences, ETH, Zurich, 8092, Switzerland

Keywords: Ice Nuclei Chamber, PINC, ZINC, ice nuclei, CRAICC

The importance of ice crystals in clouds for our climate is manifold: Their presence, number and shape influences the optical properties of clouds, the formation of precipitation and the cloud lifetime. All of these aspects impact global radiative balance and therefore the climate. Within the CRAICC (CRyosphere-Atmosphere Interactions in a Changing Arctic Climate) center of excellence we aim to investigate the ice nucleating properties of aerosols present in the Artic region using continuous measurements at different Nordic field stations.

To achieve this goal, two new transportable ice nucleation chambers (PINCii) based on the designs of the ETHZ instruments ZINC (Zurich Ice Nucleation Chamber) and PINC (Portable Ice Nucleation Chamber), are being built. The field instrument, PINC, has successfully participated in multiple laboratory campaigns (Chou et al, 2013; Kanji et al, 2013; Wex et al, 2014; Hiranuma et al, 2014) as well as field campaigns (Chou et al, 2011). A successful collaboration between ETHZ and CRAICC partners has led to technology transfer for the manufacture of the two Ice Nucleation Chambers. Our new PINCiis have two portable refrigerant compressors to directly cool the walls of the chamber without the use of an intermediate cooling liquid. In this configuration, the instrument is able to measure ambient ice nuclei (IN) concentrations at conditions as cold as -40°C and relative humidities exceeding water saturation. Our new PINCii has an elongated ice nucleation chamber (1 meter) similar to that of ZINC. An inter-comparison prior to their first campaign is scheduled for summer 2015.

In this presentation, we will explain the Ice Nucleation Chamber operational principles. We will discuss the challenges we encountered while constructing the two chambers and finally we will discuss the needs we have identified for effective operation in the field.

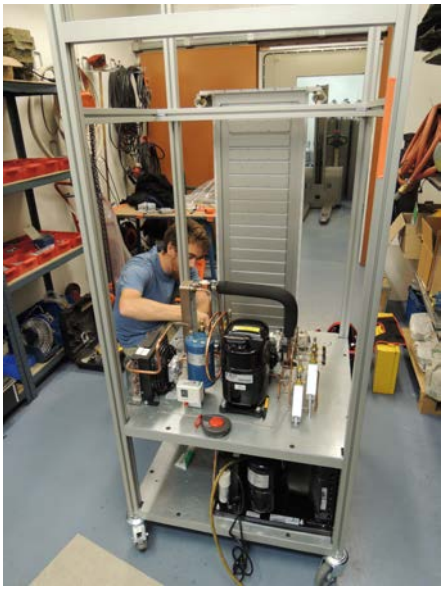

Figure 1. Installation of the 1 m ice nucleation chamber with the refrigeration unit compressors in the foreground.

ACKNOWLEDGEMENTS

This work was supported by CRAICC, the Finnish Center of Excellence (project No. 272041) and the Swedish Research Councils

REFERENCES

Chou et al. (2011), Atmos. Chem. Phys., 11, 725-4738
Chou et al. (2013), Atmos. Chem. Phys., 13,761-772
Kanji et al. (2013), Atmos. Chem. Phys., 13, 9097-9118
Wex et al. (2014), Atmos. Chem. Phys. Disc., 14, 22321–22384
Hiranuma et al. (2014), Atmos. Chem. Phys. Disc., 14, 22045–22116

A true monodisperse classifier without charge-state artefacts: Classifying nanoparticles with the Aerodynamic Aerosol Classifier

J.S Olfert[1], C. Lowndes[2], J.P.R. Symonds[2], K StJ. Reavell[2], and M. Rushton[2]

[1]Department of Mechanical Engineering, University of Alberta, T6G 2G8, Edmonton, Canada
[2]Cambustion Ltd, CB1 8DH, Cambridge, United Kingdom

Keywords: monodisperse classifier, aerodynamic aerosol classifier, relaxation time.

The Aerodynamic Aerosol Classifier (AAC) classifies particles by their relaxation time (or aerodynamic diameter). The AAC consists of two rotating coaxial cylinders. The aerosol enters through a gap in the inner cylinder and is carried axially by particle-free sheath flow. Between the rotating cylinders, the centrifugal force causes the particles to move in the radial direction. Particles with a narrow range of aerodynamic diameters exit the classifier through a gap in the outer cylinder with the sample flow. Particles with larger aerodynamic diameters impact and adhere to the outer cylinder and particles with smaller aerodynamic diameters exit the classifier with the exhaust flow.

Unlike the differential mobility analyser (DMA) or centrifugal particle mass analysers (CPMA or APM) the classification does not depend on the electrical charge state of the particles. Therefore, the AAC is a preferred classifier where a truly monodisperse aerosol is desired.

Previously work has shown theoretical models of the transfer function of the AAC (Tavakoli & Olfert, 2013), experimental validation of those transfer functions (Tavakoli et al, 2014), and tandem measurements using an AAC and DMA to measure particle mass, effective density, mass-mobility exponent, and dynamic shape factor (Tavakoli & Olfert, 2014).

In previous work most of the measurements were made between ~100–1000 nm in aerodynamic diameter due to the limited rotational speed of the first prototype AAC. Recently, a new prototype AAC has been developed with a much higher maximum rotational speed. The purpose of this presentation is to demonstrate the AAC can accurately classify particles down to ~20 nm in aerodynamic diameter.

The AAC was tested using a scanning mobility particle sizer (SMPS) as shown in Figure 1. Atomized NaCl was passed through the AAC operating at a fixed rotational speed. The SMPS was used to measure the mobility size distribution out of the AAC. Both the AAC and DMA were operated with sheath and aerosol flow rates of 3 LPM and 0.3 LPM, respectively.

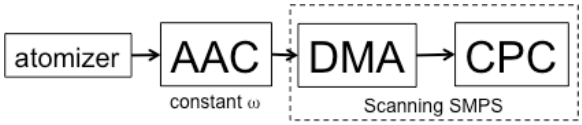

Figure 1. Experimental set-up.

The measured mobility size distributions are shown in Figure 2 for AAC rotational speeds between 2000 and 8000 rpm. These speeds correspond to aerodynamic diameters ranging between 23 and 222 nm. Given that the NaCl particles are not unit density nor spherical, these correspond to mobility diameters of 15 to 150 nm.

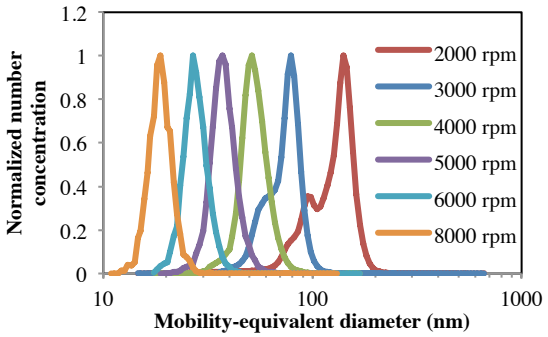

Figure 2. Mobility-diameter spectra of AAC-classified NaCl particles.

It is important to note that the aerosol exiting the ACC (and entering the SMPS) is monodisperse, however, due to multiple charge effects in the SMPS, peaks of the multiply-charged particles are seen in some spectra at smaller sizes than the singly-charged peak (i.e. to the left of the large peak). These multiply-charged peaks are clearly seen at the larger particle sizes (lower rotational speeds), where the probably of having particles with +2 or +3 charges is significant, where at smaller mobility sizes (< 50 nm) the probably of having multiply-charged particles is relatively small.

This work was supported by Cambustion Ltd.

Tavakoli, F. & Olfert, J. S. (2013). *Aero. Sci. & Tech.* 47, 916–926.

Tavakoli, F., Symonds, J.P.R. & Olfert, J. S. (2014). *Aero. Sci. & Tech.*, 48, i–iv.

Tavakoli F. & Olfert J. S. (2013). *J. Aerosol Science,* 75, 35–42.

ACTRIS WP3: Improving the observations of the in-situ aerosol properties in Europe

P.P.Aalto[1], H. Manninen[1], T. Petäjä[1] and A. Wiedensohler[2]

[1]Department of Physics, University of Helsinki, P.O.Box 64, FI-00014, University of Helsinki, Finland
[2]Leibniz Institute for Tropospheric Research, Permoserstraße 15, D-04318 Leipzig, Germany

Keywords: Atmospheric aerosols, instrumentation, size spectrometers

ACTRIS (Aerosols, Clouds, and Trace gases Research Infra Structure Network) is a European project aiming at integrating European ground-based stations equipped with advanced atmospheric probing instrumentation for aerosols, clouds, and short-lived gas-phase species. ACTRIS was funded as on Integrating Activity I3 under the EU FP7. Inside the ACTRIS WP3 the overall objective is to improve the observations of the in-situ aerosol properties. These properties at the moment are aerosol number size distributions, aerosol optical properties, sampling and analysis of organic and elemental carbon and organic tracers and cloud condensation nuclei measurements. Main European laboratories involved are Leibniz Institute for Tropospheric Research (TROPOS), University of Helsinki Department of Physics (UHEL), JRC in Ispra, University of Lund Department of Physics (ULUND) and Paul Scherrer Institut (PSI). TROPOS is also the GAW World Calibration Centre of Aerosol Physics (WCCAP) and has been hosting most of the workshops held under WP3. ACTRIS continues the work started under EU FP6 project EUSAAR In 2014 26 sites from Europe submitted aerosol data to EBAS data base hosted by Norwegian Institute for Air Research (NILU)

Inside the WP3 the improvements of the observations are attempted by organizing expert meetings, publishing Standard Operation Procedures (SOP) and construction instructions for the instruments, organizing intercomparison workshops, station audits and constructing reference instruments, which can be used as travelling standards and in intercomparison workshops (Wiedensohler, 2012).

In this abstract we concentrate on the work done with the Mobility Particle Size Spectrometers (MPSS). During EUSAAR period three intercomparison workshops were organized and during ACTRIS period two. During ACTRIS period also two expert workshops were organized which concentrated on the spectrometers optimized to sub 10nm particle measurements. First attempts to intercompare Optical Particle Counters (OPC) and Aerodynamic Particle Sizers (APS) were also started. Station audits were done during the EUSAAR period.

In a typical intercomparison workshop the Condensation Particle Counters (CPC) are checked at first. Some of the calibrated counters need at first some service, but after the service their 50% counting efficiency is within some nanometers and they reach 100% efficiency with accuracy of some percent. Next step is to check the sizing accuracy of the MPSS systems. The test is done with 200nm PSL particles and the well behaving spectrometers did not deviate more than 3.5% from the nominal size. In the first workshops the deviations reached 10% with some instruments. The final comparison is to compare the ambient size distribution against the reference MPSS and integrated concentration against the reference CPC. The goal was to achieve 10% accuracy in 10-500nm size range. However finally the agreement was found just between the 20-200nm size range.

To achieve better agreement in the ultrafine size range one has to pay attention to the accuracy of the MPSS classification voltage and calibrate each system individually for losses. That is why in both EUSAAR and ACTRIS WP3 projects a separate sub projects were initiated to improve the detection of sub 20nm particles. In UHEL a special version of the MPSS with variable sheath and aerosol flows and more accurate voltage control was built, calibrated and tested. The instrument is currently in active use in UHEL and can measure size distributions between 6-850nm. The construction can be adapted by other laboratories. The existing (UHEL and TROPOS) MPSS systems specially designed to measure particle size distributions between 3-20nm were intercompared and calibrated in UHEL The results are quite promising. Also Neutral cluster Air Ion Spectrometer (NAIS) was used during the expert workshop.

The reason for the discrepancy of the MPSS instruments above the 200nm size class is still unknown and should be studied. One reason might be the different time constants of the MPSS systems. The instruments are not reacting fast enough for the decaying concentration.

This work was accomplished by the European research infrastructure projects EUSAAR (European Supersites for Atmospheric Aerosol Research, EU FP6 Integrated Infrastructures Initiatives project, No. FP6-026140), and ACTRIS (Aerosols, Clouds, and Trace gases Research InfraStructure Network). The research leading to these results has received funding from the European Union Seventh Framework Programme (FP7/2007-2013) project No. 262254).

Wiedensohler, A.., et al. (2012). *Atmospheric Measurement Techniques*, 5, 657-685

ACTRIS: http://www.actris.net/
EUSAAR: http://www.eusaar.net/
EBAS: http://ebas.nilu.no/

Advanced Electrospray Aerosol Generator with Integrated Soft X-ray Neutralizer

Torsten Tritscher[1], Aaron Avenido[2], Axel F. Zerrath[2], Tim Johnson[2], Jacob H.T. Scheckman[2], Thomas Krinke[1], Florian Dahlkötter[1] and Oliver F. Bischof[1]

[1]TSI GmbH, Particle Instruments, Neuköllner Str. 4, 52068, Aachen, Germany
[2]TSI Inc., 500 Cardigan Road, 55126, Shoreview, MN, USA

Keywords: Nanoparticle, Electrospray, Scanning mobility particle sizer, Soft X-ray neutralizer

An electrospray is a suitable technique for the generation of aerosols from suspended particles and solutions of dissolved solutes. Electrospray (ES or nano-ES) offers significant advantages as a particle source for aerosol measurements with e.g. Scanning Mobility Particle Sizers (SMPS) due to its ability to produce stable, uniform and small (~150 nm) initial liquid droplets. The method is commonly used to disperse particles as small as 2 nm up to 150 nm or even larger. These particles can then be analyzed in applications including basic aerosol research, protein sizing, manufactured nanoparticle sizing and others.

The droplets formed by electrospray generation are highly charged and decrease in size as they dry. The surface charge on the droplet increases and the repulsive force can cause them to fragment. The droplets can be neutralized using a radioactive source like Po-210 (Kaufman et al., 1993) to avoid droplet disintegration and particle losses.

Low energy soft X-ray neutralizers are frequently employed as an alternative to radioactive sources (Shimada et al., 2002; Lee et al. 2005). Both types of neutralizers are able to bring particles to a stable bipolar charge distribution. This has recently been characterized for use in SMPS measurements (Knobel, et al., 2013).

In this paper we present a new Electrospray Aerosol Generator (EAG, TSI model 3482) with an integrated soft X-ray neutralizer, see Figure 1.

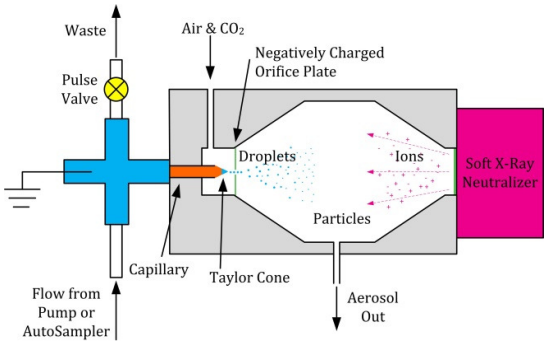

Figure 1: Schematic of the Electrospray Generator.

The advanced EAG presented here has been designed to improve usability. A key element in any electrospray is the status feedback of the Taylor cone generated by balancing flows and voltages. A digital camera is used to produce the image of the electrospray cone at the tip of the capillary and the live video image is shown on the instrument's touch panel display.

Additionally, a particularly short capillary is used, so the surface area for particle adhesion is minimized and occurrences of capillary clogging are greatly reduced. The new capillary mount is also designed for easy replacement.

Standard connectors are used for connection to an external pump, such as a high pressure piston pump, e.g. HPLC pump or an easy-to-use syringe pump. Use of an external pump also allows for an easy connection to an autosampler for automated sample analysis.

The size of the generated droplets was characterized during verification of this new device. We evaluated the stability of the particle output and the charge state of the generated droplets after neutralization. The EAG was then used to aerosolize PSL, colloidal silica (shown in Figure 2), and proteins of known molecular mass for further size distribution analysis with SMPS.

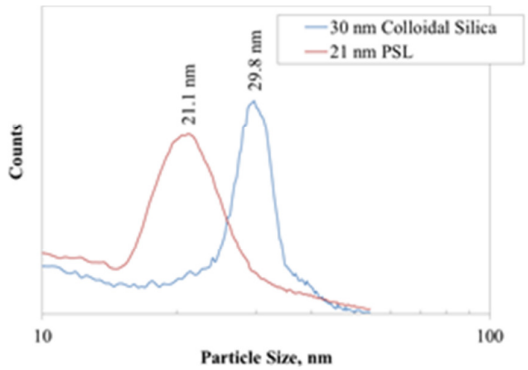

Figure 2: Number size distribution for PSL and colloidal silica generated with the new EAG.

Kaufman, S.L., Zarrin, F., Dorman, F. (1993) Electrospray Apparatus for Producing Uniform Submicrometer Droplets. *U.S. Patent* No. 5,247,842.

Knobel, L., Weinhold, K., Gandhi, J., Wiedensohler, A. and Schmid, H.J. (2013) Application of a X-ray charger for SMPS measurements", *European Aerosol Conference 2013*, Prague, CZE.

Lee, H.M., Soo Kim, C., Shimada, M and Okuyama, K. (2005). *J. Aerosol Science*, 36(7), 813-829.

Shimada, M., Han, B., Okuyama, K. and Otani, Y. (2002). *Journal of Chemical Engineering of Japan*, 35(8), 786-793.

Aerosol analysis by absorption in the mid IR regime: Application to e-cigarettes

W. Dunkhorst[1], P. Lipowicz[2], W. Koch[1]

[1]Dep. Aerosol Technology, Fraunhofer ITEM, Nikolai-Fuchs-Str. 1, 30625, Hannover, Germany,
[2] Altria Client Services Inc., Research, Development & Engineering, 601 East Jackson St. Richmond, VA USA 23219

Keywords: aerosol extinction, e-cigarette

A highly concentrated submicron condensation aerosol is formed in electronic cigarettes. Its main chemical components are the carrier substances glycerol, propylene glycol and, to minor extent, nicotine and water. Time resolved information on mean particle size and volume concentration during the puff is of interest for the assessment of mass transfer of the substances.

The aerosol parameters are measured using a three wavelength light extinction method in the near and mid-IR regime. Special use is made of the strong absorption bands at 3.4 µm caused by the excitation of C-H-vibrations of the main aerosol components. The other two wavelengths are 1.65 and 2.0 µm. The analysis is based on the ratio, R_{scat}, of the extinction values at 1.65 and 2.0 µm determining the exponent, ν, of a power law approximation of the extinction by scattering. This is used to subtract the scattering part of the extinction at 3.4 µm from the total extinction value to obtain the absorption, which is proportional to the volume concentration of the smoke. Mean particle size is obtained from the ratio of absorption at 3.4 µm to scattering extinction at 2.0 µm (Fig. 1).

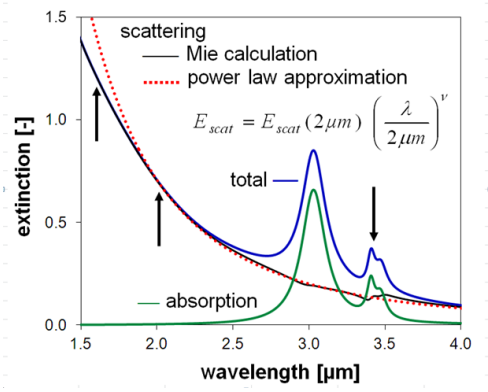

Fig. 1: Mie calculations of the extinction pattern for an aerosol with median diameter of 0.75 µm and σ_g=1.9.

In the current state, the evaluation scheme is sensitive to variation of particle size and volume concentration but not of geometric standard deviation. This has to be determined separately by impactor measurements for example.

The construction of a simple sensor became feasible due to the availability of LEDs in the mid IR regime (Roithner Lasertechnik, Vienna, Austria). The sensor is composed of the three extinction paths (0.5 cm) arranged in series in flow direction. The optics are protected by a clean air curtain flowing concentrically with the aerosol stream (Fig. 2).

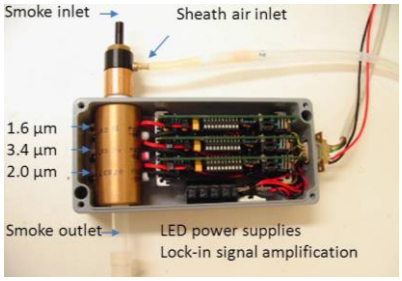

Fig. 2: 3-wavelength (mid) IR extinction sensor for the measurement of organic aerosols.

Fig. 3 demonstrates the time resolution achieved in measuring the median diameter and the mass flux of the undiluted, mainstream condensed aerosol generated by an e-cigarette during a puff.

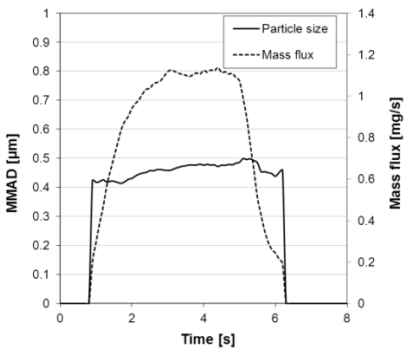

Fig. 3: Time resolved aerosol characterization

.

The aerosol quantities were measured for a wide range of operating parameters of the e-cigarette. Time integrated signals were compared with results of filter (mass generation) and impactor samples (mean particle size and standard deviation). The sensor response for concentration was independent of the relative composition of the condensate in view of glycerol and propylene glycol. The MMADs determined by the extinction method agreed well with cascade impactor measurements.

Aerosol concentrations and composition in an underground mine

K. Teinilä[1], H. Timonen[1], M. Aurela[1], S. Saarikoski[1], H. Hellén[1], H. Hakola[1], R. O. Salonen[2], A. Pennanen[2], M. Linnainmaa[3], F. Reyes[4], Y. Vasques[4], R. Hillamo[1]

[1]Atmospheric Composition Research, Finnish Meteorological Institute, FI-00560, Helsinki, Finland
[2] Department of Environmental Health, National Institute for Health and Welfare, Kuopio, Finland
[3] Finnish Institute of Occupational Health, Tampere, Finland
[4] Mario Molina Center Chile, Santiago de Chile, Chile

Keywords: particulate matter, aerosol mass spectrometry, chemical composition, mining.

Particulate matter (PM) emitted from mining operations may have adverse health effects on workers and population living nearby. In order to characterize aerosol physical and chemical properties and their emission sources in mining environment, an intensive campaign was conducted in underground mine (−500 m) between April 1 and June 17, 2014. On-line instrumentation was used to measure aerosol chemical and physical properties with high time resolution. In addition, samples for chemical analyses were collected using a PM_1 sampler and a Nano-Moudi impactor which collects particles from 10 nm to 10 µm.

On−line chemical composition of particles smaller than 1.0 µm of particle aerodynamic diameter (D_a<1.0 µm) was measured using a Time-of-Flight Aerosol Chemical Speciation Monitor (ToF-ACSM, Aeodyne Research Inc), a Soot Particle Aerosol Mass Spectrometer (SP−AMS, Aerodyne Research Inc.), and a Multi-Angle Absorption Photometer (MAAP, Thermo Fisher Scientific Inc.). Particle size-distributions between 10 nm and 10 µm were measured using combination of a Scanning Mobility Particle Sizer, (SMPS, TSI Inc.) and an Aerodynamic Particle Sizer, (APS, TSI Inc.). Particle size distributions were also measured with an Electrical Low Pressure Impactor (ELPI+, Dekati Ltd).

The total particulate mass concentration was calculated from SMPS and APS measurements using density of 1.4 g/cm^3 for particles D_p<0.5 µm (SMPS) and 2.0 g/cm^3 for particles with D_a between 0.5 and 10 µm (APS). On average 60 % of the measured particulate mass was found in particles with D_p<0.5 µm.

Chemical composition of sub−micrometer particles was quite similar over most of the time. Major components were organics and black carbon (Figure 1), both expected to be constituents of emissions from diesel engines. The chemical composition of supermicron PM was not measured with on−line systems, but most probably majority of supermicron PM was mineral dust. The analysis of Nano−Moudi samples will give more information on the chemical composition of supermicron particles.

Although chemical composition of submicron particles did not vary much during the measurements, their concentration levels and the total particle mass concentration (D_p<0.5 µm) showed large variations during the measurements. Mass concentration of particles between 0.5 and 10 µm varied also during the measurements. These changing particle mass concentrations were connected to diurnal variations in mine activities. The variations of total particle mass in particles less than 0.5 µm reflected the changes in diesel emissions, and the variations in coarse particle size was attributed to mineral dust emissions. Also longer term variations in mine activities could be seen. A 10 day lasting episode, when majority of particle mass was found in particles larger than 0.5 µm in diameter may be connected to mineral dust source close of the measurement site.

On-line measurements of chemical composition showed that concentrations of inorganic ions, ammonium, nitrate and sulphate, and also concentration of total organics occasionally increased markedly over few hour lasting periods. It seems that the peaks in their concentrations are connected to blasting situations.

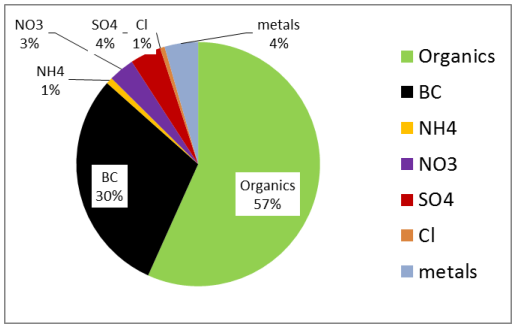

Figure 1. Average mass fractions of chemical components during ten PM_1 samplings. Total organic matter and inorganic ions were measured with ToF-ACSM, black carbon was measured with MAAP and metals were analysed from PM_1 filter samples using ICP-MS.

This work was funded by the TEKES in the Green mining programme (HIME project).

Aerosol Manufacturing of ZnO Nanorods for Catalytic Hydrogen Production

D.Q. Chie and K. Wegner

Particle Technology Laboratory, Swiss Federal Institute of Technology (ETH) Zurich
Sonneggstrasse 3, CH-8092 Zurich, Switzerland

Keywords: Nanorods, Flame Spray Pyrolysis, ZnO, Scale-up

Nanoscale zinc oxide is an extremely versatile material that finds application e.g. in electronics, optics, solar cells, catalysis, sensors or polymer nanocomposites. Improved performance has been reported frequently for one-dimensional nanostructured materials like nanorods or -wires, asking for continuous manufacturing routes for such nanomaterials.

Flame aerosol synthesis has already been proven a versatile, economic and scalable method for production of oxide nanoparticles with controlled properties. In particular, Flame Spray Pyrolysis (FSP, Mädler et al., 2002) has been employed for ZnO nanoparticle synthesis (Tani et al., 2002). However, sphere-like product particles rather than nanorods were obtained unless dopants were used (Height et al, 2006).

Here we demonstrate how careful tuning of flame conditions results in a narrow window for production of ZnO nanorods with aspect ratios as high as 20. Based on this, scale-up of the laboratory process to kg/h production rate (Hembram et al., 2013) is explored. Finally, the performance of flame-made nanorods in the catalytic generation of hydrogen from formic acid is investigated and compared to that of spherical nanoparticles.

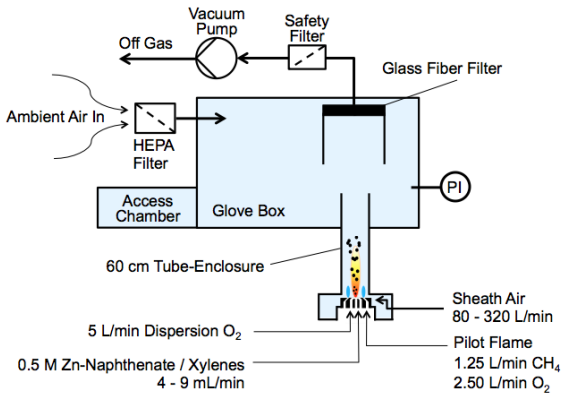

Figure 1: Glove-box enclosed flame spray pyrolysis unit for synthesis of ZnO nanorods.

Figure 1 shows the schematic of the experimental setup for ZnO nanoparticle synthesis from 0.5M Zn-naphtenate / xylenes precursor. The FSP reactor with concentric sheath air supply channel and 60 cm long Inconel tube enclosure is tightly attached to the bottom of a glove box. Product particles are collected on glass fibre filters inside the glove box with the help of a vacuum pump. During pump operation, HEPA-filtered ambient air is drawn into the glove box that is maintained at slightly sub-atmospheric pressure, preventing airborne particles from escaping into the workspace. Production of the particles within the glove box thus ensures contained and safe nanoparticle production and handling.

Precursor and sheath air flow rates are varied to generate different particle growth conditions in the flame and aerosol reactor tube. Axial and radial temperature profiles as well as flow and concentration maps by computational fluid dynamics are correlated to nanoparticle size and morphology obtained by thermophoretic sampling. Only conditions near 6 mL/min precursor and 80 L/min sheath air flow yield appropriate high temperature particle residence times for production of high-aspect ratio ZnO nanorods while outside this window rather spherical particles are made (Figure 2). Employing such particle growth conditions in a pilot-scale FSP reactor allows nanorod manufacturing at kg/h scale.

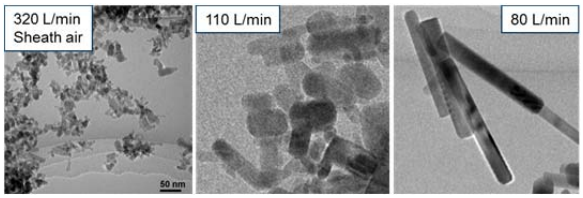

Figure 2: Effect of reactor conditions on product ZnO nanoparticle morphology: 6 mL/min precursor and 80 L/min sheath air flow yields nanorods while otherwise rather spherical particles are obtained.

These FSP-made nanorods show significantly higher activity in the catalytic generation of hydrogen from formic acid than same quantities of non-rod particles with similar specific surface area, attributed to a higher density of defect sites.

Height, M.J., Mädler, L., Pratsinis, S.E. & Krumeich, F. (2006). *Chem. Mater.*, 18, 572-578.

Hembram, K., Sivaprakasam, D., Rao, T.N. & Wegner, K. (2013). *J. Nanoparticle Res.*, 15., 1461.

Mädler, L., Kammler, H.K., Mueller, R.& Pratsinis, S.E. (2002). *J. Aerosol Sci.* 33, 369-389.

Tani, T., Mädler, L. & Pratsinis, S.E. (2002). *J. Nanoparticle Res.*, 4, 337-343.

Aerosol Nanoparticle Synthesis without Chemical Reactions

Prof. F. Einar Kruis
Institute for Technology of Nanostructures and Center for Nanointegration Duisburg-Essen,
University Duisburg-Essen, Germany

The chemistry-free synthesis of nanoparticles in the gas-phase has a certain number of advantages in comparison to synthesis based on precursors and chemical reactions, which will elaborated in this talk. After a short discussion of nanoparticle synthesis by physical methods, the talk will be guided by an extensive description of its' main challenges, namely costs, energy consumption, stability of generation, product stoichiometry, control methods, scaling-up and integration in other processes. A number of examples will be given, especially for arc and spark discharge which are characterized by simple power supplies, beneficial both for laboratory operation as well as scaling-up purposes. The characteristic energy consumption of these processes will be described, as this is essential for the final product costs. The abilities for monitoring production rate and product quality are important requirements for industrial production, as well as methods which allow to control particle size, the material stoichiometry and mixing ratio. Strategies to maximize the production rate as well as scaling-up examples will be shown. Finally, two examples of integration a chemistry-free nanoparticle generator into a subsequent material synthesis process will be given, size-selected nanoparticles for the aerotaxy process as well as incorporating particles into a PVD film at low pressures.

Aerosol of silica nanoparticles generated during the combustion of a polysiloxane nanocomposite

G. Ounoughene[1,2,3], O. Le Bihan[4], C. Chivas-Joly[5], C. Longuet[2], C. Motzkus[5], B. Debray[4], A. Joubert[1], J-M. Lopez-Cuesta[2], L. Le Coq[1*]

[1]LUNAM, Ecole des Mines de Nantes, GEPEA, CNRS, UMR 6144, 4 rue Alfred Kastler, 44307 Nantes Cedex 03, France
[2]C2MA, Ecole des Mines d'Alès, 6 Avenue de Clavières, 30319 Alès Cedex, France
[3]ADEME, 20 avenue du Grésillé, 49004 Angers Cedex 01, France
[4]INERIS, Parc Technologique Alata, 60550 Verneuil-en-Halatte, France
[5]LNE, 29 Avenue Roger Hennequin, 78197 Trappes Cedex, France
*Corresponding author: laurence.le-coq@mines-nantes.fr

Keywords: combustion, aerosol, nano-silica, polysiloxane.

This study focuses on the aerosol emitted during the combustion of a polysiloxane nanocomposite filled with nano-silica particles. This kind of nanocomposites has been extensively studied and developed by both universities and industries for many applications in various industrial areas such as electronic and electrical equipment. Since their production and their use, they are expected to end up in incineration waste plants and they could be involved during fire. Hence, these two combustion scenarios raise an issue concerning risks towards the combustion aerosol generated. Many articles have been published about the thermal degradation of polysiloxane nanocomposites but none of them relate to tests studying silica combustion aerosol. However, SiO_2 nanoparticles are studied in the problematic of siloxane in biogas.[1] The aim of our work is to investigate the behavior and the fate of the nano-silica from the polysiloxane nanocomposite during its combustion under two combustion scenarios.

Combustion tests have been performed at lab-scale using a peculiar tubular furnace for an incineration scenario[2], and a specific cone calorimeter for a fire scenario. The combustion aerosol has been sampled and characterized using various techniques devoted to the analysis of aerosols. This work reports particularly on the particles number concentration and microstructure of the aerosols produced during combustion tests. The objective of the sampling was to avoid cold spots (which would entail nucleation and condensation phenomena) before and during the first dilution. The dilutors perform two successive dilutions: the first heated dilution at 160 °C (± 10) °C and the second at room temperature. Regarding the time tracking of the particles from the combustion aerosol, an Electrical Low Pressure Impactor (ELPI, Dekati) and a DMS500 Fast Particle Analyser (Cambustion) were used downstream of dilutors. Regarding off-line imagery analyses, there were two types of sampling. In the first type, silica combustion aerosol particles were collected throughout the test using gravimetric impactors (DLPI and DGI, Dekati). The particulate matter of the combustion aerosol was collected on impaction substrates with controlled temperature during sampling (160 ± 10 °C). Then, these particles collected were analyzed by a scanning electronic microscope (SEM). This gravimetric impactor allowed an off-line qualitative analysis (imagery and chemistry) of particles collected during the whole combustion test. In the second type, combustion aerosol particles were collected over successive targeted time ranges with a MPS ® (Mini-Particle-Sampler, Ecomesure) on transmission electronic microscope (TEM) grids for the TEM imagery.

Results show aggregated and agglomerated particles of nano-silica in the combustion aerosol. The finest silica particles seem to come from nano-silica fillers (D<50nm) and the others seem to come from polysiloxane matrix decomposition (Figure 1).

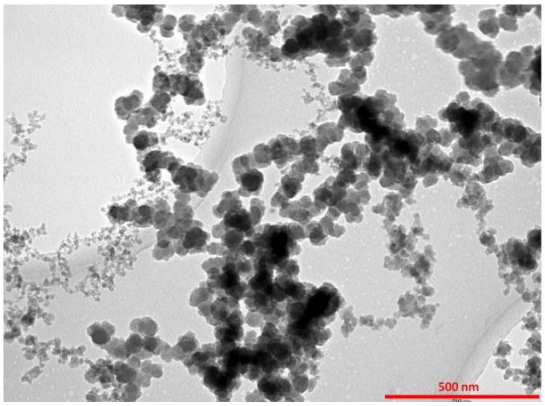

Figure 1. Silica particles collected on a TEM grid during combustion of polysiloxane nanocomposite.

References

[1]Turkin A.A., Dutka M., Vainchtein D., Gersen S., van Essen V.M., Visser P., Mokhov A.V., Levinsky H.B., De Hosson J.Th.M. (2014), *Applied Energy, 113, 1141–1148.*

[2]Ounoughene G., O. Le Bihan, C. Chivas-Joly, C. Longuet, B. Debray, C. Motzkus, S. Durécu, D. Venditti, A. Joubert, J-M. Lopez-Cuesta, L. Le Coq, *EAC 2013 Conference.*

Aerosol precursor and cluster detection by mass spectrometry: Recent advances and future research directions

M. Sipilä and M. Ehn

Department of Physics, 00014 University of Helsinki, Finland.

Keywords: nanoparticles, clusters, mass spectrometry, atmospheric aerosols.

The smallest nanoparticles and molecular clusters are subject of intensive research due to their effects on atmospheric aerosol properties and human health. Experimental methods to detect these smallest sub-3 nm particles and clusters have included different condensation based techniques such as the particle size magnifier and ion spectrometers. Mass spectrometers have typically been applied mostly for research related to chemical composition of relatively large (>50 nm) particles and for detection of some of the gaseous particle precursors such as sulphuric acid.

Recent advances in the development of mass spectrometry are, however, revolutionizing the experimental nano-cluster and secondary aerosol formation research in atmospheric sciences. Today, intensive research and development is carried out at the Department of Physics, University of Helsinki. Here we summarize our latest technological progress and related scientific key findings and discuss the future prospects.

A key leap forward was the development of an Atmospheric Pressure interface – Time-Of-Flight (APi-TOF) mass spectrometer, for highly sensitive detection of atmospheric ion clusters (Tofwerk AG, Switzerland). On top its extreme sensitivity, the instrument has a mass resolution of 4000 Th/Th – high enough for reliable identification of ion cluster atomic composition (e.g. Ehn et al., 2012). The instrument has been successfully applied in investigations related to ion cluster formation pathways in the atmosphere and in the CERN-CLOUD laboratory experiments (e.g. Almeida et al. 2013; Riccobono et al., 2014). With this instrument also the first observations regarding a previously unrecognized group of particle precursor vapours, so-called exteremely low volatile organic compounds (ELVOC) were made in the atmosphere (Ehn et al., 2012).

As the APi-TOF is only capable of detecting charged molecules and clusters, several Chemical Ionization (CI) methods and systems have been developed and applied. Jokinen et al. (2012) integrated the NO_3^- - ion based CI originally designed by Eisele and Tanner (1993) to the APi-TOF. With this NO_3^- -CI-APi-TOF neutral cluster formation pathways were resolved in certain laboratory (Kürten et al., 2014) and ambient environments (Sipilä et al., 2014). These observations are a crucial stride forward in understanding atmospheric cluster formation. Besides molecular clusters, NO_3^- -CI-APi-TOF is highly sensitive to cluster and particle precursor vapours, including ELVOC. The instrument was applied in a series of studies where ELVOC formation was shown to proceed via an auto-oxidation process (Ehn et al., 2014).

Another CI system, utilizing $HSO_4^-\cdot(H_2SO_4)_n$ –ions, was developed by Sipilä et al. (2015) for detection of atmospheric amines and ammonia. These bases may have a significant role in atmospheric aerosol formation but their sensitive detection is a challenge. With the present method, a sensitivity below 0.01 ppt for amines has been demonstrated.

NO_3^- based CI-APi-TOF has also been developed further (Taipale et al., 2014). If equipped with a suitable flow reactor system, the instrument is capable of indirectly detection gas phase radicals and oxidants – including OH, sCI, HO_2/RO_2 – which play a key role in production of aerosol precursor vapours.

Even though the CI-APi-TOF technique has thus far been mostly applied in atmospheric research the instrument is capable of detecting a variety of compounds and clusters of interest for a wider research community. The technique could be applied for example in detection of harmful or toxic compounds and clusters, including those relevant for civil security, clean room applications, medical applications, process control, etc.

Future research should therefore focus also on the above-mentioned areas of application. One of the major technological challenges in atmospheric research is still to amend the instrument sensitivity for detection of extremely low concentrations of sub-3 nm nano-clusters to resolve atmospheric secondary new particle formation.

Almeida et al. (2013). *Nature* 502, 395.
Eisele and Tanner (1993). *J. Geophys. Res.*, 98, 9001.
Ehn, M., et al. (2012). *Atmos. Chem. Phys*. 12, 511.
Ehn M. et al. (2014). *Nature* 506, 476.
Jokinen, T. et al. (2012). *Atmos. Chem. Phys*. 12, 4117.
Kulmala et al. (2013). *Science*, 339, 943.
Kürten et al. (2014). *Proc. Natl. Acad. Sci.* 111, 15019.
Mauldin III et al. (2012). *Nature*, 488, 167.
Riccobono et al. (2014). *Science.* 344, 717.
Sipilä M. et al. (2014). *Proc. Internatl. Aerosol Conf.*
Sipilä M., et al. (2015). *Atmos. Meas. Tech. Disc.*
Taipale, R. et al. (2014). *Boreal Environ. Res.* 19, 55.

Aerosol Self-Assembly of Nanoparticle Films: Densification Mechanisms of Ultra-Fine Particles in the Diffusion Regime

Noushin Nasiri[1], Tobias D. Elmøe[2], Qinghua Qin[1], Yun Liu[3], Antonio Tricoli[1,*]

[1]Nanotechnology Research Laboratory, Research School of Engineering, the Australian National University, 2601, Canberra, Australia
[2]Amminex Emissions Technology A/S, Gladsaxevej 363, 2860 Søborg, Denmark
[3]Research School of Chemistry, the Australian National University, 2601, Canberra, Australia

Keywords: Aerosol Deposition, Self-Assembly, Particle Dynamics, Scaling Laws

Nanoparticle films have shown potential for several technologies such as batteries dye sensitized solar cells (DSSCs),[1] sensors,[2, 3] fuel cells[4] and immobilized nanocatalysts. For example, chemo-resistive gas sensors made of metal oxide semiconductor nanoparticles have been successfully applied to breath analysis[5]. In general the nanoparticle film morphology can be categorized in three main categories namely dense, compact and porous[6]. Highly porous films are advantageous for gas sensors because gas molecules can diffuse rapidly into the detector and chemical interactions can occur between the gas and a large fraction of the total nanoparticle surface[6]. However, in order to benefit from the unique properties of nanoparticles in commercial products, it is crucial to develop scalable assembly methods able to provide reproducible three-dimensional morphologies.

Amongst others, aerosol deposition of nanoparticles is a highly scalable method with the potential to provide well-controlled pattern and unique miniaturization performance[7] as required by portable integrated solid state devices[8]. In addition, aerosol deposition of nanoparticle typically leads to highly porous morphologies[3] resulting in a convenient morphology for numerous applications such as chemical sensors[6] and super-hydrophilic/phobic coatings[9]. Engineering of the film structural properties to produce highly performing devices requires an advanced understanding of multi-scale phenomena such as particle-, fluid- and molecule-dynamics interaction[10]. However, recent results[11] have questioned the validity of existing models for the self-assembly of ultra-fine nanoparticle films from the gas phase[12]. Significant densifications of the resulting structures have been predicted by numerical solutions of the Langevin's equation of motion for decreasing particle size below 30 nm.[11] As the chemically most active nanostructures have often a diameter below 10 nm,[6] this variation are of considerable potential impact and an understanding of the densification mechanisms of ultra-fine particle self-assembly is of broad fundamental interest.

Here, the deposition dynamics of solid, monodisperse, freely diffusing spheres on a static, initially flat surface was investigated over four orders of magnitude in depositing body size from the micro- to the nano-scale. Grid-free numerical solutions of the Langevin's equation of motion in a continuous cuboid domain were used to predict the resulting deposition and films growth. Validation of the simulated nanoparticle film morphologies was pursued by deposition of flame-made nanoparticle aerosols on polished Si-wafer. A novel deposition regime that combines feature of the ballistic and diffusion limit is proposed to account for the divergence in the reported packing density with decreasing particle size below 50 nm. Two analytical models are derived to predict the morphology of the nanoparticle-substrate interface enabling robust predictions of the resulting film density as a function of particle size and Péclet number.

[1] A. Tricoli, A. S. Wallerand, M. Righettoni, J. Mater. Chem. 2012, 22, 14254.
[2] R. K. Joshi, F. E. Kruis, Appl. Phys. Lett. 2006, 89, 153116.
[3] L. Mädler, A. Roessler, S. E. Pratsinis, T. Sahm, A. Gurlo, N. Barsan, U. Weimar, Sens. Actuator B-Chem. 2006, 114, 283.
[4] Y. Liu, S. W. Zha, M. L. Liu, Adv. Mater. 2004, 16, 256.
[5] M. Righettoni, A. Tricoli, S. Gass, A. Schmid, A. Amann, S. E. Pratsinis, Anal Chim Acta 2012, 738, 69.
[6] A. Tricoli, M. Righettoni, A. Teleki, Angew. Chem. Inter. Ed. 2010, 49, 7632.
[7] H. Kim, J. Kim, H. Yang, J. Suh, T. Kim, B. Han, S. Kim, D. S. Kim, P. V. Pikhitsa, M. Choi, Nature Nanotech. 2006, 1, 117.
[8] A. Tricoli, M. Graf, F. Mayer, S. Kühne, A. Hierlemann, S. E. Pratsinis, Adv. Mater. 2008, 20, 3005.
[9] A. Tricoli, M. Righettoni, S. E. Pratsinis, Langmuir 2009, 25, 12578.
[10] D. Rodriguez-Perez, J. L. Castillo, J. C. Antoranz, Phys. Rev. E 2005, 72, 021403.
[11] L. Mädler, A. A. Lall, S. K. Friedlander, Nanotechnology 2006, 17, 4783.
[12] D. Rodriguez-Perez, J. L. Castillo, J. C. Antoranz, Phys. Rev. E 2007, 76, 76.011407.

Aerosol synthesis, generation, and characterization for toxicological studies

A.J. Koivisto[1,2], E.M. Rydman[2], H. Alenius[2], H. Norppa[2], K.M. Savolainen[2] and K.J. Hämeri[3]

[1]National Research Centre for the Working Environment, Lersø Parkallé 105, Copenhagen DK-2100, Denmark
[2]Nanosafety Research Centre, Finnish Institute of Occupational Health, Topeliuksenkatu 41 a A, FI-00250 Helsinki, Finland.
[3]Department of Physics, University of Helsinki, Gustaf Hällströmin Katu 2, P.O. Box 64, Helsinki FI-00014, Finland.

Keywords: inhalation exposure; nanoparticle; exposure assessment; aerosol generation; synthesis

Exposure to particulate matter (PM) has a significant impact on human health. For example, urban $PM_{2.5}$ air pollution has been recognized to be globally the 9th most powerful risk factor for burden of disease (Lim *et al.,* 2012). Several experimental and first epidemiological studies consider that the ultrafine particles are the most harmful fraction of PM with respect to pulmonary uptake (Meng *et al*., 2013).

In the years 2000 was invented nanotoxicology which focused mainly to study health effects of engineered nanomaterials (ENMs). Later, it was found that ENMs with their adjustable and well-defined properties can be used to study the toxicological mechanisms (Lison *et al.,* 2014). This requires well-controlled and repeatable methods to generate particles for inhalation studies. Here we

1) present three different setups to generate test aerosols which were applied for full body inhalation studies,
2) discuss how to disperse aerosols so that powders properties do not change significantly, aerosol concentration metrics (units: cm^{-3}, m^2 m^{-3}, and mg m^{-3}) and measurement techniques using particle counters and mobility, aerodynamic and optical particle sizers,
3) show how to perform safely inhalation studies with hazard materials.

A custom made laminar flow reactor was used to synthesize TiO_2 (74% anatase and 26% brookite) particles at a concentration range of 4×10^5 to 12×10^6 cm^{-3} (0.8 to 28.5 mg m^{-3}; Koivisto *et al.*, 2011).

A rotating brush generator (RBG 1000, Palas) was used to disperse five different types of TiO_2 powders and SiO_2 powder at concentrations of 10±2 mg m^{-3} (Rossi *et al.*, 2010).

A fluidized bed aerosol generator (TSI, FBAG model 3400A) was used to disperse carbon nanotubes (Baytubes, Mitsui, and Cheaptubes) at concentrations ranging from 8.2 to 18.5 mg m^{-3}, and ZnO and TiO_2 powders at concentrations ranging from 2.5 to 20.4 mg m^{-3}. The exposure setup is described by Rydman *et al*. (2014).

We found that different techniques are needed to aerosolize different ENM powders. For example, to achieve the same concentration using different ENM powders, the volumetric amounts may vary up to 30 times depending on the powder's density. Also, ENM powders fluidization properties differ significantly which causes *e.g*. clogging or problems in material flows. Differences in particle properties make concentration measurements challenging. We found that carbon nanotubes clog instruments sampling tubes at below 1 mg m^{-3} concentration or may cause new particles in corona charger. Finally we show how we have solved safety issues in cleaning of the exposure setup, material and waste handling, and instruments maintenance.

Lim S.S., Vos T., Flaxman A.D., *et al*. (2012) A comparative risk assessment of burden of disease and injury attributable to 67 risk factors and risk factor clusters in 21 regions, 1990–2010: a systematic analysis for the Global Burden of Disease Study 2010. Lancet; 380: 2224–2260.

Lison D., Vietti G., Van den Brule S., (2014) Paracelsus in nanotoxicology. Particle and Fibre Toxicology 11:35.

Meng X., Ma Y., Chen R., *et al*. (2013) Size-fractionated particle number concentrations and daily mortality in a Chinese city. Environ Health Perspect; 121: 1174–1178.

Koivisto A.J., Mäkinen M., Rossi E.M., *et al*. (2011) Aerosol characterization and lung deposition of synthesized TiO_2 nanoparticles for murine inhalation studies. Journal of Nanoparticle Research 13:2949-2961.

Rydman E.M., Ilves M., Koivisto A.J., *et al*. (2014) Inhalation of Rod-Like Carbon Nanotubes Causes Unconventional Allergic Airway Inammation. Particle and Fibre Toxicology, 11:48.

Rossi E.M., Pylkkänen L., Koivisto A.J., *et al*. (2009) Airway Exposure to Silica-Coated TiO2 Nanoparticles Induces Pulmonary Neutrophilia in Mice. Toxicological Sciences 113:422-433.

Aggregate Dynamics in the Transition Regime: a two Knudsen Number Problem

Prof. Christopher J. Hogan Jr.
Department of Mechanical Engineering, University of Minnesota

The production of particles at sufficiently high concentration in the gas phase invariably leads to the formation of agglomerates/aggregates, i.e. condensed phase entities composed of spherical or near spherical primary units in contact with one another. Aggregates are frequently produced in high temperature combustion and gas phase materials synthesis reactors, hence aggregate formation, growth, and measurement has garnered considerable interest. In large part, efforts in aggregate analysis have been devoted to inference of aggregate structure, including primary particle diameter, as well as the scaling between the number of primary particles per aggregate and the aggregate radius of gyration (i.e. the fractal dimension). However, a series of experimental and theoretical studies reveal that it is not these structural properties which govern aggregate transport in aerosols including aggregate mobilities/diffusion coefficients, ion attachment (charging) rates, and aggregate-aggregate collision rates. On the contrary, aggregate transport properties are determined by appropriately defined aggregate continuum radii and projected areas, which are measures of overall aggregate architecture. In this talk, an overview of the transport properties of aggregates in aerosols will be provided, including specific methods to calculate aggregate mobilities and collision rates at all background gas temperatures and pressures. These methods are based upon a series of Monte Carlo and Brownian Dynamics calculations, and experimental evidence supporting use of the developed equations will be provided. Emphasized in the presented methods will be the need to consider two Knudsen numbers in quantifying aggregate transport; the traditional Knudsen number, which governs aggregate mobility, and the diffusive Knudsen number, the parameter governing aggregate-ion and aggregate-aggregate collisions.

An experimental and theoretical assessment of the dissociation of ammonium nitrate aerosol.

Nicholas Talbot, Vladimir Zdimal, Jakub Ondracek, Jaroslav Schwarz

Laboratory of Aerosol Chemistry and Physics, Institute of Chemical Process Fundamentals of the ASCR, v.v.i., Rozvojová 2, 165 02 Prague 6 - Suchdol, Czech Republic.

Keywords: Ammonium Nitrate, Dissociation, Experiments, Modelling.

The dissociation kinetics of ammonium nitrate was investigated experimentally utilizing a tandem differential mobility analyzer/scanning mobility particle sizer system (Dassios and Pandis, 1998). Monodisperse aerosol of ammonium nitrate was produced by nebulizing 1g/ltr ammonium nitrate solution, drying the polydisperse particles, bringing them to Boltzmann charge equilibrium using a Kr^{85} aerosol neutralizer, and selecting one mobility fraction in the Vienna type DMA.

The aerosol generation system was located in a thermally insulated box kept at controlled temperature below 10˚C. The monodisperse aerosol was then diluted by mixing it with a dry, particle-free air and fed into a laminar flow reactor in which temperature, relative humidity and flow rates were controlled.

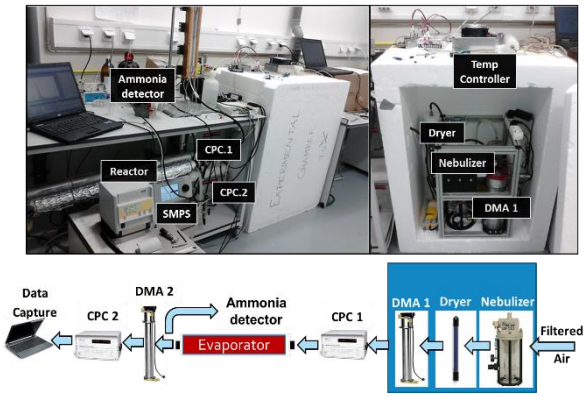

Fig. 1: Experimental setup.

Particle size distributions both upstream and downstream of the reactor were determined by an SMPS, consisting of a TSI EC 3080 provided with a long DMA, and a TSI CPC 3775. The stability of the aerosol generating system was further checked by the UCPC 3025A monitoring continuously the total particle concentrations.

In the series of dissociation experiments, we studied the size changes of the ammonium nitrate aerosol for three selected particle sizes (50, 100 and 200nm), at four reactor temperatures (15, 20, 25, and 30˚C), and several flow rates (between 0.6 to 1.6 litres per minute in 0.2 litre increments).

The observed changes of particle size were compared to the predictions of a mathematical model taking into account the ammonium nitrate dissociation kinetics, Kelvin effect and diffusion of ammonia and nitric acid from the particle to the bulk phase taking into account the measured concentration of ammonia gas in the bulk phase (equation 1).

$$\frac{d(\mathrm{d}p)}{dt} = \frac{4DvM}{RPpdp}\left(\frac{P\infty}{T\infty} - \frac{Pd}{Td}\right)\phi \qquad (1)$$

The model assumed evaporation in the continuum regime using the Fuchs-Sutugin correction term (Hinds, 1999).

Observed results indicate a strong association between increasing temperature and accelerated dissociation, tilting the reversible reactions shown in equation 2 below to the right hand side.

$$NH_4NO_3(s) \rightleftharpoons HNO_3(g) + NH_3(g)$$
$$NH_4^+(aq)\ NO_3^-(aq) \rightleftharpoons HNO_3(g) + NH_3(g). \qquad (2)$$

Results also indicate that NH_4NO_3 is most likely not completely dehydrated by the time it reaches the reactor. Therefore is likely further drying takes place in the reactor, helping explain in part the accelerated shrinking rates of the larger 200nm particles.

Shrinking and dissociation rates show a susceptibility to Kelvin surface / kinetics regime change effects when dp approaches 50nm. This is highlighted by a marked acceleration in dissociation behavior as the particle shrinks and is observed in both our dissociation rates and our modelled results.

The authors acknowledge support of this work by European Union Seventh Framework Programme (FP7/2007-2013) under grant agreement n° 315760 HEXACOMM.

References.

Dassios, K.G and Pandis, S.N, 1998, The mass accommodation coefficient of ammonium nitrate aerosol, Atmospheric Environment, **33**, pp2993-3003.

Hinds W C, 1999, Aerosol Technology, Properties, Behavior and Measurements of Airborne Particles. Wiley publications, New York.

Application of a Particle Size Magnifier under high relative humidity conditions

Daniela Wimmer, Juha Kangasluoma, Katrianne Lehtipalo, Joonas Vanhanen, Alessandro Franchin, John Backmann. Tuukka Petäjä, Markku Kulmala

Department of Physics, University of Helsinki, Helsinki, FI-00650, Finland

Keywords: nano-particles, measurement technique, condensation particle counter

Aerosol particles have been measured in various environments and play a major role in the energy balance of our planet. As well as influencing clouds and climate, they affect air quality and human health. Nanoparticles are also more and more used in technical or medical applications. Determining the size and concentration of aerosol particles is vital for advancing in all these fields.

Using condensation particle counters, allows for measurement of total concentrations of single aerosol particles down to a few particles cm^{-3}. By using the technique presented here it is possible to measure, with a high efficiency, particles of sizes as small as 1 nm in diameter. The Airmodus A20 consists of a Particle Size Magnifier (PSM) and a Condensation Particle Counter (CPC) used as a counter. The PSM working principle is based on mixing a hot saturated vapour with cold sample air, creating supersaturation, which leads to condensational growth of the aerosol from few nm to about 90 nm (Vanhanen *et al.*, 2010). The whole setup consists of two stages where the second stage allows further growth of the activated particles and their optical counting. The particles activated with DEG grow to sizes of about 90-100 nm, which is too small for optical detection (Iida *et al*., 2009).

High relative humidity (RH) conditions are a challenging environment for aerosol measurements in particular for condensation-based instruments. For overcoming these problems we designed an inlet suitable for measurements at high RH conditions, using the Airmodus A20 system. By using the newly designed inlet, the RH of the sample could be reduced from 90-100% down to about 30% at the inlet of the PSM. The high detection efficiency of the A20 is maintained and composition of the aerosol particles stays constant through the transition from the ambient environment to the time when they enter the measurement setup.

The inlet consists of dilution unit and a core sampling probe. The dilution unit is using a sintered tube where pressurized dry air is mixed with the humid ambient air, maintaining a laminar flow. To minimize diffusion losses within the inlet, a core-sampling probe is attached to the inlet of the PSM downstream of the inlet dryer. The flow rates both for the dry pressurized air and the core-sampling probe can be varied, resulting in different final RH values which mainly depend on the dry pressurized air flow.

The inlet was characterized in the laboratory both for diffusion losses and for its performance with respect to reducing the RH of the carrier gas. The results from the diffusion loss measurements show that the cut-off diameter of the PSM is shifted from 1.1 nm to 1. 5 nm. The PSM together with the inlet were used during the GoAmazon 2014/5 campaign in Brasil. Ground based measurements at the T3 site, 60 km to the west of Manaus (3°12'47.82"S, 60°35'55.32"W).

We compared the A20, equipped with the novel inlet with a commercial ultrafine TSI CPC3776. (3°12'47.82"S, 60°35'55.32"W). Good agreement was achieved comparing the inlet+PSM+CPC system and a commercial ultrafine TSI CPC3776.

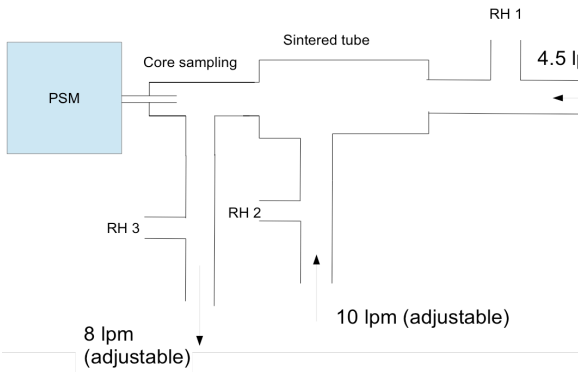

Figure 1: Design of the inlet for reducing the carrier gas RH.

This study was supported by Academy of Finland, Centre of Excellence program (project no. 272041 and 1118615).

Vanhanen J. et al., (2011). *Particle Size Magnifier for Nano-CN Detection*. Aerosol Sci. Tech.

Iida K. et al., (2009). *Effect of Working Fluid on Sub-2 nm Particle Detection with a Laminar Flow Ultrafine Condensation Particle Counter*, Aerosol Sci. Tech.

Beyond Counting– Applications of Condensation Systems to Particle Collection and Charging

S. V. Hering[1]
[1]Aerosol Dynamics Inc., 935 Grayson St, Berkeley, CA 94710, USA

Keywords: nanoparticle, condensation particle collector, electrical charging, particle imaging

Since the pioneering work of Aitken in the nineteenth century, condensational growth has been a key tool for aerosol scientists. Initially used to determine particle number concentrations, condensational particle counters continue to be a mainstay of aerosol research laboratories. Yet there are many additional types of aerosol measurement that are enabled through condensational growth as well.

As early as the 1970s, steam-injection methods were used to enlarge and capture submicrometer particles for on-line determination of chemical composition. In the 1990s condensational growth was applied to concentration systems for enriching the numbers of ultrafine particles in an air flow. It has been explored as a means to enhance the level of electrical charging. And it has been exploited to enable ultrafine particle imaging. This presentation will explore some of these applications beyond particle counting, namely collection, concentration, charging, and imaging. We focus on applications of a "moderated" approach for water-based condensation in a laminar flow that enables creation of water vapor supersaturation with relatively low water content and temperature in the output flow.

Moderated Water Condensation Growth Tube: Illustrated in Figure 1, the moderated water condensation method passes flow through a wet-walled tube, the middle portion of which is warmed. Within the warm section water vapor from the walls diffuses into the flow more quickly than it warms, creating a supersaturated flow. The cooler walls downstream remove water vapor and reduce the temperature, while maintaining the supersaturation (Hering et al., 2014) This three-stage, "moderated" approach activates particles at sub-10nm sizes without elevated temperature or water content in the output flow.

Collection: The moderated water condensation approach enables the capture of ultrafine particles as a dry, 1-mm diameter spot. Collection efficiencies are above 90% for particles larger than 8 nm. The concentrated collection interfaces readily with laboratory systems for automated sample extraction and analysis. The system has been implemented as a sequential sampler for time-resolved monitoring of inorganic ions and for polycyclic aromatic hydrocarbons, with comparable results to filter collection. The approach may also be used for the concentrated deposition of particles into liquid, capturing both soluble and insoluble fractions.

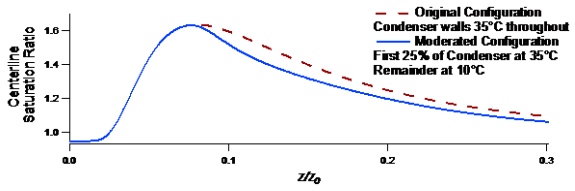

Figure 1. Saturation ratio along the flow centerline for wet-walled growth tubes operated with walls at 35°C throughout, or with walls starting at 35° and decreasing to 10°C. Entering flow is 5°C, 50%RH. z = axial distance; $z_o = Q/D$ (where Q=volumetric flow; D=water diffusivity).

Concentration: Using aerodynamic focusing as introduced by Fernandez de la Mora (1988), the droplets formed through condensational growth pass through a nozzle that focuses the droplets into the central 10% of the flow. The outer 90% of flow is removed through an annular slit in the wall of the nozzle, providing a 10:1 enrichment in particle concentration. Measured enrichments are 85-90% of the flow split for particles above 8 nm.

Charging: Many measurements of nanometer sized particles rely on size selection by electrical mobility, but charging efficiencies below 20 nm is poor, even with unipolar charging. Ion attachment is greatly increased by introducing ions along with the aerosol into a condensation growth tube. Multiple charging may be minimized through use of an ion scavenger immediately following the point of activetion, or by rapidly evaporating the droplets once formed. This approach has been combined with aerodynamic focusing to provide a 30-40 enrichment in the charging of particles at 10nm.

Imaging: Kulkarni and Wang (2006) developed a system for rapid measurements of particle size distributions through condensational growth and imaging of particles within a parallel plate mobility size separator. The original systems used an alcohol-laden sheath flow and cooled condenser to create this growth. This has now been accomplished using water condensation, wherein the water is introduced downstream of the mobility separation.

This work was supported by the U.S. Department of Energy grants DESC0004698, DESC0006312, and DESC0009644; and by the US National Institute of Environmental Health, grants ES014997, ES019081 and ES022523.

Fernandez de la Mora, J., Riesco-Chueca P. (1988) *Journal of Fluid Mechanics*, 195: 1-21.
Hering, S. V., Speilman, S. R., Lewis, G. L. (2014). *Aerosol Science and Technology* 48:401-408.
Kulkarni, P., and Wang, J. (2006) *Journal of Aerosol Science*, 37, 1326-1339.

Bimetallic platinum-palladium nanocatalysts produced by spark discharge

K. Hu, M.E.J. Stettler, S.A. Scott and A.M. Boies

Department of Engineering, University of Cambridge, Cambridge, CB2 1PZ, United Kingdom

Keywords: spark discharges, bimetallic particles, photoionisation, catalysts.

Emissions from diesel engines are a major contributor to reduced air quality and resultant human health impacts. Exhaust after-treatment devices are routinely used to reduce emissions of harmful pollutants. Diesel oxidation catalysts, mainly consisting of nanoparticles of platinum and palladium, oxidise harmful pollutants such as carbon monoxide and unburnt hydrocarbons and convert them to carbon dioxide and water. Commercial catalysts are typically produced using wet-chemistry methods, which are batch processes suffering from poor control over the ratio of platinum and palladium in the catalyst nanoparticles, and from impurities introduced by solvents and precursors.

This study presents a gas phase approach, which utilises an electrical spark discharge to generate catalyst nanoparticles from appropriate electrode metals. A high voltage current source was used to generate a potential difference across a gap between platinum and palladium electrodes in excess of the breakdown voltage, which is a function of the inter-electrode distance and carrier gas. The resultant discharge occurs on the microsecond-scale and a >200 A current pulse is accompanied by an expanding shock wave. The pulses of electrical discharge create a ~20,000 K hot spot on the tip of electrodes (Reinmann & Akram, 1997), which causes material to sublimate from the electrodes to the surrounding inert gas. The large temperature gradient results in nucleation of nanoparticles. Contaminants are minimised, depending only on the purity of the electrodes and carrier gas.

To supress agglomeration processes, photoelectric charging of the newly-formed nanoparticles was achieved by illuminating the generated catalyst nanoparticles with ultraviolet (UV) radiation. The energetic photons liberated surface electrons from the nanoparticles, resulting in a unipolar positive charge state. Excess free electrons were removed by positively biased precipitator to avoid charge recombination.

A schematic of the experimental setup is shown in Figure 1. A Scanning Mobility Particle Sizer (SMPS) was employed to measure particle size distribution at the exit of the spark generator. In situ and online characterisation of the generated catalyst nanoparticle activity was carried out in a temperature-controlled chamber in which the nanoparticles were mixed with hydrocarbon gases to directly measure oxidation activity. Furthermore, particles were analysed by transmission electron microscopy (TEM) and x-ray diffraction (XRD) to study their morphology.

Figure 2 shows that the geometric mean diameter (GMD) and geometric standard deviation (GSD) of the spark-generated nanoparticles are dependent on the gap distance between the electrodes. A larger gap distance, with constant current and hence the discharge frequency, leads to a smaller GMD and GSD. We will show the effect of other experimental parameters on the particle size distribution, catalytic activity and morphology.

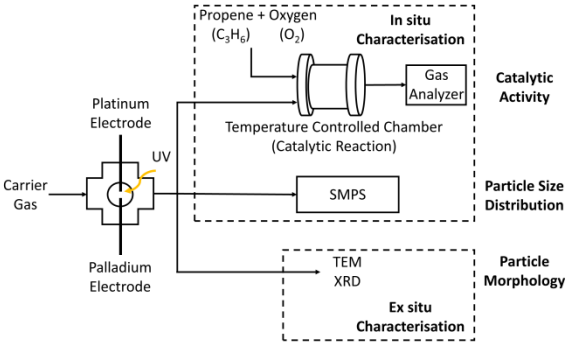

Figure 1. Schematic of the in situ and ex situ characterisations of the spark-generated catalysts.

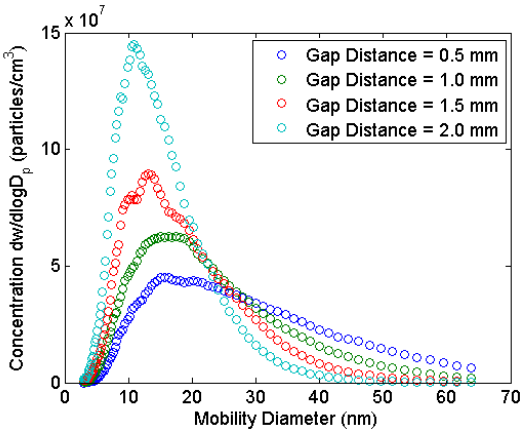

Figure 2. Particle size distribution measured by SMPS using a constant current output.

This work was supported by Johnson Matthey and UK Engineering and Physical Science Research Council.

Reinmann, R., & Akram, M. (1997). *J. Phys. D Appl. Phys.*, 30, 1125-1134.

Bipolar Charge Analyzer (BOLAR): A new device for bipolar charge measurements

[*]J. Yli-Ojanperä[1], A. Ukkonen[2], A. Järvinen[1], S. Layzell[3], V. Niemelä[2] and J. Keskinen[1]

[1] Tampere University of Technology, Department of Physics, P.O.Box 692, FIN-33101 Tampere, Finland
[2] Dekati Ltd., Tykkitie 1, FIN-36240 Kangasala, Finland
[3] GlaxoSmithKline, 980 Great West Road, Brentford, Middlesex TW8 9GS, United Kingdom

Keywords: Bipolar, Charge measurement, Charge-to-mass ratio, Pharmaceutical, Inhaler, BOLAR

Electrical charging of aerosol particles to a known charge size distribution, using unipolar or bipolar diffusion chargers, is utilized in many applications in aerosol technology. Examples of aerosol instruments that utilize the electrical charging include the Differential Mobility Analyzers (DMA; Knutson and Whitby, 1975) and the Electrical Low-Pressure Impactor (ELPI; Keskinen et al., 1992). The known charge size distribution allows the determination of other properties of the inlet aerosol, such as the number size distribution. Within the submicron particle range, operating the DMA with and without the charger also allows the measurement of the inherent charge size distribution of the aerosol (e.g. Laakso et al., 2007).

In some applications, such as in pulmonary drug delivery using various types of inhalers, the inherent charge size distribution of the aerosol and charge-to-mass ratios of the particles, are of great importance. The reason for this is that the charge of the individual particles has been shown to greatly influence on where and how efficiently the inhalable medicine gets collected on a human respiratory tract (Balachandran et al., 1997; Kulon and Balachandran, 2001). The dry powder inhalers and nebulizers tend to produce bipolarly charged aerosols that are mainly larger than 1 µm in aerodynamic size (Balachandran et al., 1997). In this size range, no commercially available instrument capable of measuring bipolar charge size distribution and charge-to-mass ratios of particles from the whole aerosol sample coming out from an inhaler has been available.

In our recent study we introduced the first commercially available instrument, which is specifically designed to measure the bipolar charge size distributions and charge-to-mass ratios from aerosol generators that are used in pulmonary drug delivery (Yli-Ojanperä et al., 2014). The device is called the Bipolar Charge Analyzer (BOLAR) and it is manufactured by Dekati Ltd. (Finland). In this work, a thorough description of the instrument is presented. We also demonstrate how this new instrument is applied to testing of the performance of various inhalers and present the first bipolar, size classified Dry Powder Inhaler (DPI) test results. The results include charge-to-mass ratios of the particles as a function of the particle size which are compared to results of other instruments in terms of net charge of the particles.

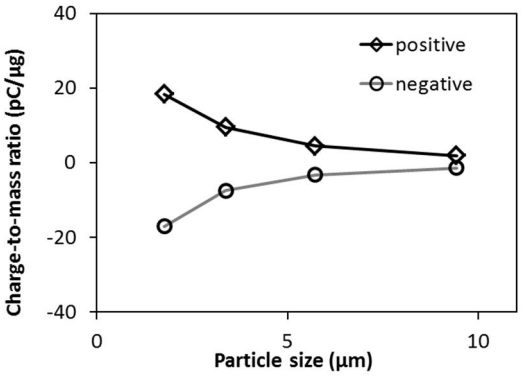

Figure 1. Charge-to-mass ratios as a function of the aerodynamic particle size for the positively and negatively charged particles.

This study was funded by Tekes–the Finnish Funding Agency for Technology and Innovation as well as by the Cluster for Energy and Environment (CLEEN, MMEA).

Yli-Ojanperä, J., Ukkonen, A., Järvinen, A., Layzell, S., Niemelä, V. and Keskinen, J. (2014) Bipolar Charge Analyzer (BOLAR): A new aerosol instrument for bipolar charge measurements. *J. Aerosol Sci* **77**, pp. 16–30.

Balachandran, W., Machowski, W., Gaura, E., Hudson, C. (1997) Control of drug aerosol in human airways using electrostatic forces, J. Electrostat. **40-41**, 579-584.

Keskinen, J., Pietarinen, K. and Lehtimäki, M. (1992) Electrical Low Pressure Impactor. *J. Aerosol Sci.* **23**, 353-360.

Kulon, J. and Balachandran, W. (2001) The measurement of bipolar charge on aerosols. *Journal of Electrostatics*, **51-52**, 552-557.

Knutson, E. O. and Whitby, K. T. (1975) Aerosol classification by electric mobility: apparatus, theory, and applications. *J. Aerosol Sci.*, **6**, 443–451.

Laakso, L., Gagné, S., Petäjä, T., Hirsikko, A., Aalto, P. P., Kulmala, M. and Kerminen V.-M. (2007) Detecting charging state of ultra-fine particles: instrumental development and ambient measurements. *Atmos. Chem. Phys.*, **7**, 1333-1345.

Calculation of deposition on fibrous filters as a function of time

S. J. Dunnett[1] and C. F. Clement[2]

[1]Department of Aeronautical and Automotive Engineering, Loughborough University, Loughborough, Leics. LE11 3TU, U.K.
[2]15 Witan Way, Wantage, Oxon, OX12 9EU, U.K.
Keywords: fibrous filter, filtration, numerical simulation, particle deposition
Presenting author email: s.j.dunnett@lboro.ac.uk

Introduction

Fibrous filters are routinely used to remove particles from the air. The filters consist of numerous fibres arranged in such a way that they are mostly perpendicular to the air flow through it. The packing fraction of such filters is generally small enabling the modelling of filter performance to be undertaken using single fibre theory. When the filters are in use particles collect on the fibres and are removed from the air. The deposit collected on the fibres affects the air flow through the filter and hence the subsequent deposit of particles. To date we have a fairly good understanding of the performance of fibrous filters at the start of their lives when no deposit is collected. The problem of filter efficiency as a deposit builds up has been addressed by Kasper et al (2009) who found empirical fits to experimental data that they have obtained. In the work presented here we will describe a method of calculating the collection efficiency and mass build up on a fibre for the case when interception or impaction are the major deposition mechanisms. The method is based on a previously developed numerical model, Dunnett and Clement (2012) and an efficient mathematical technique for determining critical trajectories Clement and Dunnett (2014).

Numerical model and procedure

The numerical model developed by Dunnett and Clement (2012) applies to deposition on a fibre, radius R_f, in a cell of radius y_c which is related to the packing fraction of the filter, c by the equation $c=R_f^2/y_c^2$. In our two dimensional model the dimension of the cell corresponding to length along the fibre is irrelevant to the deposition process, and the particle mass flux, F, mass in the deposit, M and deposit volume, V, are all in units per unit length of the fibre. The flux, F_c, entering a single cell is given by

$$F_c=2y_c n m_p v \qquad (1)$$

where n is the concentration of particles of mass m_p and velocity v. The mass deposition rate on a fibre at time t is

$$\frac{dM}{dt} = F_c E(t) \qquad (2)$$

where E(t) is the deposition efficiency which is the fraction of particles entering the cell which are deposited. This corresponds to an increase in volume of

$$\frac{dV}{dt} = \frac{F_c E(t)}{\rho_p (1-P)} \qquad (3)$$

where ρ_p is the particle density and P is the deposit porosity. The deposition efficiency depends on the geometry of the existing deposit and it is assumed in our model that E(t) remains constant, $E_L(t)$, during the deposition of a layer L of depth d at the front of the fibre. Therefore, from equation (3), the total volume deposited for a layer is given by

$$V_L = \frac{F_c E_L(t) t_L}{\rho_P (1-P)} \qquad (4)$$

where t_L is the time taken to deposit the layer L of width d.

To determine $E_L(t)$ we find the critical trajectory, using the techniques given in Clement and Dunnett(2014), which enters the cell at a height y_L so that $E_L=y_L/y_c$.

We assume that the incident fluxes forming the new deposit in figure 1 remain constant during the layer deposition. This enables us to directly determine t_L for deposition width d at the front, and V_L from integration of the fluxes over the new deposit.

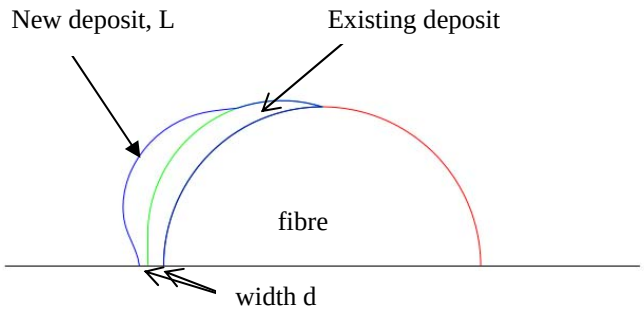

Figure 1. Deposit geometry for a new layer on an existing deposit.

Hence it is possible to investigate the volume and mass deposited as a function of time and results will be presented.

References

Clement, C.F. and Dunnett, S.J. (2014) J. Aerosol Sci., 69, 98-112.

Dunnett, S.J. and Clement, C.F. (2012) J. Aerosol Sci., 55, 85-99.

Kasper, G., Schmollmeier, S., Meyer, J. and Hoferer, J. (2009) J. Aerosol Sci., 40, 993-1009.

Calibrating an instrument measuring 1-3nm aerosol particle number size distribution

J. Vanhanen[1], J. Kangasluoma[2], M. Attoui[3] and M. Väkevä[1]

[1]Airmodus Ltd., Pietari Kalmin katu 1 F 1, 00560, Helsinki, Finland
[2]Department of Physics, University of Helsinki, Gustaf Hällströmin katu 2 A, 00560, Helsinki, Finland
[3]University Paris Est Creteil, University Paris-Diderot, LISA, UMR CNRS, Orléans, France

Keywords: cluster, CPC, calibration.

Recent development of aerosol particle counters has allowed measurement of sub 3nm particles number and size all the way down to 1nm in diameter. Airmodus A11 nano Condensation Nucleus Counter system (nCNC) including Particle Size Magnifier (PSM) (Vanhanen *et al.* 2011) and Condensation Particle Counter (CPC) allow measurement of size distribution of particles having mobility diameter between 1-3nm. The size distribution is achieved by scanning mixing ratio of PSM internal flows. This recent development has introduced new challenges in calibration of the particle counters. In the smallest size range the production and size selection of the calibration particle gets much more difficult. Also it has been shown that the particle counters are sensitive to the chemical composition of the particle (Kangasluoma *et al.* 2013).

In calibration point of view it is necessary to produce highly monodisperse aerosol with different sizes between 1-3nm. We calibrated Airmodus A11 nano Condensation Nucleus Counter system by using ammonium sulfate particles produced with evaporation – condensation – method and tungsten oxide particles by using hot wire generator (Peineke *et al.* 2006). The particles were size selected by using Herrman - type high flow differential mobility analyser (DMA) (Herrmann *et al.* 2000) with resolving power of about 20.

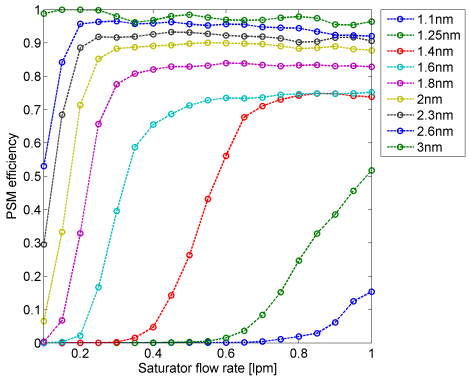

Figure 1. PSM efficiency (scaled to unity) as a function of saturator flow rate for ammoniun sulfate particles.

The inversion used to achieve the size distribution uses the cut-off diameters that can be calculated from the calibrations shown in the figure 1 (Lehtipalo *et al.* 2014). For each individual s-curve the point where 50% of the highest detection efficiency for that certain particle size was determined. Figure 2 shows 50% cut-off diameters as a function of the saturator flow rate for ammonium sulfate and tungsten oxide particles. Even though it is known that the PSM is sensitive to the chemical composition of the particle, the 50% cut-off diameters seem to agree supprisingly well. This indicates that the PSM can be calibrated with tungsten oxide particles even though the inversion is used for salt like particles. Though it has to be noted that the calibrations were conducted in 0% relative humidity and it has been shown that water vapor affects the activation behaviour of the PSM (Kangasluoma *et al.* 2013). This effect is also assumed to be dependent on the chemical composition of the particle.

We also tested the inversion based on the calibrations with monodisperse particles in laboratory environment. Also some stability tests were conducted for the full nCNC system.

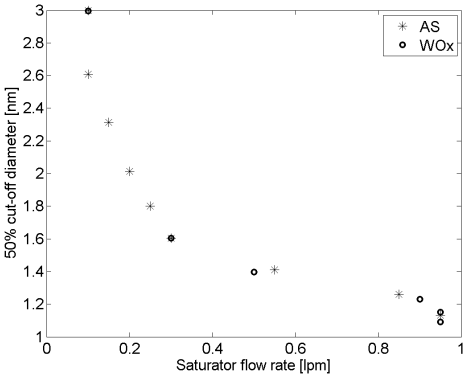

Figure 2. 50% cut-off diameter as a function of saturator flow rate of the PSM (AS=ammonium sulfate, WOx=tungsten oxide)

Vanhanen, J. *et al.* (2011). *Aerosol Science and Technology*, 45:4, 533-542.
Kangasluoma, J. *et al.* (2013). *Aerosol Science and Technology*, 47:5, 556-563.
Peineke, C. *et al.*. (2006). *J. Aerosol Science*, 37:1651.
Herrman, W. *et al.*. (2000). Abstract AAAR Conference, 15B5.
Lehtipalo, K. *et al.*. (2014). *Boreal Environment Research*, 19 (suppl. B), 215-236.

CARS microscopy as a tool to characterize bioaerosols

V. Ulevicius, G. Mordas and A. Dementjev

STI Center for Physical Sciences and Technology, Savanorių ave. 231, LT-02300 Vilnius, Lithuania

Keywords: bioaerosol, particle characterisation, CARS microscopy, imaging.

There is a strong interest in the development of rapid bioaerosol characterization techniques. Conventional methods are time consuming, use expensive instrumentation, apply chemical markers and destroy the sample during measurement. In this work, we present an application of Coherent Anti-Stokes Raman Scattering microscopy (CARS) technique for rapid analytical characterization and imaging of the bioaerosol.

The CARS (Zumbusch *et al.*, 1999) is a modern informative technique. Chemical selectivity, high spatial resolution and other advantages of CARS microscopy make this technology very attractive as a characterization tool capable to separate certain materials from surroundings, identify their geometrical shapes and uniformity. We apply the CARS microscopy as a chemical imaging tool of certain bio-chemical compounds such as lipids in biological cells of airborne particles.

The designed CARS microscope (Dementjev *et al.*, 2010) is based on a six picosecond frequency doubled Nd:YVO4 pump laser with the pulse repetition rate of 1 MHz equipped with a travelling wave optical parametric generator (OPG). For CARS implementation an OPG radiation was coupled with a fundamental laser radiation (1064 nm) used as Pump and Stokes excitation beams, respectively. Such a mixing provides probing within the 700 – 4500 cm^{-1} range of vibration frequencies. Both Stokes and pump beams were collinearly combined and directed to an inverted microscope (Olympus IX71). Measurements of the CARS spectra were performed in high-wavenumber region of Raman spectrum by tuning the OPG frequency. The spectral resolution of the CARS setup was ~8 cm^{-1}. The spectra were recorded with a typical detection rate of 5 cm^{-1} per second, thus the spectrum in the range from 2500 to 3500 cm^{-1} was recorded during about 2 minutes. A piezo scanning system (Physik Instrumente GmbH & Co) was used for scanning the sample. The 500×500 pixel images were obtained with 2 ms pixel dwell time. Excitation pulse energies from 1 to 10 nJ at the sample for both pump and Stokes beams were used. Sample scanning, data processing and the laser wavelength tuning were controlled with a computer.

Using that CARS microscope, we placed a bioaerosol sample of pollen on the microscope optical glass plate. Through the 100×100 micrometer size optical window, it was observed twelve objects. We selected an interesting object manually and scanned the CARS spectra of the object. It was determined two high picks at 2850 cm^{-1} and at 3250 cm^{-1} (Fig. 1). First pick responses C-H resonant band and it characterizes the lipids in biological cell. The second pick belongs to the N-H vibrations and can be attributed to the amino acids. In fingerprint region the spectra of such object has no distinct band and an image repeat the information given in the highwavenumber region. Going to get an image with smallest area (10x10µm), the CARS setup was tuned to the maximum of C-H resonant band at 2850 cm^{-1}, where the amplitude of CARS signal was above 500 counts. The registered image is illustrated in Fig. 2. The same measurements were done for other detected objects. The results were similar. Thus, our study demonstrates a potential of the CARS technique as a tool to characterize and imaging individual bioaerosol objects.

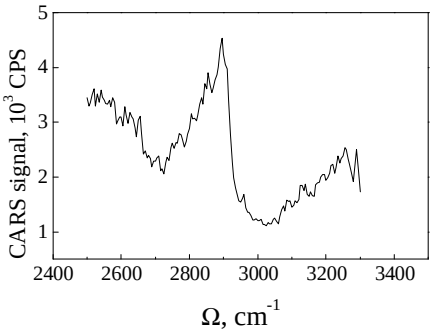

Figure 1. The CARS spectra in highwavenumber region of Raman spectrum.

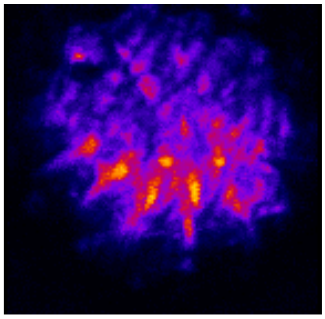

Figure 2. The CARS imaging of pollen.

Dementjev, A., Gulbinas, V., Serbenta, A., Kaucikas, M., & Niaura, G. (2010). *Journal of Modern Optics*, 57, 503-509.

Zumbusch, A., Holtom, G. R., & Xie, X. S. (1999). *Physical Review Letters*, 82, 4142-4145.

Cessna 172 light aircrafts as a platform for measuring aerosols in the lower troposphere

R. Väänänen[1], R. Krejci[2,1], H. E. Manninen[1], J. Kangasluoma[1], T. Nieminen[1], S. Mazon[1], J. Lampilahti[1], S. Schobesberger[1], A. Manninen[1], L. Ahonen[1], L. Zhou[1], T. Yli-Juuti[1], T. Pohja[1], P. P. Aalto[1], T. Petäjä[1], M. Kulmala[1]

[1]Department of Physics, University of Helsinki, Helsinki, Finland
[2]Department of Applied Environmental Science (ITM), Stockholm University, Stockholm, Sweden

Keywords: aircraft-borne measurements, planetary boundary layer, lower troposphere, number size distribution

To understand the role and processes of aerosol particles in the atmosphere, on-ground and airborne experiments are both needed. To extend the measurements into the boundary layer column and lower troposphere, University of Helsinki has performed aircraft-borne measurement campaigns using a Cessna 172 light aircraft since 2009 (Schobesberger *et al*, 2013).

Typically, the research flights have been connected to the measurement campaigns performed at SMEAR II (Hari and Kulmala, 2005) Hyytiälä field station. The aims of the flights have been to quantify the horizontal and vertical aerosol distribution up to the altitude of 3.5 km, and to study the new particle formation in the lower troposphere. In Spring 2013 the flights were a part of Pegasos Northern Mission campaign together with Zeppelin NT airship and intensive on-ground measurements. Then 45 Cessna flights with 118 flight hours were performed above the surroundings of Smear II station or Jämijärvi airfield. During year 2014 the measurements flights were a part of BAECC campaign, which was a multiplatform campaign to measure biogenic aerosols and gases emitted from forests to determine their effects on clouds, precipitation, and climate. In total 143 flight hours with 50 flights were performed in three periods in March-April, May-June, and August-September 2014.

The particle number size distribution between diameters of 2-350 nm has been measured. An aerosol and gas inlet was mounted under the right wing and the sample air was transported to the cabin where the aerosol and gas instruments were placed. During 2013 the aerosol instruments included a TSI 3776 condensation particle counter (CPC) with a cut-off size of 3 nm, a Scanning Mobility Particle Sizer (SMPS), with a size range of 10-350 nm, and an Airmodus Particle Size Magnifier (PSM) A09 together with a TSI 3772 CPC. Other instruments on-board included a Li-Cor Li-840 H2O/CO2-analyzer, a temperature sensor, a relative humidity sensor, and a GPS receiver. The power supply for the instruments were accumulators.

In May 2014 the PSM A09 was replaced by a new Airmodus PSM A10. During the campaigns, the measurement parameters of the PSMs have been optimized to meet the varying airborne conditions.

Figure 1. Two Cessna 172 aircrafts used for research flights in September 2014

In September 2014 we installed a Neutral cluster and Air Ion Spectrometer (NAIS) into another Cessna 172 plane. A 2-week measurement campaign was performed with two research aircraft flying in a formation. A new short sample air inlet was tested with the NAIS.

Over 160 measurement flight hours only during the last two years enabled us to construct the statistical vertical profile of the aerosol size distribution and of the total particle concentration, and compare them to the on-ground measurements. Also, the new particle formation has been studied. Additionally, the data set offers new views to the spatial variability of the boundary layer aerosols on scales from tens of meters to tens of kilometers. The technical details of the instrumentation as well as scientific results will be presented.

This study was supported by Academy of Finland Centre of Excellence programs (project no. 272041 and 1118615), and European Commission under the Framework Programme 7 (FP7-ENV-2010-265148).

Schobesberger, S., et al. (2013): *Boreal Env. Res.* 18: 145–163.
Hari, P. & Kulmala, M. (2005): *Boreal Env. Res.* 10: 315–322.

Characteristics and formation of natural gas engine exhaust nanoparticles

J. Alanen[1], E. Saukko[1], K. Lehtoranta[2], H. Timonen[3], J. Keskinen[1] and T. Rönkkö[1]

[1] Aerosol Physics Laboratory, Tampere University of Technology, P.O. Box 599, FI-33720, Tampere, Finland
[2] VTT Technical Research Centre of Finland, P.O.Box 1000, FI-02044 VTT
[3] Air Quality Research, Finnish Meteorological Institute, P.O. Box 503, FI-00101 Helsinki, Finland

Keywords: natural gas engine, particle formation.

Natural gas is an attracting alternative for diesel in piston engines due to smaller carbon dioxide and particulate mass emissions. However, also natural gas engines need techniques that reduce their emissions. Particle mass emissions of natural gas engines are small in comparison with diesel engines (Jayaratne *et al.*, 2009). Yet, particle number emissions can be of the same order of magnitude as those of diesel engines without particulate filters (Holmén *et al.*, 2002). Knowing the generation process and origin of the emissions helps in reducing them.

Measurements (Alanen *et al*. 2014) were steady-state tests performed at an engine dynamometer with a passenger car petrol engine. Test engine was retrofitted to run with natural gas without exhaust after-treatment and with a selective catalytic reactor (SCR). The engine was not equipped with a turbocharger.

Particle measurements were made using EEPS, Nano-SMPS and PSM with CPC. A thermodenuder (TD, maximum temperature 265 °C) was used to study particle volatility characteristics and Nano-SMPS without the neutralizer was used to study the electric charge state of particles. Particle emission sampling system consisted of a porous tube diluter, a residence time tunnel and an ejector diluter (Dekati Ltd). Residence time in the dilution system was 3 s. The dilution ratio over the porous tube diluter (PDR) during the measurements was six but also larger dilutions ratios were tested.

Results indicate that natural gas engine exhaust particles are initially formed in engine cylinders and they increase in size during sample dilution and cooling process. The growth occurs by condensation of gaseous compounds in exhaust gas if the conditions during primary dilution process are favourable.

A small fraction of the particles carry an electric charge. Particles carrying electric charge have been charged most probably in the high temperatures of the engine cylinders. Thermodenuder volatility measurements suggest that the particles have a non-volatile core but a notable part of their volume consists of volatile matter. SCR influences particles by reducing their number concentration. This can result from oxidative reactions of hydrocarbons taking place inside the SCR or from diffusion of particles on its walls.

Particles emitted from the natural gas engine were extremely small with the particle size distribution peak at about 4 nm. Number of particles with a diameter larger than 50 nm was very low (Figure 1).

This was the first time the electrical charge of the particle emission of a natural gas engine power plant was investigated or particles under 4 nm in the particle emission of a natural gas engine were measured. Also the observation of particle size reduction at 265 °C rather than complete evaporation was made for the first time in this work.

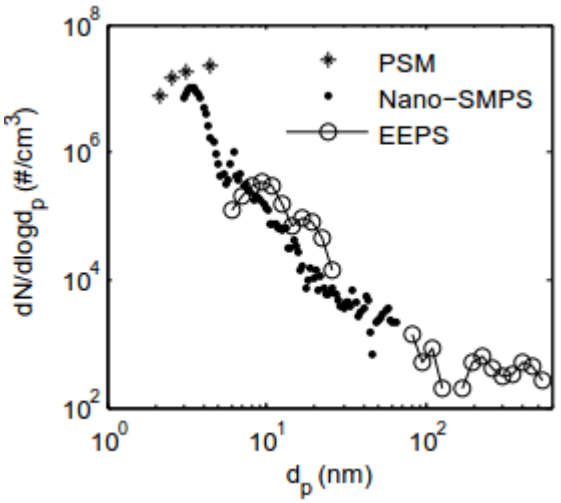

Figure 1. Natural gas engine exhaust nanoparticle size distribution measured by PSM, Nano-SMPS and EEPS

This work was supported by the The Finnish Funding Agency for Technology and Innovation (TEKES), Neste Oil Corporation, Wärtsilä Finland Oy, Dinex Ecocat Oy, AGCO Power, Dekati Ltd, Viking Line, Suomi Analytics Oy and Gasum Gas Fund.

Alanen, J. *et al.* Formation and characteristics of natural gas engine exhaust nanoparticles. Manuscript in prep.

Holmén, B. A, & Ayala, A. (2002). *Environ. Sci. Technol.*, 36, 5041–5050

Jayaratne, E. R.., Ristovski, Z. D. Meyer, N. and Morawska, L. (2009). *Science of the Total Environment*, 407, 2845–2852.

Characteristics of emission and size fractions of fine particles (PM_{10}, $PM_{2.5}$) from stationary sources using cyclone (US EPA Method 201A) and cascade impactors

S.H. Han[1], H.R. Kim[1], K.W. Jang[2], D.I. Kang[2], Y.W. Jung[1] and K.J. Jeon[1]
[1]Department of Environmental Engineering, Inha University, Inha-ro 100, Nam-Gu, 402-751, Incheon, Korea
[2]Air Pollution Engineering Division, Climate and Air Quality Research Department, National Institute of Environmental Research, Hwangyong-ro 42, Seo-Gu, 404-708, Incheon, Korea

Keywords: $PM_{2.5}$, stack PM emission, size faction, EPA Method 201A, cascade impactor

In Korea, new national air quality standard for $PM_{2.5}$ was established and implemented in 2015 due to adverse health effects caused by fine particles. To satisfy new ambient standard and control emission sources, it is very important to identify stationary emissions. For this, Korea standard method for the measurements of the filterable fine particle (PM_{10} and $PM_{2.5}$) in stack flue gas was established based on US EPA Method 201A. But at present, the information on emission characteristics of fine particles from stack is lack and the improvement of stack sampling method is also necessary.

In-stack sampling methods (US EPA 201A, ISO 23210, and so forth) with cyclone, cascade impactor, and virtual impactor have been used in order to measure filterable PM_{10}/$PM_{2.5}$ from stack, and to measure condensable PM or total primary PM, US EPA Method 202 or dilution sampling methods have been applied (Lee, 2010; Ehrlich et al., 2007; England et al., 2007; US EPA 1998). These methods have the merits and demerits that can be applied in accordance with conditions of emission facilities.

The ultimate objective of our present study is to identify the emission characteristics (emission concentration, emission factor, size fractions) and chemical source profile of PM_{10} and $PM_{2.5}$ in flue gases from large stationary sources and provides key to improve the standard methods that suits to Korea's emission facilities by comparing different sampling methods.

The concentrations of total PM(TPM), PM_{10}, and $PM_{2.5}$ were measured from stack through control devices of carefully selected stationary PM sources including coal-fired power plants (A), municipal solid waste incinerators (B), cement kiln (C), small boiler (D), and heating furnace of petroleum refining (E). In-stack sampling method of US EPA 201A with cyclone was mainly employed for determining filterable PM concentrations. For comparison of the size fractions, in-stack cascade impactors (Sierra Series 220 and Dekati 2-stage impactor according to ISO 23210) was used.

The results of these measurements show that the concentrations and size fractions of stack PM emissions are different according to the types of facility, fuel, and control device used. Most of measured emission factors are found to be lower than those of US EPA AP-42 and Korea emission inventory (CAPSS). Further the fine fractions are a little higher than previous studies. Fig. 1 shows the comparison of $PM_{2.5}$/PM_{10} ratio by facilities and sampling devices. Overall results was found to be relatively similar, but multi-cascade impactor show the tendency of relatively higher $PM_{2.5}$/PM_{10} ratio than those of EPA Method 201A. On the other hand, results of ISO 23210 (Dekati impactor) are the different tendency by facilities. Detailed results will be presented.

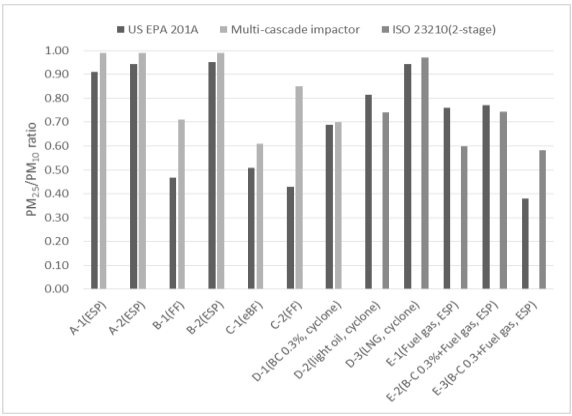

Figure 1. The comparison of $PM_{2.5}$/PM_{10} ratio by facilities and sampling devices.

This work was supported by the Korean National Institute of Environmental Research.

Ehrlich, C., Noll, G., Kalkoff, W. D., Baumbach, G., & Dreiseidler, A. (2007). *Atmospheric Environment*, 41, 6236-6254.

England, G. C., Watson, J. G., Chow, J. C., Zielinska, B., Chang, M., Loos, K. R., & Hidy, G. M. (2007). *J. of the Air & Waste Management Association*, 57, 65-78.

Lee, S. W. (2010). *Fuel*, 89, 874-882.

Woodard, K. (1998). *Stationary Source Control Techniques Document for Fine Particulate Matter*, US Environmental Protection Agency.

.

Characterization of an Open-Pored Nickel Foam with Respect to Aerosol Filtration Efficiency

A. Hellmann, M. Pitz, K. Schmidt, F. Haller, S. Ripperger, S. Antonyuk

Chair of Particle Process Engineering, University of Kaiserslautern, 67663, Kaiserslautern, Germany

Keywords: filtration, simulation, open-pored foam, particle deposition.

The deposition of micron and submicron particles in metallic, ceramic or synthetic open-pored foams has been intensively studied for the past years. Thereby, the techniques of measurement as well as simulation have been continuously enhanced. Open-pored foams are suitable for the filtration of particles from aerosols among others.

The filter efficiency for submicron particles can be measured by Differential Electrical Mobility Analyser Systems (DEMAS) or Optical Particle Counters (OPC). Also the determination of the aerosol filtration efficiency is additionally available for approximative formulas from the literature. A third method is direct numerical simulation by means of a tomography or generated model including computational fluid dynamics (CFD) and Lagrangian particle tracking.

These methods of determining the particle deposition rate on foams are evaluated and compared. An example of a real structure and a tomography is shown in figure 1.

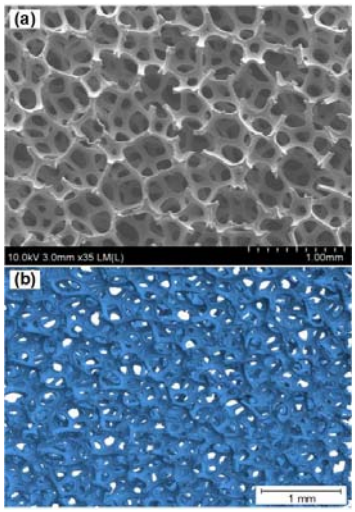

Figure 1. SEM picture of a real structure (a) and a tomography (b) of the observed open-pored foam.

In this work, the characterization of exemplary open-pored nickel foam is conducted by all 3 methods and the results for measurement and 3D simulation agree very well. In particular also statistics for varying tomography cut-outs are evaluated by Hellmann et al. (2015).

The characteristic dimensions of this foam are given in Table 1.

Table 1. Material properties of the utilized nickel foam.

Foam Type	Cell Diameter µm	Link Diameter µm
Nickel foam	450 ± 45	56.5 ± 4.4

Additionally, empirical approaches and 3D simulations of pressure drop and filter efficiency of an open-pored nickel foam are compared with experimental results. By adaption of the empirical formulas of Clark et al. (2009), Vincent et al. (1993) and Wake and Brown (1991), the filtration efficiency and the pressure drop of the nickel foam can be predicted with enhanced precision.

This work was supported by the Nano Structuring Center at the University of Kaiserslautern (NSC), the Institute for Occupational Safety and Health of the German Social Accident Insurance (IFA) and the Regionales Hochschulrechenzentrum Kaiserslautern (RHRK).

Clark, P., Koehler, K. A., Volckens, J. (2009), *An Improved model for particle deposition in porous foams*, Journal of Aerosol Science 40(7):563–572

Hellmann, A., Pitz, M., Schmidt, K., Haller, F., Ripperger, S. (2015). *Characterization of an Open-Pored Nickel Foam with Respect to Aerosol Filtration Efficiency by Means of Measurement and Simulation*, Aerosol Science and Technology 49(1): 16-23

Vincent, J. H., Aitken R. J., Mark D. (1993), *Porous plastic foam filtration media: penetration characteristics and applications in particle size-selective sampling*. Journal of Aerosol Science, 24: 929 – 44

Vincent, J.H.; Aitken, R.J., Mark, D. (1992), *Further studies of porous plastic foam filtration media*, Journal of Aerosol Science 23(1):627-630

Wake, D. and Brown, R. C. (1991), *Filtration of Monodisperse Aerosols and Polydisperse Dusts by Porous Foam Filters*. Journal of Aersosol Science, 22 (6):693-706

Characterization of nanoparticles at different workplaces

M. Miettinen, J. Leskinen, T. Torvela, A. Lähde, J. Tissari and J. Jokiniemi

Department of Environmental Science, University of Eastern Finland, P.O. Box 1627, 70211, Kuopio, Finland

Keywords: workplace aerosol, on-line characterization, nanoparticles, number concentration

INTRODUCTION

Nanoparticles form a special group among the particulate impurities in the workplace air. Due to, e.g., small size and large surface area, nanoparticles may have different health effects compared with larger particulates. However, the characterization of the nanosize fraction of the workplace aerosol is rarely conducted.

European Commission recommendation (COM 2011 696) does not differentiate manufactured and incidental nanomaterials. Incidental nanoparticles are typically formed during processes in which materials burn and transfer to the gas phase, such as in diesel engines, and welding of metals or plastic. On the other hand, many workers, such as bakers and joiners are exposed to organic nanoparticles.

Here, nanoparticles were characterized at different workplaces, i.e., bakery, carpentry shop and welding workshop. Number concentration, number size distribution and lung-deposited surface area of the particles were measured on-line and electron microscopy samples were collected to study the composition and morphology of the nanoparticles.

METHODS

Number concentration and number size distribution were measured using condensation particle counters (TSI 3007, 3775, 3776), Scanning mobility particle sizer (SMPS, TSI) and Fast mobility particle sizer (FMPS, TSI). Lung-deposited surface area was measured using Nanoparticle surface area monitor (NSAM, TSI).

Electron microscopy samples were collected on holey carbon grids and studied with scanning electron microscope (SEM, Zeiss Sigma HD/VP) equipped with two EDS detectors, and transmission electron microscope (TEM, JEOL JEM-2100F).

RESULTS AND CONCLUSIONS

Results verified that number concentrations of nanoparticles in the work-place air were high although mass concentrations were relatively low.

Nanosize fraction may consist of different particles. For example, in the bakery the number size distribution varied during the working hours (Fig. 1a) and there exist at least three types of nanoparticles in the workplace air: flour particles (Fig. 1b), agglomerates and inorganic particles, derived typically from combustion (Fig. 1 c).

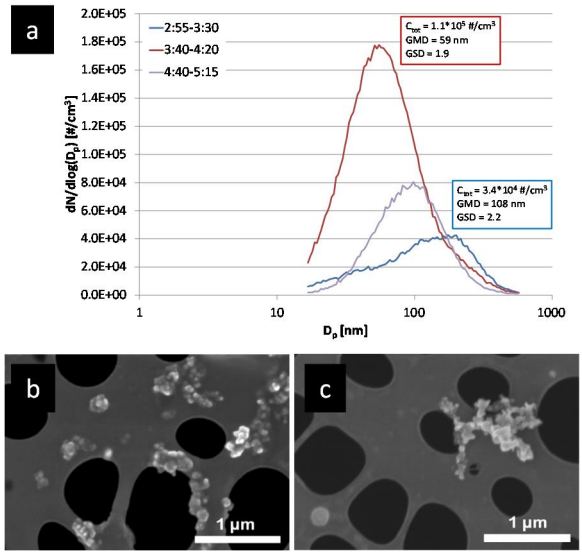

Figure 1. Averaged particle number size distributions in the bakery during working hours (a). SEM images of flour particles (b), agglomerates and inorganic particles typical for combustion processes (c).

Today, threshold limit values are not set either to manufactured or incidental nanoparticle concentration in the workplace air. Obviously, a commonly used mass concentration (mg/m^3) is not that suitable unit for a possible threshold limit.

Personal exposure levels (number, surface-area) to incidental nanoparticles, together with information of composition and morphology of these particles should be measured from different workplace aerosols for improved assessment of work related health risks.

ACKNOWLEDGEMENTS

This work was supported by The Finnish Work Environment Fund (grant 114255). This work made use of University of Eastern Finland SIB Labs facilities.

REFERENCES

COM (2011) 696. Commission recommendation on the definition of nanomaterial. *Official Journal of the European Union 20.10.2011 L 275/38-40.*

Characterization of trivalent doped zinc oxide nanoparticles synthesized via flame spray pyrolysis

M. Stanzel[1], Andreas Kunzmann[2], Rubén D. Costa[2], D.M. Guldi[2,3] and W. Peukert[1,3]

[1]Institute of Particle Technology, Friedrich-Alexander-University Erlangen-Nuremberg, Cauerstr. 4, 91058 Erlangen, Germany
[2]Department of Chemistry and Pharmacy, Friedrich-Alexander-University Erlangen-Nuremberg, Egerlandstr. 3, 91058 Erlangen, Germany
[3]Interdisciplinary Center for Engineering of Advanced Materials (EAM), Friedrich-Alexander-University Erlangen-Nuremberg, Nägelsbachstr. 49b, 91052 Erlangen, Germany

Keywords: flame spray pyrolysis, indium, gallium, aluminium, zinc oxide

Nanoparticulate zinc oxide as a wide band gap semiconductor, as well as trivalent doped zinc oxide nanoparticles (NPs) are economic and promising materials for the application in printable electronic devices. Dispersed in organic solvents and deposited as thin film on e.g. flexible substrates they can be used in solar cells, transistors or sensors. Moreover, the morphological, optical and electronic properties of the powders can be adjusted depending on the doping content and synthesis route (Hammarberg et al, 2009).

To cover the high demand of low cost materials an energy efficient and solvent free synthesis method with high production rates, for example a flame spray process, is required. Utilizing this technique particle size, shape, optical band gap and defect states of the particles can be controlled by the content of dopant and the synthesis route. In this work, doping of zinc oxide with aluminium, gallium and indium and the usage of indium doped zinc oxide in dye sensitized solar cells is investigated.

A liquid precursor of mixtures of aluminium-, gallium-, indium- and zinc acetylacetonate in 2-methoxyethanol is dispersed by a nozzle into the spray flame. In the flame, pyrolysis reactions lead to high supersaturations and therefore to particle nucleation with subsequent growth, agglomeration and sintering. The reactor set-up (Kilian et al., 2014) allows producing In-Zn-O and Ga-Zn-O with mean primary particles in the size range of 5 nm up to 12 nm. These particles are then collected with a membrane filter.

Doping with In leads to a steadily decreasing primary particle size down to a minimum for In_2O_3 with 7.4 nm, which is determined by BET, XRD and TEM. Also a steadily increasing Ga content in the precursor generates smaller particles down to a minimum for Ga_2O_3 with 5.6 nm. A similar trend can be observed for Al doping. All dopants obviously inhibit particle growth of pure ZnO. XRD, EDX and ICP-OES proof the precise composition of the trivalent doped powders. The optical band gap first decreases exponentially for increasing dopant content and then increases up to the band gap of the pure trivalent oxides. Additionally, the crystalline phase changes between 40 and 60 mol% indium and round 40 mol% gallium into an amorphous/nanocrystalline phase. PL measurements provide an overview about the defect states of the binary Al-, In- and Ga-Zn-O and the oxygen vacancies of the particles.

Due to a precisely adjustable band gap the In-Zn-O particles are favorable for the usage as photoanodes in DSSCs. By doping ZnO with indium it is possible to enhance the charge transport processes and reduce the recombination rates. For example an increased current density can be achieved as shown in Fig.1.

The aerosol synthesis will be reviewed, the properties of the doped zinc oxide particles will be discussed in detail regarding morphology, composition and opto-electronical properties. Finally, the integration in DSSCs will be illustrated.

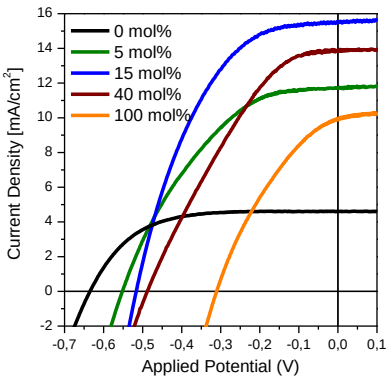

Figure 1. The current density indicates a good device performance between 5 and 20 mol% with an overall device efficiency ~ 4 % at 15 mol% Indium content

This work was supported by the German Research Council (DFG) and the Cluster of Excellence "Engineering of Advanced Materials" (EAM).

Hammarberg, E. Prodi-Schwab, A. & Feldmann, C. (2009). *Journal of Colloid and Interface Science*, 29-36

Kilian D., Engel S., Borsdorf B., Gao Y., Kögler A.F., Kobler S., Seeger T., Will S., Leipertz A., Peukert W. (2014). *Journal of Aerosol Science, 69*, 82-97.

Characterization, Fate, and Re-suspension of Aerosol Particles (0.3–10 µm) inside University Offices: the Effects of Occupancy and Carpet

Tareq Hussein [1,2], Lubna Dada [2], Hassan Juwhari [1], Dina Faouri [1]

[1]Department of Physics, The University of Jordan, Amman 11942, Jordan
[2]Department of Physics, University of Helsinki, P. O. Box 48, FI-00014 UHEL, Helsinki, Finland

Keywords: Indoor air quality, particle number size distribution, aerodynamic diameter, gravitational setting

Upon the implementation of the WHO law to the right of healthy indoor atmosphere (WHO, 2000) and due to the fact that people spend over 90% of their time indoors (Hussein et al., 2012), studies became more concentrated towards indoor air quality (IAQ) of workplaces which reflects the performance efficiency and health status of workers inside.

Both the work occupational health and work occupational exposure have been given an increased attention, however, it is still important to understand the dynamic behavior of indoor aerosols at work places and suggest methodologies and protocols, to improve IAQ.

This study focuses on measurements and characterization of particles emitted in offices due to occupancy and workers' activities inside. It presents the number based size distribution (diameter 0.3 – 10 µm with high time resolution) inside four offices (naturally ventilated). Each office has a typical environment in terms of occupancy and furniture. The differences between workdays and weekends in term of particle number and mass concentrations are investigated. Moreover, the effect of smoking, workers' activity and outdoor concentration on indoor concentrations is also presented.

During workdays, the highest measured coarse fraction concentration in the occupied office is found to be around 95µg/m^3 (Figure 1) compared to 9.0µg/m^3 in the unoccupied offices. Re-suspension of indoor dust is seen to have higher rates in occupied and carpeted offices (highest re-suspension emission rate = 235 µg/m^{3}h) in comparison to unoccupied uncarpeted offices (75 µg/m^{3}h). Carpets seem to accommodate particulate matter better than bare floors and therefore lead to increased emission rates.

Furthermore, this study utilizes a simple indoor aerosol model to estimate the ventilation rates which were found to vary between 0.15 and 0.38 h^{-1}. The proximity of offices reflects the closeness in the ventilation rates' values. Another simple model is used to calculate the gravitational settling profile of particles of different diameters. As expected, larger particles have higher gravitational settling potential (Figure 2). It is also found that the presence of carpets and furniture aids in the settling of particles and results in an increase in the total particle loss rate.

Finally, results of this study emphasize that natural phenomena such as dust storms influence indoor particle size distributions by infiltration. Also, human indoor activities such as smoking and walking contribute to increase the particle concentrations inside.

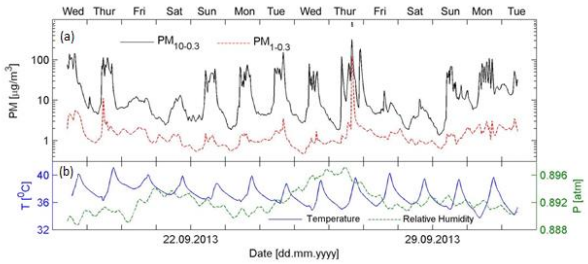

Figure 1. Half-hourly averages of measured particle size distributions within the diameter range 0.3–10 µm inside occupied office: (a) integrated particle mass and (b) indoor air temperature and pressure.

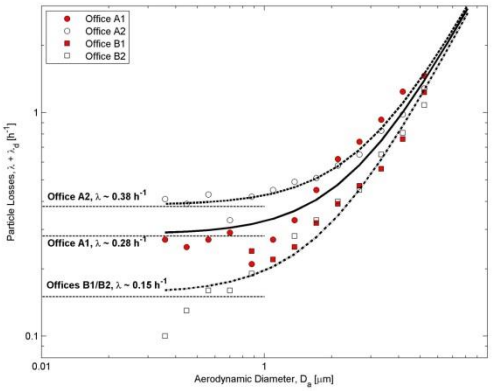

Figure 2. Particle loss rate $\lambda + \lambda_d$ [h^{-1}] inside the offices. The lines represent calculated gravitational settling rate ($\lambda_d = v_g/H$) of aerosol particles with an offset value reflecting the average ventilation rate (λ) as indicated for each office.

This study was fully sponsored by the Deanship of Academic Research at the University of Jordan.

WHO. (2000). The Right to Healthy Indoor Air.
Hussein, T., Paasonen, P. and Kulmala (2012). *Sci. Tot. Environ.*, **425**, 289-292.

Charge distribution of particles with dense and fractal structure

L. Hillemann[1], M. Seipenbusch[2] and M. Stintz[1]

[1]Institute of Process Engineering and Environmental Technology, TU Dresden, 01062 Dresden, Germany
[2]Institute for Mechanical Process Engineering and Mechanics, Karlsruhe Institute of Technology, 76131 Karlsruhe, Germany

Keywords: Charge distribution, particle shape, particle structure

For the characterization of airborne particles the SMPS is widely used. Shape and structure of the particles influence not only their classification in the DMA but also the charging process in the aerosol neutralizer.

Previous studies focused on the theoretical description of the charging process for nonspherical particles (Lamframboise 1977, Han 1991, Han 1994, Biskos, 2004) or determined only the mean number of charges on particles varying in shape (Wen, 1984, Oh, 2004, Unger, 2004, Ouf, 2009).

The presented study employs a CVS system for aerosol generation (Okuyama, 1986). This set-up generates particles with a fractal-like structure. To modify the shape of the particles, the particles were sintered at temperatures in a sintering furnace downstream the CVS-reactor.

After cooling and diluting a fraction of the aerosol with defined electrical mobility was selected by a DMA. This fraction was charged in a radionuclide-based diffusion charger. Downstream the charger this aerosol was classified according to the electrical mobility of the particles in second DMA. An example of these data is shown in Fig. 1. Here the mobility diameter of the particles under consideration was set to 200 nm.

The contribution will present more data and discuss the influence of the structure of the particles on the charge distribution.

This work was supported by the German Federal Ministry of Economics and Technology (BMWi) under grant 17051 BG / 1.

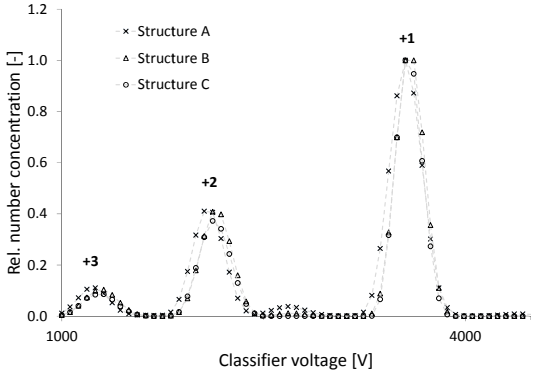

Figure 1. Example of measured distribution of electrical mobility

Okuyama, K., et al. (1986). *AIChE Journal*, 32, 2010–2019.

Biskos, G., et al. (2004). *J. Aerosol Science*, 35, 707–730.

Han, R. J., et al. (1991). *Aerosol Sci. Technol.*, 15, 184–190.

Han, R. J., Gentry, J. W. (1994). *J. Aerosol Science*, 25, 499–508.

Laframboise, J. G., Chang, J.-S. (1977). *J. Aerosol Science*, 8, 331–338.

Oh, H., et al. (2004). *Aerosol Sci. Technol.*, 38, 1045–1053.

Ouf, F.-X., Sillon, Ph., (2009). *Aerosol Sci. Technol.*, 43, 685–698.

Unger, L., et al. (2004). *J. Aerosol Science*, 35, 965–979.

Wen, H. Y., et al. (1984). *J. Aerosol Science*, 15, 103–122.

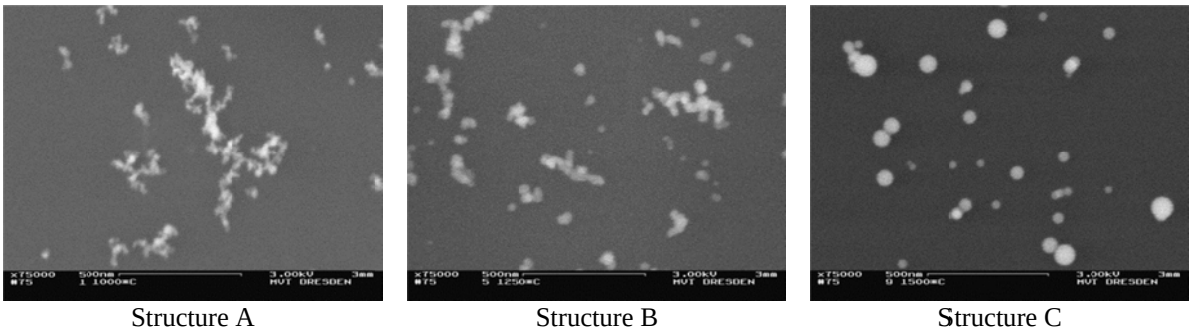

Structure A Structure B Structure C

Figure 2. SEM images of the aerosol particles sampled downstream the sintering furnace showing different particle structure

Chitosan nanoparticle generation and characterization using CARS technique

G. Mordas, V. Ulevicius, V. Dudoitis and A. Dementjev

STI Center for Physical Sciences and Technology, Savanorių ave. 231, LT-02300 Vilnius, Lithuania

Keywords: nanoparticle, generation, particle characterisation, CARS microscopy, imaging.

Chitosan due to its unique physical and chemical properties has found a widespread use in different areas from food to medicine. However, the development of novel materials based on chitosan needs chemical and physical modifications of the chitosan. This work describes such chitosan modification that allowed producing stable chitosan nanoparticles. In addition, we apply Coherent Anti-stokes Raman scattering microscopy technique (CARS) as a tool to investigate the spatial structure and chemical composition of microstructured materials based on chitosan.

In this work, we deacetylate a chitosan powder (Sunrise Nutrachem Groupe). The volume of alkali needed to neutralize the protonated amino groups was determined by alkalimetry. The molecular weight was determined viscometrically. The viscosity measurements in 0.5 mol/l acetic acid and 0.2 mol/l sodium acetate buffer solutions were performed using an Ostwald viscometer and recording the efflux time of the solution at 25C. The average molecular weight (M) of chitosan was calculated by the Mark-Houwink equation $\eta = K_m M^{\alpha}$ ($M = (\eta/K_m)^{1/\alpha}$), where η is the intrinsic viscosity, constants $K_m = 3.5 \times 10^{-4}$ and $\alpha = 0.76$. The chitosan was titrated by 0.05 mol/l H_2SO_4 solution of 100 mg sorbent placed in 50 ml of a 0.1 mol/l NaOH solution and kept there for 24 hours.

The obtained immobilized chitosan was diluted with water (dilution ratio is 1:20) and atomized using three aerosol generators (TSI model 3076, TSI model 3079 and electrospray generator TSI model 3480). The particle number concentration and the particle number size distribution were measured with Scanning Mobility Particle Sizer TSI model 3936. The generated aerosol was dried with the air dryer TSI model 3030 using silicogel. Preparing the sample for the CARS microscopy (Dementjev *et al.,* 2010) the dried particles were sediment on thin (0.17 mm) glass plate using Nanometer Aerosol Particle Sampler TSI model 3089.

The particle number size distributions of the generated chitosan nanoparticles are presented in Fig. 1. Fig. 2 shows CARS spectrum of chitosan particle. Two distinct peaks are obtained in spectrum: the band at 2880 cm^{-1} belongs to alkane vibrations and the wider band centred at 3300 cm^{-1} was assigned to amine vibrations. Images presented in Figure 3(A,B) were recorded at the wavenumber corresponding to determined alkane and amine groups, which are the markers of chitosan. The CARS image gives particle size of 0.64 ± 0.3 μm, in a perfect agreement with the measured with TSI spectrometer (0.65 ± 0.1 μm). Thus, we demonstrates the possibility to generate the modified chitosan nanopaticles in wide size range and to characterize them using CARS technique.

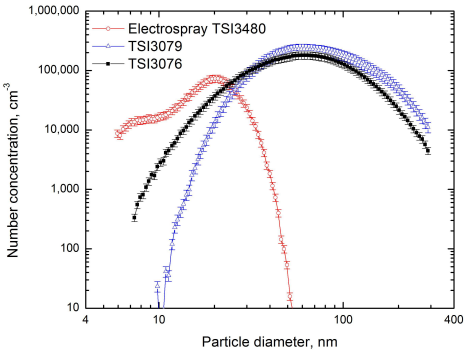

Figure 1. Chitosan particle number size distribution.

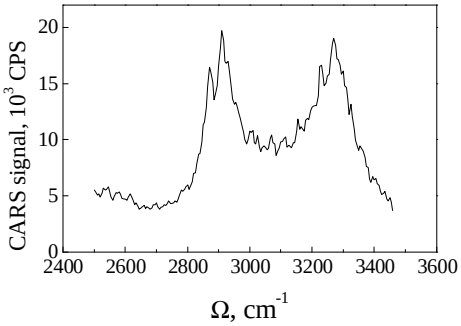

Figure 2. The CARS spectrum of chitosan particle.

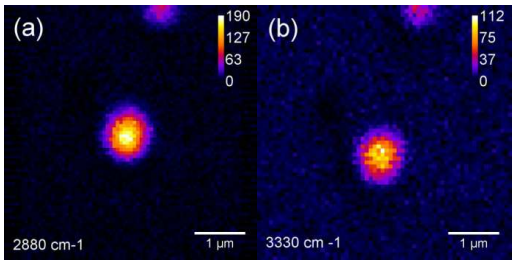

Figure 3. (a) and (b) - CARS images of particle recorded at 2880 and 3300 cm^{-1} respectively.

Dementjev, A., Gulbinas, V., Serbenta, A., Kaucikas, M., & Niaura, G. (2010). *Journal of Modern Optics*, 57, 503

Combustion Spray Synthesis of Nanoparticles: From Single Droplets to Nanoparticles

C.D. Rosebrock[1], T. Wriedt[2], K. Wegner[3], and L. Mädler[12]

[1]Department of Production Engineering, University of Bremen, Bremen, 28359, Bremen, Germany
[2]Foundation Institute of Materials Science, University of Bremen, Bremen, 28359, Bremen, Germany
[3]Particle Technology Laboratory, Swiss Federal Institute of Technology (ETH) Zürich, Switzerland

Keywords: droplet combustion, flame synthesis, decomposition, vapour nucleation, particle formation.

Combustion spray synthesis of nanoparticles is an established method for the production of a wide variety of functionalized materials. High gas-phase temperatures and short residence times offer the opportunity of scalable production of nanoparticles with high purity in a one-step process, while preserving the nanoparticle properties (Mädler, 2002).

The gas-phase synthesis in combusting sprays is intrinsically related to the formulation of the liquid metal-organic precursor solution, e.g. chemical and thermal stability. Incomplete combustion of the solution droplets due to selective vaporization or flame extinction results in undesired micron-sized (nano) particle production. Strong interaction between the solution droplets within the combusting sprays challenging the experimental investigation, confining the current research to relating the nanoparticle properties to integral process parameters.

To obtain detailed information about the transport processes during the combustion of precursor solution droplets, experiments on single isolated burning droplet appear to be a successful tool for understanding and designing liquid precursor solutions.

Recent experimental results on liquid precursor solution droplets revealed that disruptive combustion occurs (Rosebrock, 2013), where the decomposition characteristics of the metal-organic precursor significantly affecting the combustion. Thermal decomposition of the precursor during combustion inhibits vaporization, resulting in a superheated liquid solution that violently disrupts due to vapor-phase nucleation within the droplets. The disruptive burning is in contrast to the common assumption of selective vaporization of the solutions components, which occurs in descending order from high to low volatility.

It is concluded that the fundamental transport mechanisms during combustion of metal-organic precursor solutions have not been sufficiently understood, yet.

Although the liquid and gas flow rates of combusting sprays are orders of magnitudes larger compared to single isolated droplets, the physicochemical mechanisms occurring during the combustion of the liquid droplets seems to be similar, i.e. the droplet sizes, relative velocities and residence times in high temperature environment. Accordingly, the resulting nanoparticles from single isolated droplets are similar in shape and size (Figure 1). Moreover, the agglomerate/aggregate size distributions of nanoparticles from single droplet experiments are also in very good agreement with the corresponding nanoparticles from combusting sprays.

The presentation will include an overview of the experimental results from the single burning droplet and show that the single isolated droplet is a successful tool for probing suitable precursor solutions regarding the production of desired nanoparticles.

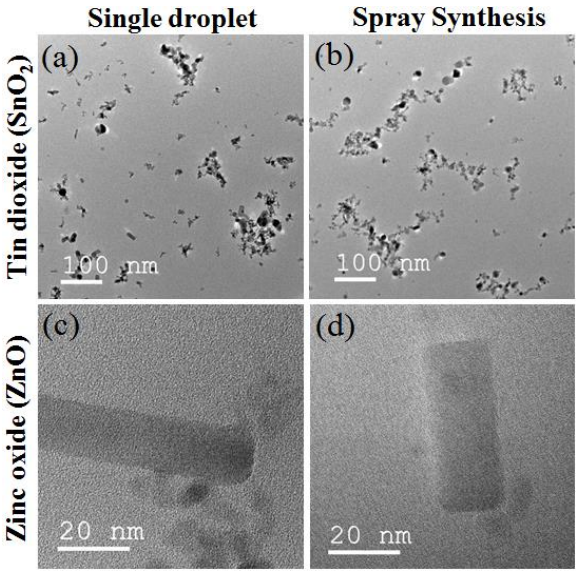

Figure 1. TEM image of Tin dioxide (a & b) and Zinc oxide (c & d) nanoparticles produced with the single droplet (a & c) and spray synthesis (b & d).

This work was supported by the Deutsche Forschungsgemeinschaft (DFG) under the grants of MA 3333/4-1.

Mädler, L., Kammler, H.K., Mueller, R., Pratsinis, S.E. (2002). *J. Aerosol Science, 33, 369-389*.

Rosebrock, C.D., Riefler, N., Wriedt, T., Tse, S.D., Mädler, L. (2013). *AIChE Journal*, 59 (12), 4553-4566.

Comparability and accuracy of personal nanoparticle exposure monitors

C. Asbach[1], H. Kaminski[1], B. Stahlmecke[1], C. Monz[2], D. Dahmann[2], M. Fierz[3], S. Clavaguera[4], B. Faure[4], N. Dziurowitz[5], A. Meyer-Plath[5], B. Dettlaff[5], A. S. Godinho de Fonseca[6], M. Viana[6], A. M. Todea[1]

[1] Institut für Energie- und Umwelttechnik e.V. (IUTA), Duisburg, Germany
[2] Institut für Gefahrstoffforschung (IGF), Bochum, Germany
[3] University of Applied Science Northwestern Switzerland, Windisch, Switzerland
[4] Commissariat à l'Energie Atomique et aux Energies Alternatives (CEA), Grenoble, France
[5] Federal Institute of Occupational Safety and Health (BAuA), Berlin, Germany
[6] Institute for Environmental Assessment and Water Research (IDÆA-CSIC), Barcelona, Spain

Keywords: personal exposure, nanoparticle, diffusion charger, personal monitor

The production and use of nanomaterials has increased constantly over the recent years. Besides the tremendous new opportunities these materials offer, the discussion on potential adverse health effects particularly caused by inhalation of nanoparticles has also gained pace. The likelihood for inhalation exposure to nanomaterials is highest in workplaces where these materials are produced or handled and exposure to airborne nanomaterials hence has to be controlled. Most published studies on inhalation exposure to nanomaterials used stationary measurement equipment (Kuhlbusch et al., 2011). However, ideally the exposure is measured in the breathing zone of a worker, i.e. within a 30 cm hemisphere around mouth and nose. While most conventional personal samplers collect all respirable particles (< 4 µm) on a filter for eventual gravimetric and/or chemical analyses, more nanospecific samplers and monitors have only recently become available. Personal monitors with time resolution up to 1 s are of particular interest for an event or activity based exposure assessment. The available monitors are all based on electrical diffusion charging of the particles, followed by charge measurement and in some cases a manipulation of the aerosol's size distribution inside the instrument. The available monitors are DiSCmini (Testo, Germany; essentially identical with miniDiSC), nanoTracer (oxility, formerly Philips Aerasense, both the Netherlands) and Partector (naneos, Switzerland). All of the instruments determine the lung deposited surface area (LDSA) concentration. DiSCmini and nanoTracer additionally also measure the number concentration and mean particle size. Due to their rather recent introduction to the market, the number of studies on their comparability and accuracy are still rather scarce (Asbach et al., 2012; Bau et al., 2015).

As part of the Eranet SIINN project nanoIndEx, we investigated both the accuracy and comparability of the monitors. Monodisperse particles with eight different sizes between 10 nm and 700 nm, i.e. within and beyond the size range of the monitors, were used to study the instruments' accuracy. The comparability of the monitors was assessed by using identical aerosols that were simultaneously sampled by the monitors. The test aerosols contained a large variety of particle sizes, morphologies and concentrations.

The results indicate that the accuracy of all instruments is within ±30% for particle sizes between approximately 20 nm and 400 nm. LDSA concentrations of particles smaller than 20 nm are overestimated and the concentration of particles larger than 400 nm underestimated.

The comparability of LDSA concentrations is also on the order of ±30% as long as the particle sizes are within the aforementioned limits. The comparability of the number concentration was slightly worse and around ±50%. Particle size (within 20-400 nm), morphology and concentration did not have a noticeable effect on the comparability. The concentrations of particles with significant fractions of particles <20 nm were typically reported as too high. Concentrations of particles >400 nm were reported as significantly too low. Both can well be explained based on the measurements with monodisperse particles.

The poster will discuss the set up and results from both parts of the study.

nanoIndEx is supported by the French National Funding Agency for Research (ANR), the German Federal Ministry of Education and Research (BMBF), the British Technology Strategy Board (TSB) and the Swiss TEMAS AG, under the frame of SIINN, the ERA-NET for a Safe Implementation of Innovative Nanoscience and Nanotechnology. IDÆA-CSIC received funding from FP7 Marie Curie ITN "HEXACOMM".

C. Asbach, H. Kaminski, D. Von Barany, T.A.J. Kuhlbusch, C. Monz, N. Dziurowitz, J. Pelzer, K. Berlin, S. Dietrich, U. Götz, H.-J. Kiesling, R. Schierl, D. Dahmann (2012), *Annals of Occupational Hygiene* **56**: 606-621

S. Bau, B. Zimmermann, R. Payet, O. Witschger, (2015), *Environmental Science: Processes & Impacts* DOI: 10.1039/C4EM00491D

T.A.J. Kuhlbusch, C. Asbach, H. Fissan, D. Göhler, M. Stintz (2011), *Particle & Fibre Toxicology* **8**: 22*;* doi:10.1186/1743-8977-8-22

Comparison between two calibration routines of the Single Charged Aerosol Reference (SCAR)

K. Pihlava, J. Keskinen and J. Yli-Ojanperä

Department of Physics, Aerosol Physics Laboratory, Tampere University of Technology, FI-33101, Tampere, Finland

Keywords: particle number concentration, calibration, SCAR.

Single Charged Aerosol Reference (SCAR, Yli-Ojanperä *et al.*, 2010) is a particle number (PN) concentration reference based on electrical detection of aerosol particles. In short, the idea of the SCAR is to generate a reference aerosol that consists of particles with a single elementary charge. The generated aerosol particles are collected to a high-efficiency filter placed inside a Faraday cup (FCUP) where the electric current, induced by the particles, is measured. Simultaneous measurement of the electric current and the volumetric flow rate through the FCUP enables determination of the PN concentration of the reference aerosol.

Several different factors contribute to the overall uncertainty of the PN concentration determination. According to Yli-Ojanperä *et al.* (2012), the random noise of the electric current measurement is the dominating uncertainty component. To eliminate the effect of the offset current, the unipolar calibration routine of the SCAR comprises *n* cycles, where the offset current (no particles) is measured before and after the actual measurement with particle output. The detailed description of the unipolar calibration method is given by Yli-Ojanperä *et al.* (2012).

In this study, the sensitivity of the electric current measurement of a single cycle was compared between two routines, namely, uni- and bipolar. In the bipolar routine, instead of measuring the offset current, particles with a positive and particles with a negative elementary charge are measured in turn. Figure 1 illustrates a measurement cycle with uni- and bipolar calibration routines.

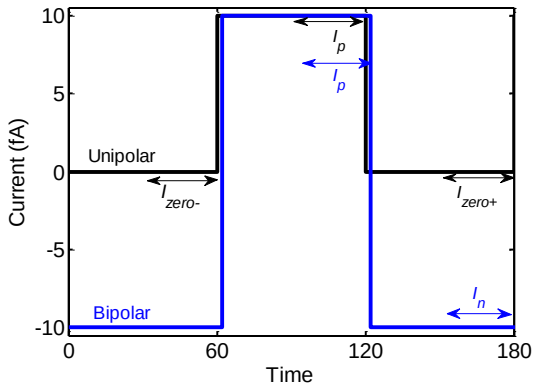

Figure 1. One measurement cycle conducted with unipolar method (black) and bipolar method (blue).

In unipolar case, one cycle produces a corrected current value ΔI

$$\Delta I = I_p - \frac{I_{zero-}+I_{zero+}}{2}, \quad (1)$$

where I_p is the mean current of the last 30 seconds of the particle (positive polarity) measurement. I_{zero-} and I_{zero+} are obtained similarly from the offset currents measured before and after the particle measurement, respectively. In bipolar routine, one corrected current value is the mean of a positive (I_p) and the following negative particle measurement (I_n) according to

$$\Delta I = \frac{I_p - I_n}{2}. \quad (2)$$

Also in bipolar method, I_p and I_n are the mean values of the last 30 seconds from the measurement as indicated in Figure 1. Therefore, the standard uncertainties of the currents of particle and zero measurements are obtained from the experimental standard deviation. Assuming the standard deviation (i.e. uncertainty) is the same for both particle polarities as well as for zero measurements, the standard uncertainty of the corrected current is

$$u^2(\Delta I) = \frac{3}{2}u^2(\Delta I_p) \quad (3)$$

in unipolar case and

$$u^2(\Delta I) = \frac{1}{2}u^2(\Delta I_p) \quad (4)$$

in bipolar case. In Equations (3) and (4), the multipliers result from sensitivity coefficients.

According to the results obtained from experimental data shown in Table 1, the standard relative uncertainty (k=2) of a cycle in bipolar method is clearly lower than in unipolar method. Hence, the bipolar method improves the sensitivity of the calibration.

Table 1. Standard relative uncertainties (k=2) of a measurement cycle in uni- and bipolar methods.

ΔI (fA)	$u(\Delta I_p) / \Delta I_p$ unipolar	$u(\Delta I_p) / \Delta I_p$ bipolar
6.8	0.0309	0.0174
14	0.0285	0.0103
25	0.0606	0.0050

Yli-Ojanperä, J., Mäkelä, J. M., Marjamäki, M., Rostedt, A. & Keskinen, J. (2010). *J. Aerosol Science*, 41, 719-728.

Yli-Ojanperä, J., Sakurai, H., Iida, K., Mäkelä, J. M., Ehara, K. & Keskinen, J. (2012). *Aerosol Sci. Technol.*, 46, 1163-1173.

Consecutive droplets-solid particles and solid particles-droplets filtration in fibrous filters

J.M. Gac[1] and A. Jackiewicz[1]

[1]Faculty of Chemical and Process Engineering, Warsaw University of Technology, Waryńskiego 1, 00-645, Warsaw, Poland

Keywords: aerosol filtration, fibrous filters, solid aerosols, liquid aerosols

Separation of aerosol particles from gas is one of the important processes in various branches of chemical industry and environmental processes. The filtration of gas on fibrous filters is very popular method because of its simplicity and relatively high efficiency of aerosol particles removal. Thus it has attracted the attention of investigators for a long time. Nowadays, the dynamics of the solid particles removal is quite well understood. The last investigations devoted to the filtration of liquid aerosols have given some insight also into this subject. In contrast, the filtration of mixed aerosols i.e. both solid and liquid particles removal, seems to be the most poorly understood.

The process of mixed aerosol filtration, when the gas contains both solid particles and liquid droplets, has been investigated experimentally by Frising et al. (2004). They have considered the case when the solid to liquid particles concentration ratio remains constant during the process. The same process has been also analysed numerically (Gac et al., 2014). However, in various applications of gas filtration this ratio may change in time. As an example, let us consider the process when in some periods of time there are only solid particles present in gas while in another ones there are only liquid droplets. The investigation of such a process of the filtration is a subject of our contribution.

It is obvious that the presence of the liquid droplets deposited on filtration fibres inside the filter influences on the efficiency of removal of solid particles and the pressure drop during the process. Roughly speaking, it is caused by the different character of the interactions between solid particles in the presence and absence of liquid. The liquid makes the solid deposits more compact (instead of dendrite-like ones, typically observed in the absence of liquid). That leads to the less pressure drop increase during the filtration of solid particles. This feature have been already observed during the filtration of solid particles on the filters pre-treated by oil. However, the presence of liquid deposited on fibres leads also to decrease of filtration efficiency of solid particles in comparison to the efficiency of filtration on dry filter. The reason of such a behaviour of the efficiency is the growth of effective fibre diameter. Indeed, in the presence of the liquid on the fibres the solid particles form the nearly uniform layer covering the fibre surface instead of thin and expanded deposits.

On the other hand, the existence of solid deposits in filter structure leads to the changes of efficiency of the removal of droplets. Similarly to the early stages of the filtration of solid aerosols, the deposits lead to increase of filtration efficiency as well as pressure drop. The efficiency then rapidly decreases (much more rapidly than in the case of the mist filtration on the filter without solid deposits). This tendency is explained as an effect of the collapse of dendrite-like deposits.

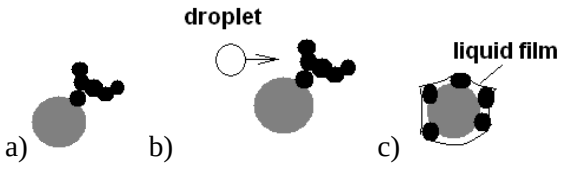

Figure 1. Change of solid deposits as an effect of mist filtration

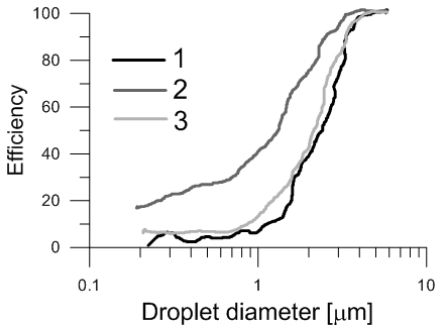

Figure 2. Mist filtration efficiency of: empty filter (1), after 1.5 h of solid aerosol filtration (2) and after 1.5 h solid filtration and 48 h liquid filtration (3)

This work was supported by the National Centre for Research and Development under the LIDER project LIDER/13/97/L-3/11/NCBR/2012.

Frising, T., Gujisaite, V., Thomas, D., Salle, S., Bremer, D., Contal, P. & Leclerc, D. (2004). *Filtration+Separation.*, 41, 36-39.

Gac, J.M., Jackiewicz, A., & Gradoń, L. (2014). in *Proc. of Oil and Gas and Chemical Filtration and Separations, AFS 2014*; Houston, U.S., Code 107351

Continuum models for nanoparticle-wall collisions

A.P. Weber[1*], C. Schöner[2], M. Gensch[1], A. Werner[1] and T. Pöschel[2]

[1]Institute of Particle Technology, Clausthal University of Technology, Leibnizstraße 19, 38678, Clausthal-Zellerfeld, Germany
[2]Institute for Multiscale Simulation, Friedrich-Alexander University, Nägelsbachstraße 49b, 91052, Erlangen-Nuremberg, Germany
*Corresponding author: alfred.weber@mvt.tu-clausthal.de

Keywords: aerosol nanoparticles, elastic-plastic transition, contact charging, bouncing, coefficient of restitution

While nanoparticles properties such as optical, electronic and magnetic behavior have been studied extensively, their mechanical behavior has been studied only for quasi-static stressing. Little is known about their mechanical properties at high shear rates such as encountered during high velocity impaction. Most of the knowledge for such stressing is based on Molecular Dynamics (MD) simulations. In contrast to the significant number of MD simulations of nanoparticles hardly any experimental data are available. Fig. 1 shows the behavior of the critical velocity, which is the minimum impact velocity for a particle to bounce, as a function of the particle size. There seems to be a transition from the micrometer range down to the nanometer range. While the extrapolation of the critical velocities, as measured in the micrometer range, to the nanoparticle sizes would predict critical velocities of several thousands of m/s, the observed critical velocities of nanoparticles are orders of magnitude lower. This raises the question if there is a transition in the mechanical material properties when reaching the nanorange. From a more general point of view, but with significant practical implications, it is of interest to elaborate how far simple continuum mechanics can be applied for nanoparticles.

Therefore, a novel approach is taken here to combine molecular dynamics (MD) simulations with nanoparticle impaction experiments to supply the first comprehensive picture of the physics behind the collision of a single dense spherical particle with a wall. While physical parameters before and after the collision are measured by modified single stage low pressure impaction (e.g. impact velocity, bounce velocity, charge transferred to the particle), the details of particle compression (e.g. acceleration due to adhesion forces, applied force and resulting contact area) are retrieved from molecular dynamics simulation.

In Fig.2 the relationship between maximum applied force F_{max} and the Hertz parameter a^3/R (with R=particle radius) as obtained from MD calculations for Pt nanoparticles impaction on a hard target (e.g. mica) is shown.

For the weakly attractive potential between the particle and the target surface a contact area is already formed without an external applied force. Therefore, the Hertz theory has to be modified to account for the nanoparticle deformation behavior (conforming contact). For larger impaction velocities the contact becomes increasingly plastic as also observed in the charge transferred to the particles.

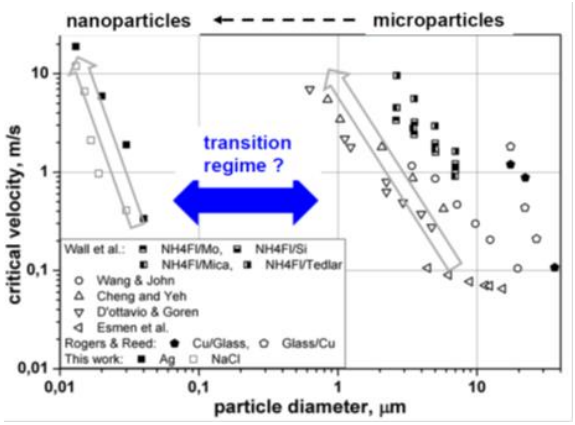

Fig. 1. Critical velocity for bounce as a function of particle size

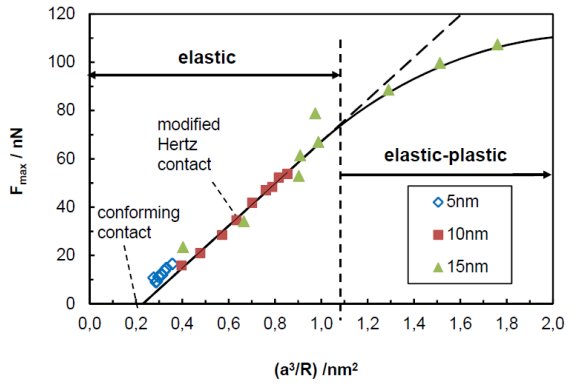

Fig. 2. Maximum force vs. Hertz parameter for Pt nanoparticles impacting on a mica target

Based on this approach the applicability of continuum models to the nanoparticle-wall collisions is tested.

Acknowledgements
This work was supported by the German Research Foundation (DFG) under the grant no. WE 2331/12-2

Control of Condensation onto 1-2 nm particles in Laminar Growth Tubes via Lewis Number Modulation in He-CO_2 Gas Mixtures

J. M. Thomas, A. Maisser , C. J. Hogan

Department of Mechanical Engineering, University of Minnesota, Minneapolis, MN 55455, USA

Keywords: CPC, nucleation, detection efficiency, size classification
Presenting author email: amaisser@umn.edu

Commercial laminar flow condensation particle counters (CPCs) are widely used as detectors in aerosol size distribution measurement, e.g. scanning mobility particle sizer (SMPS). CPCs can detect particles down to sizes of a few nanometers by exposing them to a supersaturated vapour and thus growing these particles to macroscopic sizes. The grown droplets are counted optically. The supersaturation achieved will determine the lowest particle size that can be activated and thus detected.

In many laminar flow CPCs a flow with saturated vapour is introduced into a condenser tube. The walls of the condenser are kept cold and thus supersaturation is achieved by heat and mass transfer. The supersaturation profile strongly depends on the vapour and gas properties and is governed by the ratio between thermal diffusivity of the gas and mass diffusivity of the vapour molecules (Stolzenburg and McMurry, 1991). This can be described by the Lewis number:

$$Le = \frac{Thermal\ diffusivity}{Mass\ diffusivity}$$

In the instance of Le > 1, heat transfer occurs more quickly, leaving supersaturated vapor in the center of the tube. Increasing Le, therefore, directly leads to increases in saturation ratio S, enabling condensation onto smaller particles. The idea of this study is to control the Lewis number in a commercially available CPC (TSI 3025 butanol based) by operating the CPC in a gas mixture. The two gases used in this study were CO_2 and Helium. The Lewis number in He exceeds that of air, and the Le in CO_2 is still lower. Thus, a large range of Le can be achieved by employing He-CO_2 mixtures. By operating at different gas ratios the saturation profile inside the growth tube and the maximum supersaturation achieved will be changed while all other operation parameters can be kept constant. This will shift the cut-off diameter of the instrument and thus, is a promising method to use for particle sizing using only a CPC without any pre-classification instrument required.

The supersaturation profile at different radial coordinates for a 30% Helium in CO_2 gas mixture was calculated using COMSOL is given in Fig. 1. The detection efficiency curves were measured using mobility standards (tetra-alkyl salts) of different sizes. The mobility standards were electrosprayed and size classified using a differential mobility analyser (half mini DMA, NanoEngineering corp., FL, USA). An electrometer and the CPC were used in parallel as detectors, where the electrometer was applied as a reference for total number concentration.

The results for detection efficiency are shown in Fig. 2. A shift of the activation efficiency toward bigger particle sizes can be observed between He to CO_2 mole ratios of 42% in comparison to 37%. These results seem promising to use this technique for particle sizing in the small nanometer size range. The advantages of controlling the saturation by gas mixture over controlling growth tube and presaturator temperatures is the relatively fast establishment of steady saturation profiles in at varying gas mixtures.

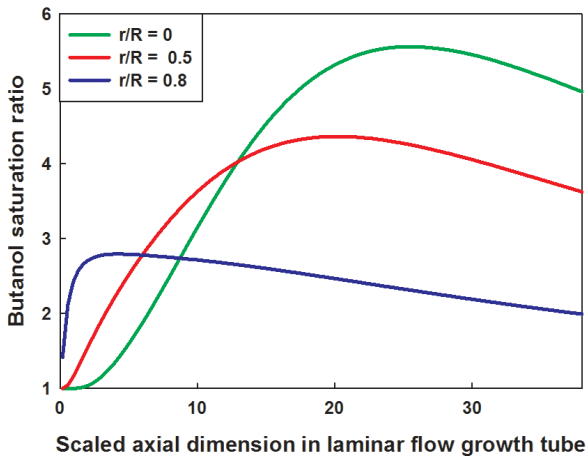

Figure 1. Axial saturation ratio profiles for laminar flow growth tube for 30 mole % He in CO_2 at three different radial coordinates. R is the growth tube radius, r is the radial coordinate.

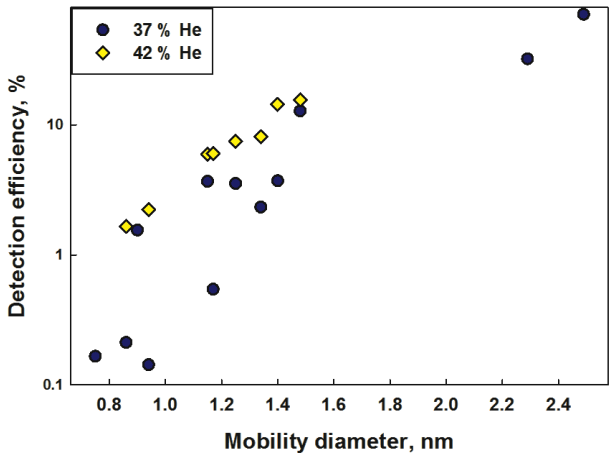

Figure 2. Detection efficiency of mobility standards at different He concentrations.

Stolzenburg, M., McMurry, P. H. An Ultrafine Aerosol Condensation Nucleus Counter. *Aerosol Sci. Technol.* 48-65 (1991).

Controlled Particle Synthesis in a Hot-Wall Reactor and Manipulation of the Aggregation Process

D. B. Rasche[1], L. Knobel[1] and H.-J. Schmid[1]

[1]Chair of Particle Technology, University of Paderborn, Paderborn, 33098, Germany

Keywords: controlled synthesis, hot wall reactor, controlled aggregation, coaxial corona charger

Particle synthesis in a hot-wall reactor is a reliable process for the production of nanoparticles due to the fact that all relevant process conditions – e.g. temperature distribution, pressure, flow field, residence time distribution – can be controlled in a wide range of values.

However, at high mass production rates, as required in industrial applications, aerosol processes typically result in highly aggregated, fractal like structures. But, it is of high interest from an application as well as research standpoint to reach high mass production rates while particles are still spherical. A necessary condition to obtain spherical particles is, that the time of cooling down the aerosol from the heated zone (here nucleation, growth, agglomeration and finally sintering takes place) to a lower temperature level (where the sintering is quenched) is rather fast to prohibit partly sintered agglomerates.

An apparatus which provides the required specifications to produce spherical particles with a sufficient mass rate has been installed recently. The main component is a ceramic tube reactor heated in three zones and able to handle temperatures up to 1650 °C. Moreover, an air heater was used upstream of the tube reactor to reduce the thermal stress in the ceramic tube occurring due to the temperature gradient caused by the incoming cold process air. Cleaned, dried and compressed air, provided by two independent flow controllers with a range from 5 to 250 SLM, are used for the process and for quenching. Adjustable air flow into the reactor allow for a wide range of possible synthesis parameters, particularly the concentration of precursor at the reactor entrance. A liquid precursor delivery system ensures an accurate flow of the precursor–nitrogen-mixture into the reactor. Downstream of the heated zone the aerosol is quenched with dry, clean air. To make quenching rapid and stop sintering almost instantly after the heated zone, an insulated and water cooled quenching probe is inserted into the tube of the hot-wall reactor. This allows to quench the hot aerosol right next to the heated zone and leads to particles being close to the final sintering stage. The heat exchanger further downstream was designed to reach a constant temperature around 200 °C offering the possibility to modify the particles in this section for the sake of further research projects. Finally, the particles are collected on a membrane filter. A vacuum pump in combination with an adjustable valve is used to control the pressure.

The characterization of the produced particles is carried out with an SMPS measurement system, by TEM image analysis and by BET surface analysis.

A first example of a follow-up research project is the manipulation of the aggregation structure downstream of the sintering process by charging particles with opposite polarities. Therefore two parallel coaxial corona chargers that can handle high flow rates and concentrations have been designed. As corona emitting source a 0.1 mm wolfram wire is used. The length of the two active corona zones is adjustable independently from each other by shielding the corona wires with a movable glass pipe.

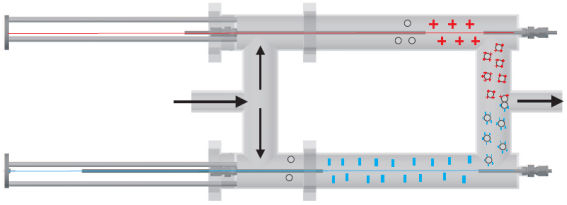

Figure 1. Designed parallel coaxial corona chargers.

The chargers are implemented downstream of the heat exchanger with opposite polarities. This offers the possibility to manipulate the agglomeration process hence the final agglomerate shape. In the focus of interest are especially chain-like aggregates with alternating sequence of different materials. To realize the chain shape, the coagulation process needs to be faster than the neutralization by recombination in the contact point, cf. Fig. 2.

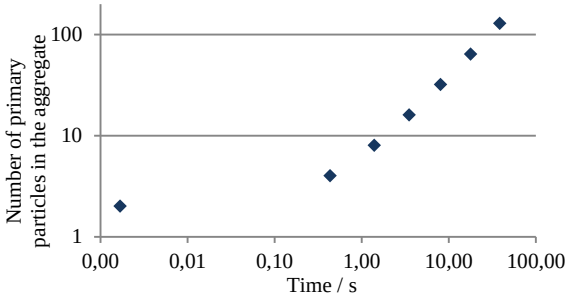

Figure 2. Coagulation time of charged 100 nm particles with an initial particle concentration of $10^{14}/m^3$.

Controlling the Size of Singlet Nanoparticles in Spark Ablation

J. Feng, G. Biskos and A. Schmidt-Ott

Department of Chemical Engineering, Delft University of Technology, 2628 BL, Delft, Netherlands

Keywords: nanoparticle production, coagulation, coalescence, atomic cluster.

Microsecond-pulsed spark ablation at atmospheric pressure is a versatile and environmentally friendly method for producing agglomerated mixtures of ultrapure inorganic nanoparticles (NPs). Here we show that the method can also be employed for synthesizing non-agglomerated singlet NPs with variable and controllable sizes down to the nanometer and atomic cluster range, where material properties are strongly size dependent. Using Au as a test material, we demonstrate that the technique can produce singlet particles having diameters in the sub-5 nm range at room temperature. In principle, larger singlets can be produced by increasing the process operating temperature. However, for spark ablation, a model that relates particle size to process variables remains absent. Here, we develop a simple analytical model to estimate the size of the resulting singlets as a function of the process conditions. The model, together with mixing capabilities and ultrapure production of spark ablation, provides a means of unprecedented versatility towards cost-effective nanofabrication on an industrial scale.

In this method, repeated sparks with 1 to 25 kHz frequency initiated between two electrodes produce vapor clouds (Pfeiffer *et al*., 2014), which are quenched and carried away by a high-purity gas flow. The vapor clouds are adiabatically expanded and rapidly cooled down to the carrier gas temperature, after which the vapor became supersaturated, resulting in homogenous nucleation and condensation to form NPs. The newly formed nuclei undergoes a coagulation growth process with complete coalescence up to a critical size, which is essentially the primary particle embedded in the agglomerates. If growth proceeds beyond the critical size, sintering only partly occurs or ceases to form agglomerated particles, below which coalescence is complete to form the non-agglomerated singlets (see Figure 1).

An analytical model is developed to describe the complete coalescence of singlets under the assumption of negligible diffusional losses:

$$d_{\mathrm{p}} = \left(\frac{3\beta V_{\mathrm{eff}}\dot{m}}{\rho\pi Q^2}\right)^{1/3} \qquad (1)$$

where d_{p} is the size of sinlets, β the coagulation coefficient, V_{eff} the effective volume corresponding to the portion of the confinement, Q the gas volumetric flow rate, ρ the material density, $\dot{m}$ the mass production rate. The concept presented in this work, where coalescence is induced in the particle growth phase, is only limited by the mass production rate of spark ablation. Considering that mass production rate of 1 g h^{-1} is feasible, the concept can lead up to about 1,000 times higher particle production rate than the commonly used post processing techniques (Pfeiffer *et al*., 2014). Additionally, the possibility of numbering up the generators can further increase the desired particle production rate (Charitidis et al. 2014).

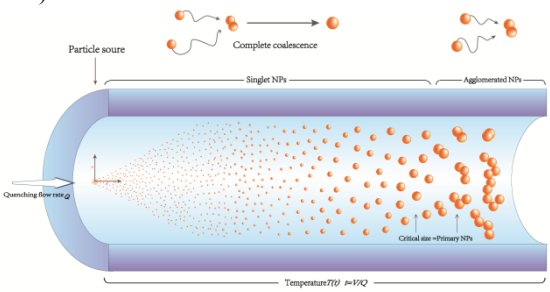

Figure 1. Schematic representation of the formation of singlet and agglomerated nanoparticles resulting from material ablation under atmospheric pressure gases.

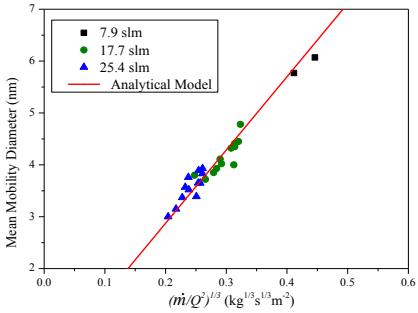

Figure 2. Mean mobility diameter vs. mass production rate and flow rate.

Figure 2 shows the variation of the mean size with the term $\left(\frac{\dot{m}}{Q^2}\right)^{1/3}$, which according to Equation 1 is linear. The product βV_{eff} derived from this slope is 5.78×10^{-20} m^6 s^{-1}, in good agreement with the theoretical value of β and an estimate V_{eff} from the geometry of the confinement.

The research leading to these results has received funding from the European Union's Seventh Framework Program under Grant Agreement No. 280765 (BUONAPART-E).

Pfeiffer, T. V., Feng J. & Schmidt-Ott A. (2014). *Adv. Powder Technol.*, 25, 56-70.

Charitidis, C. A., Georgiou, P., Koklioti, M. A., Trompeta, A. F. & Markakis, V. (2014) *Manufacturing Rev.*, 1, 1-19.

Correction method for SMPS measured particle size distributions with high number concentrations at the upper size limit

H. Kaminski, B. Stahlmecke, C. Asbach and T.A.J. Kuhlbusch

Institut für Energie- und Umwelttechnik, Bliersheimer Straße 58-60, 47229, Duisburg, Germany

Keywords: Aerosol Measurement, Electrical Mobility, SMPS

The measurement of the number size distribution of airborne particles in the size range from approximately ten nanometer up to one micrometer is usually conducted through electrical mobility analysis. The correct measurement of particle size dependent number concentrations with these instruments relies on the known charge distribution of the particles in conjunction with an algorithm to correct the obtained mobility distributions for multiply charged particles. For the most commonly used Scanning Mobility Particle Sizer (SMPS) the multiple charge correction (MCC) is realised by using a pre-separator at the instrument's inlet to fulfil the prerequisite of only singly charged particles in the highest size channels.

The standard MCC works well if the highest size channels contain no or just a few particles. If this is not the case, e.g. because of the use of an inappropriate impactor or the necessity to work without an impactor at all, MCC leads to an over-correction and thus faulty concentration data for the lower size channels.

To overcome this limitation we developed an extension of the standard MCC based on spreadsheet software and applied it successfully for the measurement of particle number size distributions (PNSD) with high particle concentrations at the upper size limit. The measurements were conducted using a TSI SMPS (model 3936) with long-DMA (model 3081) for a size range from 34 nm up to 1,000 nm without the application of an impactor.

This manual MCC is based on the assumption that the particle number size distribution to be measured follows a unimodal lognormal size distribution and that the mode diameter is within the measurement range of the SMPS. In this case, the mobility distribution of singly charged particles is also lognormal and can hence be extrapolated to complete the lognormal distribution. The manual MCC is carried out by using the principle introduced by Hoppel (1978) along with the Wiedensohler (1988) and Fuchs (1963) charge approximation with following assumptions: 1. the formulae are valid for the size range above 1,000 nm and 2. the charge behavior of the particles is similar to that of spheres.

Figure 1 shows as an example a titanium dioxide PNSD without correction, with standard MCC and with manual MCC. The blue curve shows the original SMPS measurement without MCC (transformed mobility distribution with the assumption that particles are only singly charged). The red curve is calculated based on the standard MCC implemented in the instrument's software AIM (version 8.1). Due to this MCC and the unfulfilled prerequisite of low particle numbers at the upper size range correction errors occur. This leads to the local maxima and minima within the size distribution. The dashed green curve shows the artificial lognormal extension of the measured data and the light blue curve the size distribution after manual MCC.

To check whether the size distribution after manual MCC represents the correct PNSD, an optical spectrometer (Palas Welas® 2000) was simultaneously used as an independent instrument based on a completely different measurement principle. The Welas® data (magenta curve) shows very good agreement with the manual MCC corrected SMPS data as one can see in Figure 1.

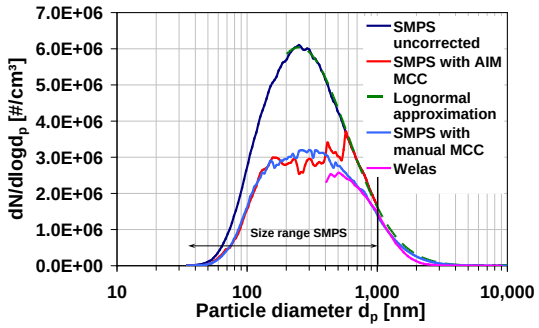

Figure 1. Comparison of measured size distribution data after standard MCC and manual MCC.

In the presentation we will discuss the rationale, possibilities and limitations of the manual MCC and show examples based on measurements with spherical particles (DEHS) and on measurements of several different aerosolised nanopowders.

This work was supported by the German Ministry for Education and Research (BMBF) within the nanoGEM project (grant no. 03X0105A) and by the EU seventh framework program within the MARINA project (grant no. 263215).

Hoppel, W.A. (1978), *J. Aerosol Sci.*, 9, 41-54.

Wiedensohler, A. (1988), *J. Aerosol Sci.*, 19, 387-389.

Fuchs, N.A (1963), *Geophysica Pura e Applicata*, 56, 185-193

Cyclone separator sampler for combustion aerosol: modelling and laboratory experiments

F. Mylläri[1], A. Karvinen[2], P. Karjalainen[1], J. Maunula[3], P. Janhunen[4], H. Ahlstedt[2], J. Keskinen[1] and T. Rönkkö[1]

[1]Department of Physics, Tampere University of Technology, 33101, Tampere, Finland
[2]Department of Mechanical Engineering and Industrial Systems, Tampere University of Technology, 33101, Tampere, Finland
[3]Valmet Power, Tampere, Finland
[4]Metso Automation, 87101, Kajaani, Finland

Keywords: aerosol sampling, high temperature, cyclone separator, computational fluid dynamics, particle losses.

Combustion aerosol consists of different sized particles: coarse and fine particles, as well as gaseous components. Coarse particles dominate the particle mass concentration and, thus can disturb the chemical analyses made for the collected sample. To achieve better resolution for the fine particle chemical analyses the coarse particles are separated from the sample by the cyclone implemented to the sampler. The sampler is designed to collect the fine particles and also the gaseous components to gas or liquid medium for further studies.

The sampler consists of a sample tube and a cyclone, which is designed to extract sample from the flue gas of power plant boilers. The sample is taken to the cyclone through a curved inlet. The inlet sample flow and the cyclone are driven by an ejector, placed inside the cyclone. The cyclone separates the larger particles from the smaller ones due to their inertia. The smaller particles are collected from the core region whereas the larger ones are blown out of the cyclone by the ejector.

The sampler was studied by computational simulations and measuring in a laboratory-scale test bench. The laboratory measurements were made with an Electrical Low Pressure Impactor (ELPI) containing sintered collection plates. The studied particle size range was 110-10000 nm. The measurement size range of ELPI was adjusted due to the test aerosol (standard test dust by Particle Technology) grain size, 500-10000 nm. The test aerosol was generated with a dust disperser (Palas GmbH PGB 1000).

The sampler was tested at three different temperatures and with five different ejector flows. In addition to laboratory tests, the sampler was modelled in two stages. At first, the gas flow was simulated with computational fluid dynamics (CFD). Secondly, the motion of the particles was simulated using the discrete element method (DEM). The calculation platform was OpenFOAM 2.2.x and computational grids were constructed using so called cutcell-method (snappyHexMesh). Three different computational grids were tested: fine, normal and coarse. Fine and coarse grids were tested once, and majority of the simulations were made with the normal grid.

Based on the simulations, the ejector mass flow was the most crucial factor in terms of penetration efficiency of the particle through the cyclone. Higher ejector flows lowered the amount of particles in the sample. In addition to ejector flow, also, the particle density and inlet temperature had effect on the penetration efficiency of the particles to the sample.

Experimental results showed that the D50% values for the cyclone were from 1-4 µm depending on the ejector flow and inlet temperature. The higher the temperature and faster the ejector flow the better the cyclone sampler works. Figure 1 shows the experimental and computational results for the cyclone separator sampler.

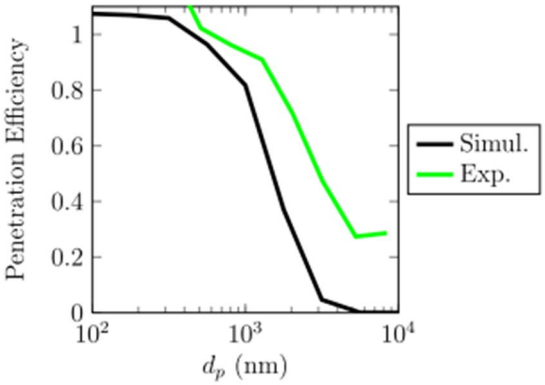

Figure 1. Penetration efficiency of the particles through sampler by simulation and experiments at 800 °C. Simulation case: ejector mass flow 2.5 kg/s, particle density 1000 kg/m^3. Measurement case: ejector flow 20 slpm, which corresponds to the ejector flow used in simulations.

This work was conducted in MMEA research program supported by Tekes (the Finnish Funding Agency for Innovation) and coordinated by the CLEEN Ltd.

DENSMO: A straightforward on-line quality monitor for nanoparticle manufacturing processes

Paxton Juuti[1], Anssi Arffman[1], Antti Rostedt[1], Juha Harra[1], Jyrki M. Mäkelä[1] and Jorma Keskinen[1]

[1]Aerosol Physics Laboratory, Department of Physics, Tampere University of Technology, Tampere, Finland

Keywords: effective density, electrostatic precipitator, slit impactor.

When producing nanoparticle based materials, whether it is a colloid, a powder or a nanoparticle coated surface, it is especially important to monitor the size and morphology of the aerosol particles as the process is running. This is true for all production lines, but is paramount when the performance of the material is strongly dependent on these parameters. Usually the quality of the produced material is tested from the final product using off-line methods or a combination of expensive on-line aerosol instrumentation (Ristimäki et al., 2002). Neither of these methods produce information without the need of post processing of the measured data.

Here, we present simplified standalone version of the measurement device introduced by Rostedt et al. (2009), DENSMO (abbreviated from density monitor). The device is capable of measuring simultaneously aerodynamic and mobility diameters and the total number concentration of an aerosol particle size distribution as well as calculate the effective density with a time resolution of one second.

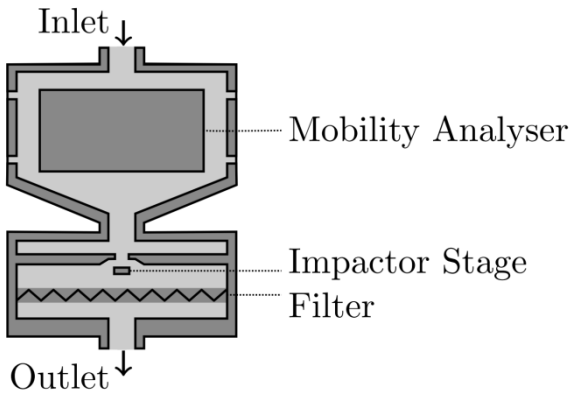

Figure 1. Cross section of the instrument and the labelled collection regions.

DENSMO functions by charging aerosol particles with a corona charger and then subsequently measuring that charge after it has been collected in one of three separate regions. The first one is an electrostatic precipitator, which characterizes the inbound aerosol distribution based on the mobility diameter. The second one is a low pressure slit impactor (Arffman et al., 2012), which collects aerosol particles based on their aerodynamic diameters. Lastly, any aerosol particle that has not been collected in the previous regions is deposited on a filter. A schematic cross section of the device is depicted in Figure 1.

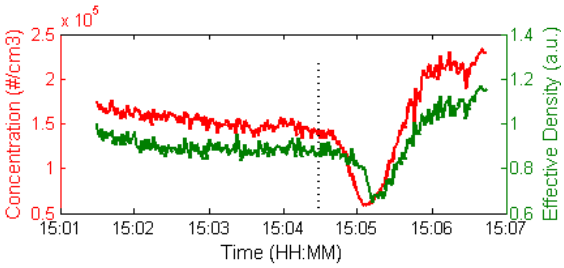

Figure 2. Measurement results from an intentionally disturbed (at the dotted line) nanoparticle production.

DENSMO is best suited for monitoring production lines, which are designed to produce certain kind of aerosol particles over long periods of time. In Figure 2, a stable production setup has been intentionally disturbed and its effect on the effective density and the total number concentration can be clearly seen. In this case, the drop in both of these values happen in less than a minute, which can only be seen due to the fact that there is measurement data with a time resolution of one second.

This research and the results produced by it have received funding from the European Union's Seventh Framework Programme under Grant Agreement n°280765 (Buonapart-E).

Arffman, A., Yli-Ojanperä, J., Keskinen, J. (2012). The influence of nozzle throat length on the resolution of a low pressure impactor, -- An experimental and numerical study. *J. Aerosol Sci. 53*, 76-84.

Ristimäki, J., Virtanen, A., Marjamäki, M., Rostedt, A., Keskinen, J. (2002). On-line measurement of size distribution and effective density of submicron aerosol particles. *J. Aerosol Sci., 33*, 1541-1557.

Rostedt, A., Marjamäki, M., Keskinen, J. (2009). Modification of the ELPI to measure mean particle effective density in real-time. *J. Aerosol Sci., 40*, 823-831.

Deposition of silver nanoparticles on carbon nanotube arrays

Eleftheria Roumeli[1], Juha Harra[1], Paxton Juuti[1], Mari Honkanen[2], Chiara Daraio[3] and Jyrki M. Mäkelä[1]

[1]Department of Physics, Tampere University of Technology, Tampere, Finland
[2]Department of Materials Science, Tampere University of Technology, Tampere, Finland
[3]Department of Mechanical and Process Engineering, Swiss Federal Institute of Technology, Zurich, Switzerland

Keywords: silver nanoparticle, carbon nanotube, particle deposition, electrostatic precipitator.

The exceptional electronic, mechanical and thermal properties of carbon nanotubes (CNTs) have inspired academic and industrial research to find ways to integrate them in robust and diverse applications. Utilizing macroscopic CNT-based structures, including mats, fibers and foams, and incorporating other nanoparticles in these structures is a rather promising method to efficiently combine high-performance building blocks to get superior hybrid materials (Georgakilas *et al.*, 2007).

The incorporation of nanoparticles in CNT-structured matrices has been mainly obtained through wet chemistry strategies. However, they usually require tedious procedures and end up altering the electronic properties of CNTs. In this study, we used a facile dry physical deposition method to prepare silver (Ag) nanoparticle-decorated CNT arrays which could be used, for example, in antibacterial applications (Akhavan *et al.*, 2011).

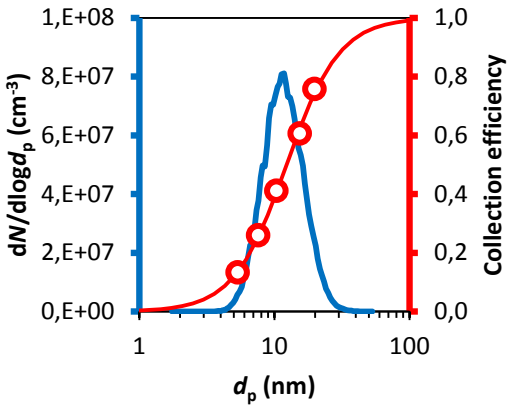

Figure 1. The number size distribution of the generated Ag nanoparticles (blue line) measured with the SMPS and the particle collection efficiency of the system (red markers).

The CNT arrays used in this study were synthesized in a chemical vapor deposition system with floating catalyst (Raney *et al.*, 2011). Ag aerosol nanoparticles with diameters of approximately 10 nm were generated through an evaporation–condensation method (Harra *et al.*, 2012). Figure 1 shows the particle number size distribution (blue line) measured with a scanning mobility particle sizer (SMPS). After generation, the nanoparticles were charged with a small corona charger introduced by Arffman et al. (2014), and collected on top of the CNT arrays using an electrostatic precipitator. The particle collection efficiency of the used system (red markers) is presented in Fig. 1. A collection efficiency of 50 % was achieved for particles with a diameter of 12 nm.

Figure 2 shows a scanning electron microscopy (SEM) image of the surface of a CNT array with deposited Ag nanoparticles. The inset in figure shows an individual CNT, with a thickness of approximately 100 nm, coated uniformly with nano-sized Ag particles. The homogeneous distribution of the Ag nanoparticles on the surface of the CNT array was further confirmed with elemental mapping.

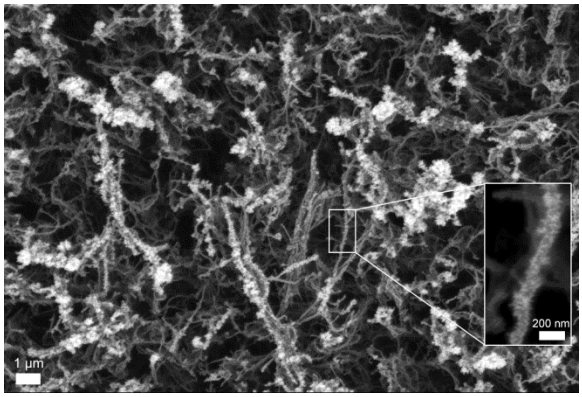

Figure 2. An SEM micrograph from the surface of an Ag-decorated CNT array. The inset shows a higher magnification of an individual decorated CNT.

J. Harra acknowledges the TUT's graduate school for financial support.

Akhavan, O., Abdolahad, M., Abdi, Y., & Mohajerzadeh, S. (2011). *J. Mater. Chem.*, 21, 387–393.

Arffman, A., Yli-Ojanperä, J., Kalliokoski, J., Harra, J., Pirjola, L., Karjalainen, P., Rönkkö, T., & Keskinen, J. (2014). *J. Aerosol Sci.*, 78, 97–109.

Georgakilas,V., Gournis, D., Tzitzios, V., Pasquato, L., Guldie, D.M., & Prato, M. (2007). *J. Mater. Chem.*, 17, 2679–2694.

Harra, J., Mäkitalo, J., Siikanen, R., Virkki, M., Genty, G., Kobayashi, T., Kauranen, M., & Mäkelä, J.M. (2012). *J. Nanopart. Res.*, 14, 870.

Raney, J.R., Misra, A., & Daraio, C. (2011). *Carbon*, 49, 3631–3638.

Design and characterisation of a probe for particle sampling in boilers of waste incineration plants

S. Schumacher[1], J. Lindermann[1], B. Stahlmecke[1], T. Zeiner[1], T. van der Zwaag[1], H. Nordsieck[2], R. Warnecke[3], and C. Asbach[1]

[1]Institut für Energie- und Umwelttechnik e.V. (IUTA), Duisburg, Germany
[2]bifa Umweltinstitut GmbH, Augsburg, Germany
[3] GKS Gemeinschaftskraftwerk Schweinfurt GmbH, Schweinfurt, Germany

Keywords: Waste incinerator, particle sampling, probe design, computational fluid dynamics

The particle phase in the flue gas of waste incineration plants has been under intense investigation for many years and is not yet fully characterised. A special interest is focused on chlorine-containing particles with diameters between approximately 1 and 25 µm, which are assumed to essentially contribute to corrosion in the boilers. In former works, the aerosol was usually exhausted from the boiler followed by dilution and cooling, in order to make it available for conventional aerosol measurement techniques [Deuerling2010]. However, at high temperatures this method involves tremendous artefacts by condensation of salt vapours during the cool-down. To prevent those artefacts, dilution factors of more than 10^7 would be required, which make the particle concentration immeasurably small.

Within the frame of the project VOKos we developed a probe, which allows collection of the particles on sample substrates in the hot zones of a waste incineration boiler.

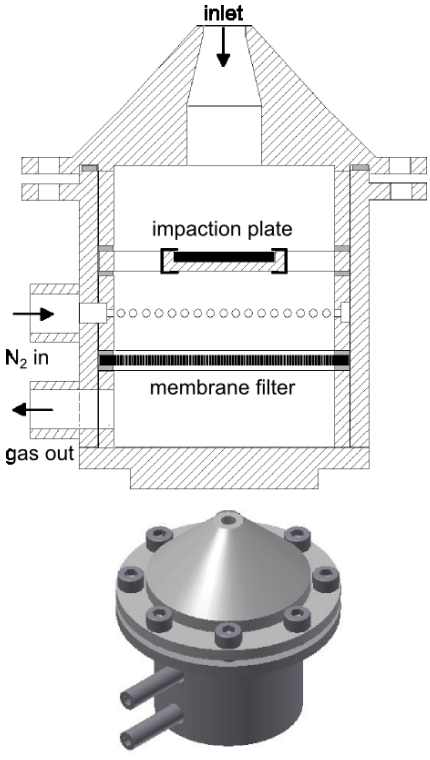

Figure 1: Cross section and model of the probe.

The probe consists of two stages: Firstly, larger particles are sampled on an impaction plate with 40 µm cut-off. Secondly, the remaining smaller particles are collected on a metallic membrane filter with well-defined pore size and arrangement. Together, a broad particle size range from a few nanometres up to several 100 µm is covered. The residence time of the probe inside the boiler is kept short to reduce potential reactions of the sampled material. In addition, the probe is flushed with an excess of clean nitrogen heated to the sampling temperature before and after sampling, which on the one hand avoids condensation of salts and post-reactions and on the other hand facilitates well defined sampling times.

Both types of substrates are well-suited for scanning electron microscopy (SEM), which provides a comprehensive investigation of the morphology and chemical properties of single particles. Using computational fluid dynamics (CFD) the collection efficiencies of the impactor as well as of the membrane filter were studied in detail. Based on that, a data evaluation strategy has been developed which allows to deduce the airborne particle number and mass size distributions from counting the collected particles in SEM.

The sampling probe was manufactured from corrosion resistant materials and successfully tested in a waste incineration plant. First results show that our method yields a reliable and efficient way for particle collection in waste incineration boilers. The design and characterisation of the probe will be presented along with first results from field measurements.

This work was supported by the Federal Ministry of Education and Research (BMBF) within the project VOKos (Grant No 03X3589).

Deuerling, C.F. et al. (2010): *Aerosol Sci. Technol.* **44**: 1

Detection of highly condensable aerosol precursors from oxidation of aromatic compounds

O. Garmash, M. P. Rissanen, O. Kausiala, M. Kulmala, M. Sipilä and M. Ehn

Department of Physics, University of Helsinki P.O. Box 64, 00014 Finland

Keywords: anthropogenic VOC, nano-clusters, mass spectrometry, atmospheric aerosols.

Volatile organic compounds (VOC) are a group of molecules emitted from both biogenic and anthropogenic sources. In the atmosphere, VOCs get oxidised (initiated by the reaction with hydroxyl radical, ozone and nitrate) and form condensable vapours that contribute to secondary organic aerosol (SOA) formation (Jimenez *et al.*, 2009; Ziemann & Atkinson, 2012).

Anthropogenic VOCs are most significant in urban areas and near industrial sites as they are emitted predominantly from biomass burning, fuel refineries and vehicle exhaust. Aromatic organic compounds are known to constitute up to 20% of non-methane organic compounds in urban air, being mostly $C_{7\text{-}10}$ molecules (Calvert *et al.*, 2002; Velasco *et al.*, 2007).

Recently, previously unidentified highly-oxidised molecules were discovered by Ehn *et al.* (2012 & 2014) from the reaction of monoterpenes (VOC emitted by a boreal forest) with ozone and hydroxyl radical. Due to the high mass and level of oxygenation of these compounds, they were titled extremely- low volatility organic compounds (ELVOC), and are likely to play a major role in initial growth of nano-clusters. ELVOC formation was also observed in oxidation of other alkenes such as cyclohexene and methyl-cyclohexenes (Rissanen *et al.*, 2014 & 2015).

In this study, we investigated the formation of ELVOC from oxidation reaction of benzene, toluene and naphthalene. This is of great importance for assessing the SOA forming potential of anthropogenic emissions. Toluene and benzene are among the dominant aromatic compounds found in fuels and their combustion exhaust gas.

Oxidation experiments were performed in a 2.5 litre flow tube reactor at atmospheric pressure and laboratory-maintained temperature of 24°C. Water was fed into the reactor by bubbling nitrogen through a Milli-Q water reservoir. It was photolysed at 184.9nm using a mercury UV lamp with a low-pass filter to form hydroxyl radicals (OH). Precursor VOC was introduced into the flow by bubbling nitrogen through a vial filled with the liquid sample. Due to the high vapour pressures of the studied compounds, the flow could be assumed saturated. The residence time in the reactor was approximately 10 seconds.

The products were detected using a high-resolution chemical ionisation atmospheric pressure interface mass spectrometer (CI-APi-TOF, Tofwerk AG, Switzerland). In detail, the instrument is described by Jokinen *et al.* (2012). Chemical ionisation is a soft ionisation method which can be used to avoid the fragmentation of the big molecules. We used nitrate ion (NO_3^-) oxidation scheme.

ELVOCs were observed from the oxidation of all three investigated compounds. The products of the oxidation were identified using tofTools software (Junninen *et al.*, 2010) and were concluded to be seen for the first time (Master Chemical Mechanism, University of Leeds). The detailed results will be presented in the conference.

There are still a discrepancies in the SOA yield measurements from oxidation of aromatic compounds, e.g. for toluene (Hildebrandt *et al.*, 2009). Understanding the initial steps of new particle formation, potentially involving ELVOCs, will help to predict SOA yields from e.g. combustion processes with higher accuracy, and also, give us a tool towards understanding the differences reported in the literature. The results from this study can be utilised further to understand anthropogenic influence on new particle formation in urban areas and global climate.

Calvert, J.G. *et al.* (2002). Oxford University Press, New York.

Ehn, M. *et al.* (2012). *Atmos. Chem. Phys.*, 12, 511.

Ehn, M. *et al.* (2014). *Nature*, 506, 476.

Jimenez, J. L. *et al.* (2009). *Science*, 326, 1525.

Jokinen, T. *et al.* (2012). *Atmos. Chem. Phys.*, 12, 4117.

Junninen, H. *et al.* (2010). *Atmos. Meas. Tech.*, 3, 1039.

Hildebrandt, L. *et al.* (2009). *Atmos. Chem. Phys.*, 9, 2973.

Rissanen, M. *et al.* (2014). *J. Am. Chem. Soc.*, 136, 15596.

Rissanen, M. *et al.* (2015). *J. Phys. Chem. A.*, Article ASAP.

Velasco, E. *et al.* (2007). *Atmos. Chem. Phys.*, 7, 329.

Ziemann, P. J. & Atkinson, R. (2012). *Chem. Soc. Rev.*, 41, 6582.

Development of a technology for online measurement of total and water-soluble copper (Cu) in ambient PM

Dongbin Wang[1], Martin M. Shafer[2], James J. Schauer[2] and Constantinos Sioutas[1]

[1] Department of Civil and Environmental Engineering, University of Southern California, Los Angeles, CA, 90089, USA

[2] Environmental Chemistry and Technology Program, University of Wisconsin, Madison, WI, 53718, USA

Keywords: Online Cu measurement, cupric ISE, Aerosol-Into-Liquid Collector, modified BioSampler.

A novel monitor for online unattended, in-situ measurement of total/water-soluble Cu of ambient PM was developed. For PM2.5, a high flow rate Aerosol-Into-Liquid Collector (Wang et al. 2013) was deployed to collect PM directly as concentrated aerosol slurry samples. For coarse PM, two virtual impactors combined with a modified liquid impinger (BioSampler) were used as the particle-into-liquid collection module. The Cu concentration in slurries is determined by a Cu Ion Selective Electrode (ISE).

Laboratory tests were conducted to evaluate the performance of the Cu ISE. The calibration curve of the Cu ISE was determined using $Cu(NO_3)_2$ standard solutions prepared by serial dilution, with the concentration ranges from 10 ppb to 1000 ppb. Figure 1 presents a typical calibration curve of the Cu ISE obtained in these tests. Meanwhile, the effect of ionic strength, temperature and pH of the slurries to the Cu ISE measurement were also evaluated (Rundle, 2006).

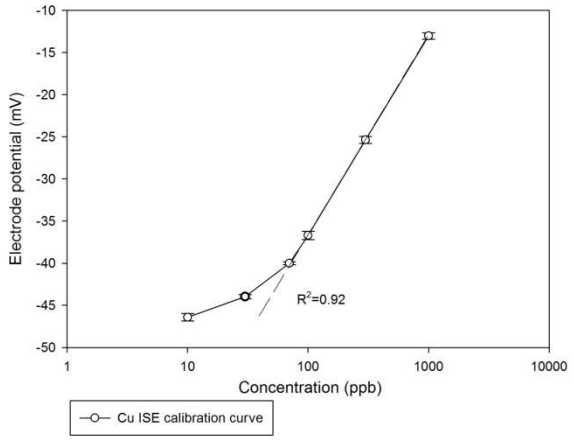

Figure 1. Calibration curve of Cu ISE.

The Cu ISE measurement accuracy was also evaluated using Cu particles generated by atomizing solution of $Cu(NO_3)_2$ with a constant output nebulizer. The generated particle was collected by the Aerosol-Into-Liquid Collector and the size distribution and total volume of the generated particle were determined by Scan Mobility Particle Size (SMPS). The mass concentration of the generated particle was calculated by multiplying the total particle volume obtained from the SMPS scan with the density of $Cu(NO_3)_2$. The Cu concentration in collected slurries was also measurement by the Cu ISE. Generally the agreement between the theoretical value from calculation and measured value from ISE is very good, indicating the excellent overall measurement accuracy of the Cu ISE. Results of these tests are presented in Figure 2.

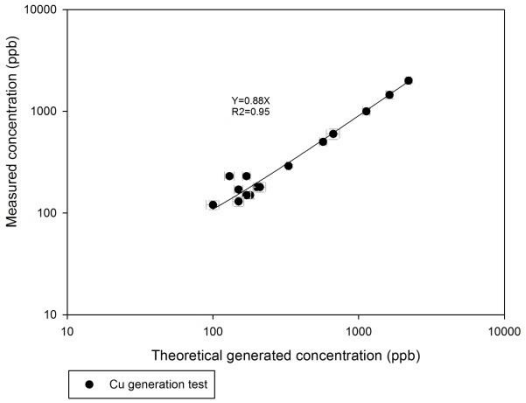

Lastly, the whole system was deployed in the field and ambient PM samples were collected both in the new system and on filter substrates to validate that the Cu compositions of suspension samples measured by Cu ISE are equivalent to those from ICPMS analysis. Very good agreements for total and water-soluble Cu concentrations were obtained for both $PM_{2.5}$ and coarse PM Cu monitor. Moreover, the field tests indicated that the Cu monitor could achieve near-continuous collection and measurements for at least 4-7 consecutive days without obvious shortcomings. These results suggest that it is an effective technology for characterization of Cu in ambient PM.

Rundle, C.C., (2006). *Beginner guide to ISE measurements*, Nico 2000 Ltd, London, UK.

Wang, D., Pakbin, P., Saffari, A., Shafer, M. M., Schauer, J. J., & Sioutas, C. (2013). Development and Evaluation of a High-Volume Aerosol-into-Liquid Collector for Fine and Ultrafine Particulate Matter. Aerosol Science and Technology, 47(11), 1226-1238.

Differential mobility analysis of soot nuclei in a laminar C2H4/air premixed flame

F. Carbone[1], M. Attoui[2] and A. Gomez[1]

[1]Department of Mechanical Engineering and Materials Science, New Haven, 06477, CT, USA
[2]Department of Physic, University Paris-Est Creteil, University Paris-Diderot, LISA, UMR CNRS 7583, France

Keywords: Soot, Nucleation, Mobility, Sampling.

Sampling followed by High-resolution Differential Mobility Analysis (DMA) of nascent soot was performed in a moderately sooting, burner-stabilized ethylene/air premixed flame with a C/O ratio of 0.69 and unburnt gas velocity of 5.87cm/s. The goal was to shed light on the still poorly understood soot inception stage using a Half-Mini type nano-DMA and a horizontal rapid dilution probe to focus on the gas-to-particle transition dimensional range (≤30nm). The flame was characterized also in terms of temperature and soot load by performing thermocouple and light extinction measurements, respectively.

Particles with positive and negative polarity, either naturally charged or neutralized by a bi-polar diffusion charger, were measured at several heights above the burner, corresponding to different residence time into the flame, and applying different dilution ratios. Some of the measured mobility diameter (MD) distribution functions are shown in fig. 1 and 2 for self-charged and neutralized aerosols, respectively. The first clearly identifiable nuclei were observed, both in the self-charged and neutralized samples, to have mobility diameters (MD) of approximately 2nm at HAB=7.5 mm. Some molecular clusters with MD=1.25nm can be already detected at HAB=5mm but their contribution to the signal in the neutralized sample can be only tentatively distinguished from that of the ions generated in the bipolar diffusion charger. When the neutralizer is used, the nuclei preferentially get a negative charge and the negatively charged nuclei appear to have multiple peaks in the size distribution function.

As expected, the average particle size increases as the sampling position is moved further downstream in the flame, resulting in an approximately lognormal distribution for sizes exceeding 5nm, which indicates that such particles are generated by coagulation of smaller ones. The presence of the nuclei in the neutralized aerosol persists even when the larger particles have been formed, suggesting that particle nucleation may still be active in the coagulation region. Nonetheless, in this region, the smallest particles cannot be detected within the naturally charged aerosol because of the low signals measured for those samples and of the higher efficiency that larger particles have in capturing the available charge.

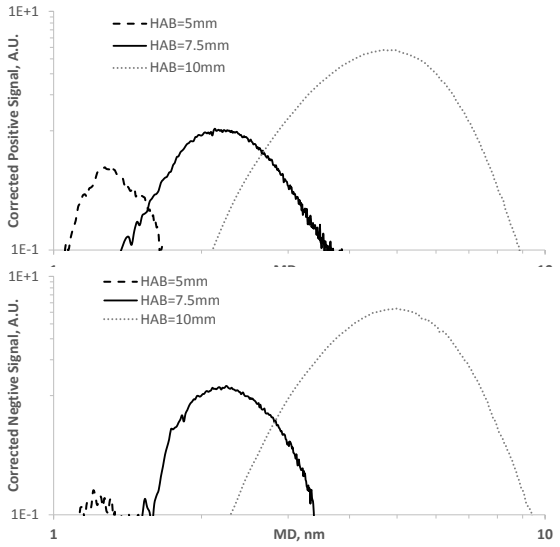

Figure 1. Mobility diameter distribution functions of positive (top) and negative (bottom) self-charged particles.

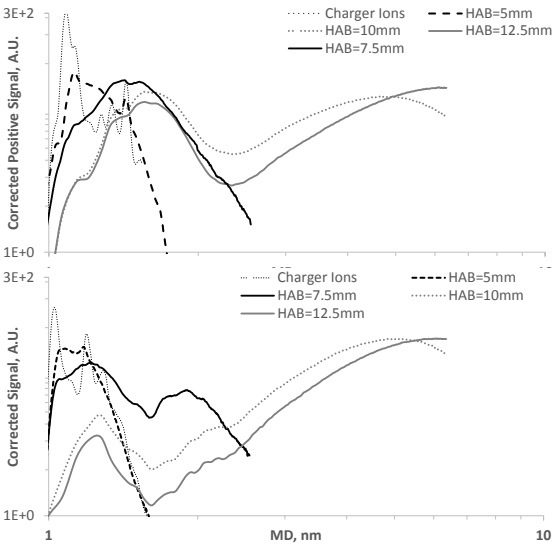

Figure 2. Mobility diameter distribution functions of neutralized particle with positive (top) and negative (bottom) charge.

Dose determination in the Air-liquid interface exposure of cell cultures for in vitro toxicological studies

S. Mülhopt[1*], T. Krebs[2] and H.-R. Paur[1]

[1]*Institute for Technical Chemistry, Karlsruhe Institute of Technology, 76021 Karlsruhe, Germany*
[2]*VITROCELL Systems GmbH, 79183 Waldkirch, Germany*
**Corresponding author: muelhopt@kit.edu*

Keywords: nanoparticle, aerosol exposure, lung toxicity.

Despite numerous efforts to reduce the ambient air concentrations of fine particles by improved combustion and filter technologies, the health effects due to inhalation of ultrafine particles are still the most important problem in environmental health.

The on-line characterization of physico-chemical properties of combustion derived particles has progressed by application of novel particle sizers and mass spectrometry. The assessment of health effects is still conducted by epidemiology or costly animal experiments. Characterization of biological effects of ultrafine particles to human cells by in-vitro studies, with particle extracts induces numerous artifacts during sampling, extraction, dose determination and biological testing, all of which renders the results derived hardly reproducible. The application of air-liquid interface exposure of human lungs cells to characterize the biological effects of combustion aerosols will avoid many of the pitfalls of the previous method (Paur et al., 2011).

For the reproducible assessment of lung toxicity of airborne particle emissions from combustion processes the Karlsruhe Exposure System was developed as described in detail before (Mülhopt *et al.*, 2007). In this fully automatic system cell cultures (A549, BEAS-2B) grown on porous membrane inserts, which are in contact with nutrient medium, are exposed directly to diluted aerosol from different particle sources. For the interpretation of the biological endpoints the applied dose on the cell culture surface is necessary. Simulating the breathing pattern in the lower lung region low gas velocities of less than 0.01 m/s are used in the air-liquid interface exposure. Therefor the submicron particles only deposit by diffusional processes and the deposition efficiencies in the range of 1 – 2 % percent of the exposed aerosol.

To determine small doses in the range of ng/cm² two dosimetry methods were developed by KIT Institute for Technical Chemistry: the fluorescein sodium dosimetry (Mülhopt, et al., 2007) and the online dose monitoring by quartz crystal microbalance (Mülhopt et al., 2009). By both methods the dose is determined over the whole particle collective. As the diffusional behaviour of airborne particles strongly depends on the particle diameter a numerical simulation is performed using Comsol Multiphysics 4.4. The deposition efficiencies and therefore doses are calculated depending on particle diameter in the range of 10 nm to 1 µm. The results show a good agreement compared to the experimental data determined by fluorescein sodium dosimetry.

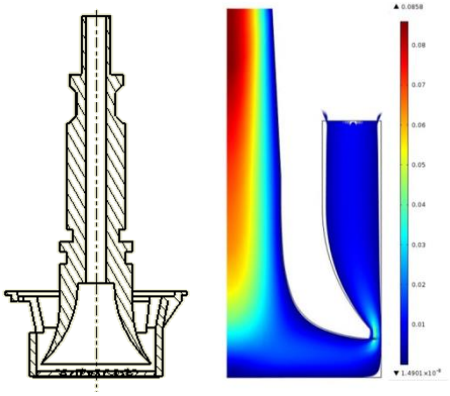

Figure 1. cross sectional view of the aerosol inlet above a cell culture membrane insert (left) and the particle trajectories of particles with a diameter of d_P = 100 nm passing it (right).

Additionally is shown how the deposition efficiency increases by the use of electrical forces depending on the electrical field. The results are compared with previous studies (Comouth *et al.*, 2013).

Comouth, A., Saathoff, H., Naumann, K.-H., Muelhopt, S., Paur, H.-R., & Leisner, T. (2013). *Journal of Aerosol Science*, 63, 103-114.

Mülhopt, S., Diabaté, S., Krebs, T., Weiss, C., & Paur, H.R. (2009). *Journal of Physics: Conference Series*, 170, S.012008/012001-012004.

Mülhopt, S., Paur, H.R., Diabaté, S., & Krug, H.F. (2007). *Advanced Environmental Monitoring.* Springer Netherlands: Dordrecht, 402-414.

Paur, H.-R., Cassee, F.R., Teeguarden, J., Fissan, H., Diabate, S., Aufderheide, M., Kreyling, W.G., Hänninen, O., Kasper, G., Riediker, M., Rothen-Rutishauser, B., & Schmid, O. (2011). *Journal of Aerosol Science*, 42, 668-692.

Drop fragments generated by bursting air bubbles on oil mist filters

S. Wurster[1], J. Meyer[1] and G. Kasper[1]
[1]Institut für Mechanische Verfahrenstechnik und Mechanik, Karlsruhe Institute of Technology (KIT), 76131 Karlsruhe, Germany

Keywords: mist filtration, coalescence filter, bubbling, fragment formation.

Oil mist, consisting of fine droplets mostly below 1 µm is generated in large amounts by various processes of industrial relevance, such as the movements of pistons in an engine crankcase, by oil lubricated air compressors, metal cutting tools and during natural gas extraction and processing. As the emission of oil aerosol into the environment is undesirable and therefore strictly regulated, machines are equipped with abatement devices, most commonly fibrous filters. The functioning of such air filters as capture devices for fine particles is generally well understood (Brown, 1993). In the case of droplet aerosols however, the accumulating liquid is transported by the air flow until it reaches the filter's rear face (Kampa et al. 2014). There it will either drain downwards or be re-entrained. The mechanisms responsible for causing droplet entrainment are a topic of current research.

One likely mechanism leading to the generation of a secondary droplet aerosol is due to the bursting of bubbles. In fact, the frequent formation of air bubbles (Figure 1) on the surface of mist filters has been observed for wettable or non-wettable media. Aerosol generation by bursting air bubbles has been investigated extensively for water (Cipriano, 1981; Resch, 1986; Blanchard, 1988) and it is well known that this mechanism can lead to the formation of multimodal spectra. However for oil practically no information is available with regard to break-up or the resulting drop spectra.

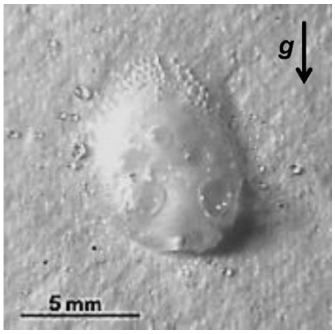

Figure 1: Bubbling on a draining oil drop on the surface of an oil mist filter medium. Fragment drops generated by collapsing bubbles are seen scattered around the drop.

An experimental set-up will be described to generate air bubbles of defined size, both on free liquid surfaces and on the surface of filter media. Bubbles were observed my photographic means, including high-speed camera to follow the process of growth, bursting and collapse.

It will be shown that the shape of the bubbles differs depending on whether they form on wettable or non-wettable mist filters. The viscosity of the oil also plays an important role during bubble formation, and especially during the bursting of a bubble with subsequent formation of oil droplet fragments. High-speed movies will show how bubbles break up, how the number of fragments generated per bubble depends on the oil viscosity, and also how the proportion of film drops resulting from the break-up of the bubble cap changes in proportion to the number of jet drops originating from the column of liquid ejected by the collapsing bubble. A final part of the presentation is dedicated to the direction(s) in which droplet fragments are ejected by bursting bubbles for oils (Figure 2).

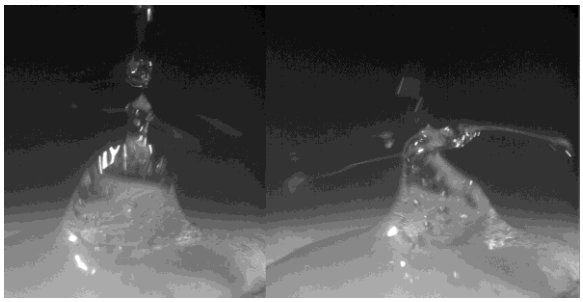

Figure 2: Direction of fragments from bubbles bursting on the surface of a mist filter.

Funding for this research was provided by Atlas Copco Airpower n.v. and by MANN+HUMMEL GmbH.

Blanchard, D. C. & Syzdek, L. D. (1988), *J. Geophys. Res. C:Oceans*, 93, 3649-3654.

Brown, R. C. (1993), *Air Filtration*. New York, USA: Pergamon Press.

Cipriano, R. J. & Blanchard, D.C. (1981), *J. Geophys. Res. C: Oceans*, 86, 8085-8092.

Kampa, D., Wurster ,S., Buzengeiger ,J., Meyer, J. & Kasper, G. (2014), *Int. J. Multiphase Flow*, 58, 313-324.

Resch, F. J., Darrozes, J. S. & Afeti, G. M. (1986), *J. Geophys. Res. C: Oceans*, 91, 1019-1029.

Dual-wavelength light scattering measurements for composition specific, single particle differentiation

Zs. Jurányi, E. Weingartner, M. Loepfe, M. Nenkov and H. Burtscher

Institute of Aerosol and Sensor Technology, University of Applied Sciences Northwestern Switzerland, 5210 Windisch, Switzerland

Keywords: light scattering, dual-wavelength, particle differentiation.

The method of analysing light pulses scattered from individual particles is a widely used aerosol measurement technique. For example, optical particle counters measure the particle number size distribution by determining the size and concentration of the individual particles based on their scattered light intensity.

At the University of Applied Sciences Northwestern Switzerland, a new method is being developed, which is similar to the method of optical particle counters with the vital difference that the measurement is conducted with two distinct different wavelengths of incident light. This allows to discriminate between different aerosol types with different optical properties.

The goal of the existing dual-wavelength light scattering setup is to be able to discriminate between water droplets, and other aerosols. For this discrimination, the specific optical properties of water are used. It is expected, that at the light absorption line of water, the scattering behaviour of water droplets is significantly different compared to other aerosols. Analysing the ratio of the scattered light at two specific wavelengths makes the envisaged particle differentiation possible.

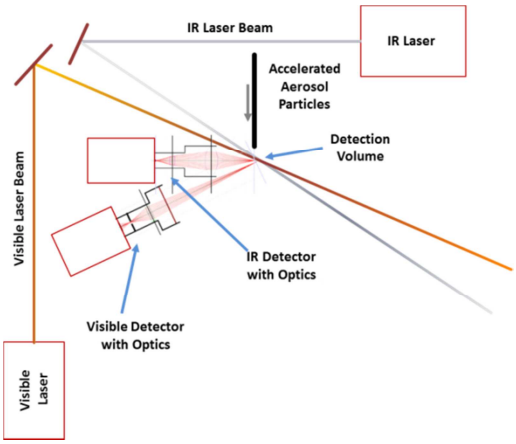

Figure 1. Drawing of the laboratory measurement setup

Theoretical calculations using the Mie theory assuming spherical particles showed that the ratios of the scattered light in the visible and at an infrared wavelengths with a backscattering angle of 150° is significantly different for water and non-water aerosol particles. An open measurement setup was built (see Figure 1) and the scattered light pulses at the two different wavelengths were measured simultaneously for single, well-defined, micrometer sized particles (such as cement, Arizona test dust and water droplets).

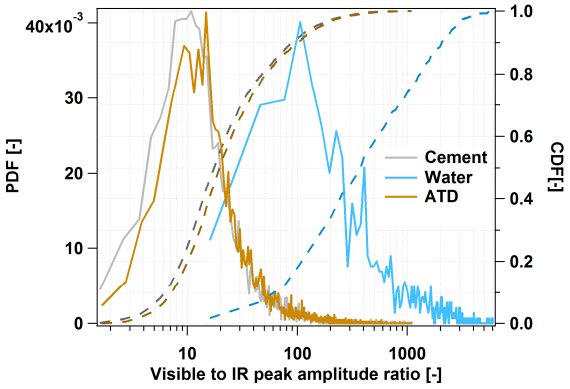

Figure 2. Probability distribution functions (left) and cumulative distribution functions (right) of the visible to IR peak amplitude ratio measured for Cement, Arizona Test Dust (ATD) and water droplets

Figure 2 shows the measured scattered light ratios (Visible to IR) for the different aerosol types. One can see that the measured scattering ratios are significantly different for water droplets: the median visible to peak amplitude ratio is 17 for cement powder, 20 for Arizona test dust and 376 for water droplets. With this, our theoretical considerations are experimentally verified.

In the future, the measurement setup will be further developed to make it deployable in the environment to measure the aerosol number and mass concentration for water and non-water aerosols separately.

This work was supported by the Swiss Federal Office of Civil Aviation. We would like to thank the Fraunhofer Institute for Applied Solid State Physics, Freiburg, Germany for providing the IR laser for the experiments.

Dynamics of the droplet formation process in periodic electric microdripping

A.J. Hijano[1], I.G. Loscertales[1], S.E. Ibáñez[2] and F.J. Higuera[2]

[1]Departamento de Ingeniería Mecánica y Mecánica de Fluidos, Universidad de Málaga, Campus de Teatinos s/n, 29071, Málaga, Spain

[2]Departamento de Mecánica de Fluidos, Universidad Politécnica de Madrid, 28040, Madrid, Spain

Keywords: microdripping, EHD, microdroplets, electrospray.

We investigate the formation of monodisperse droplets from an electrified meniscus of a low viscosity, highly conductive liquid in the periodic electric microdripping mode, termed *Axial Spray Mode II* by Juraschek & Röllgen (1998).

The meniscus, attached at the tip of a capillary tube of diameter D, is fed with a flow rate Q and connected to a voltage ϕ. A flat metallic counter electrode connected to ground is located at a distance L in front of the capillary tube tip. Within a certain range of flow rates and applied voltages, the meniscus sets in the periodic microdripping mode, in which its tip elongates forming a ligament that ultimately detaches to form a droplet. This mode produces monodisperse droplets whose diameter may be one tenth of D, the diameter of the capillary tube.

The process is governed mainly by two dimensionless parameters: the dimensionless flow rate $q = \rho^{1/2}Q/(\gamma D^3)^{1/2}$, where ρ and γ are the liquid density and surface tension, and the electric Bond number $B_E = \epsilon_0\phi^2/[\gamma D \ln^2(4\,L/D)]$, where ϵ_0 is the permittivity of the air surrounding the meniscus. Parameter q is small but can be varied by a factor of about 100 within the microdripping mode, whereas B_E is bound to a narrow range of order unity values.

High speed video has been used to analyze the dynamics of the meniscus, and the electric charge carried by the emitted droplets has been measured.

At low flow rates, the whole meniscus recedes during each oscillation except for the tip, which is pinned by the electric field, thus forming a tiny ligament; the time required to form this tiny ligament is a very small fraction of the oscillation time, so the oscillation frequency is constant of the order of the inverse of the capillary time $t_c = (\rho D^3/\gamma)^{1/2}$. On the other hand, at large flow rates the electric field continuously pulls the tip, thus forming a much longer filament; the oscillation time is basically the ligament formation time, so the oscillation frequency decreases as the ligament length increases. These two qualitatively different dynamics, combined with order-of-magnitude estimates, lead to scaling laws for the dimensionless ligament length, L_s/D, and width, D_s/D, just before its detachment, for low and high flow rates. Experimental measurements of L_s and D_S agree with the scaling laws proposed (See Figure 1).

The electric charge on the droplet is about 1/4 of the Rayleigh charge regardless of the conditions.

We also find that the product of the dripping frequency and the capillary time is nearly constant for small q and decreases as $q^{-1/2}$ for large q, as expected.

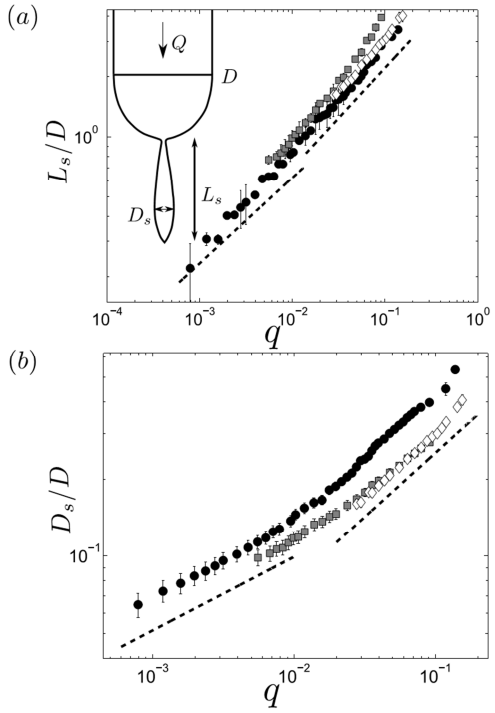

Figure 1. Dimensionless length and width of the ligament immediately before detachment as functions of q for B_E = 0.20 (circles), 0.27 (squares) and 0.37 (diamonds). The dashed straight lines at the left-hand sides have slopes 3/7 (for L_s/D in (a)) and 2/7 (for D_s/D in (b)). The dashed lines at the right-hand side have slope 1/2.

This work has been supported by the Spanish Ministerio de Economía y Competitividad through projects DPI2010-20450-C03 and DPI2013-47372-C02. SEI and FJH also acknowledge support through project CSD2010-00010.

Juraschek, R., & Röllgen, F. W. (1998). *Pulsation phenomena during electrospray ionization. Int. J. Mass Spectrometry*, 177, 1-15.

Effect of humidity on the pressure drop of nanostructured deposit

Q. Ribeyre[1, 2], A. Charvet[1, 2], C. Vallières[1, 2] and D. Thomas[1, 2]

[1] Université de Lorraine, Laboratoire Réactions et Génie des Procédés, UMR 7274, Nancy, F-54000, France
[2] CNRS, Laboratoire Réactions et Génie des Procédés, UMR 7274, Nancy, F-54000, France

Keywords: filtration, nanoparticles, adsorption-condensation, pressure drop modelling.

In recent years, there has been much interest in industrial and research development in the field of nanomaterials. This quick development leads to an exposure to ultrafine particles of a growing part of the population. Thus, in most cases, High Efficiency Particulate Air Filters (HEPA) are used to protect workers and environment. However, almost all the available data on the clogging of these filters were obtained at ambient temperature and humidity. But, some accident scenarios can lead to a high moisture environment. This is the case of a fire in the nuclear facilities where the fumes trigger the anti-fire devices and therefore, increase the air humidity (Mocho and Ouf, 2011). Despite these extreme conditions, the HEPA filters used in these institutions must maintain the containment.

The lack of experimental data regarding the pressure drop changes of clogged filters at high humidity has inspired this study. Some laboratory measurements have shown that the behaviour of the filters is strongly impacted by the presence of moisture (Schröter and Poon, 2012) and that the interaction between water vapour and particles are responsible for these variations (Joubert, 2010).

From an experimental point of view, two nanostructured powders (fumed silica and amorphous carbon) has been selected and generated using a Palas RBG 1000. When the nanostructured deposit is formed, we gradually increase the relative humidity and continuously record the thickness of the bed with the help of a laser device (based on the method developed by Altmann and Ripperger (1997)). When the pressure drop and the bed thickness remain stable, these values are recorded. The same operation is repeated for several humidity step between 0 and 90%.

The second phase of this study concerns the modelling of pressure drop variations with humidity. In a previous paper, we have developed a semi-predictive model of adsorption-condensation on nanoparticles beds in order to calculate the water mass sorbed by a powder (Ribeyre et al. 2014). This model has been implemented in three pressure drop models available in the literature (described by Kozeny-Carman, Mauret-Renaud and Thomas) in order to predict the pressure drop evolution of a nanostructured deposited at various humidities. We modified them by introducing cake thickness and porosity variation according to relative humidity.

We choose to represent the relative pressure drop (denoted $\Delta P/\Delta P_0$) versus water activity (denoted a_0) for experiments with the fumed silica (Figure 1). As we can see, the experimental pressure drop values and modelling data are in good agreement. Consequently, our modified pressure drop model correctly represents the increase of pressure drop for high humidities.

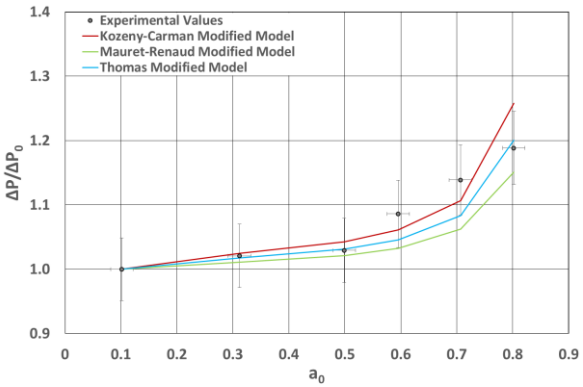

Figure 1. Pressure drop vs water activity for the fumed silica sample.

Acknowledgments: This study was conducted with the French Institute for Radiological Protection and Nuclear Safety in the joint research program on Media-Aerosol Interactions (IRSN/ LRGP CNRS N° 083332).

Altmann, J. & Ripperger, S. (1997). *Journal of Membrane Science*, 1, 119-128.

Joubert, A., Laborde, J.C., Bouilloux, L., Callé-Chazelet, S. & Thomas, D. (2010). *Aerosol Science and Technology*, 44, 1065–1076.

Mocho, V.M. & Ouf, F.-X. (2011). *Nuclear Engineering and Design*, 241 (n°5), 1785-1794.

Ribeyre, Q., Grévillot, G., Charvet, A., Vallières, C. & Thomas., D. (2014). *Chemical Engineering Science*, 113, 1-10.

Schröter, M. & Poon, M. (2012). In proc. *11th World Filtration Congress*, Graz, G18 – 02-148.

Effect of material properties on filtration efficiency and deposits structure in fibrous filters

R.Przekop[1], A.Jackiewicz[1], P.Woźniak[2,3] and L.Gradoń[1]

[1]Faculty of Chemical and Process Engineering, Warsaw University of Technology,
ul. Waryńskiego 1, 00-645, Warsaw, Poland
[2]Faculty of Materials Science and Engineering, Warsaw University of Technology,
ul. Wołoska 141, 02-507, Warsaw, Poland
[3]University Research Centre Functional Materials, Warsaw University of Technology,
ul. Wołoska 141, 02-507, Warsaw, Poland

Keywords: fibrous filters, lattice-Boltzmann, Brownian Dynamics, deposition, Atom Force Microscopy.

Filtration is one of the effective methods for the removal of particles from an aerosol stream. The development in the formation of specific fibrous structures promises the construction of highly efficient filters for the collection of aerosol particles. A fibrous material operates by capturing an aerosol particle on the fibers within the filter depth, the result being the deposition of particles approaching the collector. Its effectiveness depends on the particle and fiber size filter porosity, and the material properties of both objects. Performance of the filter can be defined by its efficiency, pressure drop and lifetime.

Complete information on the statistical description of a gas at, or near, thermal equilibrium is assumed to be contained in the one-particle phase-space distribution function $f(x, t, \Gamma)$ for the atomic constituents of the system. The variables x and t are the space and time coordinates of the atoms and Γ stands for all other phase-space coordinates e.g. momentum, momentum flux. To build the cellular-space picture with a dynamics of the collective motion predicted by Navier-Stokes equation, a lattice on which particles move, a collision rules and other restrictions characteristic for a chosen model should be defined (Qian *et. al*, 1992). In this work 3-dimensional lattice with 19 allowed directions of movement, usually referred as D3Q19 was used.

Particle trajectory is calculated for the generalised Besset-Boussinesqu-Ossen equation, which takes into account drag, external and random Browian forces. The equation was solved using the Brownian Dynamics (BD) method established by Chandrasekhar (1943) for a Stokesian particle in stationary fluid and for a force-free field. In this work extension of BD for the case of moving fluid at presence of the external forces derived by Podgórski (2002) was used.

The interaction model base on works by Reeks *et. al* (1988) and Ziskind *et. al* (2000). Authors assumed that adhesion force and elastic reaction force, considered in JKR theory, could be described by equation of harmonic movement with dumping effect.

The constants in mentioned equation are the function of material properties such as Young modulus or Poisson ratio and work of adhesion. The work of adhesion was estimated using Atom Force Microscopy (AFM)

The calculations of monodisperse particles deposition on single fiber were done for deposition of silica and KCl particles on polymer fiber. Results were compared with calculations assuming 100% effectivity of particles deposition. For the KCl particles the calculations predict formation of the monolayer on the surface of collector., while for silica particles, with higher value of the work of adhesion, the dendrite growth is observed. The collisions between suspended and deposited particles are ineffective for deposition for low values of work of adhesion and for deposited particles the reentrainment is more probable. This result is consistent with experimental SEM analysis.

This work was supported by National Science Centre under the grant number DEC-2012/07/B/ST8/03996
This work was supported by National Centre for Research and Development under the grant LIDER/13/97/L-3/11/NCBR/2012

Chandrasekhar, S. (1943) Stochastic Problems in Physics and Astronomy, *Reviews of Modern Physics*, 15, 1-89

Podgórski, A. (2002) *On the transport, deposition and filtration of aerosol particles in fibrous filters: Selected problems*., Oficyna Wydawnicza Politechniki Warszawskiej, Warsaw

Qian, Y.H., d?umieres, D. and Lallemand, P. (1992) Lattice-BGK Models for Navier-Stokes Equation, *Europhysics Letters* 17, 47984.

Reeks, M.W., Reed, J. and Hall D. (1988) On the resuspension of small particles by turbulent flow. *J. Phys. D* 21, 574-589

Ziskind, G., Fichman, M. and Gutfinger, C. (2000) Particle behavior on surfaces subjected to external excitations, *J. Aerosol Sci.* 26, 703-720

EFECT OF MESOSCALE INHOMOGENITY ON FIBROUS FILTER PERFORMANCE – CFD INVESTIGATION

Arkadiusz Moskal*, Łukasz Makowski

Warsaw University of Technology, Faculty of Chemical and Process Engineering

Ul. Waryńskiego 1, 00 – 641 Warsaw, POLAND

Keywords: filtration, inhomogeneity, CFD modelling

Aerosol particles are present in many industrial processes. Aerosol filtration in fibrous filters is one of the principal methods of accurate removal of particulate matter from stream of gas. During the past fifty years, many researchers have investigated the filtration process using "classical theory" of filtration: (Davies, 1973), (Brown, 1993) The "classical theory" of depth filtration of aerosol particles in fibrous structures based on the assumption of existing single fiber efficiency, E, which may be used to recalculation of overall efficiency of entire filter, according to well-known formula:

$$P = \exp(-\lambda L) \tag{1}$$

where: P is penetration of aerosol particles through a filter, L is filter thickness and λ is filter coefficient, related to the single fiber efficiency, E, as:

$$\lambda = \frac{4E}{\pi d_f}\left(\frac{1-\varepsilon}{\varepsilon}\right) \tag{2}$$

where: d_f is the fiber diameter and ε denotes the fiber porosity. The single fiber efficiency E is defined as a ratio of the flux of particles depositing onto one fiber to the flux of particles passing a surface being the projection of the fiber on to a plane perpendicular to the direction of the mean gas motion. Deposition of the aerosol particles on fibrous surface may occur due to different mechanisms, which may be divided into two groups: deterministic mechanisms (inertial impaction, sedimentation, electrostatic forces, interception), E_{det}, an stochastic one (Brownian diffusion), E_{diff}. Taking into account assumption of independent action of deterministic and stochastic deposition mechanisms, the overall deposition efficiency of the filter may be calculated as follows:

$$E = 1-(1-E_{\text{det}})(1-E_{diff}) \tag{3}$$

Using "classical theory" of filtration one may introduce some errors. There are several reasons for inappropriate estimation of the single fiber efficiency: i) neglecting of short-range interactions, ii) separation of the inertial and Brownian effects, ii) perfect adhesion of the particles to the fiber, iv) assumption of perfect mixing of aerosol particles in the gas stream, v) assumption of negligible effect of the presence of neighboring fibers and vi) assumption of perpendicular orientation of the homogenous fibers in the filtration structure. The aim of this work is to investigate influence of mesoscale inhomogeneity on fibrous filters performance using CFD calculations in models of filters differ by internal structure (Figure 1).

a) b)

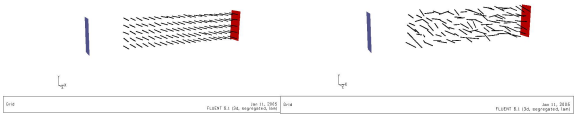

Figure 1. Different filtration structures a) regular, b) random;

Obtained results show that for structures with small porosity there are optimal value of "randomness" of internal structure, which guarantee high value of aerosol deposition. (Figure 2)

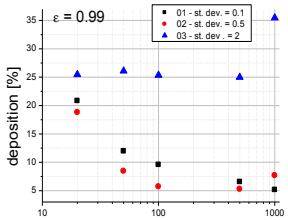

a)

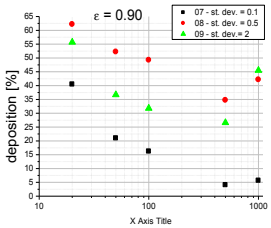

b)

Figure 2. Deposition as a function of particle diameter for two different porosities of the filter structure;

This research was funded in part by Fleedgard Ltd and financed by National Science Centre granted by decision number: DEC-2012/07/B/ST8/03996.

Brown R.C., (1993) , *Air filtration*, Oxford U.K.: Pergamon Press

Davies, C.N, (1973), *Air filtration*, London U.K.: Academic Press

Effective density measurements of aircraft soot particles and surrogates

F.X. Ouf[1], A. Bescond[2], D. Ferry[3], I. Marhaba[3], F. Salm[1], S. Peillon[1], J. Yon[2], D. Delhaye[4], D. Gaffie[4], C. Guin[4], J.J. Lecout[4], L. Ait-Ali-Yahia[5], A. Forthomme[5], B. Sagot5, and A. Vandestoc[4]

[1]Institut de Radioprotection et de Sûreté Nucléaire (IRSN), BP 68, 91192 Gif-sur-Yvette Cedex, France
[2]UMR 6614 CORIA, CNRS, Université et INSA de Rouen, Saint Etienne du Rouvray, BP12, 76801, France
[3]Aix-Marseille Université, CNRS UMR 7325, CINaM, 13009, Marseille-France
[4]Onera – The French Aerospace Lab, F-91123 Palaiseau, France
[5]ESTACA, Laboratoire Fluide et Energétique, 92300, Levallois-Perret, France

Keywords: aircraft emissions, effective density, fractal dimension, soot, primary diameter, CAST.

The effective density is defined as the ratio between the particle mass and the volume of the sphere having the same mobility diameter. In case of spherical particles, this measurement informs us about the particle density. For particles with more complex morphologies as soot fractal aggregates, the effective density is a decreasing function of the mobility diameter. This curve is useful because it permits to determine the particle mass concentration from conventional mobility diameter based granulometers (SMPS, DMS…). Yon et al. (2014) have proposed a unification method in order to compute the fractal dimension but also the density of soot particles according to the effective density. We propose here to apply this method on aircraft soot particles and to compare these results with those obtained for surrogates produced by a MiniCAST burner.

The experimental setup for measurements of the effective density is composed by a Scanning Mobility Particle Sizer (SMPS 3085 from TSI) and a Centrifugal Particle Mass Analyser (CPMA from Cambustion). Instead of scanning the particle mass for each fixed mobility diameter (driven by CPMA), we fix the mass selection by inserting the CPMA between the DMA and CPC and a mobility scan is driven by the SMPS. That configuration decreases the measurement duration and increases the sensitivity of the measurement. This setup has been previously applied (Yon et al., 2014) to soot particles produced by a propane diffusion flame (MiniCAST SP1 and SPA) and we report here results recently obtained for aircraft emissions. These measurements have been conducted with a tubular furnace, representative of the SAM 146 turbofan (SNECMA, Ouf et al., 2014), and implemented on the ONERA's M1 test bench (Ouf et al., 2015).

Results obtained by this approach for different operating conditions (fuel to air ratio) of the miniCAST soot generator and the tubular furnace for cruise conditions are presented in figure 1. Considering aircraft emissions, two different measurements have been conducted. One after two dilutions (2 PALAS VKL10 respectively with nitrogen at 65°C and 35°C as dilution gas) and the other one with only one dilution at 65°C. The effective density appears to be slightly sensitive to dilution conditions for particles with a mobility diameter smaller than 60 nm. Besides this dilution effect, a good agreement is noticed between the effective densities of aircraft particles and CAST SP1 soot particles. Further analysis is in progress to compare the diameter of spherical particles composing the soot aggregates and, considering the approach proposed by Yon et al. (2014), to compute the real density of these particles which is an important parameter poorly documented for aircraft soot particles.

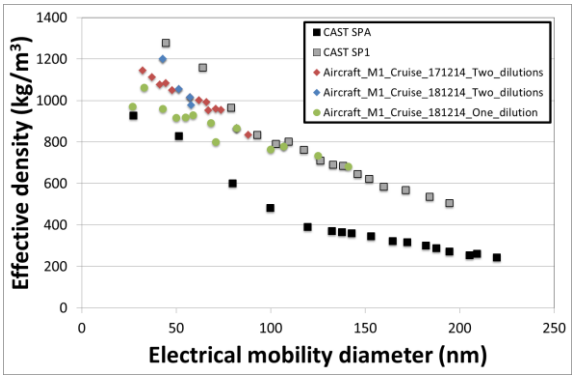

Figure 1. Effective density determined for different operating conditions of the miniCAST soot generator and the M1's aircraft tubular furnace.

This work was supported by the MERMOSE project, financially supported by DGAC (French national funds) - see http://mermose/onera/fr/en. This work is dedicated to the memory of Jean-Jacques LECOUT.

Yon, J., Bescond, A., Ouf, F.X. (2014). T280A21, *Conference on Aerosol Technology*, Karlsruhe, Germany.

Ouf, F.X., Delhaye D., Ferry D., et al. (2014). T280A17, *Conference on Aerosol Technology*,, Karlsruhe, Germany.

Ouf, F.X., Delhaye D., Ferry D., et al. (2015). *Submitted to Conference on Aerosol Technology*, Tampere, Finland.

Effects of spatial sensitivity on particle detection with microfabricated electro-acoustic resonators

A.T. Zielinski[1], A. Prasad[2], A.A. Seshia[2], M. Kalberer[1], and R.L. Jones[1]

[1]Centre for Atmospheric Science, Department of Chemistry, University of Cambridge, Lensfield Road, CB2 1EW, Cambridge, UK
[2]The Nanoscience Centre, Department of Engineering, University of Cambridge, JJ Thomson Avenue, CB3 0FF, Cambridge, UK

Keywords: instrument development, MEMS, particle mass, microresonators.

Micromechanical resonators, fabricated in a range of geometries, have recently seen increased use as mass sensors (e.g. Arlett *et al.*, 2011). By modelling the resonator as a single degree-of-freedom mass-spring-damper system, the resonant frequency, f_0, can be related to the effective mass, M, and stiffness, K, by $f_0 = (1/2\pi)(K/M)^{1/2}$. An increase in mass therefore corresponds to a decrease in resonant frequency assuming all other parameters remain unchanged.

This study examines the application of micromechanical resonators as particulate detectors with a focus on characterising their non-uniform spatial sensitivity to deposited particles. Square bulk acoustic mode resonators were used, rather than flexural mode resonators, as they typically show higher quality factors (Mattila *et al.*, 2007) which enables improved resonant frequency shift resolution in air. Previous studies (Lee *et al.*, 2007) have shown agreement with a linear sensitivity model based on Sauerbrey's principle for a uniform thin film, but this model is not applicable for non-uniform particle deposition.

In this study, two square 1400 µm micro-fabricated silicon resonators were actuated in the square-extensional mode at ~3.14 MHz to study their response to particle adsorption by monitoring their resonant frequencies and quality factors. The resonators were of the same design except for surface treatments with one being hydrophilic (via plasma cleaning) and the other hydrophobic (via a perfluoro-decyltrichlorosilane self-assembled monolayer). Microdroplets containing known concentrations of 300 nm polystyrene latex (PSL) particles were deposited onto each resonator and quickly evaporated in a vacuum chamber to adsorb the PSL particles to the resonator surface. Results were compared with our newly developed spatial sensitivity model (inspired by Prasad *et al.* (2014)) which accounts for the resonators' spatial sensitivity based on residue images. The comparison, shown in Figure 1 for the hydrophilic resonator, suggests three stages of particle deposition: (i) residue growth, where the size and location of the residue is variable, (ii) uniform mass addition, where the residue shape has stabilised and the response is linear, and (iii) particle stacking, where fluctuations are present due to rearrangement of particles after each droplet.

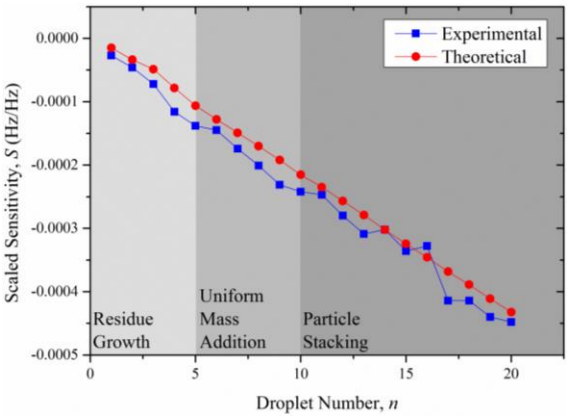

Figure 1. Sensitivity relative to original, unloaded resonant frequency using experimental and theoretical results for the hydrophilic resonator. Theoretical results scaled in magnitude to focus on per-droplet trends.

The spatial sensitivity model is most effective in the residue growth phase due to the changing size and location of the residue, highlighted by matching sensitivity shifts for droplets one through five. Differences in magnitude are due in part to elevated mass depositions which were confirmed by SEM imaging and macro-scale mass experiments.

We will present an overview of the resonators, expand on the results discussed above (including a comparison between surface treatments) and provide insight into their application to aerosol particle deposition from gaseous mediums.

Arlett, J. L., Myers, E. B., & Roukes, M. L. (2011). *Nat. Nano*, 6, 203-215.

Lee, J. E.-Y., Zhu, Y., & Seshia, A. A. (2007). *Appl. Phys. Lett.*, 91, 234103.

Mattila, T., Kiihamäki, J., Lamminmäki, T., Jaakkola, O., Rantakari, P., Oja, A., Seppä, H., Kattelus, H., & Tittonen, I. (2002). *Sens. Actuators, A*, 101, 1-9.

Prasad, A., Zielinski, A. T., Kalberer, M., Jones, R. L., & Seshia, A. A (2014). in *Proc. 28th European Frequency and Time Forum*, Neuchâtel, 23-26.

Effects of vehicle technology on real exhaust particle emissions from city buses

L. Pirjola[1], A. Dittrich[2], J.V. Niemi[3], S. Saarikoski[4], A. Malinen[1], H. Kuuluvainen[5], H. Wihersaari[5], H. Timonen[4], A. Kousa[3], T. Rönkkö[5], and R. Hillamo[4]

[1]Department of Technology, Metropolia University of Applied Sciences, P. O. Box 4021, FI-00180 Helsinki, Finland
[2]Department of Vehicles and Engines, Technical University of Liberec, 461 17 Liberec 1, Czech Republic
[3]Helsinki Region Environmental Services Authority HSY, P.O. Box 100, FI-00066 HSY, Helsinki, Finland
[4]Finnish Meteorological Institute, P.O. Box 503, FI-00101 Helsinki, Finland
[5]Department of Physics, Tampere University of Technology, P.O. Box 692, FI-33101 Tampere, Finland

Keywords: mobile measurements, size distribution, particle chemistry, volatility, fuel

Regardless of many improvements in vehicle technology diesel exhaust particles constitute major air pollutants in urban environments. Although, due to the tightened emission regulations, the mass emissions have been reduced, the number emission of exhaust nanoparticles has been reported to be significant (Rönkkö et al., 2013). Recently, the World Health Organization reclassified diesel engine exhaust as carcinogenic to humans (WHO, 2012). Exhaust particle concentration significantly depends on the engine and exhaust after-treatment technology, operation and environmental conditions as well as fuel and lubricant oil properties.

As a part of the MMEA Programme (Measurement, Monitoring and Environmental Assessment 2010-2014), one week chasing campaign by mobile laboratory ´Sniffer´ (e.g. Pirjola et al., 2004) was performed in November 2013 to study exhaust emissions from individual city buses at a bus depot area in Helsinki and on the normal route of bus line 24. Twenty three individual buses were selected to represent Euro 3, Euro 4 and EEV (Enhanced Environmentally Friendly Vehicle, ≥ Euro 5) classes, different after-treatment systems (SCR, EGR+DPF, three-way catalyst, no after-treatment), different fuel (diesel, ethanol, natural gas CNG) and engine.

Particle number concentration was measured by UCPC (diameter > 2.5 nm) and size distribution by EEPS (diameter > 5.6 nm). Particle volatility was studied by two ELPIs, ELPI+ (diameter > 6 nm) before the thermodenuder and ELPI (diameter > 7 nm) after it. Furthermore, PM_1 was monitored by DustTrak, black carbon (BC) by Aethalometer AE33, and particle chemistry by soot particle aerosol mass spectrometer SP-AMS. Also recorded were NO, NO_2, NOx, CO, CO_2, meteorological and geographical parameters. All instruments were operated with 1 s time resolution.

As expected, highest particle emissions were measured from the Euro 3 buses, and lowest from the CNG buses (Fig. 1). The bimodal average number size distributions were obtained for all diesel-fuelled buses with peak modes of ~10 nm and 70-80 nm; however, the Euro 4 buses had very low nucleation mode even in the accelerating mode. No clear effect of the use of electricity by the hybrid buses to reduce particle emissions was observed in this campaign. In the accelerating mode the ethanol-fuelled buses emitted high number of very small particles, the modes peaked at ~10 nm and ~30 nm. Similar results were also obtained from the buses operating bus line 24.

The CNG buses showed lowest BC emissions, and both in the accelerating and in the constant speed modes the ratio of organics and BC was even eight times larger than those for the other buses. More details of the nonvolatile properties of the emissions were further investigated.

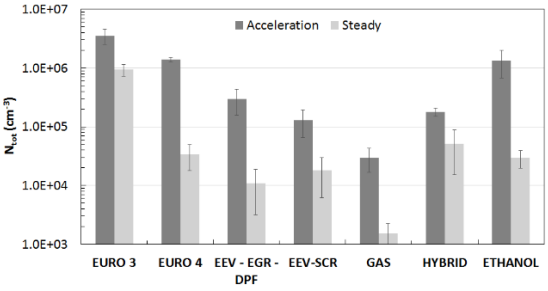

Figure 1. Averaged total particle number concentrations for different bus types when the buses were accelerated from idle to 25 km/h uphill and when they were run at constant speed 25 km/h. Background particles were subtracted.

This work was supported by CLEEN Ltd (the cluster for Energy and Environment), by the Ministry of Education, Youth and Sports of Czech Republic, and the OPR&DI project "Centre for Nanomaterials, Advanced Technologies and Innovation".

Pirjola, L., Parviainen, H., Hussein, T., Valli, A., Hämeri, K., Aalto, P., Virtanen, A., Keskinen, J., Pakkanen, T., Mäkelä, T., Hillamo, R. (2004). *Atmos. Environ.*, 38, 3625-3635.

Rönkkö, T., Lähde, T., Heikkilä, J., Pirjola, L., Bauschke, U., Arnold, F., Schlager, H., Rothe, D., Yli-Ojanperä, J., and Keskinen, J. (2013). *Environ. Sci. Technol.*, 47, 11882-11889.

WHO (2012). *Bulletin of the World Health rganization* 90, 477–556.

Electrical impedance spectroscopy for the determination of the agglomeration state of nanoparticles

R. Wernet[1], W. Baumann[2], H.-R. Paur[2] and M. Seipenbusch[1]

[1]Institute for Mechanical Process Engineering and Mechanics,
Karlsruhe Institute of Technology (KIT), 76131, Karlsruhe, Germany
[2]Institute for Technical Chemistry, Karlsruhe Institute of Technology (KIT), 76131, Karlsruhe, Germany

Keywords: impact fragmentation, characterisation of deagglomeration, electrical impedance spectroscopy.

The strength of nano-scaled soft-agglomerates, primarily held together by attractive Van der Waals forces, is a significant parameter to the physical properties and manageability of powders. The mechanical stability can be measured by impaction under low-pressure conditions; however this method requires the knowledge of the impaction energy and the resulting degree of fragmentation. In order to determine the impaction energy, the impact velocity has to be detected either by measurement or by calculation. TEM image analysis is utilized to identify the degree of fragmentation. Since image analysis is a time-consuming off-line technique, the present work is aiming for qualitative information as to the size of particles after impaction via electrical impedance spectroscopy (EIS).

In the liquid phase a size effect on the impedance spectrum was demonstrated for silica particles ranging from 12 nm to 220 nm in diameter (Zhao et al., 2013). For the size change associated with fragmentation a shift in the impedance spectrum can therefore be expected.

The experimental set-up includes a spark discharge generator, a sinter furnace and an agglomeration tank in order to obtain metallic soft-agglomerates made of spherical primary particles. The fragmentation occurs in a molecular beam apparatus (MBA) which provides high-vacuum conditions. A laser device to measure the time of flight over a definite distance is implemented into the MBA before the impaction plate. Due to the vacuum conditions drag forces acting on the particles can be neglected and the measured velocity needs no correction. To the impaction plate TEM grids for image analysis and interdigitated electrodes for EIS measurements can be attached. Thereby impedance spectra can be correlated to the degree of fragmentation determined by TEM image analysis.

Figure 1 shows the impedance spectra of preliminary tests using an interdigitated comb electrode (Novocontrol, Montabaur/Germany). Commercial Carbon Black was dispersed and introduced into the MBA where it deposited on the electrode. Impedance spectra were taken from the empty electrode and after the deposition (level 1). Afterwards the deposition process and the impedance measurement were repeated (level 2.) EIS identifies the three states of the electrode clearly.

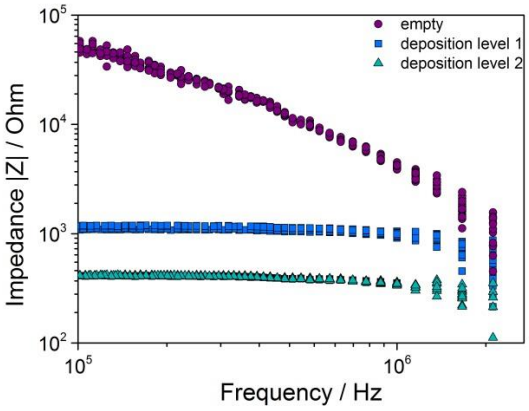

Figure 1. EIS measurements on an interdigitated comb electrode covered with Carbon Black.

The authors acknowledge the financial support from the German Research Foundation (SE 1782/4-1).

Zhao, Y., Wang, M., Hammond, R. B. (2013). *Journal of nanoscience and nanotechnology*, 13.2, 808-812.

Electrospray Deposition Method for TEM sample preparation

P. Dohányosová[1], P.Ballorca[2], I. G. Loscertales[2] and S. Lopéz-Vidal[1]

[1]RAMEM S.A., Sambara 33, 28027, Madrid, Spain
[2]Yflow, Parque Tecnológico de Andalucía, 29590, Malaga, Spain

Keywords: electrospray, deposition, TEM.

The rapid development of nanotechnology and spreading of nanomaterials in almost all sectors of human activities, including i.e. food production or cosmetics industry, require establishing reliable methods of nanomaterial characterization. At present, one of the most important nanoparticle characterization methods is Transmission Electron Microscopy (TEM) for its robustness and its ability to measure particles even bellow 5 nm where the majority of instrumental methods fail.

The crucial aspect of TEM measurement is the sample preparation. It consists of the deposition onto an electron transparent grid of a very thin layer of the nanomaterial to be studied from a liquid dispersion of it and the subsequent solvent evaporation by drying. Generally, nanomaterials are dispersed in non-dissolving liquid in an ultrasonic bath. Established methods of TEM sample preparation are i.e. centrifugation of suspension on TEM grid, drop deposition or rapid dipping of the grid into the dispersion. These methods have their limitations. Their main disadvantages are that during sample preparation particle agglomeration and non-homogenous particle deposition can occur.

In this work we prepare samples by directly electrospraying the nanoparticle suspension onto TEM grids. Highly-charged, submicron-drops containing the nanoparticles of the nanomaterial to be analyzed are steadily produced from the electrospray (ES) in the cone-jet mode. The solvent evaporates in the presence of drying gas and the solvent-free airborne nanoparticles reach the collector (counter-electrode) placed at a short distance in front of the electrospray emitter. The collector is an electrically conductive plate that holds the TEM grid. The electric field is established between the electrospray emitter and the collector. Conditions of steady cone-jet operation (liquid flow rate in the capillary, high voltage, distance between capillary tip and collector, etc.) depend on the physical chemical properties of the liquid dispersion and must be determined for each sample particularly.

The performance of this ES deposition system was tested with the commercially available gold nanoparticles of 5 nm in aqueous dispersion (BBI Solutions).

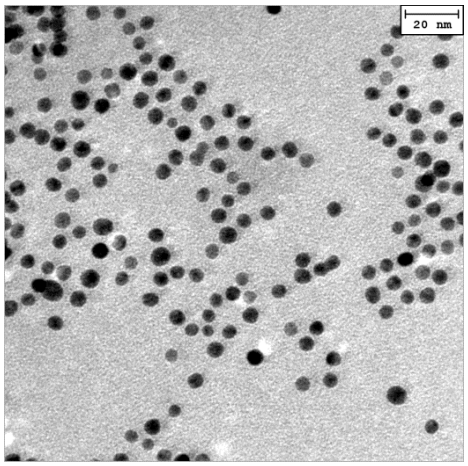

Figure 1.TEM image of 5 nm gold particles deposited by electrospray.

The nanoparticles were deposited homogenously into a circular spot. The grid holding the collected nanoparticles was analysed by TEM and its image is presented in Figure 1. It can be seen that particles are nearly monodisperse and seldom form agglomerates.

Further samples of water-based dispersions of various nanoparticles were studied and the results will be presented.

The research leading to these results has received funding from the European Union Seventh Framework Programme under grant agreement nº 604347.

Electrospray Synthesis of PLGA TIPS Microspheres

S.A. Malik[1], W.H. Ng[1], J. Bowen[2], J. Tang[3], A. Gomez[3], A.J. Kenyon[1] and R.M. Day[4]

[1]Department of Electronic & Electrical Engineering, University College London, Torrington Place, WC1E 7JE, London, United Kingdom
[2]School of Chemical Engineering, University of Birmingham, B15 2TT, Birmingham, United Kingdom
[3]Department of Mechanical Engineering & Materials Science, Yale University, New Haven, CT, 06520-8286, USA
[4]Division of Medicine, University College London, 21 University Street, WC1E 6JJ, London, United Kingdom

Keywords: Electrosprays, Poly(lactic-*co*-glycolic) acid (PLGA), Microspheres

We successfully demonstrate the synthesis of polymer microspheres using a single electrospray source, and show their physical characterisation. Electrospray has proven to be a versatile method to manufacture particles, giving tight control over size with quasi-monodisperse size distributions. It is a liquid atomisation technique that generates a monodisperse population of highly charged liquid droplets over a broad size range (nanometres to tens of microns). The droplets contain liquid precursors for the in-flight synthesis of particles, and control over the trajectory of these droplets can be precisely manipulated with the use of electric fields to drive them to a grounded substrate.

This study reports a method to synthesize poly(lactic-co-glycolic) acid (PLGA) microspheres using the electrospray and thermally induced phase separation (TIPS) techniques, followed by subsequent freeze-drying, for particle production. These microspheres are of interest as vehicles for controlled drug release systems.

Materials and Methods

A 5% w/v polymer solution of PLGA (Purasorb PDLG 5004A, 50:50 DL-lactide/glycolide copolymer) was prepared using a solvent formulation of dimethyl carbonate (DMC), formic acid and deionized (DI) water with the following ratio, 99:0.5:05 v/v. The solution was electrosprayed in the cone-jet mode at 1ml/hr using a dual-electrode configuration (i.e. needle and extractor plate) and one 19G needle source positioned concentrically 1mm above a 0.4mm diameter extractor hole. Care was taken to avoid misalignment between the nozzle and the extractor hole, which may cause the jet to discharge asymmetrically leading to an electrical short between the two components.

The electrodes were maintained at different potentials to achieve the desired electric field with $V_{needle} > V_{extractor} > V_{collector}$ (ground). The voltages applied to the needle and extractor were 10.2kV and 7.0kV, respectively. The electric field driving the droplets between the extractor electrode and the collector was high enough to avoid reversal of the droplet motion near the extractor (satellite trapping). Particles were collected in a liquid nitrogen bath (40mm below the extractor plate) held within a non-stick Teflon casing. Particles were subsequently lyophilised for 24 hours to produce porous, spherical particles (Figures 1A and 1B).

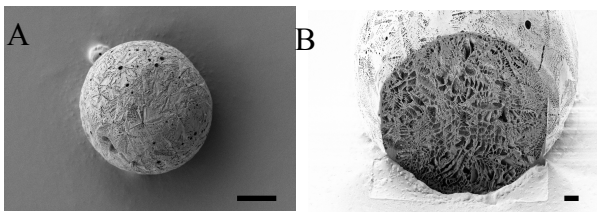

Figure 1 – (A) SEM micrograph of a PLGA TIPS microsphere. Scale bar 10μm. (B) FIB-SEM slice through a microsphere. Scale bar 2μm.

Results and Discussion

SEM images revealed the successful synthesis of freeze-dried polymer particles. Particle size was measured using a particle size analyser (Morphologi G3, Malvern Instruments, UK), and results revealed a median particle size of 14μm. Spectroscopic analyses (Alpha 300R Confocal Raman Microscope, WiTec, Germany) revealed identical spectra for the electrosprayed PLGA and PLGA as-received. Hence, the electrospray process did not alter the composition of the polymer. Further, imaging the internal structure of electrosprayed PLGA particles using confocal Raman microscopy yielded images similar to those in Figure 1B; such structures were not present for PLGA as-received.

This research was supported by the Engineering and Physical Sciences Research Council (EPSRC), the UCL Institute of Biomedical Engineering (IBME)-led Yale-UCL Medical Technologies Collaborative and the Department of Biomedical Engineering, Yale University.

Entrainment rates and spectra of oil drops from the surface of mist filters

S. Wurster[1], J. Meyer[1] and G. Kasper[1]
[1]Institut für Mechanische Verfahrenstechnik und Mechanik, Karlsruhe Institute of Technology (KIT), 76131 Karlsruhe, Germany

Keywords: mist filtration, coalescence filter, blow-off, optical size analysis.

Oil mist, consisting of fine droplets mostly below 1 µm is generated in large amounts by various processes of industrial relevance, such as the movements of pistons in an engine crankcase, by oil lubricated air compressors, metal cutting tools and during natural gas extraction and processing. Most commonly such aerosols are removed by fibrous filters. Oil accumulating in such a filter is transported by the air flow until it reaches the rear face (Mullins, 2005; Kampa, 2014a) where it can be re-entrained to form a secondary aerosol. The mechanisms responsible for causing droplet entrainment and the resulting spectra are a topic of current research. The scientific literature on oil entrainment from fibrous filters media is sparse (Payet, 1992; Raynor, 2000; Contal, 2004). Drop formation mechanisms are not well understood on the microscale, and there are no macroscale models to express dependence of entrainment on operating conditions, oil properties or filter structure parameters.

At first, an experimental set-up is described to measure size spectra of entrained oil drops and entrainment rates from glass microfiber filter media. It will be shown that the entrainment spectrum of such media ranges from below 1 µm to several millimeters and thus requires the combination of several techniques including CPC and OPC for the range below about 10 µm, as well as a newly developed optical technique for drops larger than about 150 µm. Only the gap between 10 and 150 µm is covered by an off-line method.

The second part discusses entrainment rates from wettable (oleophilic) and non-wettable (oleophobic) glass-fiber media as a function of time, flow velocity, and oil concentration. Early work by Saemundsson (1968) and Bürkholz (1970) suggests that blow-off rates from relatively open structures should increase with drag by force and thus with filtration velocity. Bürkholz also reports higher entrainment concentrations with increasing liquid load. Kampa et al. (Kampa, 2014a and Kampa, 2014b) had shown that these drainage patterns can take the form of either isolated large drops or continuous films, depending on wettability (Fig. 1). While hanging drops suggest blow-off as the dominant mechanism of entrainment, the presence of an oil film makes bursting bubbles the more likely cause for the generation of new drops.

In order to test the relevance of these hypotheses for glass-fiber media and oil, time resolved entrainment rates are compared to changes in oil coverage and drainage patterns on the back of these filter media.

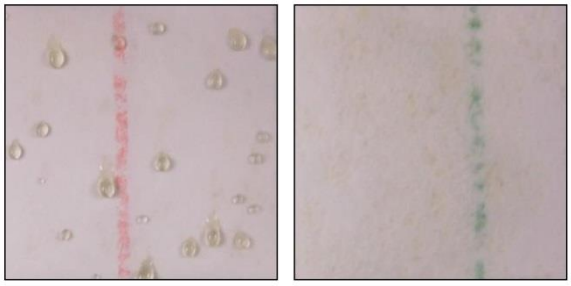

Figure 1: Oil drainage patterns on the back surface of a non-wettable (left) and wettable (right) glass-fiber filter medium.

Funding for this research was provided by Atlas Copco Airpower n.v. and by MANN+HUMMEL GmbH.

Bürkholz, A. (1970), *Chem. Ing. Tech.*, 42, 1314-1321.

Contal, P., Simao, J., Thomas, D., Frising ,T., Calle, S., Appert-Collin, J. C. & Bemer, D. (2004), *J. Aerosol Sci.*, 35, 263-278.

Kampa, D., Wurster ,S., Buzengeiger ,J., Meyer, J. & Kasper, G. (2014a), *Int. J. Multiphase Flow*, 58, 313-324.

Kampa, D., Wurster, S., Meyer, J. & Kasper, G. (2014b), *Chem. Eng. Sci.*, 122, 150-160.

Mullins, B. J., Braddock, R. D., Agranovski, I. E., Cropp, R. A. & O'Leary, R. A. (2005), *J. Colloid Interface Sci.*, 284, 245-254.

Payet, S., Boulaud, D., Madelaine, G. & Renoux, A. (1992), *J. Aerosol Sci.*, 23, 723-735.

Raynor, P. C. & Leith, D. (2000), *J. Aerosol Sci.*, 31, 19-34.

Saemundsson, H. B. (1968), *Verfahrenstechnik*, 2, 480-486.

Establishing SI-traceability for the measurement of particle number concentration with condensation particle counters

Hans-Georg Horn*

TSI GmbH, Neuköllner Straße 4, 52068 Aachen, Germany

Keywords: number concentration, CPC, standards, tracability

The measurement of particle number concentration (PNC) plays an increasing role in regulated measurements. Therefore, the requirement of SI-traceability of the measure and PNC got into focus over the recent years. The most important step to achieve SI-traceability is standardization of the calibration of measurement instruments.

The Condensation Particle Counter (CPC) is the most common tool to measure "total" PNC. A meanwhile established example for the regulated application of CPCs is the measurement of particle number concentration for the certification of new vehicles and engines (UN-ECE Regulations 49 and 83, Euro 6 and VI). Actually, standardization of the measurement of total PNC in ambient air, e.g. for monitoring purposes, is underway (CEN TC 264/WG 32). To support traceable CPC calibration, ISO TC 24/SC 4/WG 12 just published the International Standard ISO 27891. In parallel, several National Metrology Institutes (NMI) completed a project (EMRP ENV-02) which enables them to offer national particle number concentration standards based on aerosol electrometers. NMI-calibrated PNC instruments filled the last remaining gap to close the traceability chain.

ISO 27891 standardizes how to calibrate the detection efficiency of CPCs for a certain particle size and PNC. It also sets requirements for valid calibration measurements and provides the tools to determine the associated calibration measurement uncertainty. However, this International Standard does not pre-define which aerosol particle material, particle size or PNC shall be used. Application standards, regulations or guidelines must serve this purpose. For example, the UN-ECE/GRPE/PMP working group proposed that a CPC used for vehicle and engine exhaust measurements shall have a detection efficiency of 50 % ±12 % at 23 nm and >90 % at 41 nm. Linearity of response to PNC must be within 0.9 to 1.1 for PNC up to 10,000 cm^{-3}. For ambient "total" PNC measurement, CEN TC264/WG 32 proposes a CPC detection efficiency of 50 % at 7 nm ±10 % and >90 % at 14 nm; it also sets linearity requirements for PNC measurement up to 100,000 cm^{-3}.

For both applications, the calibration particle material must be understood as a model substance. Available aerosol generation methods, their stability over time and achievable repeatability and reproducibility of particle properties play the key role in their selection. When applied after calibration, the CPC will measure particles which are different from the calibration particles. However, activation of droplet growth on particles at the size-wise low end of a CPC's detection efficiency depends on both the measured particle material and the working fluid of the CPC. The goal of the standardization is to achieve good inter-comparability of measurements in the field. If a model aerosol is chosen for calibration, this inter-comparability can only be guaranteed if the CPC's working fluid (n-butanol in both before mentioned cases) is standardized. While the reference calibration material for vehicle/engine emission measurement is PAO 4; the CEN working group proposes calibration with sintered Ag particles.

To achieve SI-traceability for PNC measurements with CPCs, all components discussed above must be obeyed.

*) Dr.-Ing. Hans-Georg Horn
Global Product Manager at TSI; convenor of ISO TC 24/SC 4/WG 12; member of UN-ECE/GRPE/PMP and CEN TC 264/WG 32.

EUSAAR extended range mobility particle size spectrometer

F. Korhonen, P.P. Aalto, E. Siivola, H.E. Manninen and T. Petäjä

[1]Department of Physics, University of Helsinki, P.O.Box 64, FI-00014, Helsinki, Finland

Keywords: atmospheric aerosols, instrumentation, size distribution, spectrometers.

EUSAAR (European Supersites for Atmospheric Aerosol Research) was an EU-funded I3 (Integrated Infrastructures Initiatives) project carried out in the FP6 framework of the specific research and technological development programme "Structuring the European Research Area - Support for Research Infrastructures". EUSAAR work was continued in project ACTRIS in Integrating Activity I3 under the EU FP7. Inside EUSAAR the networking activity NA3 objective 3 was to extend the size range of existing size spectrometers below 10 nm

To achieve this, particle losses inside the spectrometer must be minimized. This can be achieved by increasing the aerosol flow rate of the spectrometer and minimizing the effective length of the spectrometer aerosol lines. These losses have to be experimentally verified. In the spectrometer developed the size range from 6 to 200nm is measured with sheath flow rate of 20LPM and aerosol flow 4LPM. Above 200nm sheath flow rate is 3-5LPM and aerosol flow 1LPM or the CPC inlet flow. Typical detection efficiency in 10nm is 50% and 6nm 30%. The differential mobility analyser used in the spectrometer is a modified version of the Vienna VIE-06 analyser (Winklmayr *et al.* 1991). The main modifications are minimizing the distance the charged aerosol flows inside the insulator and fixing the central electrode to the bottom of the analyser (Figure 1.). It is also possible to exchange the original plastic insulator with a slightly conducting insulator to avoid charge accumulation to the insulator.

The particle counter used in the spectrometer should able to measure concentration in as low particle sizes as possible with decent aerosol flow rate, like 1 LPM. Particle counter should be also fairly fast to react to rapid concentration changes. In some particle counters one has to increase the temperature difference between condenser and saturator to reach the required particle sizes. However by doing this one might lose the guarantee.

It is also important that the classifying voltage inside the differential mobility analyser is set as accurately as possible. This is especially important in the low end. To achieve this a special high voltage supply was built (Korhonen, 2013). The supply is working with an accuracy of 0.2% or 200mV, whichever is greater. The supply is operated via serial interface, not with an analogue signal typical for the standard supplies.

Otherwise the design follows the ACTRIS standard spectrometer (Wiedensohler, 2013). Sheath flow is generated with a blower and measured with mass flow meter, which outputs also volumetric flow. Temperature and pressure are measured so that they correspond the conditions inside the analyser. Aerosol inlet flow relative humidity and volumetric flow are measured. Aerosol flow is dried with a special Nafion drier especially designed for aerosol measurements by Leibniz Institute for Tropospheric Research (TROPOS), Leipzig. Particles are brought to charge balance with 370 MBq C-14 source producing beta radiation.

Instruments have been operated on the field over many years and have proven to be fairly reliable (Herrman, 2014). The instrument is operated with MBED lpc1768 microcontroller, which can operate the system independently or under computer control via serial or Ethernet line.

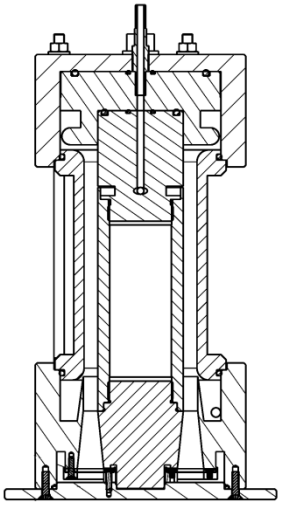

Figure 1. Modified version of the VIE-06 analyser.

This work was accomplished by the European research infrastructure project EUSAAR

Herrman, E., *et al. (2014). Atmospheric Chemistry and Physics*, 14 , 2169-2183

Korhonen, F., (2013). *http://urn.fi/URN:NBN:fi:amk-201303123212*

Wiedensohler, A.., *et al.* (2012). *Atmospheric Measurement Techniques*, 5, 657-685

Winklmayr, W. *et al.*, (1991). *J. Aerosol Sci*. 22, 289

ACTRIS: http://www.actris.net/

EUSAAR: http://www.eusaar.net/

Evaluation of SMPS and ELPI methods for the on-line determination of the morphology of aggregated copper nanoparticles at different sintering stages

D. Kiesler, M. Stein, Y. Beckmann, D. Pawlak and F.E. Kruis

Institute of Technology for Nanostructures and CENIDE, University Duisburg-Essen, 47057, Duisburg, Germany

Keywords: Agglomerate structure, On-line measurement, DMA, ELPI.

On-line measurement techniques, which offer not only information about one specific size parameter but also information about the morphology of aerosol nanoparticles, are relevant for the production of technical aerosols. Multi-parameter characterization by measuring different physical properties like electrical mobility (DMA), Stokes-number (ELPI) or mass (APM) can lead to further information about the morphology, such as the effective density or the mass-mobility-exponent D_{fm}. However, in order to obtain all required parameters for the applied models, information about the primary particles still requires off-line measurements, like BET or TEM.

In this work, we focus on the measurements of Stokes-number and electrical mobility. The aerosol is produced by an anodic-arc evaporation of copper. A small fraction of the product aerosol is used for the online measurement with a scanning mobility particle sizer (SMPS) and an electrical low-pressure impactor (ELPI). Different aggregate morphologies can be created by sintering the Cu aggregates. Additionally, a differential mobility analyzer (DMA1) can be used, to characterize only a size fraction of the input aerosol. An electrostatic precipitator (ESP) can be used to acquire samples for TEM investigation.

This setup allows the investigation off different techniques for the determination of the mass-mobility-exponent D_{fm}. By turning off DMA1, the parallel methods can be tested. The simplest approach is the fit suggested by Stein et al. (2013) assuming a constant effective density ρ_{eff} for the full size range. A more refined method adapts ρ_{eff} for different sizes and thus extracting D_{fm}, as suggested by Virtanen et al.(2010). To validate these results, it is also possible to measure only one size-fraction of the aerosol and measure a size-dependent ρ_{eff} as has been done by Maricq et al. (2004). For the evaluation of D_{fm} two techniques can be applied to the data. The first approach is to directly fit ρ_{eff} as a function of the mobility diameter d_{b}. Another way is use ρ_{eff} to calculate the aggregate mass m_{p} and apply the dimensionless formula used for APM data evaluation by Eggersdorfer et al. (2012):

$$\frac{m_{\mathrm{p}}}{m_{\mathrm{prim}}} = k_{\mathrm{b}} \left(\frac{d_{\mathrm{b}}}{d_{\mathrm{prim}}} \right)^{D_{\mathrm{fm}}}$$

An example for this comparison is shown in figure 1. The temperature where sintering starts changes between 550°C-600°C depending on the method used.

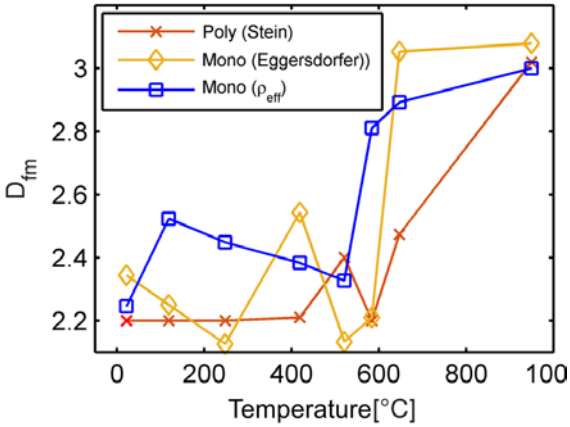

Figure 1: Obtained mass-mobility exponents D_{fm} for different sintering temperatures by using parallel or serial DMA-ELPI measurements.

The research leading to these results has received funding from the European Union's Seventh Framework Program under Grant Agreement No. 280765 (BUONAPART-E) as well as from the Deutsche Forschungs Gemeinschaft in the framework of the joint research program "multi-parameter characterization of particle-based functional materials by innovative online measurement technology" (PAK688).

Stein, M., Kiesler, D., & Kruis, F.E. (2013). *J. Nanopart. Res.*, 15(1), 1400.

Stein, M., Kiesler, D., & Kruis, F.E. (2013). *Aerosol Sci. Technol.*, 47(11), 1276-1284.

Virtanen, A., Ristimäki, J., & Keskinen, J. (2004). *Aerosol Sci. Technol.*, 38(5), 437-466.

Maricq, M. M., Podsialik, D. H., & Chase, R. E. (2000). *Aerosol Sci. Technol.* 33, 239–260.

Eggersdorfer, M. L., Gröhn, A. J., Sorensen, C. M., McMurry, P. H., & Pratsinis, S. E. (2012). *J. Colloid Interface Sci.*, 387(1), 12-23.

Experimental and Algorithmic Study of Soot Oxidative Fragmentation

A. D. Melas[1,2], P. Baltzopoulou[1], M. Kostoglou[1,3], E. Daskalos[1], Y. Drossinos[4], A.G. Konstandopoulos[1,2]

[1]Aerosol and Particle Technology Laboratory, CPERI/CERTH, P.O. Box 60361, Thermi 57001, Greece
[2]Department of Chemical Engineering, Aristotle University, Thessaloniki, Greece
[3]Department of Chemistry, Aristotle University, Thessaloniki, Greece
[4]Join Research Centre, European Commission, Ispra, Italy

Keywords: soot, aggregate, fragmentation, oxidation .

Over the last years, legislation on particulate matter emissions of diesel cars focuses on ultrafine particles (smaller than 100nm) which are claimed to be responsible for climate change and irreversible health effects. It is characteristic that in Euro 5b, a particle number limit was introduced in addition to the already existing particulate mass limit. Particle number and size distribution are unstable and depend on internal processes like coagulation and fragmentation (Friedlander, 2000). While the coagulation kernel has been extensively studied in the literature (e.g. Kostoglou and Konstandopoulos, 2001), there is still lack of understanding about the fragmentation mechanism.

Harris and Maricq (2002) found that soot particle size distributions from various types of diesel engines have a lognormal shape which may be predicted from the solution of the fragmentation-aggregation equation with Brownian coagulation in the continuum regime. Kostoglou and Konstandopoulos (2003) introduced a more-physically based fragmentation mechanism. Accordingly, fragmentation of the soot aggregates is assumed to occur due to surface oxidation of the solid contacts between the primary particles, the so-called “necks”. Necks are smaller than the primary particle size and fragmentation may occur before a significant reduction of the primary particle size.

Herein, we study the behavior of well-characterized soot aggregates generated by CAST in a heated reactor at temperatures up to 850^{o}C. Two different oxidants are used (O2, mixture of O2 & NO2) and different measurement techniques are applied in parallel. For both oxidants, after the burnout of 50 to 70% of soot, a particle number increase and a new particle size distribution are observed. Particles with diameters similar to primary particle diameters appear initially in small concentration, which increases as the temperature increases. A preliminary attempt to understand the fragmentation process impact on the aggregate population dynamics is done by formulating a Monte-Carlo simulation of aggregate fragmentation. The results of the simulation substantiate some of the experimental observations. from the atmosphere (so called air-capture).

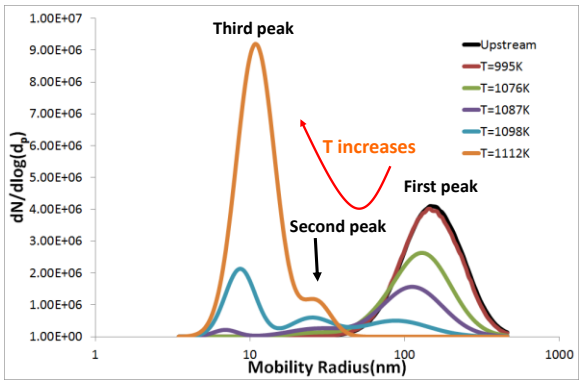

Figure 1. Appearance of oxidative fragmentation modes as temperature is increased.

This work was supported by the European Commission through Project APT-STEP.

Friedlander, S. K. (2000) Smoke, Dust and Haze. Fundamentals of Aerosol Dynamics, 2nd Ed., Oxford.
Kostoglou M. and Konstandopoulos, A.G. (2001) Journal of Aerosol Science, 32 (12), pp. 1399-1420.
Harris, S.J. & Maricq, M.M. (2002). The Role of Fragmentation in Defining the Signature Size Distribution of Diesel Soot. J. Aerosol Science, 33, 935–942.
Kostoglou M. and Konstandopoulos, A.G. (2003) Journal of Aerosol Science, Special Issue, S1061-S1062.

Experimental characterization of the air flow in a ventilated duct in contribution to particle resuspension mechanism study at micro scale

F. Théron[1], L. Le Coq[1], D. Debba[1] and C. Solliec[1]

[1]GEPEA, CNRS, UMR 6144, Ecole des Mines de Nantes, BP 20722, 44307 Nantes, France

Keywords: Resuspension of dry particles, Velocity profile, Turbulence characterization, Hot Wire Anemometry

Even if particle resuspension has been well studied through experimental, theoretical and numerical approaches (Kassab *et al.*, 2013; Henry and Minier, 2014), there are still issues to be addressed to well describe the involved mechanisms. Among these issues is the influence of the flow structure at the wall vicinity on particles trajectories.

This study thus deals with the experimental characterization of the air flow in a duct dedicated to further investigate the resuspension mechanism at local scale. The aims are to get information about the air velocity profiles in the duct, especially at the close vicinity of the wall, and about the characteristic scales of eddies in the boundary layer which will be encountered by the particles.

For that purpose Hot Wire Anemometry has been used as it represents the advantage to obtain instantaneous velocity recording. Velocity measurements have been performed in a ventilated duct of rectangular cross section (4x20 cm²), and of 2 meters length, made of transparent antistatic polycarbonate material. In order to well investigate the flow close to the wall (in the viscous boundary layer) a boundary layer probe has been used, and a camera equipped with a magnification system has been implemented to accurately measure the distance between the HWA probe and the wall. Thus velocity measurements have been acquired up to 50 µm from the wall.

Velocity profiles have been obtained at three mean velocities of 3; 5 and 7.6 $m.s^{-1}$. Velocity profiles involved about 100 points along the vertical axis. Each point consists in the instantaneous recording of velocity during about 80 seconds, with a frequency of 200 Hz.

Instantaneous velocity data were firstly treated in terms of mean velocity and turbulence intensity. This first step enabled to characterize the flow profiles to validate the duct design (flow symmetries, established character of the flow), and to compare the dimensionless velocity profiles to the theory (cf. Figure 1).

These dimensionless velocity profiles fitted well to the theory up to y^+ values of about 3, which enabled to calculate the viscous sub-layer thickness δ (770 to 350 µm), and the friction velocity U* (0.16 – 0.36 $m.s^{-1}$).

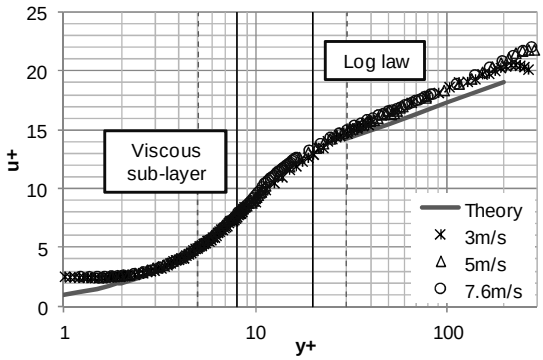

Figure 1. Dimensionless velocity profiles

The second step of this study consisted in investigating the instantaneous velocity recordings at different wall distances. Each temporal signal was decomposed in terms of mean and fluctuating components of the velocity which enabled to calculate the skewness and flatness factors. The values obtained fitted well with data reported in the literature for flow in a larger scale duct (Keirsbulck *et al.*, 2012). Then temporal data were converted in terms of auto correlation coefficients, amplitude and power spectrum. Thanks to these last data eddies time and length scales have been evaluated. The values of major interest are those at the closest wall distance (which is here included in the viscous sub-layer) where particles will be located before resuspension. At this location eddies length scale which has been evaluated ranges from 1 to 2 mm and time scale ranges from 0.010 to 0.003 s.

These results will be related to the resuspension mechanism which is under investigation at local scale in the laboratory, for particle sizes of the order of magnitude of 2 to 30 µm (lower than the viscous sub-layer thickness). Resuspension will be studied for mono-layer particles deposits prepared by sedimentation. Resuspended fraction will be measured thanks to particle counting, and individual particle trajectories will be observed thanks to high-speed imaging.

Henry, C., Minier, J.P. (2014). *Progress in Energy & Combustion Sci.*, 45, 1-53.

Kassab, A.S., Ugaz, V.M., King, M.D., Hassan, Y.A. (2013). *Aerosol Sci. & Technol.*, 47, 351-360.

Keirsbulck, L., Fourrié, G., Labraga, L., Gad-el-Hak, M. (2012). *C. R. Mécanique*, 340, 420-433.

Experimental study and modelling of droplet growth and activation efficiency for efficient aerosol separation by heterogeneous condensation

F. Haller[1], B. Daumann[2], K. Schaber[3], S. Antonyuk[1] and S. Ripperger[1]

[1]Chair of Particle Process Engineering, University of Kaiserslautern, Gottlieb-Daimler-Straße 44, 67663, Kaiserslautern, Germany
[2]Department of Chemical and Process Engineering GCP/TP, BASF SE - L540, 67056, Ludwigshafen, Germany
[3]Institute for Technical Thermodynamics and Refrigeration Engineering, Engler-Bunte-Ring 21, 76131, Karlsruhe, Germany

Keywords: gas cleaning, wet scrubber, heterogeneous condensation, energy effciency

Due to the trend of the reducing emission limit values and the increasing energy costs in Europe, it will be essential to have a smart combination of economic and efficient wet scrubber processes, to abate the last fine particular aerosol fractions with a diameter of smaller than 1µm. Usually for a fine aerosol fraction, a high energy consumption is necessary. The Holzer (1974) figure was developed as a connection between energy consumption and the limit particle diameter of different wet scubbers, shown in Figure 1.

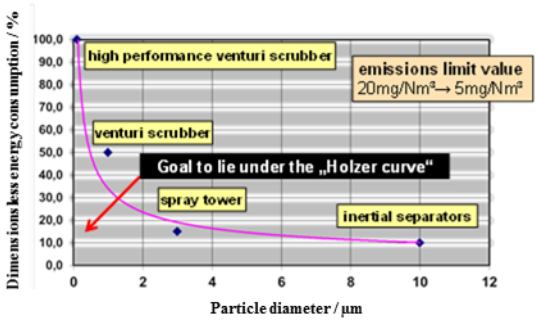

Figure 1: Simplified Holzer diagram of wet scrubbers

In a joint project with industry and university, our focus is lying on the heterogeneous condensation and the growing of aerosol particles to generate a separable aerosol diameter for the wet scrubbers. From the last 10-15 years a lot of knowledge is available about the heterogeneous condensation, about saturation and the growing of the aerosols, according to Gretscher et al. (1999). Our goal of this R&D project is beyond the limits of inertial separation <1.5µm, what means: High raw gas particle concentrations, low saturated and the particle diameter before growing is in a range of 100nm till 300nm.

For the better understanding of efficient separation of submicron aerosols it is necessary to have more knowledge about heterogeneous condensation that will be influenced from the particle shape, kind of surface, surface morphology or agglomeration. The evaluation in lab scale experiments is also important for an industrial scale implementation.

One of the current research activities involves kinetics of heterogeneous condensation of different aerosols. Especially the particles differ in wetting properties, particle shape, surface morphology or agglomeration degree. For this the activation efficiency (ratio of wetted particles relating to total particles) and also the droplet size is examined. Figure 2 shows an example for an investigated carbon black aerosol.

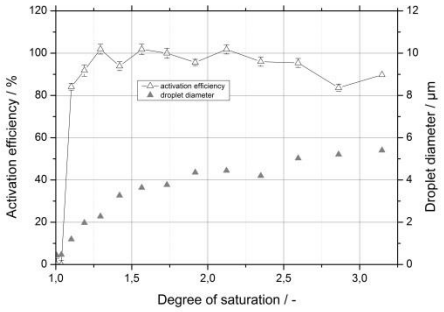

Figure 2. Example for investigated wetting properties of a carbon black aerosol with regard to activation efficiency and droplet diameter

In this study the set up for the experimental investigation of characteristics of different methods to achieve a supersaturated gas phase is presented. Furthermore results from different types of aerosol particles will be shown. Emphasis will be put on methods where a transfer from laboratory to industrial application is possible. Additionally potential concepts of separation as well as model calculations on decreasing the energy consumption will be presented.

Holzer, K. Erfahrungen mit naßabscheidenden Entstaubern in der chemischen Industrie. Staub-Reinhalt. d. Luft 34 (1974) Nr. 10, S. 361-365

Gretscher, H., Schaber, K.: Aerosol formation by heterogeneous nucleation in wet scrubbing processes. Chem. Eng. and Processing 38 (1999) 541 – 548

Niklas, J.; Ripperger, S.: Heterogene Kondensation in Membrankontaktoren. In: Ripperger, S. (Publisher): Fortschritt-Berichte, Wissenschaftliche Schriftenreihe des Lehrstuhls für Mechanische Verfahrenstechnik. Band 8. Technische Universität Kaiserslautern, 2013.

Extending the first nucleation theorem into real environments

J. Malila[1], R. McGraw[2], A. Laaksonen[1,3], and K. E. J. Lehtinen[1,4]

[1]Department of Applied Physics, University of Eastern Finland, 70211 Kuopio, Finland
[2]Biological, Environmental & Climate Sciences Department, Brookhaven National Laboratory, 11973 Upton, New York, USA
[3]Finnish Meteorological Institute, 00101 Helsinki, Finland
[4]Finnish Meteorological Institute, 70211 Kuopio, Finland

Keywords: fundamentals of particle formation, nucleation, nucleation theorem, sum rules

Aerosol synthesis of nanoparticles via nucleation of primary particles and their subsequent assembly into nanostructures is vital for production of novel nanomaterials (Motl *et al*., 2013). To gain further information on the molecular parameters affecting primary particle formation and aggregation, Lümmen and Kraska (2005) applied kinetic nucleation theorems (Ford, 1997) on molecular dynamics-derived formation data of platinum nanoparticles. Although an acceptable practice in the analysis of simulated data—describing nucleation in homogeneous environment, conditions inside actual particle reactors are inhomogeneous (see, *e.g.*, Damour *et al*., 2005), leading to scavenging of subcritical clusters due to coagulation with pre-existing particles and/or sticking on reactor walls, consequently invalidating assumptions used to derive the nucleation theorems. Similar situation is also encountered in an atmospheric setting, where a naïve application of nucleation theorems into measured new particle formation data gives spurious results (Kupiainen-Määttä *et al*., 2014).

We have recently (2015) derived an extended version of the kinetic first nucleation theorem (Ford, 1997; McGraw & Wu, 2003) together with two sum rules that can be used to study the effect of cluster loss on observed g-mer formation rates J_g and on the critical size: Let us consider the Szilárd process, *i.e.* addition or evaporation of a single monomer at time to/from the cluster. Let G be an integer, substantially larger than the kinetic critical size $\bar{g}$ that forms a bottleneck for the nucleation process. In the absence of cluster loss, flux through each size g is the given by $J = J_g$, and it is easy to derive the standard form of the kinetic first nucleation theorem:

$$\left(\frac{\partial \ln J}{\partial \ln n_1}\right)_T = \sum_{g=1}^{G-1} gP(g) + 1, \qquad (1)$$

where n_1 is the concentration of monomers and T is temperature; we identify $\bar{g} = \Sigma_g gP(g)$, where $P(g)$ is the normalised distribution inverse forward rate coefficients p_g (McGraw & Wu, 2003). Extending the analysis into case where each size is scavenged by linear rate $L_g = q_g n_g$, where n_g is the concentration of g-mers, we get the first sum rule

$$\sum_{g=1}^{G-1} J_g P(g) = J, \qquad (2)$$

i.e., the average net forward rate equals J and does not depend on loss rates L_g. Taking logarithmic derivatives on both sides and reorganising we get the second sum rule that generalises the first nucleation theorem [Eq. (1)] into lossy cases:

$$\sum_{g=1}^{G-1} \left[\left(\frac{\partial \ln J_g}{\partial \ln n_1}\right)_{T,\{q_g\}} - g\right] \frac{J_g P(g)}{J} = 1. \qquad (3)$$

Together Eqs. (2) and (3) can be used to, for example, reconcile measurements of J_g from different instruments for nucleation under lossy conditions to estimate the critical size that controls the primary particle size distribution.

Further results can also be obtained (Malila *et al*., 2015): It is possible to give an analytic expression for each $\partial \ln J_g / \partial \ln n_1$, and also for the kinetic critical size averaged over the generalised distribution $J_g P(g)/J$. However, the first mentioned result is too cumbersome to be of any practical use, and the second one does not allow straightforward physical interpretation, as there is no single rate limiting step for the new particle formation if clusters are scavenged. Further work is needed to derive a corresponding generalisation of the second nucleation theorem and to extend the treatment for multicomponent systems, and also to tackle other known deficiencies of nucleation theorems (Kupiainen-Määttä *et al*., 2014).

This work was supported by the Academy of Finland through the Centre-of-Excellence Programme and the ASR Program of US DOE.

Damour, T. M., Ehrman, S. H., Karlsson, M. N. A., Karlsson, L. S., & Deppert, K. (2005). *Aerosol Sci. Tech.*, 39, 444–451.

Ford, I. J. (1997). *Phys. Rev.* E, 56, 5615–5629.

Kupiainen-Määttä, O., Olenius, T., Korhonen, H., Malila, J., Dal Maso, M., Lehtinen, K. E. J., & Vehkamäki, H. (2014). *J. Aerosol Sci.*, 77, 127–144.

Lümmen, N., & Kraska, T. (2005). *Nanotechnology*, 16, 2870–2877.

Malila, J., McGraw, R., Laaksonen, A., & Lehtinen, K. E. J. (2015). *J. Chem. Phys.*, 142, 011102.

McGraw, R., & Wu, D. T. (2003). *J. Chem. Phys.*, 118, 9337–9347.

Motl, N. E., Mann, A. K., & Skrabalak, S. E. (2013). *J. Mater. Chem.* A, 1, 5193–5202.

Filtration of gaseous and particulate iodine with a wet electrostatic precipitator

M. Gouëllo[1], T. Kärkelä[1], J. Hokkinen[1], A. Auvinen[1], P. Rantanen[1]
[1]VTT Technical Research Centre of Finland, P.O. Box 1000, FI-02044 VTT, Finland

Keywords: Particle filtration, electrostatic precipitation, iodine oxide particles

The electrostatic precipitation (ESP) technique is widely used in the industry to filter out impurities in gases. It has been found to be a reliable and effective filtration method in a variety of applications (Riehle 1997). The filtration efficiency of a modern wet electrostatic precipitator (WESP) can be higher than 99.9 % for the particles (Chang 2011). That leads to a decontamination factor higher than 1000. Another advantage of the WESP is that the impurities are removed from the system with water. They can thus directly be transported to a water container, such as a sump in a nuclear power plant (NPP). Radiotoxic iodine has a significant contribution to a possible source term in a severe NPP accident. Therefore, the applicability of the WESP technique on the filtration of fission products, especially gaseous and particulate iodine, is investigated in this study.

Inside an ESP a corona is formed on the tip of the centre electrode in a high electric field. Ions travelling from the centre electrode to the collection electrode charge particles during their flight. In the electric field charged particles drift to the collection electrode. For small particles, less than 1 µm in diameter, charging efficiency may be too low for effective filtration. These particles are filtered with an ion wind principle. Momentum of the ions travelling to the collection electrode drives small aerosol particles there as well. The filtration efficiency has been further enhanced in the studied WESP filter by spraying water droplets to the gas flow. Inside the filtration unit large droplets are charged and driven to the collection electrode. The droplets are very efficient in trapping small particles.

The ESP technique can also be used to filter gaseous pollutants when the gas flow is pre-treated before the filtration unit. The water droplets fed into the system adsorb gaseous impurities. The effect can be enhanced by injecting additives with the water. The gaseous compounds can also be oxidized to form solid particles which are filtered with the ESP technique. In this study on iodine filtration with a WESP, both proposed methods are used for the decontamination of gaseous species in containment conditions. Gaseous iodine is oxidized with additional ozone and water droplets are fed to the gas flow just before the filtration unit of WESP. The oxidation of gaseous iodine by ozone has previously been studied at VTT (Kärkelä 2009).

The preliminary experiments were carried out with TiO_2 aerosol. The applied electric voltage between the electrodes, the residence time of particles inside the ESP chamber and the injection of water droplets before the ESP chamber were varied in the first experiments. As it is shown in Figure 1, the injection of water droplets significantly increased the trapping efficiency of TiO_2 particles for applied electric voltage less than 15 kV (negative).

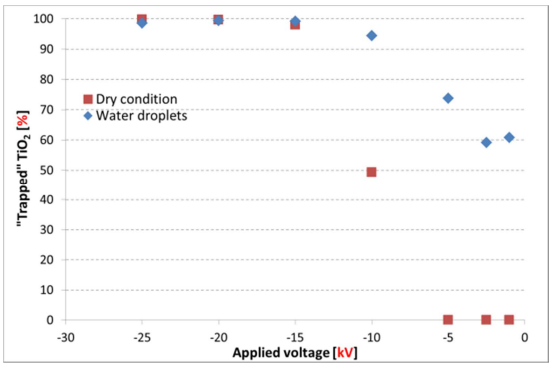

Figure 1. Evolution of the fraction of trapped TiO_2 particles with the WESP filter, as a function of applied electric voltage, with or without the presence of water droplets in the gas flow.

In the iodine experiments, the gas flow containing elemental iodine (2.2 l/min, 16 ppm of I_2) was mixed with ozone (3 l/min, > 1000 ppm) in order to oxidize all gaseous iodine to iodine oxide particles. The number size distribution and the number concentration of the formed iodine oxide particles were measured online with ELPI and SMPS devices. A result of the first filtration experiments with iodine oxides, more than 98 % of IO_x particles was filtered with the WESP when the applied electric voltage was in a range from -10 kV to -25 kV.

This study is partly funded by the European Atomic Energy Community's (Euratom) Seventh Framework Programme FP7/2007-2013 under grant agreement n° 323217.

Riehle, C. (1997). *Basic and theoretical operation of ESP's*, in Parker, K.R., Applied electrostatic precipitation, Chapman & Hall, London, UK.

Chang, J-S. Dong, Y., Wang, Z., Wang, P., Chen, P., Man, C (2003). *Journal of Aerosol Science*, 42, 544–554.

Kärkelä, T., Holm, J., Auvinen, A., Ekberg, C., Glänneskog, H. (2009). *Iodine Chemistry (EXSI)-Containment Experiments with Elemental Iodine*, .Nordisk Kernesikkerhedsforskning, Roskilde (Denmark), No.NKS-204.

First measurements of the number size distribution of 1 – 2 nm particles released from manufacturing processes in a cleanroom environment

L. R. Ahonen[1], J. Kangasluoma[1], J. Lammi[2], K. Lehtipalo[1], T. Petäjä[1] and M. Kulmala[1]
[1]Department of Physics, University of Helsinki, P.O. Box 64, FI-00014, Helsinki, Finland
[2]Beneq Oy, P.O. Box 4, FI-02201 Espoo, Finland

Keywords: nanoparticles, cleanroom, CPC.

Airborne particles in a cleanroom environment are monitored and controlled for product quality and worker safety point of view. In this study we used an instrument capable of measuring total number concentration of particles starting from particles consisting of just a few molecules, and the number size distribution between 1-3 nm (mobility equivalent diameter). This was the first time when these kinds of measurements have been performed in a cleanroom environment where the processes could possibly induce particle formation and produce nanoparticles.

An Airmodus A11nCNC system consisting A10 Particle Size Magnifier (PSM) and A20 condensation particle counter and an extra A20 CPC was installed to different locations of production site including different levels of cleanliness. The PSM is a diethylene glycol based continuous flow particle size magnifier where DEG-saturated flow is mixed turbulently to the sample air. The mixture is cooled in a growth tube where supersaturation is achieved. Particles starting from 1 nm are grown to approximately 90 nm (Vanhanen et al., 2011). A20 is a traditional n-butanol based CPC with cut-off diameter around 7 nm. Novel calibration with material similar to the materials used in some of the coating processes performed in the cleanroom was conducted in the laboratory after in situ measurements. The calibration was used for the data-inversion which gives the number size distribution in 1 – 3 nm diameter range when the instrument is used in a mode where the saturator flow is changed periodically (Lehtipalo et al., 2014).

The measured concentrations varied a lot between different sampling locations, like assumed. The largest area, which was the least clean space, had by far largest concentrations. The base level concentration was really low, less than 0.1 cm^{-3} for > 1.3 nm particles and 10 - 1000 cm^{-3} for 1.05 – 1.3 nm particles, but during short peaks the concentration climbed from around thousand to million for 1 nm particles and from less than 1 to 20 000 for 2 nm particles per cubic centimetre. The concentration between 1-2 nm was a couple of orders higher than in the > 7 nm size class during these peaks of high concentration. These kind of peaks where observed in a daily basis in this one location during morning time. At other sampling locations base level concentrations were similar to the largest area but only slightly elevated concentrations where observed.

We introduced a novel technique for monitoring airborne particles released from manufacturing or maintenance processes in a cleanroom. We observed 1 - 2 nm particles at all sampling locations and high concentrations in one location, although a specific source was not identified within this study.

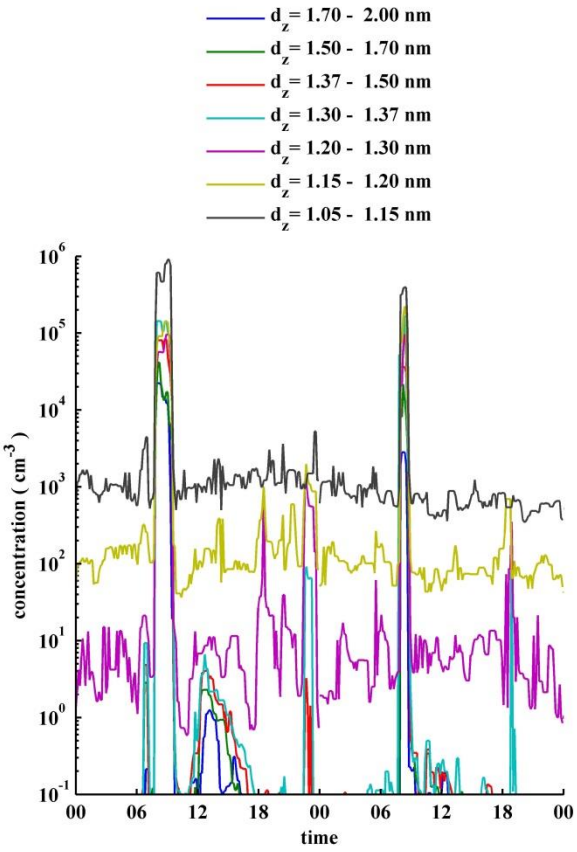

Figure 1. An example of the observed number concentration in different size classes between 1-2 nm at the sampling location with the highest concentrations during a two day period

This work was supported by the Academy of Finland Center of Excellence (project no. 272041).

Lehtipalo, K., et al (2014). *Boreal Environment Research, 19*, 215-236.

Vanhanen, J., et al (2011). *Aerosol Science and Technology, 45*(4), 533-542.

Flame spray pyrolysis of Co_2AlO_4 catalytic nanoparticles

A. Lähde[1], L. Modesto[2], T. Karhunen[1], R.J. Chimentão[3], F. Medina[4], and J. Jokiniemi[1]

[1]Department of Environmetal Science, University of Eastern Finland, 70211, Kuopio, Finland
[2]Department of Aerospace Engineering and Fluid Mechanics, University of Seville, Spain
[3]School of Chemistry, Yachay Tech, Yachay City of Knowledge, Urcuqui, Ecuador
[4]Universitat Rovia i Virgili, Av. Països Catalans 26, ES-43007, Tarragona, Spain

Keywords: flame spray pyrolysis, catalyst, cobalt

The catalytic nanoparticles are typically prepared in a solution followed by thermal treatments in air [Dumond et al. 2007]. However, thermal treatments induce migration of a fraction of cobalt into alumina to form an aluminate spinel that cannot be reduced below 800 ºC. In addition, Co_3O_4 and γ-Al_2O_3 have isotype crystal structures which enables the migration of ions from cobalt oxide into the underlying support. The optimization of dispersion and degree of reduction is therefore demanding.

In this paper we describe one-stage flame spray pyrolysis for production of Co catalytic particles. Unlike the typical wet-based methods, flame spray pyrolysis ensures uniform dispersion of Co and alumina. However, due to the high temperatures of FSP and large amount of water formed during the process, the particles consists mainly of cobalt aluminate spinel.

In order to regain the catalytic activity, the produced powders were reduced using a temperature programmed reduction (TPR) at 850 ºC for 1h. A gas flow of 50 cc/min of 5% H_2 in Ar was used for the reduction. A thermal conductivity detector (TCD) was used to monitor the hydrogen consumption. The powders were characterized with XRD, BET, TEM and SEM/EDS. The catalytic activity of the powders was tested for glycerol hydrogenolysis. The catalytic conversion of glycerol was carried out in gas phase in a quartz fixed bed down flow reactor at 573 K for 6h.

Table 1 shows the elemental composition of as-synthesized Co_2AlO_4 powder. According to the XRD and BET analysis the total surface area of the as-synthesized powder was around 174 m^2/g with a mean pore diameter of 10 nm.

Table 1. Elemental composition of as-synthesized Co_2AlO_4 material.

Element	Weight %	Atomic %
C	5.32	10.09
O	33.46	47.67
Al	37.03	31.28
Co	20.39	7.89
Si	3.79	3.08

The TPR profile of the catalyst powders showed two major fingersprints. A broad peak between 200 ºC and 250 ºC can be related to a two-step reduction as follows Co_3O_4 ➔ CoO ➔ Co. The peaks between 500 ºC and 800 ºC can be assigned to the reduction of cobalt oxides species (Co^{2+} and Co^{3+}) which are strongly interacting with the support to metallic cobalt ($Co_xO_yAl_2O_3$ ➔ Co metal) [Arnodly and Moulijin 1985].

Figure 1 shows catalytic activity of Co_2AlO_4 as a function of time. The reduced Co_2AlO_4 consisting of Co and Al_2O_3 promotes dehydration and dehydrogenation of glycerol, thus yielding hydroxyacetone, lactid acid, and lactide as main products. However, a decrease in the glycerol conversion from 80 % at the beginning to ~ 35 % after 4 h of reaction suggests catalyst deactivation (see Figure 1). The formation of carbon deposits during the dehydration of glycerol presumably contributes to catalyst deactivation. The carbon deposits may result from consecutive reactions of glycerol, e.g., oligomerization on acidic catalyst surface sites and/or side reactions between dehydrated products such as hydroxyacetone.

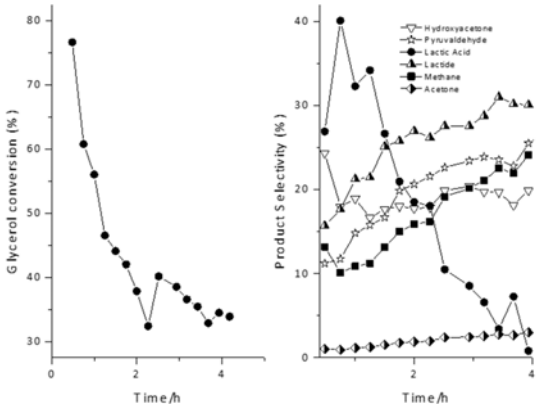

Figure 1. Conversion of glycerol and product selectivity of Co_2AlO_4 catalyst as a function of time of reaction.

This work was supported by the strategic funding of the University of Eastern Finland (Namber).

P. Arnoldy and J.A. Moulijn, J. Catal. (1985), 93, 38.
F. Dumond et al. J. Phys. Chem. C (2007), 111, 4780.

Fluorescence based real-time bioaerosol measurements in urban environment

S. Saari[1], J.V. Niemi[2], T. Rönkkö[1], H. Kuuluvainen[1], A. Järvinen[1], L. Pirjola[3], Minna Aurela[4], Risto Hillamo[4]and J. Keskinen[1]

[1]Department of Physics, Tampere University of Technology, Korkeakoulunkatu 3, 33720, Tampere, Finland
[2]Helsinki Region Environmental Services Authority (HSY), P.O. Box 100, FI-00066 HSY, Finland
[3]Department of Technology, Metropolia University of Applied Science, Kalevankatu 43, FI-00180 Helsinki, Finland
[4]Atmospheric Composition Research, Finnish Meteorological Institute, Erik Palménin aukio 1, FI-00560 Helsinki, Finland

Keywords: fluorescence, bioaerosol, BioScout, UVAPS.

Bioaerosols such as bacteria and fungal spores can cause adverse health effects for people and animals both in indoor and outdoor environments. Atmospheric bioaerosols have been recognized to have important influence in the climate acting as cloud condensation nuclei and ice nuclei and thus contribute cloud formation and precipitation processes. Information on concentrations, particle size distributions and sources of bioaerosols is needed to estimate their health risks and climatic relevance.

In this study, two fluorescence based real-time bioaerosol instruments, BioScout and UVAPS, were used to study atmospheric fluorescent bioaerosol size distribution and concentration in Helsinki metropolitan area during winter and summer. We also demonstrate that comparison between the real-time bioaerosol data and particle mass (PM2.5), black carbon (BC) and nitrogen oxides (NO_x) as well as meteorological data enable to estimate bioaerosol sources and transportation. Contrary to the accepted custom, we especially extend the analysis also to the fluorescent fine particles.

The results showed that there were typically two fluorescent bioaerosol modes (0.5-1.5 µm and 1.5-5 µm) during the summer, whereas the fine mode dominated in the winter. We assume that the modes are mainly originating from fungal spores and bacteria. The concentrations and ratio of the fluorescent particle modes varied between the season periods. Sometimes there was strong diurnal variation in the fluorescent particle concentrations (Fig. 1), which is indication of significant local sources. We found also that the BioScout had typically much higher fluorescent particle counting efficiency than the UV-APS. This is consistent with our laboratory results (Saari et al., 2014).

The previous studies typically treated fine fluorescent particles as non-biological particles, but our results indicate that this is not necessarily the case. The types and sources of fine fluorescent particles should be studied more and compared fluorescence based measurements with other analyzing techniques such as microscopy and quantitative polymerase chain reaction (qPCR).

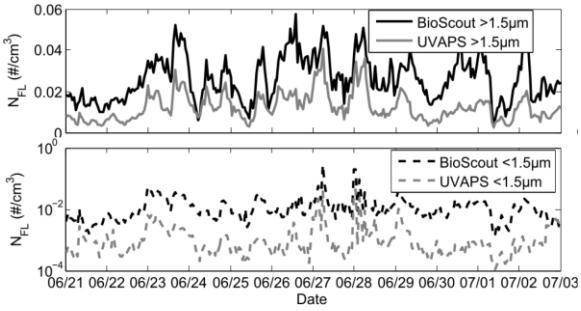

Fig. 1: Time series of fluorescent particle concentrations for the coarse mode (D_p>1.5 µm; above) and fine mode (D_p<1.5 µm; below) measured by the BioScout and the UVAPS during the summer campaign 2012. (Adapted from Saari et al., 2015)

This study provides information on atmospheric bioaerosol characterization by two fluorescence based instruments. The results can be used to estimate health risks and climatic relevance of bioaerosols in urban environments.

This work was supported by the Doctoral School of Tampere University of Technology.

Saari, S., Reponen, T. and Keskinen, J. (2014). *Aerosol Sci. Technol.* 48(4), 371-378.

Saari S., Niemi J.V., Rönkkö, T., Kuuluvainen, H., Järvinen, A., Pirjola, L., Aurela, M., Hillamo, R. and Keskinen, J. (2015). Submitted to *Aerosol and Air Quality Research*.

Formation of particles by radiolytical oxidation of organic iodine

T. Kärkelä[1], A. Auvinen[1], T. Kekki[1], P. Kotiluoto[1], J. Lyyränen[1] and J.K. Jokiniemi[1,2]

[1]VTT Technical Research Centre of Finland, FI-02044 VTT, Finland
[2]University of Eastern Finland, FI-70211 Kuopio, Finland

Keywords: radiation, particle formation, iodine oxide particles.

During a severe nuclear power plant (NPP) accident, iodine is transported from damaged fuel rods through a primary circuit into the gas phase of the containment building. There iodine is exposed to air radiolysis products as well as to the ionizing radiation (such as alpha, beta, gamma and X-ray) itself. This may lead to oxidation of gaseous iodine and subsequent formation of iodine containing aerosol particles. Currently, the effect of radiation on the speciation of gaseous inorganic and organic iodine compounds is not well known. In the large-scale Phébus FP tests one of the most surprising finding for iodine behaviour in containment was a steady state iodine concentration in the containment gas phase, which was reached in every test. While the processes leading to this are not known, several hypotheses have been formulated. One of the hypotheses was that gaseous iodine species released from the containment surfaces would be radiolytically destroyed to form fine particulate iodine oxides or iodine nitrogen oxides. The aim in this study was to find out experimentally, whether UV or beta radiation would be efficient in oxidizing gaseous methyl iodide (CH_3I).

In experiments gaseous methyl iodide was fed into the EXSI CONT facility in an air mixture [Kärkelä et al., 2010]. In some experiments the flow contained also humidity. The reactions took place in a quartz tube heated either to 50 °C, 90 °C or 120 °C. UV-light (including 185 nm wavelength) was used as a source of radiation to produce ozone from oxygen. A separate generator was also applied to reach higher ozone concentrations. Further studies on the radiolytical oxidation of CH_3I in oxygen by beta radiation at 20 °C were carried with the BESSEL facility [Kärkelä et al., 2015].

As a result of CH_3I experiments with EXSI-CONT, there was a clear trend in the formation of gaseous reaction product species. The main gaseous reaction products were methanol and formaldehyde. Especially at elevated temperature other reaction products, such as formic acid and methyl formiate, became important as well. Increasing amount of reaction product species were detected while the concentration of ozone was increased. Similarly, the mass concentration of aerosols increased as well, thus aerosol nucleation was enhanced. Increase in temperature seemed to increase also the aerosol mass concentration. This is probably partly due to more efficient decomposition of gaseous CH_3I and subsequent aerosol formation by ozone.

In the beta irradiation experiments with the BESSEL facility, it was found out that the concentration of formed particles (ca. 10 nm to 50 nm in diameter) decreased very slowly with increasing irradiation time, see Figure 1. It seemed that an equilibrium was reached between gas phase iodine compounds and iodine species deposited on wall surfaces. At that equilibrium the rate of new particle formation was low. When the facility was purged with oxygen, a new formation of particles was observed in every CH_3I experiment. It suggested that the radiolysis reaction products were limiting the particle formation. Oxygen, a precursor of ozone when irradiated, was also needed for the nucleation to take place, since the new particle formation was not observed without irradiation or when the atmosphere was pure nitrogen. The formed particles were highly water soluble and volatile. These findings could also partially explain the constant concentration of iodine, which was observed in the gas phase of containment at the end of every Phébus FP test.

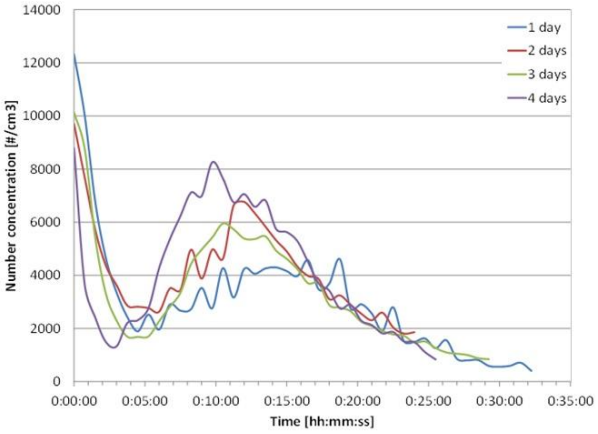

Figure 1. The measured number concentration of IOx particles after an irradiation period of 1 to 4 days when purging the BESSEL chamber with O_2.

Kärkelä, T., Holm, J., Auvinen, A., Zilliacus, R., Kajolinna, T., Tapper, U., Glänneskog, H. & Ekberg, C. (2010). in *Proc. Int. Conf. on Advances in Nuclear Power Plants 2010, San Diego*, Vol. 2, 1084 – 1091.

Kärkelä, T., Auvinen, A., Kekki, T., Kotiluoto, P., Lyyränen, J. & Jokiniemi, J.K. (2015). Submitted to *Radiochimica Acta.*

Generation of neutral calibration clusters

G. Steiner[1,2,*], A. Franchin[1], J. Kangasluoma[1], M. Rissanen[1], T. Petäjä[1] and M. Kulmala[1]

[1] Department of Physics, Division of Atmospheric Sciences, University of Helsinki, P.O. Box 64, 00014, Finland
[2] Institute of Ion Physics and Applied Physics, University of Innsbruck, 6020 Innsbruck, Austria
[*] present address: Faculty of Physics, University of Vienna, 1090 Vienna, Austria

Keywords: electrospray, high resolution DMA, ion recombination, neutral clusters

In recent years, comprehensive efforts have been made for the development of new instrumentation for the detection of airborne neutral molecular clusters and neutral ultrafine aerosols in the size range below 3 nm. These instruments comprise mobility analysis based instruments like the NAIS (neutral air and ion spectrometer, e.g. Manninen et al. 2011), chemical ionization mass spectrometers (Jokinen et al. 2012) and new types of condensation particle counters (Iida et al., 2009, Vanhanen et al. 2010). Despite their different measurement techniques, all these instruments share one requirement: the need for adequate neutral calibration clusters.

This work addresses this issue and concentrates on two possible generation methods of neutral clusters: the neutralization of well-known charged molecular clusters and the recombination of positive and negative ion species of the later clusters. Especially the second method will be discussed in more detail. In this experiment, two high resolution DMAs (e.g. Steiner et al 2010) classify electrospray generated positive and negative monomobile molecular clusters of the ionic liquid ñmethyl trioctylammonium bis (trifluoro methyl sulfonyl) imideò ï in short ñMTOAò. Figure 1 shows a schematic overview of the setup:

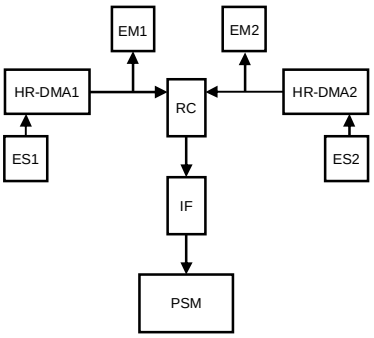

Figure 1. Experimental setup ES1/2: electrosprays; HR-DMA1/2: high resolution DMAs; EM1/2: electrometers; RC: recombination cell; IF: ion filter; PSM: Airmodus A10 Particle Size Magnifier.

After classification, two electrometers determine the total number concentration of charged clusters exiting the DMAs. Subsequently, the airflows containing the positive and negative ion clusters are merged in a recombination cell. Between the recombination cell and the Airmodus A10 PSM, an ion filter ensured that no charged clusters obscured the neutral cluster detection in the PSM.

Figure 2 shows preliminary data of first experiments of the recombination of positive dimer [+2] and negative dimer [-2] MTOA clusters. The upper panel in figure 2 shows a time series of the signal recorded by the two electrometers downstream of the high-resolution DMAs; the lower panel a time series of the signal detected with the PSM.

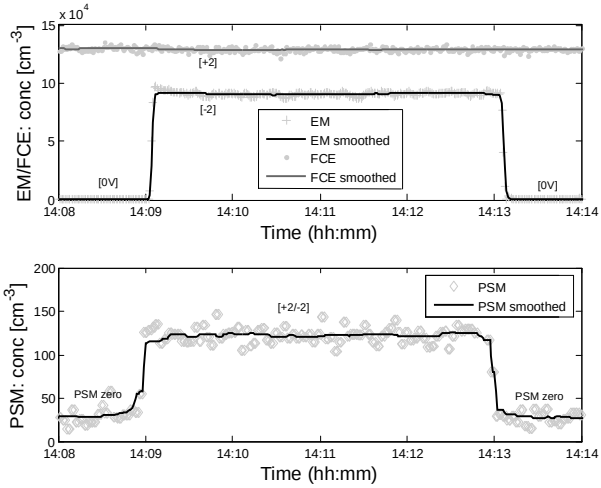

Figure 2. Neutral clusters [+2/-2] detected by the PSM. The clusters are recombination products of positive [+2] and negative [-2] dimers of the ionic liquid ñMTOAò.

A reproducible signal of neutral clusters [+2/-2] originating from the recombination of positive and negative dimers is found.

This work has been funded by the Academy of Finland (Center of Excellence project no. 1118615) and by the University of Innsbruck promotion grant four young researchers.

Manninen H. et al. (2011) *Atmos. Meas. Tech., 4, 2767ï 2776.*
Jokinen, T., et al. (2012) *Atmos. Chem. Phys., 12, 4117-4125.*
Iida, K., et al. (2009) *Aerosol Sci. Technol., 43:1, 81-96*
Vanhanen, J., et al. (2011) *Aerosol Sci. Technol., 45:4, 533-542*
Steiner, G., et al. (2010) *Aerosol. Sci. Technol., 44:4, 308-315*

Generation of Water Soluble Standards Ions in the in the sub 2 nm range

Michel ATTOUI
University Paris-Est Creteil, University Paris-Diderot, LISA, UMR CNRS 7583, France
attoui@u-pec.fr

Keywords: Ions, Standard, Calibration, Nucleation, Nanoparticles

Tetraalkylammonium ions in gas phase produced by electrospray atomization are widely used as mobility standards for drift tube, ion mobility studies coupled to mass spectrometry (IMS-MS) and aerosol instrument calibration (Ude & Fernandez de la Mora 2005,). They are also used in nucleation studies and CPC detection efficiency measurement. It's well known that the nucleation process is significantly dependant of the properties of the site particles such as size, charge state and polarity, solubility, hygroscopicity and or hydrophilicity. Non soluble standard ions produced with electrospray atomization method are widely used in aerosol science technology since the work of Ude and Fernandez de la Mora (2005). Water soluble and or hygroscopic standard ions in the sub 2 nm range were missed until now.

This presentation is focused on the generation of singly charged positive and negative ions of water soluble and or hygroscopic non soluble salts. The particles are produced by electrospray atomization followed bya DMA of high resolution for the mobility measurements in air. The isotopic distribution in both gases of the different ions produced by each salt is measured with a tandem DMA-Mass spectrometer A home-made electrospray source is used in both cases.

Because of the water surface tension needles of 70 to 100 mm ID and 30 mm at the tip are used to spray aqueous solution without CO2 sheath gas around the tip. All the experiments are done with compressed filtered air of the lab.

The following water soluble salts give well defined sharp and singly charged peaks in the sub 2 nm range:

tetrabutylammonium bromide;
tetrabutyl ammonium iodide;
tetrabutyl ammonium chloride;
tetrabutylphosphonium bromide;
tetrahexadecyl ammonium bromide;
tetrahexylammonium bromide;
tetrabutylphosphonium bromide;
tetrapropyl ammonium iodide,…

The figure 1 below gives the size (mobility diameter) distribution of the tetrabutylphosphonium bromide in positive mode. The peaks are sharp well defined drop to zero and are separated by a negligible back ground signal which shows their purity.

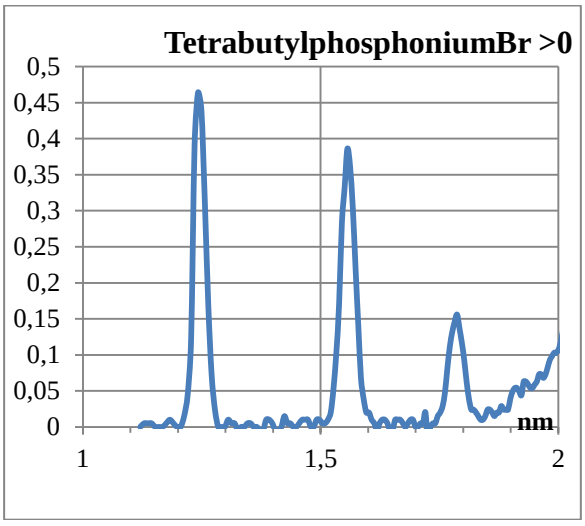

Ude, S. Fernandez de la Mora, J. (2005) J. Aerosol Sci. 36 ; 1224–1237

Generation, characterization and sizing of neutral sub 3 nm metallic clusters

J. Kangasluoma[1], M. Attoui[2], H. Junninen[1], K. Lehtipalo[1], A. Samodurov[1], F. Korhonen[1], N. Sarnela[1], A. Schmidt-Ott[3], D. Worsnop[1,4], M. Kulmala[1], T. Petäjä[1]

1 Department of Physics, P.O. Box 64, 00014, University of Helsinki, Helsinki, Finland
2 University Paris Est Creteil, University Paris-Diderot, LISA, UMR CNRS 7583, France
3 Nanostructured Materials, DelftChemTech, Delft University of Technology, Julianalaan 136, NL-2628BL Delft, The Netherlands
[4] Aerodyne Research Inc., Billerica, MA, USA

**Corresponding author: juha.kangasluoma@helsinki.fi*

Keywords: neutral cluster, nanoparticles, CPC

Neutral particle sizing in the nanometer size range usually relies on known particle charge equilibrium and size resolved charged concentration measurement. At sizes below 3 nm the method becomes unusable due to high particle diffusion losses and low charging probabilities, in addition to the charging method generated ions overlapping with the sample particles. Thus methods to size-resolve particles without charging are needed in the sub 3 nm sizes, and their characterization requires instrumentation to directly measure the composition, as well as methods to generate neutral sub 3 nm particles. These three are the focus of this study.

The test particles were generated with a hot wire generator [*Peineke et al.*, 2009]. One nice feature of the generator is that it generates self-charged particles without an additional charger. We show how to generate four different types of clean metal clusters, clean in the sense that we know exactly the molecular formula from a direct measurement (Figure 1).

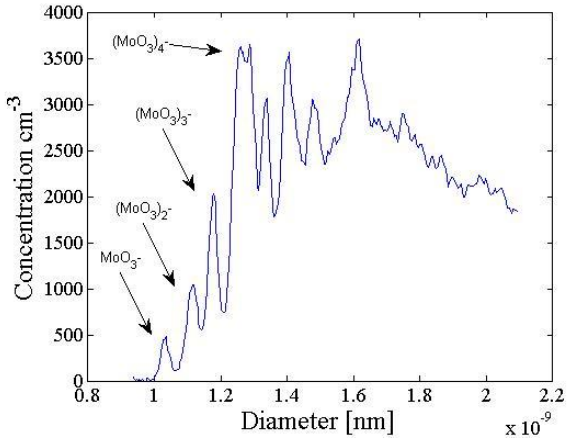

Figure 1. Example mobility spectrum of MO3. Peak identification is done with a mass spectrometer.

With a high resolution mass spectrometer we measured the chemical composition of the self-charged particles, and mechanism for the formation self-charged particles is suggested based on the mass analysis. The composition of the neutral particles was obtained with a controlled nitrate ionization in front of the mass spectrometer.

Finally, with control over the composition of the test aerosol, we calibrated our particle size magnifier (PSM) [*Vanhanen et al.*, 2011], which can measure particle size distributions of 1-3 nm particles. The accuracy of the calibration was tested against another independent method of measuring the same size distribution, which was a combination of high resolution differential mobility analyzer and an electrometer. These experiments provide the first direct verification of the PSM's ability to measure accurately neutral sub 3 nm size distributions.

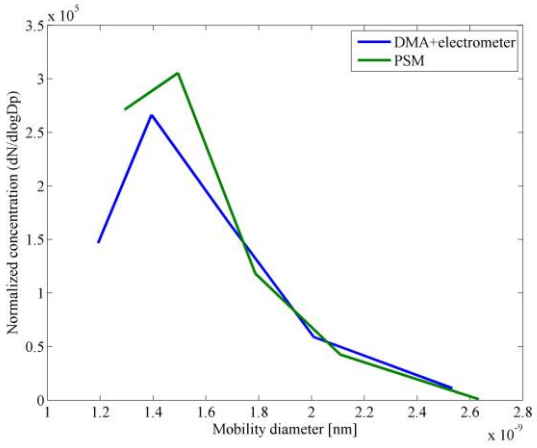

Figure 2. Size distribution of sub 3 nm neutral particles measured with two independent methods.

Acknowledgements

This work was partly funded by European Research Council (ATMNUCLE, 227463), Academy of Finland (Center of Excellence Program projects 1118615 and 139656), Nordic Center for Excellence (CRAICC), European Commission seventh Framework program (ACTRIS, contract no 262254; PEGASOS, contract no 265148) and Maj and Tor Nessling Foundation.

References

Peineke, C., et al. (2009), *J Aerosol Sci*, *40*(5), 423-430.
Vanhanen, J. et al. (2011), *Aerosol Sci Tech*, *45*(4), 533-542.

Heavy-duty diesel vehicle particle emissions during engine braking

P. Karjalainen[1], T. Murtonen[2], F. Mylläri[1], H. Wihersaari[1], J. Keskinen[1] and T. Rönkkö[1]

[1]Department of Physics, Tampere University of Technology, P.O. Box 692, FI-33101 Tampere, Finland
[2]VTT Technical Research Centre of Finland, P.O. Box 1000, FI-02044 VTT, Finland

Keywords: particle emissions, engine braking, diesel, lubricant

Particle emissions from vehicles have been studied and regulated extensively during the last 20 years mainly due to the adverse health effects associated with combustion generated nanoparticles. Recent studies (Rönkkö et al., 2014; Karjalainen et al., 2014) have reported vehicle nanoparticle emissions also during engine braking when the simultaneous fuel consumption is zero. New road diesel engines are equipped with diesel particle filters (DPFs) in Europe and the US, whereas there are no particle filters in the majority of heavy-duty vehicles currently operating. With particle filters the particle emissions during engine braking are considered negligible whereas for the vehicles without the filters these emissions are reality. Here two heady-duty diesel vehicles operating in Helsinki (Finland) area were studied in terms of particle emissions under engine braking conditions.

Two vehicles (Table 1) were tested in the heavy-duty chassis dynamometer facilities of VTT. Test runs consisted of controlled 40-20 km/h and 80-20 km/h deceleration routines and standardized World Harmonized Vehicle Cycle (WHVC) test. The acceleration/deceleration routines were driven in order to study the phenomena related the particles during engine braking in detail. The WHVC test was driven to estimate the role of engine braking related particle emissions over a standardized driving routine.

Table 1. List of studied heavy-duty vehicles. EL = emission level, EC = emission control.

Vehicle	Year	EL	EC	Transmission
Bus	2005	Euro III	EGR	Automatic
Truck	2007	Euro IV	EGR	Manual

The particle sampling was executed with a system consisting of a porous tube diluter, ageing chamber and an ejector diluter. Exhaust particles were measured in real-time with condensation particle counters (CPCs), a high-resolution low pressure impactor (HRLPI) (Arffman et al., 2014) and an engine exhaust particle sizer (EEPS). The particle volatility was studied utilizing a thermodenuder at 265 °C. Exhaust particles were also collected during engine braking and later analysed with a transmission elector microscope.

An example of particle emission profiles measured by the CPCs (top) and EEPS (center) are shown in Figure 1 during the 40-20 km/h test for the truck. The particle concentration levels were comparable between accelerations and decelerations but the particle size was different. During deceleration conducted by engine braking the particle GMD was close to 20 nm, and both the particle size and number concentration had a decreasing trend in time.

The particle emissions during engine braking were found to correlate with engine coolant and oil temperatures. Also it was found that the gear changes during deceleration increased the amount of emitted particles. This can lead to excess particle emissions caused by automatic transmission.

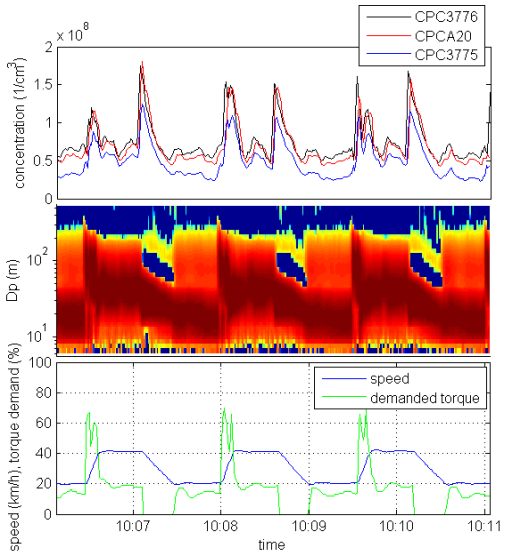

Figure 1. Exhaust particle number concentrations measured by the CPCs (top), size distributions measured by the EEPS (centre), wheel speed and driver's demanded torque on-board diagnostics data (bottom). Cut-sized for CPCs were: 2.5 nm (CPC 3776), 7 nm (CPC A20) and 23 nm (CPC 3775, tuned).

Finnish Transport Safety Agency (Trafi) is acknowledged for the financial support of the study.

Arffman, A. *et al.* (2014). Journal of Aerosol Science, 78, 97-109.

Karjalainen, P. *et al.* (2014). Atmospheric Environment, 97, 262-270.

Rönkkö T. *et al.* (2014). Environmental Science & Technology, 48, 2043-2050.

High-resolution low-pressure cascade impactor

A. Arffman, J. Harra, J. Kalliokoski, P. Karjalainen, T. Rönkkö, J. Yli-Ojanperä and J. Keskinen

Department of Physics, Tampere University of Technology, Aerosol Physics Laboratory, 33101, Tampere, Finland

Keywords: cascade impactor, aerodynamic size

Probably the most important characteristic of nanoaerosol is the particle size distribution. Particle size defines in large extent the behaviour of an aerosol particle in many processes, such as transportation, aerosol dynamics, particle charging, etc. Thus, the measurement of particle size is one of the key aspects in nanoparticle research. In nanoparticle synthesis, emission characterization, and atmospheric research focus is in the particle size range of below 100 nm, and often the phenomena are highly transient (e.g. Karjalainen et al., 2014). This drives the need for high-end measurement devices that operate in real-time and in nanoparticle size range.

There are only a few instruments that are capable to measure below 100 nm particle size in real-time (excluding integral quantities measuring instruments): Electrical Low Pressure Impactor (ELPI, Keskinen et al., 1992) and Engine Exhaust Particle Sizer (EEPS, TSI Inc.) ELPI measures aerodynamic size distribution using the electrical detection of particles with a cascade impactor, and has 12 channels in the measurement range of 16 – 10000 nm, and below 100 nm, 4 channels. EEPS measures electrical mobility size distribution using electrical detection of particles and has 22 current measurement channels in the size range of 6–560 nm. ELPI has coarse resolution under 100 nm compared to EEPS, limiting its applicability in nanoparticle studies.

In this study, we present a new high-resolution low-pressure cascade impactor (HRLPI, Arffman et al., 2014) that has 10 impactor stages in the size range of 7.7–142 nm and a filter stage. The HRLPI impactor operates at 40 mbar pressure with the sample flow rate of 1.1 lpm. The HRLPI was fitted to the ELPI body, and a small self-made corona charger was used before the impactor to produce a known charge distribution for particles. HRLPI uses a separate pressure reduction inlet to bring the aerosol from the ambient pressure to the impactor inlet pressure. The essential feature in the HRLPI is to use slit type, short throat length nozzles in the impactor stages. The nozzles of this type have been shown to produce very steep collection efficiency curve shape (Arffman et al., 2012). Sharp cut-curve shape allows doubling the number of measurement channels below 100 nm compared to ELPI impactor without significant overlap of kernels. The minimal overlap of the kernels makes the inversion or interpretation of the measurement results simple and robust, as the cut-point concept works well with HRLPI. All the impactor stages, charger and inlet were fully calibrated with monodisperse dioctylsebacate (DOS) particles produced by SCAR instrument (Yli-Ojanperä, 2010) and an evaporation-condensation method.

In the laboratory, the performance of HRLPI was compared to ELPI+, ELPI with improved nanoparticle resolution (EELPI), EEPS, and two SMPSs (DMA models TSI 3071 and TSI 3085). The instrument was also tested in the field measurements, where the diesel exhaust of a modern passenger car engine was characterized with HRLPI, EELPI and EEPS in parallel. Figure 1 shows an example of the test measurement results.

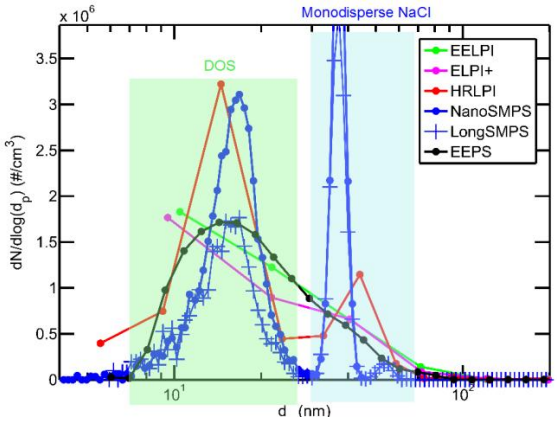

Figure 1. Particle size distribution measured with different instruments for externally mixed DOS and NaCl aerosol.

Results of the test measurements showed that HRLPI is a well-suited aerodynamic size measurement instrument for the cases where the interesting size range is approximately 5–200 nm. Compared to the other low-pressure impactors, it has a better size resolution and the lowest cut point. By combining the mobility and aerodynamic particle size distribution measurements of EEPS and HRLPI, the effective density of the particles down to at least 7 nm can be determined in real time.

Keskinen J. et al. (1992) *J. Aerosol Sci. 23*, 353-360
Karjalainen P. et al. (2014) *Environ. Sci. Technol. 48* (4), 2336-2343
Arffman A. et. al. (2014) *J. Aerosol Sci.. 78*, 97–109
Arffman A. et al. (2012) *J. of Aerosol Sci, 53*, 76-84
Yli-Ojanperä et al. (2010) *J. Aerosol Sci. 41*, 719-728

High-speed fabrication of superhydrophobic nanocoating by Liquid Flame Spray

J. Haapanen[1], M. Aromaa[1], H. Teisala[2], M. Tuominen[2,3], M. Sillanpää[4], M. Stepien[5], J.J. Saarinen[5], M. Toivakka[5], J. Kuusipalo[2] and J.M. Mäkelä[1]

[1] Aerosol Physics Laboratory, Department of Physics, Tampere University of Technology, Tampere, Finland
[2] Paper Converting and Packaging Technology, Department of Materials Science, Tampere University of Technology, Tampere, Finland
[3] SP Technical Research Institute of Sweden, Chemistry, Materials and Surfaces, Stockholm, Sweden
[4] Laboratory centre, Finnish Environment Institute, Helsinki, Finland
[5] Laboratory for Paper Coating and Converting, Abo Akademi University, Turku, Finland

Keywords: aerosol synthesis, Liquid Flame Spray, nanoparticles, nanocoatings

Liquid Flame Spray (LFS) is an aerosol synthesis method for production of nanoparticles and nanostructured coatings. High-speed fabrication of nanocoated surfaces has been an issue for decades. We present high-velocity roll-to-roll fabricating of superhydrophobic surfaces by LFS. With paperboard line speeds up to 300 m/min, method gives promising results in pilot scale and shows a great potential for up-scaling.

LFS is a versatile method for synthesizing nanoparticles. In LFS method, liquid precursor solution is fed via burner nozzle to a turbulent hydrogen-oxygen flame. Through various aerosol processes, nanoparticles are formed (Haapanen et al.). With variable process parameters, nanoparticle production rate, size and rate of agglomeration can be fixed on desired level.

In this study, TiO_2 nanoparticles were deposited on paperboard surface in roll-to-roll process. LFS-made TiO_2 nanocoating is known to produce superhydrophobic surface on paperboard with the line speed of 50 m/min (Aromaa et al., Teisala et al.). Precursor solution was prepared by mixing titanium(IV) isopropoxide (TTIP) and isopropanol. Produced nanoparticles are analysed in aerosol stage by SMPS and as deposits on paperboard surface by SEM. Wetting behavior of nanocoated paperboard surface is determined as water contact angle values, measured by goniometer. Total mass of deposited nanoparticles has been evaluated by inductively coupled plasma mass spectrometry (ICP-MS). Yield of the coating process is determined from ICP-MS results.

As a result, roll-to-roll line speeds from 50 m/min to 300 m/min are demonstrated succesfully. Results of water contact angle measurement 1 day after the coating process are displayed in Figure 1. Results show high level of hydrophobicity even with line speed of 300 m/min. All measured water contact angle values are above 140° and the reference value of uncoated paperboard is 80°. According to these results, LFS is a competitive method for fabricating superhydrophobic TiO_2-nanocoatings for paperboard in large scale. Primary particle size for TiO_2-deposits is mainly 20-50 nm, verified by SEM and TEM analyses.

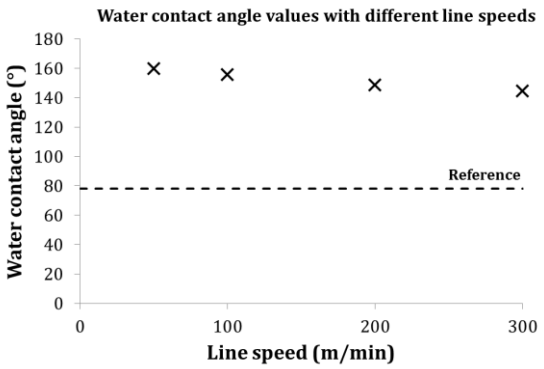

Figure 1. Water contact angle values for TiO_2-nanocoated paperboard with line speeds of 50, 100, 200 and 300 m/min.

This work was funded by the Finnish Funding Agency for Innovation (Tekes), project Nanorata 2.

Haapanen et al. (2014). *Binary TiO_2/SiO_2 nanoparticle coating for controlling the wetting properties of paperboard*. Mater. Chem. Phys., doi: 10.1016/j.matchemphys.2014.10.011 (in press)

Aromaa et al. (2012). *Atmospheric Synthesis of Superhydrophobic Carbon Coated TiO_2 Nanoparticle Deposits in a Single Step using Liquid Flame Spray*, J. Aerosol Sci. 52, pp. 57-68

Teisala et al. (2013). *Wettability conversion on the liquid flame spray generated superhydrophobic TiO2 nanoparticle coating on paper and board by photocatalytic decomposition of spontaneously accumulated carbonaceous overlayer*, Cellulose: Volume 20, Issue 1 (2013), pp. 391-408

High temperature sample and low particle concentration – challenge for measurements

V. Niemelä[1], J. Kannosto[1], K. Lehtoranta[2], T. Rönkkö[3], J. Alanen[3], A. Ukkonen[1]

[1]Dekati Ltd., FI-36240, Kangasala, Finland
[2]VTT, Technical Research Centre of Finland, FI-02044, Espoo, Finland
[3]Department of Physics, Tampere University of Technology, FI-33101, Tampere, Finland

Keywords: ELPI+™, HT-ELPI+™, engine exhaust,

In engine exhaust particle measurements, the sample is usually warm. Sample temperature needs to decrease before it can be measure with real-time aerosol measurement instruments. By decreasing the sample temperature, there is possibility to have condensation and/or nucleation of water, sulphuric compound and VOC. When the aim of the research is to study solid exhaust particles this problem is typically handled with a dilution system that decreases the temperature and vapor pressures in two dilution stages including thermal treatment. However with low-emission vehicles, this might also lower the particle concentration below instrument detection limit. Also, despite the controlled temperature profile dilution might still affect the size, composition and structure of particles, and uncertainty in dilution factor might decrease the measurement accuracy.

To avoid these issues a new version of the Electrical Low Pressure Impactor ELPI+™ was developed for high temperature, low concentration measurement. In this system, the detector part, impactor, is heated to a sample temperature up to 180C, see Figure 1. This allows high temperature tailpipe aerosol measurement without dilution, without sample cooling and without VOC condensation. In other words, the particles are measured as they exist in the tailpipe.

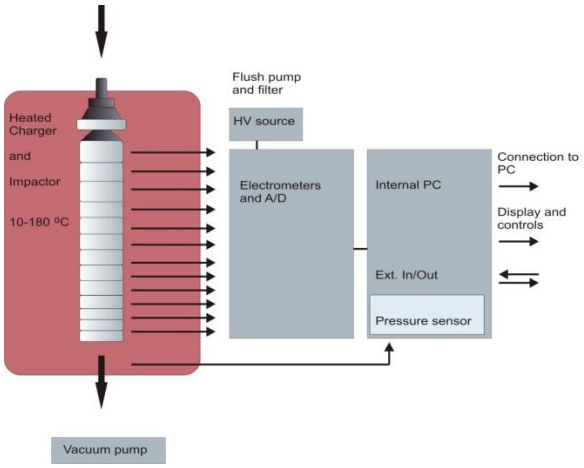

Figure 1. Operating principle of the High Temperature ELPI+™. Impactor is heated to be able to operate with high temperature sample

The system was tested with a 2-litre passenger car engine that was modified for natural gas fuel, known to produce very low particle emissions. In the test setup, the exhaust gas composition was made adjustable by adding methane, propane, ethane and ethene to tailpipe-extracted side flow to mimic large bore engine (ship / power plant) emission composition.

The developed High Temperature ELPI+™ was used to measure the particle size distribution and concentration from tailpipe environment before catalysts. A bimodal particle number size distribution was detected, one mode at below 10 nm particle size range and the other mode at around 30 nm, see Figure 2. A volume-weighed size distribution also shows a large particle mode at around 750 nm.

In this presentation, we describe the HT-ELPI+™ and the engine and exhaust conditioning setup and present the particle measurement results from the system. We also discuss about the detected particles and their origin and present comparison results from other instruments (EEPS, SMPS and gravimetric filter measurement) that simultaneously measured diluted exhaust.

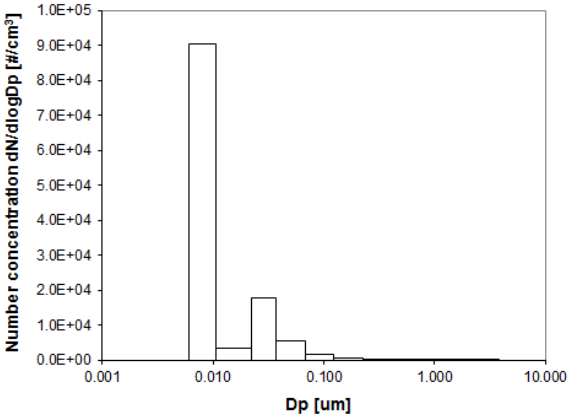

Figure 2. Number size distribution measured with HT-ELPI+™.

Homogeneous coating of aerosol nano particles in a cold plasma at atmospheric pressure

P. Post[1], S. Dahle[2], W. Maus-Friedrichs[2] and A.P. Weber[1]

[1]Insitute of Particle Technology, Clausthal University of Technology, Leibnizstraße 19, 38678, Clausthal-Zellerfeld, Germany
[2]Insitute of Energy Research and Physical Technologies, Clausthal University of Technology, Leibnizstraße 4, 38678, Clausthal-Zellerfeld, Germany

Keywords: plasmas, particle surface coatings

The coating of nano particles for passivation is an essential step in many applications by improving the long-term stability or by creating a protective layer between particle and environment. The flame synthesis, an established aerosol coating technique, requires high temperatures which on the one hand could change the particle morphology and on the other hand might complicate the process control, due to different viscosities of the gases.

Techniques that use non-thermal "cold" plasmas do not have those same difficulties but often some of their own. Monosilane (SiH_4) is the preferred precursor for creating SiO_2 coatings in plasmas since it does not form any by-products that might contaminate the film. The downside to using silane is its high reactivity with oxygen which often results in uneven coatings when SiO_2 starts forming in the gas phase before contacting with the particles. Methods to solve this problem include complex fluid mechanical systems or the use of alternate oxygen sources, which in turn might also contaminate the coating.

The approach presented here solves the problem of the reactivity by dividing the process into two slower reactions. In the first step a dielectric barrier discharge (DBD) plasma is used to coat the core particles with silicon nitride which is then converted into silicon oxide in a second DBD reactor. These reactions are comparatively slow and allow the formation of geometrically defined layers around the core particles. While one part of this project consists of coating particles on substrates to study the mechanics of the deposition (Dahle et al., 2013), the one presented here aims to coat particles in a continuous process directly in the gas phase.

At this point in the project the goal has been to coat particles produced in a spark discharge generator with a silicon nitride layer. The experimental setup shown in figure 1 was used for this purpose. As shown there, the spark generated particles were (optionally) sintered to spheres which improved the visibility of the coatings in TEM pictures. Diluted Silane was added to the aerosol after the oven. In contrast to pure monosilane this diluted form is basically hazard free which much simplifies the handling. The DBD reactor itself is self-build and consists of an outer Al_2O_3 dielectric which also serves as the flown-through tube. The electrode on this side is applied with silver conductive varnish on the outside of the dielectric. Inside the reactor is the second electrode which is made of copper and also covered with a dielectric. The discharge area is about 25 mm long and 1 mm in distance between the electrodes. The dielectrics are fixed to two metal holders through which the aerosol flows.

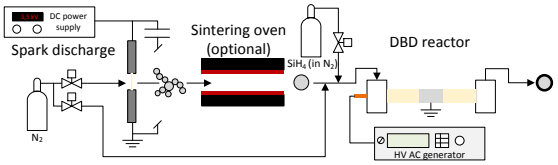

Figure 1. Experimental setup.

While there are some challenges with this experimental setup like high particle losses in the electric field of the plasma, first experiments show promising results. Thus it was possible to reliably coat different core materials, two examples of which are shown in figure 2. Current experiments aim to answer the question why the films seem to consist of oxides and not nitrides (as shown with EDX). Findings whether the source is in the system or if the nano sized particles react at the point of removal of the TEM grid are of course planned to be presented at the conference in June.

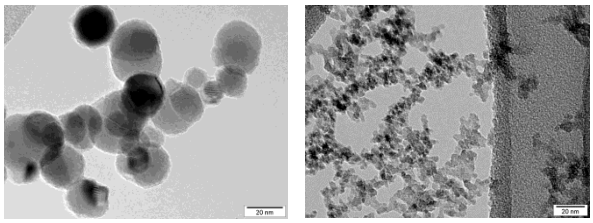

Figure 2. SiO_2 coated copper (left) and titanium (right) particles

The authors acknowledge the support by the German Research Foundation (DFG) under grants WE 2331/18-1 and MA 1893/23-1.

Dahle, S., Wegewitz, L., Qi, F., Weber, A. P., & Maus-Friedrichs, W. (2013). *Plasma Chemistry and Plasma Processing*, 33(5), 839–853.

Hydration and mobility of bisulfate ion-sulfuric acid-ammonia/dimethylamine clusters from computational studies

N.T. Tsona[1], H. Henschel[1], N. Bork[1,2] and H. Vehkamäki[1]

[1]Division of Atmospheric Sciences, Department of Physics, University of Helsinki, Helsinki, FI-00014, Helsinki, Finland

[2]Department of Chemistry, University of Copenhagen, Copenhagen, 2100, Copenhagen, Denmark

Keywords: aerosol, particle formation, particle dynamics, electrical mobility.

Secondary atmospheric aerosol particles are known to form almost everywhere around the world. A high proportion of these particles are formed from sulfuric acid vapor, which binds strongly to some base molecules (ammonia or dimethylamine) to form stable small clusters susceptible of further growth. The stability of these clusters can be affected by their charging state, thus modifying both the collision and evaporation rate constants and hence their dynamics (Ortega et al., 2014).

We performed calculations on a set of bisulfate ion-sulfuric acid-ammonia and bisulfate ion-sulfuric acid-dimethylamine clusters (HSO_4^-)(H_2SO_4)$_s$(NH_3/$(CH_3)_2NH$)$_b$, with s = 0-3, b = 0-2) using ab initio methods. Up to five water molecules were involved in the calculations. The clusters equilibrium structures and the energies of stepwise hydration were determined. The equilibrium hydrate distributions of the investigated clusters were further predicted at 298.15 K and various relative humidities between 1 and 100%.

As opposed to the traditional approach used to derive cluster structures from ion mobility measurements, we used a particle dynamics model (Larriba et al., 2013) to predict the mobilities in air of the cluster ions investigated in this study, under standard conditions. The cartesian coordinates of the lowest energy configurations were taken as inputs.

We found that the hydration of the HSO_4^-(H_2SO_4)$_s$(NH_3/$(CH_3)_2NH$)$_b$ clusters is weaker than that of their corresponding protonated counterparts (Henschel et al., 2014). Furthermore, we find that the hydration of clusters containing base molecules is more energetically favourable than that of base-free clusters, while the hydration of ammonia-containing clusters is more favourable than that of dimethylamine-containing clusters. As a consequence, the hydrate distribution of ammonia-containing clusters is wider than that of dimethylamine-containing clusters.

We predicted ion mobilities falling in the range of 1.05-3.42 cm^2/Vs, corresponding to the mobility diameter range of 0.52-1.11 nm. The ion mobility decreases with hydration as can be seen from Figure 1, most likely due to the increase in the collision cross section with increasing hydration. It is also apparent from Figure 1 that the change in ion mobility is weakly sensitive with hydration in large clusters.

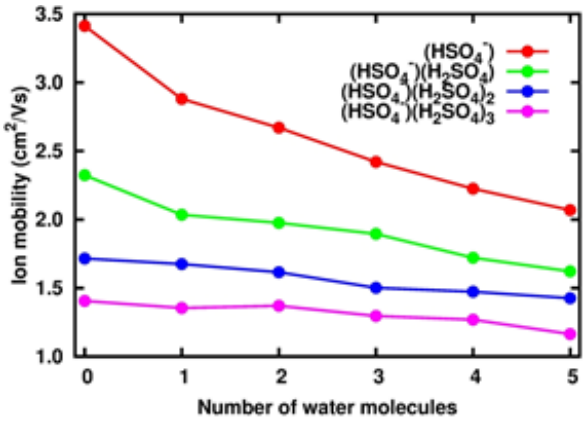

Figure 1. Variation of the electrical mobilities (at 1 atm and 298.15 K) in air of the HSO_4^-(H_2SO_4)$_s$ clusters (s=0,1,2,3) with hydration.

This work was supported by Academy of Finland Center of Excellence (grant no. 272041) and ERC Project No. 257360-MOCAPAF. We acknowledge the CSC IT Centre for Science in Espoo, Finland for computer time.

Ortega, I. K., Olenius, T., Kupiainen-Määttä, O., Loukonen, V., Kurtén, T., & Vehkamäki, H. (2014). *Atmos. Chem. Phys.*, 14, 7995–8007.

Larriba, C., & Hogan, Jr., C. J. (2013). *J. Phys. Chem. A*, 117, 3887−3901.

Henschel, H., Acosta Navarro, J. C., Yli-Juuti, T., Kupiainen-Määttä, O., Olenius, T., Ortega, I. K., Clegg, S. L., Kurtén, T., Riipinen, I., & Vehkamäki, H. (2014). *J. Phys. Chem. A*, 118, 2599−2611.

Hydrogen assisted spark discharge generation of metal particles

R. T. Hallberg[1], K. D. Thelander[1, 2], M. Magnusson[1], M. Messing[1, 3]

[1] Solid State Physics, Lund University, Box 118, 221 00 Lund, Sweden
[2] Centre for Analysis and Synthesis, Lund University, Box 124, 221 00, Lund, Sweden
[3] Synchrotron Radiation Research, Lund University, Box 118, 211 00 Lund, Sweden

Keywords: Spark discharge, aerosol sintering.

Spark discharge generation is a method to generate aerosol particles of varying materials depending on the choice of electrodes. The generation is typically done in an inert environment (N_2 or Ar), but as the system is not completely leak-tight, there are also small amounts of oxygen present. This can cause oxidation of the agglomerated particles that inhibit the thermal compaction into spherical particles and may affect the material properties. To prevent this we don't use an inert gas flow but a reducing gas flow by mixing two nitrogen mixtures before the particle formation. The mixtures used are 100 % N_2 and 95 % N_2 with 5 % H_2, and by changing the ratio of the two mixtures the hydrogen concentration is controlled.

The experiments have been done for different electrode materials, compaction temperatures and hydrogen concentrations. The set-up uses DMA filtering before and after the compaction furnace combined with an electrometer for measuring the particle concentration[1]. In complementary electron microscopy has been used to verify the size and investigate eventual differences in the produced particles.

We have observed a reduction in compaction temperature for bismuth and cobalt particles with hydrogen concentrations below 1 %. For bismuth, we have observed a compaction of 80 nm agglomerates sintered at different temperatures. This is clearly observable in figure 1 as the hydrogen-assisted particles consistently compact more than particles generated in an inert environment. For cobalt the system was not able to generate spherical particles without the aid of hydrogen, as the particles did not compact satisfactorily within the furnace operation limit < 1200 °C. With the addition of hydrogen the particles were sintered at already 800 °C.

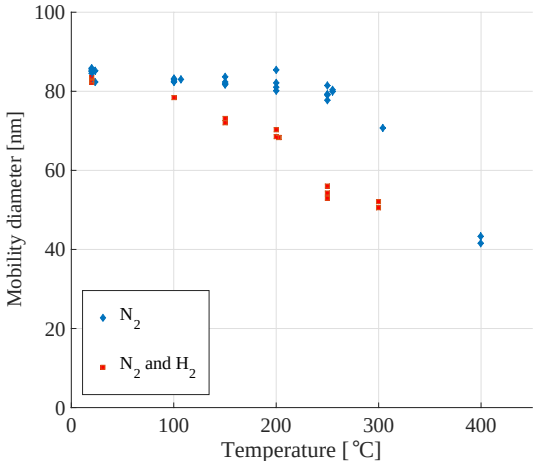

Figure 1 Sintering of 80 nm agglomerated bismuth particles show that particles generated in a hydrogen environment compact at lower temperatures compared to an inert environment.

In conclusion, we have shown that hydrogen improves the compaction for at least two material systems. Similar results are expected for other material systems and for methods that instead remove oxygen. Nonetheless, hydrogen has shown great promise and may prove to be essential when producing easily oxidised material.

References

1. Meuller, B. O. *et al.* Review of Spark Discharge Generators for Production of Nanoparticle Aerosols. *Aerosol Sci. Technol.* **46,** 1256–1270 (2012).

Impact of the Filtration Velocity on the Pressure Drop and Internal Liquid Transport of Fibrous Oil Mist Filters

H.E. Kolb, S. Wurster, J. Meyer and G. Kasper

Institute of Mechanical Process Engineering and Mechanics, Karlsruhe Institute of Technology, 76131 Karlsruhe, Germany

Keywords: filtration, coalescence filter, oil-mist, liquid transport.

Sub-micron oil aerosols ("oil mist") are generated by a wide range of processes, such as metal cutting, engine crankcase ventilation or compressed air generation. An efficient and commonly practiced way to clean gases from oil mist is by filtration with fibrous media. As opposed to dust filters which clog with increasing particle load and begin to form a cake, mist filters reach a steady state with constant Δp. This steady-state Δp is determined entirely by the way fluid is arranged and transported through the media. Kampa et al. (2014) showed that once the aerosol is captured in the front-most layer of the filter, the subsequent internal transport of coalesced liquid occurs in distinct oil channels, which are "pumped" by the air flow. The number and width of these parallel channels determines the internal Δp contribution of an oil loaded filter.

In the case of solid particle filtration, the internal arrangement of dust is little affected by the air flow velocity (Thomas et al., 2001). In fact, the Δp vs. loading curves for a dust filter become identical when normalized as Δp/v. With droplet aerosols however, the arrangement of oil channels appears to be highly dependent on the gas flow in a way that is not at all understood, because the normalized Δp curves do not collapse at all (Fig. 1).

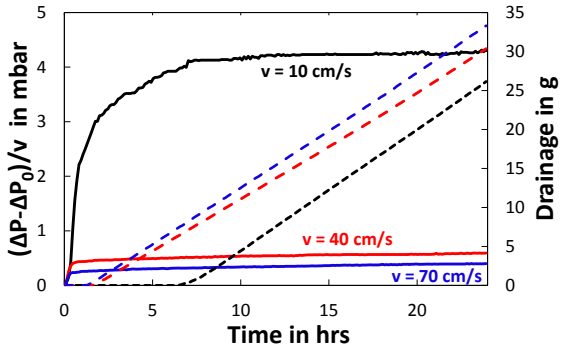

Fig. 1. Pressure drop and drainage curves for a non-wettable filter medium at various filtration velocities.

Past investigations were limited to a narrow range of flow velocities (Frising et al., 2005) or kept the filtration velocity constant (Kampa et al., 2014). The present work investigates the impact of a wide range of flow velocities (10 cm/s – 70 cm/s) on Δp and makes first comparisons with the structure of the oil channels inside the media. The experiments were carried out with flat, wettable and non-wettable glass fiber media assembled in multiple layers and loaded with a constant oil aerosol concentration until well past steady-state (constant Δp). The oil loading rate was kept constant, regardless of each flow velocity. At the end of an experiment the individual layers were photographed and the global saturation per layer was measured. These images reveal a significant and systematic evolution of the channel pattern toward more and finer oil channels with increasing filtration velocity (Fig. 2). These results are discussed on the basis of experimental data and existing models. Understanding channel structure and liquid transport are thus as crucial for the performance of oil mist filters, as is the deposition efficiency.

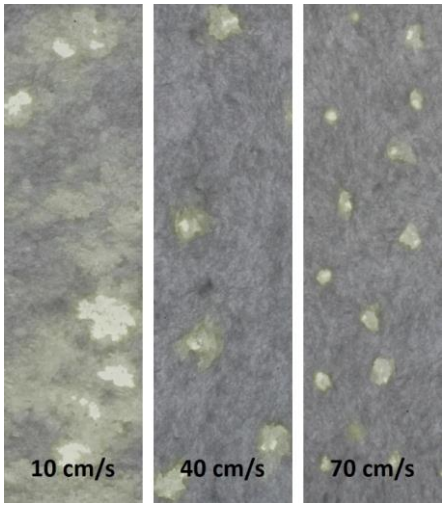

Fig. 2. Oil-channels in a non-wettable filter midsection at various filtration velocities.

Frising, T., D. Thomas, D. Bémer, & Contal, P. (2005). Chem. Ing. Science, 60, 2751-2762.

Kampa, D., S. Wurster, J. Buzengeiger, J. Meyer, & Kasper, G. (2014). Int. J. Multiphase Flow, 58, 313-324.

Thomas, D., P. Penicot, P. Contal, D. Leclerc & Vendel, J. (2001). Chem. Ing. Science, 56, 3549-3561.

Inactivation of microorganisms on filter elements of Tion A air cleaners

A.S. Safatov[1], O.V. Pyankov[1], V.A. Vechkanov[1], V.V. Solodkii[1], G.A. Buryak[1] and D.A. Trubitsyn[2]

[1]Department of Biophysics and Ecological Researches, FBRI SRC VB "Vector", Koltsovo, Novosibirsk region, 630059, Russian Federation
[2]«Aeroservis», Ltd., 14, Maxim Gorky Str., Novosibirsk, 630099, Russian Federation

Keywords: bioaerosols, air cleaner, Ebola virus, *Staphylococcus aureus*.

Bioaerosol removal from indoor air is an urgent task. Disinfecting air cleaners running in recirculation mode, in particular, Tion A designed by *Aeroservise* provide a high degree of air purification. These devices and other recirculation type devices comprise filter elements which remove various types of aerosol particles from the purified air flow. Microorganisms deposited on filter elements accumulate in the device operation and can be reaerosolized during planned replacement of filter elements, which presents a threat to the health of staff replacing the filters and those working in these areas if microorganisms remain viable.

The goal of this work was to study the inactivation rates of some microorganisms on filter elements of Tion A disinfecting air cleaners running in normal mode under the influence of ozone and air ions generated by corona discharge during the device operation. Tion A running in normal mode reduces the concentration of viable microorganisms in aerosol by not less than 99.999% in one pass.

The study was conducted in a Class III biological safety cabinet at the temperature T = 30 ± 1 ºC, relative humidity φ = 60 ± 5 %, ozone concentration inside the particle charger of Tion A disinfecting air cleaner running in normal mode being 0.200 ± 0.006 mg/m^3, and air ion concentration at the output of this unit being 33.16 ± 40.48 and 26.46 ± 43.15 ions/cm^3 for positively and negatively charged ions, respectively. The following standard microorganism suspensions (SMS) were used:

- Viral suspension containing Ebola virus (Zaire strain);
- Bacterial suspension containing *Staphylococcus aureus* bacteria.

To minimize the risks, AFA-HA filters coated with known amounts of SMS in the form of small droplets were placed on filter elements of the particle charger of Tion A disinfecting air cleaner instead of bioaerosol.

The control exposure time was 90 minutes for the test involving the viral suspension and 180 minutes for the bacterial suspension.

Colorless Hanks' solution was used as a flushing solution for the bacterial suspension, and Hanks' solution supplemented with bovine serum (2% by volume), 100 μg/ml of penicillin and 100 μg/ml of streptomycin was used for the viral suspension.

After the experiment, the exposed filters were placed in a container with 5 ml of flushing solution, and microorganisms were flushed from the filters into the solution for 15 min at regular shaking, followed by biological analysis of flushing samples and processing of experimental results.

The microbial inactivation rate was calculated on the basis of biological activity values of the original SMS and the corresponding values of this activity after fixed periods of the device operation.

The dynamics of the inactivation process of *Staphylococcus aureus* bacteria on the surface of filter elements of the particle charger of Tion A disinfecting air cleaner are approximated by the exponential law with a logarithmic factor of inactivation being 0.5/hour. The experiment revealed that 99.952% of *Staphylococcus aureus* bacteria were inactivated during two-hour operation of the device.

The obtained values of the rate constants for inactivation of Ebola virus (Zaire strain) placed on the output filters of the particle charger of the disinfecting air cleaner with corona discharge switched on (Experiment) and off (Control) were 0.1353 ± 0.1123 and 0.0588 ± 0.0875 min^{-1} respectively. Based on the experimental data, the value of Ebola virus inactivation under the influence of ozone and air ions is estimated at 99.994% (as the difference between the means of all determined inactivation rate constants for the Experiment and the Control) after two-hour operation of the device.

Thus, the inactivation rates of some microorganisms on filter elements of the particle charger of Tion A disinfecting air cleaner were determined, and it was shown that *Staphylococcus aureus* bacteria and Ebola viruses (Zaire strain) deposited on these elements are almost completely inactivated within a few hours of the device operation.

Increasing the sampling efficiency of sub-3 nm particles measurements using the "sampling box"

Franchin A.[1], J. Duplissy[1], J. Kangasluoma[1], F. Korhonen[1], T. Petäjä[1]

[1]Department of Physics, P.O. Box 64, 00014, University of Helsinki, Helsinki, Finland

Keywords: sub-3 nm particles, sampling efficiency, automatic measurements.

Recently, new technologies have made possible the detection of sub-3 nm sized particle. For example, the Particle Size Magnifier (PSM, Vanhanen et al., 2011), has improved the particle detection threshold from 3 nm down to 1 nm. The PSM has been successfully tested in laboratory and field campaigns, making direct measurements of formation and growth rates for sub-3 nm particle possible (Kulmala et al., 2013).

Nevertheless, carrying out successfully measurements of sub-3 nm particles in the field is a challenging task.

Firstly, sampling sub-3 nm can be problematic. In fact, a large fraction of such small particles can be lost in the sampling line, because of their high diffusivity. For example, if the sampling line is only 40 cm long, corresponding to the line length to cross a wall to measure outside, the losses for 1 and 2 nm particles can be as high as 45% and 35%, respectively.

Secondly, the instruments used to detected sub-3 nm particles, such as PSM, are operated at the limit of homogeneous nucleation. For this reason there is the need for periodic measurements of the background concentration, in order to correct, for example, if the onset of homogeneous nucleation, which is related to the detection efficiency, has shifted with ambient conditions.

Thirdly, discriminating between charged and neutral particles at these size ranges is of great of interest. In fact a mode of ions is omnipresent in the range between 0.8 or 2 nm and overlaps with the neutral clusters.

The "sampling box" is a solution for those three points. It provides 1) an efficient sampling, with losses less than 10% through a 80 cm sampling line to the instrumentation, 2) an automatic zero background measurement, and 3) an electrostatic filter that removes efficiently (>95%) ions up to 4 nm in diameter making it possible to study only the neutral fraction of sub 3-nm clusters.

An important aspect of the electrostatic filters is that they are designed in a way that uncontrolled extra losses in the line are avoided, for example minimizing stray electric-fields from the insulators. In this way they can be used in reversible filtering, i.e. either all particles and ions or only neutral particle, and can be switched on and off at will, without introducing bias in the measurement.

The prototype of the "sample box" has been successfully tested in 2014 at the SMAEAR II measurement station in Hyytiälä, Finland. The "sampling box" we present here, is now made as a compact solution for automated measurements of the background, minimizing the diffusion losses in the sampling line and removing ions with a switchable electrostatic filter. It is currently running continuously in front of PSMs at different field stations in Finland.

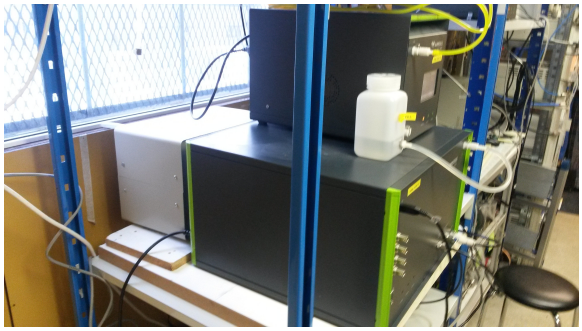

Figure 1. Setup showing the "sampling box" (in white) deployed in front of a PSM-CPC system (Airmodus A20).

This research has been funded by the Academy of Finland (Center of Excellence project no. 1118615).

Kulmala et al., (2013). *Science* 339 (6122): 943–46.

Vanhanen, J. et al., (2011). *Aerosol Science and Technology* 45 (4): 533–42.

Influence of particle concentration in the exhaust gas from wood combustion boiler on their charging and precipitation

A. Bologa[1], M. Ecker[2], H.-P. Rheinheimer[3], H.-R. Paur[1]

[1]Karlsruhe Institute of Technology, D-76344 Eggenstein - Leopoldshafen, Germany
[2]HDG Bavaria GmbH; D- 84323 Massing, Germany
[3]CCA-Carola Clean Air GmbH, D-76344 Eggenstein – Leopoldshafen, Germany

Keywords: combustion aerosol, particle charging, electrostatic precipitation

Wood combustion is widely used for domestic heating. The biomass combustion is the source of fine particle emissions which contribute significantly to the PM-burden in many cities. Among the environment pollution, fine particles are strongly associated with various diseases and illnesses. Particle emission can be reduced by improvement of combustion process and by use of various filter systems installed downstream or integrated into the combustion facility.

In the current report we present the results of the study of the influence of particle concentration in the exhaust gas from a wood-chips combustion boiler on their charging and precipitation.

The study was carried out at the KIT test set-up. A wood-chips combustion boiler HDG Compact 100 (HDG Bavaria GmbH) was used as the source of particles emissions.

Figure 1. ESP CCA-50

The exhaust gas was delivered to the electrostatic precipitators (ESP) CCA-50 or CCA-100 (CCA-Carola Clean Air GmbH), Fig.1. The boiler and ESPs were operated over 2500 h both at normal and minimum fuel load of the boiler. In the ESP particles were charged in the DC negative polarity corona discharge and further precipitated in the brush-electrode collectors under the influence of space charge effects.

Particle mass concentrations were measured simultaneous upstream and downstream the ESP using Wöhler SM 500 suspended particulate analyzer. Over 130 gravimetric measurements were carried out at various operation conditions. Particle size distribution and number concentrations were measured using SMPS (Fa. Grimm) and ELPI+ (Fa. Dekati).

The corona current decreases with increase of particle concentration η in the exhaust gas due to corona suppression (Fig.2). At rather the same η the decrease of current takes place due to loading of the HV corona electrode with aerosol.

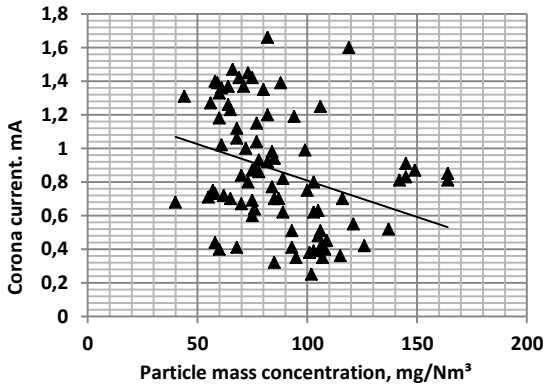

Figure 2. Corona current for various particle mass concentrations in the exhaust gas, U=19,8-201, kV

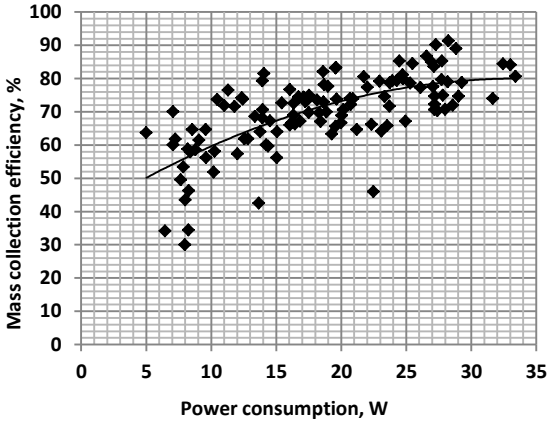

Figure 3. Dependence of mass collection efficiency on power consumption for particle charging

The increase of power consumption P for particles charging enhances the ESP efficiency (Fig.3). There is rather clear value of P over which the increase of power consumption results in small increase of ESP efficiency. If P increases from 10W up to 20W, η mean value increases from 60% to 74% (Fig.3, approximation curve). With further increase of P from 20W to 30W, η mean value increases from 74% to 82%.

Acknowledgement: The authors thank Ulrich Frei, Klaus Woletz, Wolfgang Aich and Damir Brand for their able technical assistance. Funding by the Federal Ministry for Economic Affairs and Energy (BMWi), Germany (FKZ-Nr: 03KB083A).

Investigating the potential for secondary aerosol formation in rural area of Central Chile

S. Saarikoski[1], F. Reyes[2], Y. Vázquez[2], M. Tagle[2], M. Aurela[1], H. Timonen[1], W.H. Brune[3], D. Worsnop[1,4,5], P. Oyola[2] and R. Hillamo[1]

[1]Atmospheric Composition Research, Finnish Meteorological Institute, FI-00560, Helsinki, Finland
[2]Centro Mario Molina Chile, 7510121, Santiago, Chile
[3]Department of Meteorology, Pennsylvania State University, University Park, 16802, USA
[4]Aerodyne Research, Billerica, MA, 01821-3976, USA
[5]Department of Physics, University of Helsinki, FI-00014, Helsinki, Finland

Keywords: secondary aerosol, PAM, SP-AMS.

Sources of anthropogenic pollution have mostly been investigated in urban areas with rather well-known pollution sources such as traffic, biomass/coal burning, cooking and energy production. Fewer studies have concentrated on the emissions from industry that is typically situated near small towns or in sparsely populated areas. Ideally, industrial facilities would be located far away from habitation but in most cases that is unfeasible because of the need of labor and efficient transportation system.

The aim of this study was to investigate the formation of secondary aerosol in Valle Alegre, V Region of Chile. Valle Alegre is a rural valley that has lot of agricultural activity but there is a large industrial area with smelter, power plant, oil refinery and cement factory less than 10 kilometres from the measurement site. The industrial site also incorporates one of the most important port activities of the region. This study focuses especially on the secondary aerosol formed from the precursor gases of industrial origin.

Secondary aerosol formation was studied by using a Potential Aerosol Mass (PAM) –chamber that is a small flow-through chamber flushed with oxidants (ozone (O_3), hydroxyl (OH), and hydroperoxyl (HO_2)) and irradiated with ultraviolet light in order to produce secondary aerosol (Kang et al., 2007). Potential aerosol mass is defined as the maximum aerosol mass that is produced in the chamber as the precursor gases are oxidized. The sampling system will be built so that the flow was directed through the PAM-chamber or past the PAM-chamber by switching the magnetic valves automatically in order to measure the ambient and oxidized sample air with the same set-up of instruments.

The chemistry and size distribution of aerosol was determined by a Soot Particle Aerosol Mass Spectrometer (SP-AMS; Onasch et al. 2012). SP-AMS provides a unique method for measuring the mass of non-refractory (organics, sulfate, nitrate, ammonium, chloride) and refractory aerosol species (black carbon, metals) and particle size. Besides the SP-AMS a nephelometer and multi-angle absorption photometer were used to measure the optical properties of aerosol. Next to our measurement container there was also an air quality monitoring station measuring continuously PM_{10} and some inorganic gases (NO, NO_2, NO_x, SO_2, O_3) operated by local industrial enterprises. Measurements were performed from January 6 to 28, 2015.

Most of the secondary aerosol mass formed in the PAM-chamber mass consisted of nitrate, ammonium and sulfate. Nitrate and ammonium were typically formed at the same time of the day (maximum from 4 to 6 pm in local time) whereas secondary PAM-sulfate followed different trend by peaking earlier than ammonium and nitrate. That was probably due to the local meteorology like wind direction. Regarding organics the formation of secondary organic aerosol (SOA) was smaller than that for secondary inorganic aerosol (SIA) and the diurnal pattern for SOA was not as clear as for SIA.

This work was funded by the Chilean Minister of Environment and the Academy of Finland (grant no 259016).

Kang, E., Root, M.J., Toohey, D.W., Brune, W. H. (2007): *Atmos. Chem. Phys*. 7, 5727-44.

Onasch, T.B., Trimborn, A., Fortner, E.C., Jayne, J.T., Kok, G. L., et al. (2012). *Aerosol Sci. Technol.* 46, 804–817.

Laser scattering for *in situ* monitoring of aerosol particles and growth of nanowires by Aerotaxy

M. H Magnusson[1], P. Samuelsson[2], Z.S. Li[2], W. Metaferia[1], B. O. Meuller[1], and K. Deppert[1]

[1]Solid State Physics, Lund University, Box 118, SE-221 00, Lund, Sweden
[2]Combustion Physics, Lund University, Box 118, SE-221 00, Lund, Sweden

Keywords: laser scattering, aerosol particle, nanowire, aerotaxy, monitoring.

Semiconductor nanowires are key building blocks for the next generation of light-emitting diodes (Qian *et al.*, 2005), solar cells (Wallentin *et al.*, 2013) and batteries (Chan *et al.*, 2008). To fabricate functional nanowire-based devices on an industrial scale requires an efficient method that enables mass production of nanowires with perfect crystallinity, reproducible and controlled dimensions and material composition, at low cost. Aerotaxy, an aerosol-based growth method (Deppert & Samuelson, 1996), can be used to grow nanowires continuously with controlled dimensions, a high degree of crystallinity and at a high growth rate. In the Aerotaxy approach, an aerosol of Au catalyst nanoparticles in N_2 is mixed with metal organic chemical vapor deposition (MOCVD) precursors (TMGa, AsH_3) in a flow-though reactor at atmospheric pressure (Heurlin *et al*, 2012). The nanowires grow at high concentrations and at a rate of > 1 µm/s, which is 20 to 1,000 times higher than previously reported for traditional, substrate-based growth of nanowires made of group III–V materials (Borgström *et al.*, 2007, Joyce *et al.*, 2009).

In order to monitor the quantity and quality of the Aerotaxy-grown nanowires *in situ*, laser scattering in a glass flow-through cell is employed. We here report on characterization of aerosol flows consisting of size-selected Au particles with diameters ranging from 100 nm to below 30 nm and concentration on the order of 10^6 cm^{-3}. We also report on scattering from Aerotaxy nanowires, typically with 80 nm diameter and 0.5–2 µm in length. By aligning the wires in an electric field (Kim *et al.*, 2007), the effects of wire orientation on scattered light polarization may be studied, providing a way of differentiation between scattering from parasitic dust and nanowires.

Figure 1 (top) shows a simple example, where we move from no particles (left), via 80 nm Au particles (center) to GaAs nanowires (right). In the top part of the left image, scattering due to residual particles can be seen; this is due to turbulence in the glass cell, giving the aerosol a longer residence time outside the main central jet of aerosol (going from right to left). Figure 1 (bottom) shows a flow-through cell with a large dead volume, where the flow of 80 nm Au particles was recently interrupted. The intensity in the central part is mainly due to fluorescence in the N_2 carrier gas.

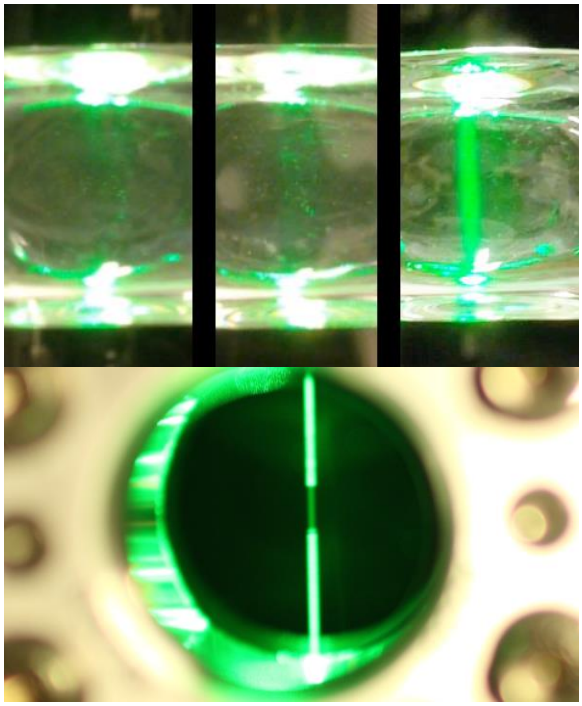

Figure 1. Laser scattering in an aerosol stream, laser coming in from the top. Top left: no particles (residual particles due to turbulence visible in the top part). Top center: 80 nm Au particles, and Top right: 80 nm wide and 1 µm long GaAs nanowires. Bottom: residual 80 nm Au particle scattering with core of clean gas in a larger cell. All concentrations were on the order of 10^6 cm^{-3}.

This work was supported by the Knut and Alice Wallenberg foundation.

Borgström, M. T. *et al.* (2007). *Nature Nanotechnol.* **2**, 541–544.
Chan, C. K. *et al.* (2008). *Nature Nanotechnol.*, **3**, 31–35.
Deppert, K. & Samuelson, L. (1996). *Appl. Phys. Lett.*, **68**, 1409–1411.
Heurlin, M. *et al.* (2012). *Nature.* **492**, 90-94.
Joyce, H. J. *et al.* (2009). *Nano Lett.* **9**, 695–701.
Kim, S. H. *et al.* (2007). *J Aerosol Sci* 38, 823–842.
Qian, F. *et al* (2005). *Nano Lett.*, **5**, 2287–2291 (2005).
Wallentin, J. *et al* (2013). *Science*, DOI:10.1126/science. 1230969

Lift off and dispersion of fractal-like aggregates

Ł. Żywczyk, A. Moskal, R. Przekop

Faculty of Chemical and Process Engineering, Warsaw University of Technology, 00-645, Warsaw, Poland

Keywords: lift off, fractal-like aggregate, *DLA*.

Effective process of drug delivery deep into the lungs is a subject of a special importance in the medical treatment. In order to deliver active medical substance effectively into the target organ, dry powder inhalers (DPI) are used commonly (Moskal & Sosnowski, 2012). DPI provides delivery of the medication absorbed on the solid platform (carrier) in a form of powder composed of particles often with diameter less than 5μm. Powder structure initially needs to be lifted off to the air inside the inhaler (Telko & Hickey, 2005) and then dispersed onto the smaller parts (Gac *et al.*, 2008, Iimura *et al.*, 2009).

The question arises, whether the morphology of formed powder will guarantee its effective dispersion, therefore significant increase of dose of medicine in lungs. Very little information has been provided in the literature so far regarding this stage of drug delivery (Grzybowski and Gradoń, 2005, Iimura *et al.*, 2009, Gac *et al.*, 2008).

Table 1. Parameters chosen to the numerical experiment.

parameter	Value
primary particle diameter [μm]	4
density of primary particle [kg/m^3]	1100
number of particles in structure	40
fractal dimension	1.6;. 2.0; 2.5
Young's modulus [Pa]	$2 \cdot 10^8$
Poisson's ratio [-]	0.27
surface energy [J/m^2]	0.15
viscosity of the air [Pa s]	$18.14 \cdot 10^{-6}$
temperature of the air [K]	293
time step [s]	$1 \cdot 10^{-9}$
average air velocity [m/s]	~1
spring constant [kg/s^2]	55.56
damp factor [kg/s]	$3.26 \cdot 10^{-19}$

In the present work flexible fractal-like aggregates model was used (Żywczyk & Moskal, 2015) to investigate lift off phenomenon and dispersion process of aggregates. Interactions in normal directions between primary particles are described by spring – damp system. In order to control flexibility of aggregate structure, additionally harmonic interaction functions has been employed, which controls resistance to bending and torsion between connected constituent particles. Numerical simulation conducted here used aggregates with different sizes and fractal dimensions. *Diffusion Limited Aggregation* algorithm was used to generate population containing different aggregates characterized with specified fractal dimension and number of primary particles. Aggregates, one at the time, are placed on the rigid surface and subjected to the air flow. Simulation has been conducted for parameters given in Table 1.

As the numerical results show, average value of hydrodynamic radius of fragments formed after specified time interval, strongly depends on fractal dimension of aggregate structure, Figure 1. This indicate that dispersion of aggregates is less effective for more compacted structures of aggregates.

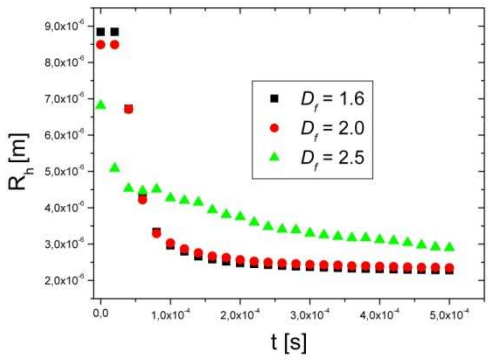

Figure 1. Evolution of the average value of hydrodynamic radius of remaining fragments in particular time interval. Aggregates with different fractal dimensions (D_f).

This work was supported by the National Science Centre, Poland granted by decision number: DEC-2012/07/B/ST8/03996.

Iimura, K., Watanabe, S., Suzuki, M., Hirota, M., & Higashitani, K. (2009). *Chem Eng Sci*, 64, 1455 – 1461.

Gac, J., Sosnowski T.R., & Gradoń L. (2008). *J. Aerosol Sci*, 39, 113-126.

Grzybowski, K., & Gradoń, L. (2005). *Adv Powder Technol*, 16, 105–121.

Moskal, A., & Sosnowski, T.R., (2012). *J. Drug Deliv. Sci. Tec.*, 22 (2) 161-165.

Telko, M.J., & Hickey, A.J. (2005). *Resp Care*, 50, 1209-1227.

Żywczyk, Ł., & Moskal, A. (2015). *J. Aerosol Sci*, 81, 75–89. DOI: 10.1016/j.jaerosci.2014.12.002.

Liquid Flame Spray synthesis of TiO_2/CeO_2 nanoparticles

M. Sorvali, J. Haapanen and J.M. Mäkelä

Department of Physics, Tampere University of Technology, P.O. Box 692, FI-33101 Tampere, Finland

Keywords: Liquid flame spray, nanoparticles, synthesis, composite

INTRODUCTION

Nanotechnology is a rapidly growing area that requires an enormous amount of studies to understand its applications well. Multiple components can be added together to develop new functionalities for nanoparticles and -coatings. An aerosol method called Liquid Flame Spray (LFS) offers a fast and well-scalable method for fabrication of versatile nanomaterial. Nanoparticles consisting of CeO_2 and TiO_2 were synthesized with LFS using various Ce/Ti ratios. Both of these compounds are known to absorb UV radiation, but not much research has been conducted regarding their composites (Gogarshadi et al. 2011). They have also been separately used in catalytic applications due to their reactivity (Qian et al. 2011). Mixing these two components together provides an interesting possibility to discover new or enhanced properties of nanoparticles.

METHODS

In LFS process, atomized droplets of a liquid precursor solution are fed into a turbulent H_2/O_2-flame for evaporation. Chemical reactions occur in the gaseous phase followed by nucleation into nanoparticles that often grow in the flame thereafter. The primary particle size is usually quite small depending on the process parameters and the used materials. Controllable parameters, such as precursor feed rate and gas flows also affect the morphology of the produced nanomaterial. Titanium(IV) isopropoxide (TTIP) and cerium(III) 2-ethylhexanoate were the two precursors used to fabricate TiO_2 and CeO_2 particles, respectively. Five different precursor solutions were prepared with Ce/Ti mass ratios of 9:1, 3:1, 1:1, 1:3 and 1:9. Xylene was chosen as a solvent in order to get both precursors to dissolve completely into the same precursor solution.

CONCLUSIONS

Nanoparticles consisting of CeO_2 and TiO_2 were fabricated successfully. Figure 1 shows TEM images of the produced nanoparticles with different Ce/Ti mass ratios. The widest, but still not very wide, size distribution (~2-15 nm) was formed with the highest Ce concentration, but it shifted closer to a bi- or trimodal distribution as the Ti concentration was increased. Agglomeration and sintering of agglomerated particles was more clearly observed with higher Ti concentrations, whereas the CeO_2 particles stayed reasonably separate and preserved their spherical shape well. The presence of Ce in the precursor seemed to slow down also the coalescence of TiO_2 particles, provided that the concentration was sufficient.

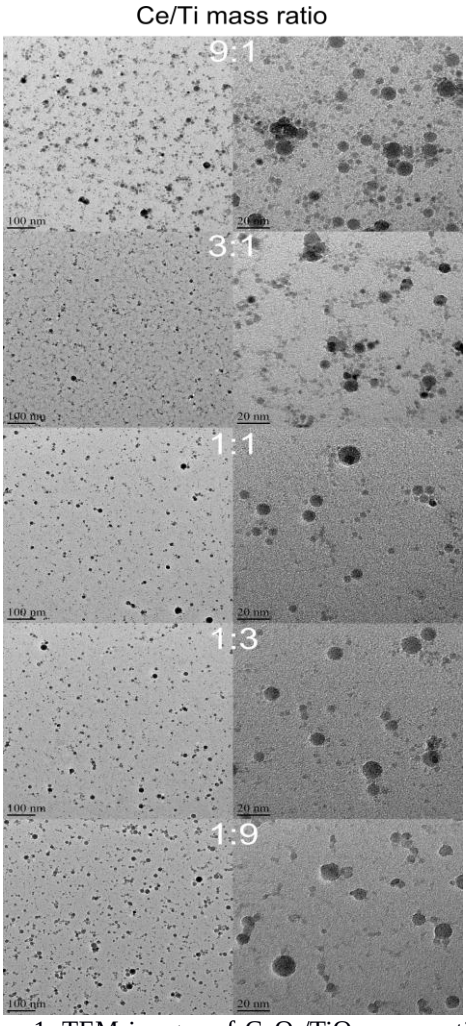

Figure 1. TEM images of CeO_2/TiO_2 nanoparticles with five different Ce/Ti mass ratios in the precursor solution and two different magnifications.

Goharshadi, E.K., Samiee, S. and Nancarrow, P. (2011). J. Colloid Interf. Sci., 356, 473-480.

Qian, L., Chen, F., Zhao, X. and Chen, Z. (2011). J. Nanopart. Res., 13, 7149-7158.

Lung deposited surface area size distributions in different urban areas

H. Kuuluvainen[1], A. Järvinen[1], L. Pirjola[2], J.V. Niemi[3], R. Hillamo[4], J. Keskinen[1] and T. Rönkkö[1]

[1]Tampere University of Technology, Department of Physics, Tampere, Finland
[2]Department of Technology, Metropolia University of Applied Sciences, Helsinki, Finland
[3]Helsinki Region Environmental Services Authority HSY, Helsinki, Finland
[4]Finnish Meteorological Institute, Helsinki, Finland

Keywords: urban air, surface area, health effects, ELPI

Numerous of studies are reporting particle mass and number concentrations in urban areas (e.g. Putaud et al., 2004). However, it has been argued that none of these metrics properly describes the negative effect of particlulate matter on human health. In this respect, particle surface area concentration is more relevant (Oberdörster, 2001). Some surface related quantities, as the lung deposited surface area or the active surface area, have been proposed to be the metric for the negative health effects. Common for these surface related quantities is that they are rather close to the response of a diffusion charger. For example, the nanoparticle surface area monitor (NSAM) is based on diffusion charging and it measures the lung deposited surface area concentration. In this study, an electrical low pressure impactor (ELPI) is calibrated and used to measure the lung deposited surface area concentrations in different urban environments. The advantage of the ELPI is that, in addition to the total concentration, also the surface area size distributions can be analyzed.

Three different measurement campaigns were carried out in the metropolitan area of Helsinki. The first campaign was held in December 2010, the second in February 2012, the third campaign in October 2012. All the campaigns included stationary measurements at different measurement sites and on-road measurements with a mobile laboratory 'Sniffer'. The stationary measurements were carried out at two traffic sites (TS), at two residential area sites (RA) and in the city center. The on-road measurements represent the variety of different routes in the metropolitan area including the city center, major roads and residential areas. In order to use the ELPI for surface area measurements, the instrument was calibrated by comparing the output of the instrument to the signal of an NSAM and to the size distributions given by a differential mobility particle sizer (DMPS). In all the experiments, the ELPI was used to measure particle surface area size distributions. The results were also compared to simultaneous PM2.5, PM10 and particle number measurements.

The average surface area size distributions for different urban environments are shown in Figure 1. It is seen that the shape of the distributions varies and the surface area is emphasized in different size ranges at different environments. The total surface area concentration is clearly higher at the traffic sites and in the city center compared to the results from the residential areas, as expected. Especially, the soot mode and non-volatile particles from traffic seem to dominate in the surface area distribution. In the residential areas, the surface area size distribution can also be affected by the amount of long range transported background aerosol. By analyzing the size distributions, the role of different particle modes on the total exposure of the lung deposited surface area can be estimated.

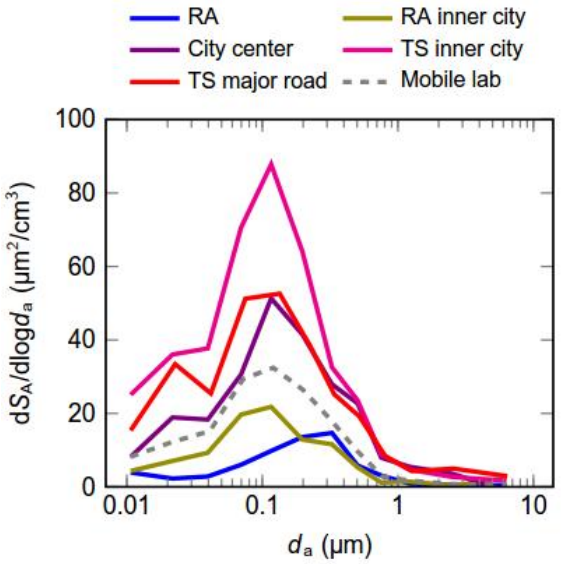

Figure 1. The averaged surface area size distributions from the stationary measurements and from the on-road measurements. TS refers to traffic site and RA to residential area.

This work was supported by CLEEN Ltd., the Cluster for Energy and Environment through the Measurement, Monitoring and Environmental Assessment (MMEA) research program.

Oberdörster G. (2001). Pulmonary effects of inhaled ultrafine particles. *Int. Arch. of Occup. Environ. Health*, 74, 1–8.

Putaud J.-P. et al. (2004). A European aerosol phenomenology – 2: chemical characteristics of particulate matter at kerbside, urban, rural and background sites in Europe. *Atmos. Environ.*, 38, 2579–2595.

Measurements of aerosol composition at coastal site in Antarctica using Time-of-Flight Aerosol Chemical Speciation (ToF-ACSM) monitor

H. Timonen[1], M. Aurela[1], D. Brus[1], H. Lihavainen[1], R. Hillamo[1], M. Cubison[2], B. Nekat[3], R. Weller[3], D. Worsnop[4], E. Asmi[1]

[1]Atmospheric composition research, Finnish Meteorological Institute, Helsinki, Finland
[2] Alfred-Wegener-Institut Helmholtz-Zentrum für Polar- und Meeresforschung, Bremenhaven, Germany
[3] Tofwerk AG, Thun, Switzerland
[4] Aerodyne Research, Inc., Billerica, MA 01821-3976, USA

Keywords: Aerosol online characterization, ToF-ACSM, SP2, CCN.

Aerosol chemical composition was studied with a recently developed Time-of-Flight Aerosol Chemical Speciation Monitor (ToF-ACSM) during austral summer at the Neumayer III station in Antarctica (70.6744° S, 8.2742° W http://www.awi.de/en/go/air_chemistry_observatory). In addition, a single particle photometer (SP2, Droplet Measurement Technologies Inc., USA) was used to measure black carbon concentrations and size distributions and a thermal-gradient cloud condensation nuclei counter (DMT-CCNC, model No. CCN-100, Droplet Measurement Technologies, Inc. DMT, USA) to measure cloud particle number concentrations. Antarctica is geographically isolated from anthropogenic particle sources, therefore the majority of measured particulate matter is originated from nearby sea areas.

ToF-ACSM (Aerodyne Research Inc., USA, (Fröhlich et al., 2013)Fröhlich et al., 2013) is designed for long-term monitoring of submicron aerosol composition with high-time resolution (minutes to hours) and high mass resolution (M/ΔM =600). ToF-ACSM contains a critical orifize to constrain the flow to 1.4cm^3 s^{-1}, and an aerodynamic lens to focus particles in a narrow beam into the vacuum chamber while the gases diverge. A Pfeiffer turbo pump and a MD1 diaphragm pump combination is used to create vacuum to the chambers. After particle beam is transmitted though the chambers particles are vaporized (600°C) and ionized (tungsten filament). ToF-ACMS has an EToF mass analyser and a SGE dynode detector. ToF-ACSM was calibrated with ammoniumnitrate (NH_4NO_3) prior to campaign and with ammoniumsulphate ($(NH_4)_2SO_4$) at the Neumayer. Time resolution of approximately 10 min (1 min filter background and 9 min ambient) was used in the measurements ToF-ACSM measures concentrations of sulphate, nitrate, ammonium, chloride and organics in submicron PM. Additionally, the mass resolution of the ToF-ACSM is sufficient for basic mass defect resolved peak fitting of the recorded spectra, which allows for quantification of certain hydrocarbon and oxygenated fragments, as well as improving inorganic/organic separation.

First results show that the ToF-ACSM suits well for continuous measurements in clean Antarctic areas. Measured concentrations were typically low (sulphate 0.5-3µg m^3, organic < 1µg m^3, nitrate < 1 µg m^3, and ammonium below detection limit, containing mainly of sulphate compounds.

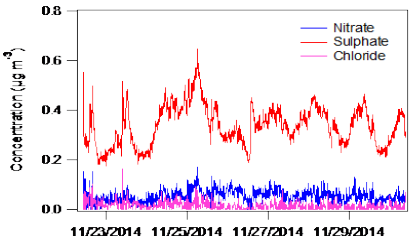

Figure 1. Timeseries of submicron ions.

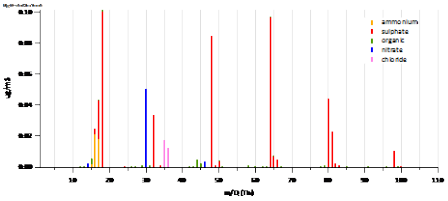

Figure 2. Average MS spectra

Higher sulphate concentrations were measured in January when emissions from open sea areas were influencing aerosol concentrations. Sea salt (NaCl) and methane sulphonic acid (MSA$^-$) were clearly seen in mass spectra when air masses originated from sea areas. The nearly complete absence of organic compound in higher mz's and abundance of sea emitted compounds next to large sea areas improved the separation of seasalt and MSA from organics greatly.

This work was supported by the Kone Foundation, Academy of Finland (ACPANT). Neumayer staff is gratefully acknowledged for their help in running the instruments.

Fröhlich, R., et al., 2013. The ToF-ACSM: a portable aerosol chemical speciation monitor with TOFMS detection. Atmos Meas Tech 6, 3225-3241, doi:10.5194/amt-6-3225-2013.

Measuring Number, Mass and Size of Diesel Exhaust Particles with the Dual Pegasor Particle Sensor

S. Amanatidis[1], L. Ntziachristos[1], M. M. Maricq[2], Z. Samaras[1], J. Tikkanen[3]

[1]Lab of Applied Thermodynamics, Aristotle University, GR 54124, Thessaloniki, Greece
[2]Research & Advanced Engineering, Ford Motor Company, MI 48121, Dearborn, USA
[3]Pegasor Oy, FIN 33100 Tampere, Finland

Keywords: PM sensor, particle mass, particle number, mean particle size

The Pegasor Particle Sensor (PPS) is an aerosol instrument designed to measure directly the hot, undiluted vehicle exhaust. The sensor operates by combining diffusion charging with the "escaping current" method. The PPS charging area is followed by an "ion trap"; this is an electrostatic precipitator that collects free ions which failed to collide with particles, so that the escaping current measured is proportional only to particle concentration. Except from free ions, the ion trap has the capacity to trap particles as well, and this presents the opportunity to use PPS as a size selective sensor.

The PPS signal is proportional to the "active" particle surface; it can be converted to particle mass and number concentrations if one assumes values for other aerosol parameters, primarily mean diameter. In the case of diesel and GDI vehicle exhaust the PPS has been successfully tested with the assumption of Dg=50nm (Ntziachristos *et al*, 2013). While this approximation is reasonable, it would be preferable to avoid using a fixed mean particle size.

In this study we demonstrate the possibility to measure exhaust particle mass, number and mean size in real time with the dual-PPS. The concept is based on sampling in parallel with two PPS units set at different ion trap voltage, so that each sensor detects a different fraction of the size distribution. Comparing the two signals can be used to first estimate mean particle size, and with this to convert PPS signal to number and mass concentrations.

The PPS charging efficiency as a function of particle size was measured with CAST soot particles. Ion trap penetration as a function of flowrate, particle size and trap voltage was explored with both CAST soot and diesel exhaust particles. Based on these, a data inversion algorithm was developed and evaluated with diesel engine exhaust.

The results demonstrate that the dual-PPS was generally in good agreement with reference instruments. Size estimation during drive cycles was much more challenging than steady state tests due to the highly transient aerosol. Nevertheless, the dual-PPS could clearly detect particle size fluctuations (Figure 1) as a result of the very good linearity between the two PPS units.

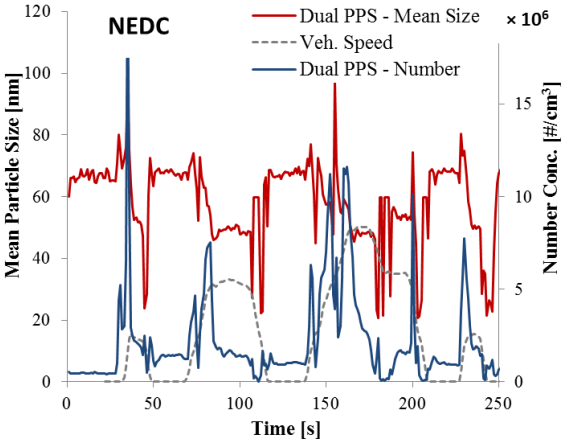

Figure 1. Real-time measurement of particle number and mean size during the NEDC drive cycle.

In addition to providing information on the mean particle size as an aerosol parameter, the dual-PPS offered significant improvements to the original, fixed-size, mass and number calibration. In specific cases, error reductions exceeded 50%. This present prototype may likely be optimized by integrating the two separate PPSs into a single unit with two measuring cells, as well as with continuously monitoring sample inlet and sheath air flowrates.

Ntziachristos, L., Amanatidis, S., Samaras, Z., Janka, K., & Tikkanen, J. (2013). *Application of the Pegasor Particle Sensor for the Measurement of Mass and Particle Number Emissions*. SAE International Journal of Fuels and Lubricants, 6

Mesoporous SiO_2-coatings on glass by a novel aerosol based coating method called nFOG

M. Tuominen[1], M. Järn[1] and S. Tammela[2]

[1]SP Technical Research Institute of Sweden, Drotning Kristinas Väg 45, SE-11486, Stockholm, Sweden
[2]Beneq Oy, Olarinluoma 9, FI-02201, Espoo, Finland

Keywords: nFOG, aerosol coating, mesoporous SiO_2-coating, up-scalable.

nFOG is a novel wet coating technology, which combines the advantages of the speed of spray-coating, the quality of dip-coating, and the high material yield of roller-coating. nFOG operates in atmospheric pressure and uses a unique contact-free deposition method to coat sensitive substrates, along with those of different thicknesses, shapes, or size variations. Typical coating uniformity is better than ±3 % and the substrate size can be up to meter scale. The aerosol-based process works with a wide range of liquid source materials, including water- or alcohol-based solutions or colloids. Typical dry coating thicknesses range from 20 to 500 nm. The majority of material used in the process can be recycled, therefore enabling a high material yield of up to 95%. Additionally, the modular approach allows scaling up to be simple and efficient.

Since the discovery of surfactant-templated silica some 20 years ago, there has been extensive research in the field. The applications for mesoporous silica and other metal oxides range from catalysis, chromatography, gas separation, water purification, chemical sensing, uptake and release of active components, and low dielectrical and optical coatings. (D. Grosso et al, 2001)

Mesoporous SiO_2 thin films were prepared using the evaporation induced self-assembly (EISA) technique. In the EISA process, the evaporation of solvent (typically ethanol) concentrates the initial diluted solution of surfactant molecules and inorganic species, leading to a hybrid inorganic-organic mesostructured network. By carefully controlling the synthesis parameters, one can synchronize the formation of micelles and their organization in a liquid crystal network with the condensation of inorganic species. The organic template is finally removed by calcination, resulting in an inorganic network with pores in the mesoporous range. (D. Grosso et al. 2004)

Thin mesoporous SiO_2 films with pore diameters of roughly 5 nm were successfully prepared by dipcoating the substrate in the precursor solution. The mesoporous SiO_2 films have been characterized with high resolution scanning electron microscopy (SEM), small angle X-ray scattering (SAXS), and gas sorption.

The pores were highly ordered in a hexagonal or cubic network, depending on the followed synthesis protocol. The film thickness could be varied between 150-500 nm. A SEM image of a mesoporous SiO_2 film prepared by dipcoating with pores ordered in a cubic phase is shown in Figure 1 (upper picture).

Mesoporous silica thin films have traditionally been prepared by dipcoating or spincoating, which put limitations when it comes to upscalability. The object of this work was thus to deposit the precursor solution by nFOG. Silicon wafers and glass slides were used as substrates. A SEM image of a mesoporous silica film on a Si wafer prepared by nFOG is shown in Figure 1 (lower picture). A well-ordered pore structure was achieved, comparable to the film prepared by dipcoating. Films were also deposited on glass slides. The transmittance of these films was excellent. Such coatings have promising applications as anti-reflective coatings on e.g. solar panels.

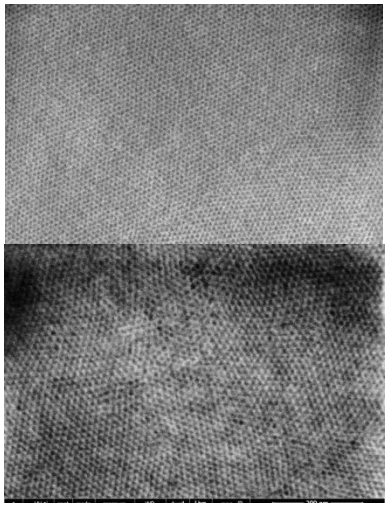

Figure 1. SEM-image of mesoporous SiO_2 coating on glass fabricated by dip coating (up) and nFOG

M.T. would like thank Nils Dorthi Tröedsson foundation for financial support.

D. Grosso, A. R. Balkenende, P. A. Albouy, A. Ayral,| H. Amenitsch, F. Babonneau, *Chem. Mater.* **2001**, 13, 1848.

D. Grosso, F. Cagnol, G. J. de A. A. Soler-Illia, E. L. Crepaldi, H. Amenitsch, A. Brunet-Bruneau, A. Bourgeois, C. Sanchez, *Adv. Funct. Mater.* **2004**, *14*, 309.

Miniature electrical nanoparticle detector for simultaneous measurement of particle number, average size and lung-deposited surface area

D.Meier[1], D.Egli[2], P.Steigmeier[2], H.Burtscher[2] and M.Fierz[1,2]

[1]naneos particle solutions llc, 5210 Windisch Switzerland
[2]University of applied sciences Northwestern Switzerland, 5210 Windisch Switzerland

Keywords: instrumentation, personal monitoring

We have recently introduced the concept of aerosol measurements by induced currents, where pulsed unipolar charging leads to a varying space charge in an open Faraday cage, thereby inducing a compensating current to the Faraday cage. (Fierz et al, 2014). This technique allows a contactless / non-collective measurement of aerosol charge, and, since only a signal amplitude is measured, the measurement is insensitive to the electrometer offset. We also built a miniature instrument based on this principle, which measures the charge transfer to an aerosol in unipolar charging, the naneos partector. This instrument is very similar to standard diffusion chargers (like the TSI NSAM).

Here, we present an extension of the original partector, the partector 2 (Figure 1):

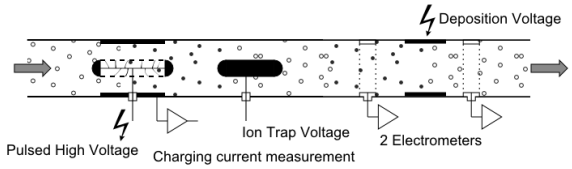

Figure 1. A scheme of the new instrument

Like its predecessor, the partector 2 is based on pulsed unipolar charging, followed by contactless electrical detection of the charges by induced currents in Faraday cages.

The partector 2 contains two Faraday cages for detection, which are separated by an electrostatic precipitator. As in the standard partector, the first Faraday cage electrometer measures an amplitude proportional to the total charge acquired by the aerosol, which is approximately proportional to the lung-deposited surface area of the nanoparticles (LDSA) (Wilson, 2007). In the electrostatic precipitator, small particles are preferentially removed, and thus the electrometer amplitude in the second Faraday cage is reduced. The ratio of the two signal amplitudes on the two Faraday cages is a measure for the average particle diameter of the aerosol, as can be seen in Figure 2. Once the average particle diameter is known, the particle number can be inferred from the signal amplitude on the first cage, as in other simple electrical detectors (Matter Aerosol DiSCmini, Grimm NanoCheck, Philips Nanotracer)

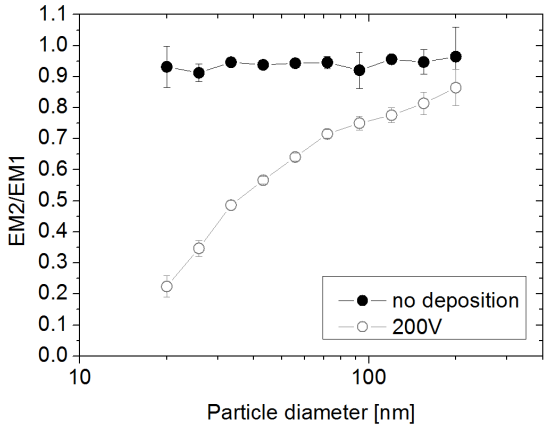

Figure 2: ratio of the 2 electrometer amplitudes as function of particle mobility diameter with deposition voltage 200V and no deposition voltage in a prototype instrument.

As with the standard partector, there are several advantages of this detection principle compared to similar instruments:

- The measurement is non-collective, which leads to long service intervals
- Electrometer offsets are irrelevant since only an amplitude is measured, so the usual drift of the zero offset due to temperature/humidity variations does not disturb the measurement
- The Faraday cages can be made very small allowing a very compact device

We will present an overview of the instrument and first results obtained with the device.

This work was supported by Forschungsfonds Aargau

M. Fierz, D. Meier, P. Steigmeier, & H. Burtscher (2014) Aerosol Measurement by Induced Currents. Aerosol Sci. Technol., doi:10.1080/02786826.2013.875981

Wilson W.E. et al. (2007) *J. Air & Waste Manage. Assoc.* **57**:211-220.

Mobility calibration standards in air in the 20-80ºC temperature range

M. Attoui[1], J. Fernández-García[2] and J. Fernandez de la Mora[2]

[1]Department of Physics, University Paris Est Creteil, LISA, UMR CNRS 7583, France
[2]Department of Mechanical Engineering, Yale University, New Haven, CT 06520-8286, USA

Keywords: DMA, mobility standard, variable temperature

Molecular ions of the tetraalkylammonium$^+$ family $(C_nH_{2n+1})_4N^+$ (referred to subsequently as Cn) have been widely used for DMA calibration in nanoparticle work at room temperature air (Ude et al, 2005; Jiang et al. 2011). Interest in mobility measurements at higher temperatures and in different gases provides a need for data on temperature dependent mobilities for these or other calibrants. Viidanoja et al. (2005) have reported the mobilities in N_2 for Cn ions with n=2-8, 10 and 12, in the temperature range from 25 ^{o}C to 88 ^{o}C. They note the interesting property that their reduced mobility Z_o $(=Z\rho/\rho_o)$ are almost temperature independent. For example, their figure 4 shows that Z_o for tetraheptylammonium decreases less than 2% from the lowest to the highest temperature studied. This valuable property has been used recently in the determination of ion-dipole corrections to the Millikan law in air and CO_2 in a comparable temperature range, under the still untested assumption that Z_o is also T-independent in air and CO_2 (Fernandez Garcia et al, 2014).

The original purpose of the present study was to check experimentally the validity of the hypothesis that the reduced mobility of C7 in air and CO_2 is also independent of temperature. To do so we have developed a mobility calibration technique in which the DMA and the blower moving the sheath gas are in a closed circuit, where the temperatures T_{DMA} and T_B in the DMA and the blower are controlled independently, so that T_p may be kept constant as T_{DMA} varies. Keeping also constant the blower speed of rotation and pressure ensures fixed operating conditions in the blower, which therefore delivers a fixed mass flow ρQ to the DMA, independently of T_{DMA}. This mass flow rate may then be determined at room temperature based on available room temperature mobility standards, yet can be used to infer ion mobilities at other values of T_{DMA}. The method appears to be of considerable interest for DMA measurements.

Contrary to our expectation, this approach reveals that the reduced mobility in air of all the Cn ions tested increases with temperature, very slightly for the two larger ions (C16, C18), but appreciably for the smaller ions. In view of the small mass and size differences between O_2 and N_2, it is difficult to ascribe observed disagreements with Viidanoja et al. (2005) to our shift from N_2 to air. Even if our new calibration method were incorrect for some unknown cause, just in terms of relative mobilities between the various members of the tetralkylammonium series Cn, if the reduced mobility of C3 is independent of T, then that of C12 must depend on T. It therefore seems that the measurements of Viidanoja et al. (2005) may contain errors of several %. Another widely used protonated mobility standard with reported T-independent reduced mobility in air is protonated 2,6-Di-tert-butyl pyridine (DtBP; Eiceman et al). In relative measurements we observe that the temperature dependence of this ion is closest to that of C3, whence C3 should have the same property, contrary to our present observations.

We are currently investigating how to resolve these contradictions with prior literature

Eiceman, G. A., E. G. Nazarov and J. A. Stone, Anal. Chim. Acta, 2003, 493, 185–194.

Fernández-García, J., Fernández de la Mora, J. (2014), *Phys. Chem. Chem. Phys.*, 2014, 16, 20500-20513

Jiang, J., M. Attoui , M. Heim , N. A. Brunelli , P. H. McMurry , G. Kasper, R. C. Flagan, K. Giapis & G. Mouret (2011). *Aerosol Sci. Tech*. 45, 480-492

Ude S., J. Fernández de la Mora (2005), *J. Aerosol Sci*. 36,1224-1237.

Viidanoja, J., A. Sysoev, A. Adamov and T. Kotiaho, *Rapid Commun. Mass Spectrom.* (2005) 19, 3051-3055

Abstract classification: Aerosol measurement techniques and particle characterization

Molecular Dynamics Simulation on Aerosol Formation of Water

D. Suh[1] and K. Yasuoka[1]

[1]Department of Mechanical Engineering, Keio University, Hiyoshi 3-14-1 Kohokuku, 223-8522, Yokohama, Japan

Keywords: molecular dynamics, heterogeneous nucleation, water.

Heterogeneous nucleation of water on solid seed particles is a critical phenomenon in understanding atmospheric aerosol formation. (Koehler *et al*., 2000; Vehkamaki *et al*., 2007). In order to understand how the solid seed geometry can influence heterogeneous nucleation and growth, seed particles with various shapes and sizes were placed inside a superheated water vapor system and studied by molecular dynamics. Two seed shapes, sphere and cube, made of aluminum were examined. Three different size classes were tested for each shape and a broad spectrum of supersaturation ratios were simulated based on the canonical ensemble. The Yasuoka-Matsumoto method was used to calculate the growth rate around the seed (Yasuoka & Matsumoto, 1998; Yasuoka & Matsumoto 1998). Though the number of molecules in each seed shape is nearly identical, just by changing the seed shape, the growth around the seed increases for the cube compared to the sphere, which was also observed in monatomic vapor systems (Suh and Yasuoka, 2011; Suh and Yasuoka, 2012). This is in spite of the fact that the sphere has a greater surface area than the cube.

The results show that different rates of heterogeneous nucleation can be obtained by changing the precursor particle configuration. The findings from this study are applicable not only to the qualitative analysis of aerosol formation and growth, but also quantitative correlation to experimental results.

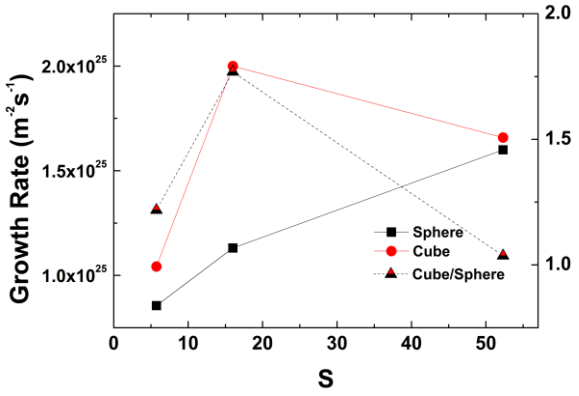

Figure 1. Heterogeneous growth rate for both shapes. The left scale is the actual growth rate for each shape, whereas the right shows the ratio.

Table 1. Dimensions for seed particle.

Shape	Seed Size	Characteristic Length (σ)	Surface Area (σ^2)
Sphere	110	5.64	100.0
Cube	108	3.65	79.97

Koehler, K. A., DeMott, P. J., Kreidenweis, S. M., Popovicheva, O. B., Petters, M., D., Carrico, C. M., Kireeva, E., D, Khokhlova, T. D., and Shonija N. K.. (2009) *Phys. Chem. Chem. Phys.*, **11** 7906-7920.

Suh, D. and Yasuoka, K., (2011) *J. Phys. Chem. B*, **115**, 10631-10645.

Suh, D. and Yasuoka, K., (2012) *J. Phys. Chem. B*, **116**, 14637-14649.

Vehkamaki H, Maattanen A, Lauri A, Kulmala M, Winkler P, Vrtala A, and Wagner P E, (2007) *J. Chem. Phys.*, **126**, 174707.

Yasuoka, K. and Matsumoto, M., (1998) *J. Chem. Phys.*, **109**, 8451-8462.

Yasuoka, K. and Matsumoto, M., *J. Chem. Phys.*, (1998) **109**, 8463-8470.

Monitoring the transport behaviour of toluene through protective polymer gloves using quartz crystal microbalance

M.J. Chen[1], L.H. Cheng[1] and T.P. Tseng [1]

[1]Department of Occupational Safety and Hygiene, Fooyin University, 151 Chin-Hsueh Rd., Ta-Liao Dist., Kaohsiung 83102, Taiwan

Keywords: Protective polymer glove, Solvent permeability, Quartz crystal microbalance

Introduction

The permeability of solvents through the polymer gloves is commonly determined using the ASTM F739 standard testing procedure associated with gas chromatography (GC) analysis (Chao et al., 2007), which characterises the solvent transport properties, such as breakthrough time and permeation rate, and provides an overall decrease in resistance rating. The observed data from the ASTM F739 method can be directly apprehended in terms of an outlet solvent concentration-time profile, i.e., concentration-versus-time (*C*-*t*) curve (Cheng et al., 2012). However, the main drawback of ASTM F739 method is that it is time consuming and costly on the laboratory processes including sampling, GC analysis and data processing. In addition, data obtained from discrete sampling cannot reflect the dynamic behavior of real permeation process as well. With regard to this background, quartz crystal microbalance (QCM) is a highly mass-sensitive sensor that is capable of measuring the mass change, corresponding to the frequency shift (Δf), in on-line and real-time mode. In this work, a gas-phase QCM was employed to conduct permeation testing instead of the ASTM-F739 method to investigate the permeation properties of organic solvent through protective polymer gloves.

Methodology

A stainless steel permeation test cell for ASTM F739 **(**Pesce Lab Sales, Inc.**,** USA) was used to perform the permeability experiments for the solvent transport through protective polymer gloves. An industrial grade toluene with 99.76 % purity was used as the test solvent. A commercial protective polymer gloves, composed of butyl rubber (North B131/9 Butyl Gloves, USA), was chosen for the permeation testing. An open-loop ASTM F739 method was employed for the permeation testing, in which a gas-phase QCM with a resolution 0.1 Hz (Model ADS; Asia New Technology, Taiwan) was directly coupled at the outlet of the collection chamber for the continuous in-situ measurements of toluene vapour concentration. The toluene sensor based on fine activated carbon particles which were coated on QCM sensor chip. During the test, 1.0 ml toluene vapour samples were manually taken from the collection chamber every 10 min and analysed by GC (Hewlett Packard 6890, USA). The detailed operating conditions for the GC are described elsewhere (Cheng et al., 2012).

Results and Discussion

The QCM sensor has a good linear relationship (r^2=0.99) between the adsorbed mass on the sensor chip and the shift frequency on the 9MHz AT-cut quartz crystal oscillator (Figure 1). The result shows that the *C*-*t* profiles obtained from QCM monitoring are similar to those from GC measurement (Figure 2). The QCM technique has been demonstrated to be a useful tool for the permeation test with direct *in situ* real-time measurement.

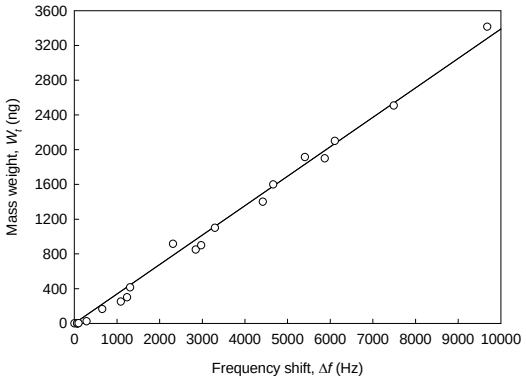

Figure 1. Absorbed mass on sensor chip versus frequency shift, Δf.

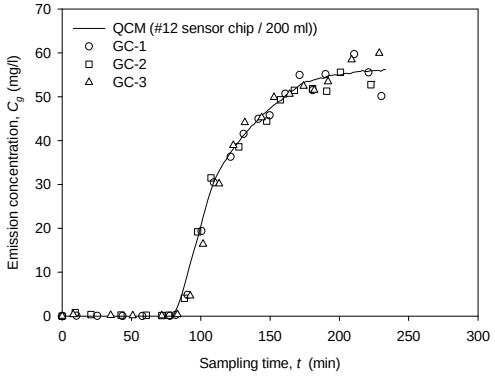

Figure 2. The comparison of *C*-*t* profiles between GC measurement and QCM detection.

This work was supported by the Ministry of Science and Technology of Taiwan under Grant No. NSC 102-2221-E-242 -001-MY2.

Chao, K. P., Wang, P., Wang, Y. T. (2007) *J. Hazard. Matrs*., 142, 227-35.

Cheng, L. H., Chen, M. J., Cheng, W. H., Lin, C. H., Lai, C. H. (2012) *J. Membr. Sci.*, 409-410, 180-90.

Multiple Electrospraying from Extractor-Free Linear-Arrays

N. Sochorakis[1], E. Bodnár[1], J. Grifoll[1] and J. Rosell-Llompart[1,2]

[1]Chemical Engineering Department, Universitat Rovira i Virgili, 43003, Tarragona, Spain
[2]ICREA - Catalan Institution for Research and Advanced Studies, 08010, Barcelona, Spain

Keywords: multiplexing, EHD atomization, electrospray, polymer particles

Reaching industrially relevant microdroplet production rates by electrospraying requires the simultaneous operation of many electrospray emitters. Electrostatic shielding between the emitters makes it challenging to design *compact* multiplexed systems. As a result, compact 2D designs must incorporate an extractor electrode (Bocanegra *et al.*, 2005; Deng *et al.*, 2006). However, unwanted deposition of very small droplets may take place on the extractor electrode (Deng *et al.*, 2009).

We are aiming to develop robust multiplexed geometries for the production of polymer microparticles, which are based on stacked one dimensional (1D) arrays of electrospray emitters (shaped as capillary tubes, or "needles"). We are studying how the system behavior (spray plumes characteristics, operation conditions, stability) depends on the geometrical parameters of arrays provided with a back plate, but no extractor plate (Figure 1(a)). An extractor electrode is not necessary in a 'compact' 1D array since it is much sparser than a compact 2D array of equal inter-needle pitch. In addition, solvent vapor is more easily removed from the sprays, a requirement for making solid particles by droplet drying. We also study the effect of non-spraying *end electrodes* (Fig. 1(a)), as previously introduced by Rulison & Flagan (1993), and by Hubacz & Marijnissen (2003).

Figure 2 shows collections spots of polymer particles obtained with 3- and 5-needle arrays (without end electrodes) and 7-needle arrays (with 4 end electrodes as shown in Fig. 1(a)). In going from N=3 to N=5 needles, the spots compress along the array direction ("horizontally"), but not in the cross direction ("vertically"), resulting in a smaller area for the center spot when N=5. In this case electrostatic shielding between the needles is increased; therefore, the applied voltage difference had to be raised by 8% in order to have stable electrospraying (in cone-jet mode), and, as a result, the spray's residence times were reduced, and the sprays became less expanded. A similar effect is observed on reducing the needles' pitch from 4.6 mm in Fig. 2(c) to 2.3 mm in Fig. 2(d). However, at the smaller pitch, unequal shapes for the 5 central spots are found because slight needle misalignments are magnified.

The similarity in area and shape among the central spots in Fig. 2(b), as well as in 2(c) (and to some extent in 2(d)) shows that the electric field is fairly repeatable for the different spray positions, except at the array-end positions. We are quantifying these effects using image analysis. In addition, this work is complemented with numerical simulations of multiplexed electrospray systems.

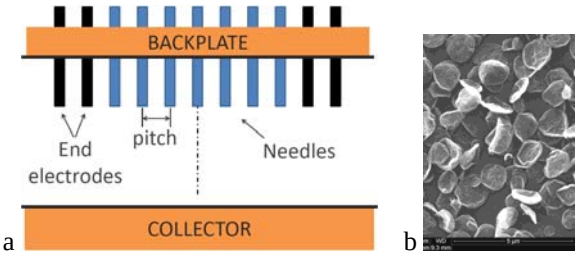

Figure 1. (a) Schematic of linear array with end electrodes; (b) SEM of ethyl cellulose particles.

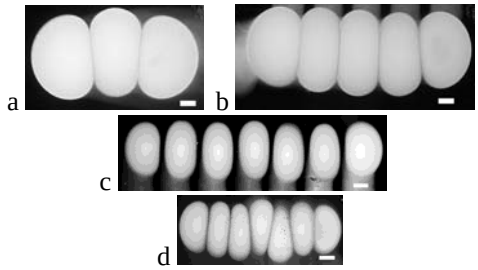

Figure 2. Collection spots of EC particles (Fig. 1(b)) from 3-, 5-, and 7-needle arrays. Inter-needle pitch is 4.6 mm for (a-c), and 2.3 for (d). Scale bars = 2 mm.

This work has been supported by MINECO (Spain), project DPI2012-35687 and predoctoral contract (N.S.), and Generalitat de Catalunya, grant 2014SGR-1640.

Bocanegra, R., Galán, D., Márquez, M., Loscertales, I. G., Barrero, A. (2005). *J. Aerosol Science*, **36**, 1387-1399.

Deng, W., Klemic, J. F., Li, X., Reed, M. A., & Gomez, A. (2006). *J. Aerosol Sci.*, **37**, 696-714.

Deng, W., Waits, C. M., Morgan, B., & Gomez, A. (2009). *J. Aerosol Science*, **40**, 907–918.

Hubacz, A. N., & Marijnissen, J. C. M. (2003). *J. Aerosol Science*, **2**, S1269-S1270.

Rulison, A. J., & Flagan, R. C. (1993). *Rev. Sci. Instr.*, **64**, 683-686.

Nanostructured materials for efficient and inexpensive NO_2 sensing using spark discharge generator

N.A.Isaac[1], M. Valenti[1], A. Schmidt-Ott[1] and G. Biskos[1,2,3]
[1]Faculty of Applied Sciences, Delft University of Technology, 2628 BL Delft, The Netherlands
[2]Faculty of Civil Engineering and Geosciences, Delft University of Technology, 2628 CN Delft, The Netherlands
[3]Energy Environment and Water Research Center, The Cyprus Institute, Nicosia 1645, Cyprus

Keywords: Spark Discharge, gas sensors, nanomaterial characterization

In this study we show that spark ablation techniques (Schwyn et al., 1988) can be used for fabrication of inexpensive NO_2 sensors with Tungsten Oxide (WO_3) nanomaterials, an n-type semiconductor, which shows an increase in resistance in the presence of oxidising gas NO_2. These sensing films on exposure to 1 ppm of NO_2 in air provide a sensitivity of 100 approximately as shown in Figure 1. Some preliminary tests with promising results have also been done for 250 ppb NO_2 in air. The response time of these sensors are in the order of 10 minutes. Cyclic measurements are performed on the sensor and they are observed to be stable over cycles of NO_2 exposure and removal.

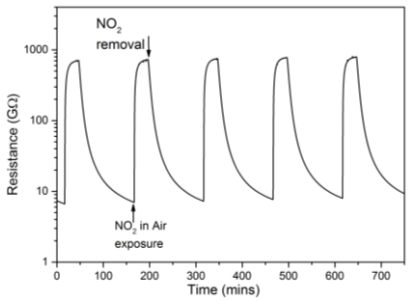

Figure 1 Cyclic measurements of sensor performance on exposure to 1 ppm NO2 in Air

WO_3 nanomaterials are synthesized in a flow of Argon gas between Tungsten electrodes. The nanomaterial generated is deposited as thin film with inertial impaction. In order to make a smooth film, aerodynamic lenses are used for focusing the aerosol before it impacts on to a substrate. Deposition is carried out on commercial substrates of Alumina with inter-digitized Au electrodes.

Material characterization is performed using techniques of SEM, TEM, XPS and XRD. The as-deposited films are amorphous in nature with primary particle size between 10 -15 nm. Before they can be used as a sensor at operating temperatures of 200°C for optimum sensitivity (Kunert et al., 2013) they need to be annealed in air at 500°C for 1 hour for crystallization. XRD (Figure 2) and XPS measurements of post-annealed films confirm crystallization of the films.

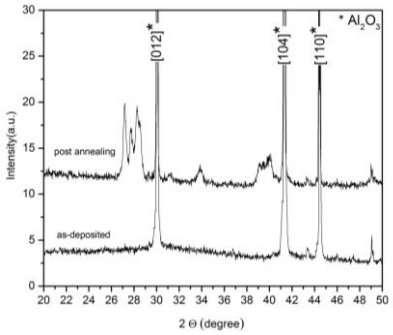

Figure 2 X-Ray Diffractogram of as deposited and post annealed tungsten oxide films. Unmarked XRD peaks are from tungsten oxide.

SEM micrographs as shown in Figure 3 depict the surface morphology of the films before and after annealing. Due to intrinsic and thermal stress on the films they develop cracks. With films becoming thicker the cracks increase in size and numbers. These cracks are also believed to help increase the sensitivity of the film by providing more surface area for film-target gas interaction.

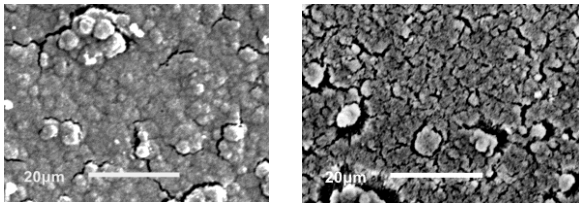

(a)As-deposited film (b) Post annealed film

Figure 3 SEM micrographs of as-deposited and annealed films showing cracks on a scale of 20 µm. With annealing the cracks increase their branches and become larger due to increased thermal stress.

References

[1] A. Schmidt.-Ott. E. Garwin, S. Schwyn, "Aerosol generation by spark discharge," vol. 19, no. 5, pp. 639–642, 1988.

[2] M. Govender, D. E. Motaung, B. W. Mwakikunga, S. Umapathy, S. Sil, a. K. Prasad, a. G. J. Machatine, and H. W. Kunert, "Operating temperature effect in WO_3films for gas sensing," *2013 Ieee Sensors*, pp. 1–4.

Nitrogen containing exhaust emissions for consideration in the aerosol research

P. Aakko-Saksa[1], T. Murtonen[1], P. Koponen[1], K. Lehtoranta[1], P. Roslund[1], P. Karjalainen[2], T. Rönkkö[2], H. Timonen[3], S. Saarikoski[3], R. Hillamo[3].

[1]VTT Technical Research Centre of Finland Ltd., P.O. Box 1000, FI-02044 VTT, Finland
[2]Tampere University of Technology, Department of Physics, FI-33720, Tampere, Finland
[3]Atmospheric Composition Research, Finnish Meteorological Institute, FI-00560, Helsinki, Finland

Keywords: ammonia, nitrogen oxides, secondary aerosol, traffic emissions.

Transformation of primary exhaust emissions into secondary products is an important aspect when traffic emissions are assessed. For example, about 30% of PM10 measured is in the form of secondary inorganic sulphate and nitrate aerosols, which are formed from the transformation of gaseous SO_2, NO_x and NH_3 emitted from various sources. These aerosols are presumably even more important as regards PM2.5. Secondary organic aerosols are formed from atmospheric oxidation and subsequent condensation of various VOCs (EEA 2012). Ammonia originates mainly from agricultural sources. However, concern of traffic sources in the production of ammonium aerosols increased as the use of urea-based SCR systems for NO_x control for diesel engimes became common. Ammonia is also formed by the three-way catalysts of the spark-ignited gasoline cars. Nitrous oxide (N_2O), a strong greenhouse gas, is also induced by catalyst chemistry under lean conditions. (Meija-Centeno 2007, EEA 2012). In this study, an extensive set of emission constituents, including ammonia emissions, were measured from two flexible-fuel cars. These results are discussed in relation with nirtogen containig emissions from other types of internal combustion engines.

Emissions from two passenger cars (VW Passat MultiFuel, DISI engine, Ford Mondeo 2.0 FlexFuel, natural aspirated MPI engine) using fuels with different alcohol content (E10, E85, and E100) were measured on chassis dynamometer using the cold-start European exhaust emissions driving cycle (NEDC) and the hot-start FTP driving cycle. Several compounds were measured on-line using Fourier transformation infrared (FTIR) equipment (Gasmet Cr-2000) from the raw exhaust gas at two-second intervals. In-depth analyses of other emissions, also secondary organic aerosols were analysed in co-operation of three research organisations.

The NO_x emissions were low for the three-way catalyst (TWC) equipped spark-ignited cars in the NEDC tests. However, surprisingly high NO_x emissions were observed for the MPI car in the hot-start FTP test (up to 228 mg/km). The highest emissions are typically observed in the beginning of the cold-start test and during accelerations, whereas here the highest NO_x concentrations occurred in the hot-start FTP test after a 10 minutes pause. This indicates engine adjustments optimised for low HC emissions leading to non-favourable conditions NO_x reduction (possibly lean air-to-fuel ratio). Nitrogen dioxide emissions were low (below 3 mg/km), as well as nitrous oxide emissions (below 5 mg/km). Both cars emitted quite similar emission levels of ammonia. The highest single emission result, close to 50 mg/km, was obtained for the the DISI car over the NEDC test cycle at -7 °C. High ammonia concentrations observed, typically over 10 ppm and substantial peaks up to 300-500 ppm. These ammonia concentrations are high when compared to limit value of 10 ppm for SCR equipped heavy-duty engines, for example. In theory, ammonia formation is enhanced in slightly rich air-to-fuel ratio at high temperatures (aggressive accelerations) when sufficiently HC and NOx emissions are present (Li et al. 2010, Mejia-Centeno 2007, Heeb et al. 2006). These results suggest that nitrogen containing emissions would deserve attention in the research of secondary aerosol formation for internal combustion engines.

This work was supported by Tekes within contribution in the IEA's Implementing Agreement on Advanced Motor Fuels (AMF) as Annex 44 (www.iea-amf.org/content/projects/annexes/44), and by the Academy of Finland (Grant No. 259016), Helsinki Energy, Ministry of Traffic and Communications, Tekes in the CLEEN/MMEA programme (WP4.5.2) and HERE and CENGE-projects (Tekes).

European Environment Agency. Air quality in Europe. EEA Report No 4/2012.

Heeb N.V., Saxer C.J. et al. Correlation of hydrogen, ammonia and nitrogen monoxide (nitric oxide) emissions of gasoline-fueled Euro-3 passenger cars at transient driving. Atmospheric Environment, Vol 40, 2006, pp. 3750-3763.

Li, W., Perry, K., Narayanaswamy, K., Kim, C. et al., Passive Ammonia SCR System for Lean-burn SIDI Engines, SAE Int. J. Fuels Lubr. 3(1):99-106, 2010, doi:10.4271/2010-01-0366.

Mejia-Centeno, I., Martínez-Hernández, A. and Fuentes, G. Effect of low-sulfur fuels upon NH_3 and N_2O emission during operation of commercial three-way catalytic converters. Topics in Catalysis. Vols. 42–43, May 2007.

Nucleation barrier for complex materials determined by guided molecular dynamics

Ian Ford

Department of Physics and Astronomy and London Centre for Nanotechnology, UCL, London WC1E 6BT, U.K.

Keywords: nucleation, free energy, molecular dynamics, sulphates, ionic materials

Aerosol nucleation is a process that depends very sensitively on the thermodynamics of extremely small molecular clusters. Considerable efforts have been made to understand these properties, with theoretical modelling being a key technique since the clusters are nanoscale in size and very short lived. The two most important elements in the process of developing useful models are to establish a realistic representation of the interactions between the nucleating molecular species, and then to employ this in the determination of free energies, which are central to the understanding of cluster thermodynamic stability and ultimately material synthesis. A third element in developing a useful practical tool is to demand agreement with experimental data where available, by parameter adjustment if necessary, to gain confidence in predictions in circumstances beyond those measured.

I shall present studies of the nucleation barrier for the formation of liquid-like water clusters modelled by the TIP4P/2005 force field, and for water-sulphuric acid mixed clusters modelled by a recently developed reactive model that can account for proton transfer (Stinson et al 2015). Both involve molecular dynamics simulations where a cluster is guided into two or more subclusters through the action of external mechanical forces. By recognising that free energy changes correspond to quasistatic, isothermal external work, we can relate the distribution of work performed over many repetitions of the guided dynamics to the excess free energy of the initial cluster, a quantity often regarded as a surface free energy and an important contribution to the nucleation barrier (Tang and Ford, 2015).

The technique is most powerful when the cluster is divided mechanically into two parts, a process termed mitosis (Lau et al, 2015). This allows us to relate the excess free energy of a cluster of N molecules to that of two subclusters of size $N/2$. In order to compare the free energy of a cluster to that of the molecules in a gas at a given molecular density, a full disassembly of the cluster is necessary, which we do by way of a lattice of independently tethered molecules. In Figure 1 we illustrate the excess free energy F_s of clusters of water molecules at 300 K, and compare the results with the capillarity approximation that underlies classical nucleation theory (CNT) and a derivative of that model known as internally consistent classical theory (ICCT). The results are also consistent with earlier calculations obtained by a grand canonical Monte Carlo technique (Merikanto et al, 2004).

These studies do not require use of the harmonic model of cluster entropy that is very often used in this area, and is based on the spectrum of vibrational modes of the cluster at low temperature. We can determine to what extent the entropy of a cluster can be represented by thermal excitation of these modes; at high temperatures such excitations are likely to provide a poor approximation.

Our methods are currently being extended to describe a range of inorganic materials, in particular fission product materials such as CsI and CsOH important for studies of nuclear safety analysis. In addition to using guided separation, the key to the approach is to employ a realistic force field (Cooper et al, 2014).

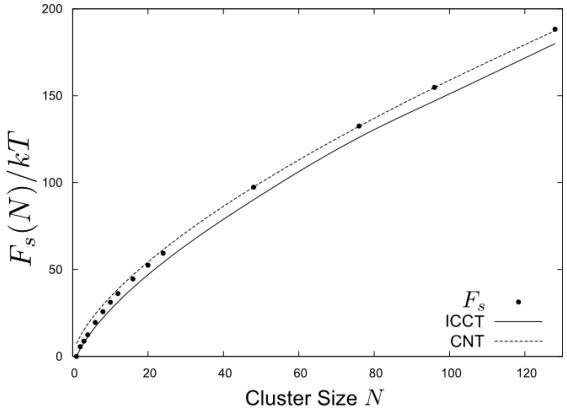

Figure 1. Computed 'surface' free energies of water clusters at 300 K described by the TIP4P/2005 force field, compared with the capillarity approximation of classical nucleation theory (CNT) and the shifted version ICCT.

This work was supported by the EPSRC and the US Department of Energy.

Cooper, M.W.D., Rushton, M.J.D. and Grimes, R.W. (2014) *J. Phys. Cond. Matt.* **26**, 105401.

Lau, G.V., Hunt, P.A., Müller, E.A., Jackson, G. and Ford, I.J. (2015) in preparation.

Merikanto, J., Zapadinsky, E., Vehkamäki, H. (2004) *J. Chem. Phys.* **121**, 914.

Stinson, J.L., Kathmann, S.M., and Ford, I.J. (2015) in preparation.

Tang, H.Y. and Ford, I.J. (2015) to appear in *Phys. Rev. E*.

Number calibration of optical airborne particle counters for sizes Ó5 µm.

B. Thaveau, A. Duarte, O. Brouste

Aerolab, ZA des Meuniers, 4 Rue Arago, 91520 Egly, France
Keywords: Calibration, traceability, uncertainties

The number calibration of optical airborne particle counters (OPC) is a prerequisite for the acceptance and approval of clean rooms and controlled-environment areas, which are classified according to their particulate concentrations.

In collaboration with the IPSNôs ñ*Laboratoire de Physique et Métrologie des Aérosols et du confinement*ò (Aerosol physics, metrology and containment laboratory) at the French Atomic Energy Agency's (CEA) site at Saclay,France, Aerolab developed a number calibration method for airborne particle counters for the particle size range of 0.1 to 1 µm and obtained COFRAC (French Accreditation Committee) accreditation in 2007 (No. 2-1810, scope available at www.cofrac.fr).

A new calibration method has been developed for 5 µm particles, which means that the entire dimensional range of the ISO 14644-1 standard [1] ôôCleanrooms and associated controlled environments Part 1 : Classification of air cleanlinessôô is now covered. This method uses a calibration bench that takes account of physical phenomena relating to 5 µm particles, principally sedimentation and impaction.

Like the 0.1 to 1 µm method, this method consists of generating a monodispersed aerosol of 5 µm latex spheres which allows for the primary calibration of a working reference instrument or reference counter, which will be subsequently used for the calibration of optical particle counters.

Particle generation consists of dispersing a dry powder of 5 µm diameter NIST (National Institute of Standards and Technology)-certified monodisperse latex particles in a concentration at a rate of 1 particle/cm^3 and for counters with a flowrate of between 0.1 cfm and 2 cfm (2.83 l/min to 56.6 l/min).

The primary calibration consists of comparing the mean particulate concentration measured by the reference counter or working reference instrument with the reference particulate concentration calculated on the basis of the total number of particles collected by a membrane during the same collection time. The membrane allows for the collection of all particles above a diameter of 1 µm at a flowrate close to the flowrate of the working reference counter. Photographs taken on a scanning electron microscope are used for counting the number of particles collected on the membrane.

The working reference instrument is an optical particle counter and all of the particles counted in the channel below 5 µm are taken into consideration.

The counting efficiency of the reference counter is calculated by comparing the mean concentration measured by the working reference counter with the mean reference concentration calculated by counting particles on photographs of the membrane.

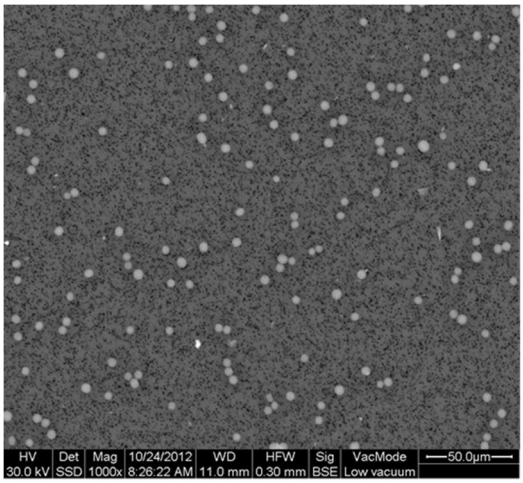

Latex microspheres on the membrane

The counting efficiency of a counter at a diameter of 5 µm is determined by placing the counter to be calibrated and the working reference counter in parallel via an isokinetic splitter dimensioned according to the flowrate of the reference counter.

The common point of both calibration methods (0.1 to 1µm and 5µm) is the traceability of reference appliances with regard to the international benchmarks [2], which allows uncertainties to be associated with counting efficiencies.

The calculation of uncertainty was developed according to the GUM method, based on a mathematical model in which the output magnitude depends on different input values, each of which is affected by a standard uncertainty.

[1] NF EN ISO 14644-1 "Cleanrooms and associated controlled environments. Part 1: Classification of air cleanlinessôô July 1999.

[2] Fletcher R.A., Mulholland G.W., Winchester M.R., King R.L. & Klinedinst D.B., (2009) National Institute of Standards and Technology (NIST). *Calibration of a Condensation Particle Counter using a NIST traceable method*

Numerical and experimental study of a spark discharge used for nanoparticle production

A. Voloshko[1], A. Kohut[2], J-Ph. Colombier[1], G. Galbács[3], Zs. Geretovszky[2] and T.E. Itina[1]

[1]Laboratoire Hubert Curien, CNRS, UMR5516/Lyon University, 42000, Saint-Etienne, France;
[2]Department of Optics and Quantum Electronics, University of Szeged, 6720 Szeged, Hungary
[3]Department of Inorganic and Analytical Chemistry, University of Szeged, 6720 Szeged, Hungary

Keywords: spark discharge, numerical modelling, spectroscopy.

Spark discharge is proven to be an efficient source of nanoparticles (Pfeiffer et al., 2014; Meuller et al., 2012). The development of plasma column during spark discharge precedes nanoparticle formation. In the present study, both numerical modelling and experiments were performed to assess the plasma properties. The ultimate aim is to understand how plasma properties influence nanoparticle formation.

The developed model consists of hydrodynamic calculations of plasma column parameters. Neutral atom, ion and electron densities are calculated in assumption of local thermal equilibrium. Energy transfer and transformations are calculated considering Joule heating by electric current, ionization energy losses, recombination-induced heating, heat conduction and radiation losses.

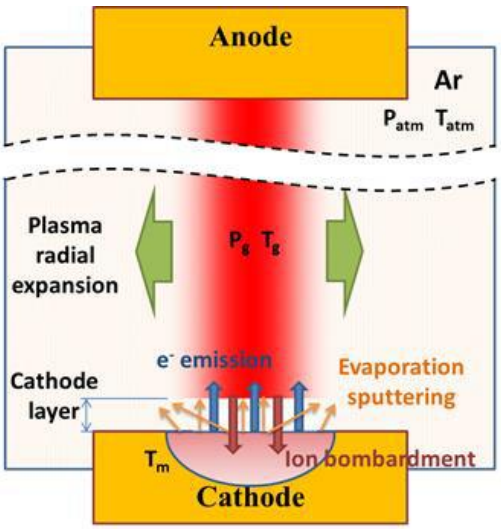

Figure 1. Schematics of the electrode material injection into the expanding plasma column.

The numerically derived plasma parameters were measured experimentally by means of temporally and spatially resolved emission spectroscopy together with time-resolved imaging. To this end, the light of the emitting plasma was imaged onto the tip of an optical fiber connected to an Echelle spectrograph equipped with a high sensitivity ICCD camera. The electron concentration was calculated from the Stark-broadening of the singly charged ion spectral lines, and the temperature was derived by the Boltzmann plot method. A separate ICCD camera was used to take time-resolved images of the plasma, in order to gather information about the time-evolution of the plasma morphology and plasma channel width.

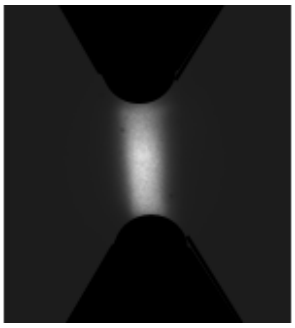

Figure 2. Image of plasma column in Ar obtained by time-resolved imaging 190 ns after the breakdown with 50 ns exposure time.

The comparison of modeling results and the data calculated from experimental data will be discussed in out presentation. In general, we found that in the case of noble gasses the match of the results is fairly good, whereas for molecular gasses a further improvement of the model is needed.

The research leading to these results received funding from the European Union Seventh Framework Programme (FP7/2007-2013) under Grant Agreement n° 280765 (BUONAPART-E).

Pfeiffer T. V., Feng J. & Schmidt-Ott A. (2014). *Adv. Powder Technol.*, 25, 56-70.

Meuller B. O., Messing M. E., Engberg D. L. J., Jansson A. M., Johansson L. I. M., Norlén S. M., Tureson N. and Deppert K. (2012). *Aerosol Sci. and Tech,*. 46, 1256–1270.

Numerical prediction of single fibre efficiency for nanoparticles filtration

N. Bardin-Monnier[1,2], A. Charvet [1,2], D. Thomas[1,2]

[1]Université de Lorraine, Laboratoire Réactions et Génie des Procédés (LRGP), UMR 7274, F-54000, Nancy, France

[2] CNRS, Laboratoire Réactions et Génie des Procédés (LRGP), UMR 7274, F-54000, Nancy, France

Keywords: Fibrous filters, Simulation, Nanoparticles, Single fibre efficiency.

The filtration of nanoparticles is becoming an important issue as they may pose a health risk due to their increased toxicity. It is commonly admitted that only Brownian diffusion takes part in the collection process. Despite this apparent simplicity, no less than 14 theoretical models can be found in the literature (Brochot, 2012). They are mostly based on the resolution of the convection-diffusion equation around a cylinder and the study of the boundary layer. They all exhibit that the single fibre efficiency due to diffusion, η_D depends on the Peclet number, most of them on $Pe^{-2/3}$. Nevertheless, the comparison between experiments and these models revealed some discrepancies and conducted some authors to propose corrective terms (Liu *et al*., 1990 ; Wang *et al.*, 2007). This work proposes a numerical study in order to investigate the role of the Peclet number for nanoparticles (10 to 100 nm).

The simulations are performed with the GeoDict® code (Math2Market, GmbH). The approach is based on the generation of microstructures representing the fibrous filter. The fibre orientation, the sizes of the domain and of the discretization element (voxel) have to be chosen to simulate the fluid flow. Secondly, the collection efficiency of the medium is deduced from the calculated particle trajectories and the fibre/particle interactions. Each simulation gives a global efficiency value (η_t) and the corresponding single-fibre efficiency η_D can be deduced from Equation 1.

$$1-\eta_T = \exp(-4.\eta_D.\frac{\alpha}{1-\alpha}.\frac{Z}{\pi.d_f}) \qquad (1)$$

In this equation, α represents the filter packing density, Z the thickness of the domain and d_f the fibre diameter. The fibre diameter ranges from 0.8 µm to 10 mm, the packing density from 1 % to 30 % and the particles diameter from 5 nm to 100 nm.

The microstructures are generated by setting the fibre diameter, the medium porosity and the fibre orientation in the domain. The distribution of the fibres is built thanks to a stochastic process via a random seed. Simulations are carried out for 5 different random seeds in order to avoid statistical bias. The fibres are supposed to be preferentially oriented in the plane perpendicular to the flow and isotropy is assumed in this plane.

The sizes of the microstructure and the discretization element are chosen in order to fit the permeability of the medium and to achieve a detailed description of the flow around the fibre. A fibre diameter is described by 7 to 20 cells. The size of the domain respects Brinkman's criteria (size in one direction > $14.k_{th}^{0.5}$ where k_{th} is the theoretical medium permeability). The values of k_{th} are deduced from well-know correlations (Davies, 1950 ; Jackson *et al.,* 1986). Once the dimensions of the microstructure are evaluated, a simulation of pure air flow is performed and the corresponding value of k is deduced. A gap of 5 % between k_{th} and k is tolerated. If it exceeds this value, the dimensions are modified until the threshold value is reached. For each simulation 5,000 trajectories are simulated.

The compilation of all the simulation results allows proposing an analytical equation to calculate single fibre efficiency :

$$\eta_D = \left(\frac{1-\alpha}{1+\alpha}\right)^{1/3}.Pe^{-1/2} + \left(\frac{1+\alpha}{1-\alpha}\right)^{2/3}.Pe^{-2/3} \qquad (2)$$

The comparison between simulation results and those issued from the correlation exhibits a mean agreement around 15%. As a consequence, these first results are quite encouraging and a thorough study is being performed for low Peclet numbers and higher packing densities in order to improve this model.

Brochot C. (2012) Filtration des nanoparticules-Application aux appareils de protection respiratoires, Thèse de Doctorat, Université de Lorraine

Liu B.Y.H., Rubow K.L. (1990) 5th World Filtration Congress, June 5-8 1990, Nice, France.

Wang J., Chen D.R., Pui D.Y.H (2007) Modeling of filtration efficiency of nanoparticles in standard filter media, *Journal of Nanoparticle Research*, 9, 109-115.

Davies C., (1952) The separation of airborne dust and mist particles. *Proc. Institution of Mechanical Engineers, Part B : Journal of Engineering Manufacture*, 1B:185-198

Jackson G., James D., (1986). The permeability of fibrous porous media. *Canadian Journal of Chemical Engineering*, 64(3): 364-374

On-chip microacoustic aerosol generation

A. Winkler, S. Harazim, S.B. Menzel, H. Schmidt
IFW Dresden, SAWLab Saxony, PF 270116, 01171 Dresden, Germany

Keywords: surface acoustic wave, atomization, SU-8, microchannels.

In this work, we present an acoustofluidic aerosol generation method suited for mass-scale device production and aerosol source miniaturization. Our method is based on the interaction of standing Surface Acoustic Waves (sSAW) of the Rayleigh-type with a fluid delivered to the surface of a piezoelectric chip. With this technique, it is possible to generate droplets with diameters in the low µm-range without the need for moving parts, nozzles or pumps. The droplet diameter can be controlled via the surface acoustic wave characteristics as well as by the liquid properties (Collins, 2012).

In conventional SAW-based atomizer lab systems, liquid wetted tissues (Rajapaksa, 2014) or capillaries (Qi, 2009) are used to supply the liquid to the acoustic propagation path. These approaches are limited in their practical applicability and regarding the mass-scale manufacturing. In order to transfer the sSAW atomization principle from the lab to real world applications, we developed a continuous fluid supply method using integrated microchannels with well-defined micro-outlet lithographically structured directly on the chip surface at the boundary of the acoustic propagation path. These channels are created via standard photolithography within SU-8 photopolymer, showing optical transparency, good chemical, thermal and mechanical resistance, and biocompatibility (Nemani, 2013).

The interaction of the sSAW with the fluid meniscus at the channel outlet generates and dynamically stabilizes a thin fluid film, which is laterally spreading into the center of the acoustic propagation path, where atomization takes place due to higher SAW amplitude. Due to this lateral separation of fluid delivery zone and atomization zone, secondary acoustofluidic actuation effects, i.e. jetting and mixing, are suppressed and the aerosol formation is stabilized. This unique approach makes SAW fluid atomization highly controllable and reproducible. Small plume opening angles of approx. 5° together with a coverage of several cm can be realized at atomization rates of around 100 µl/min. Furthermore, by variation of the interfering SAW amplitude ratio within the atomization zone, the aerosol emanation angle can be controlled within the limits of the Rayleigh-angle (e.g. approx. ±22° for water, measured from the surface normal).

Our method of SAW fluid atomization with integrated microchannels shows high potential for miniaturization and brings the production of handheld devices for inhalation therapy or various technological purposes into reach.

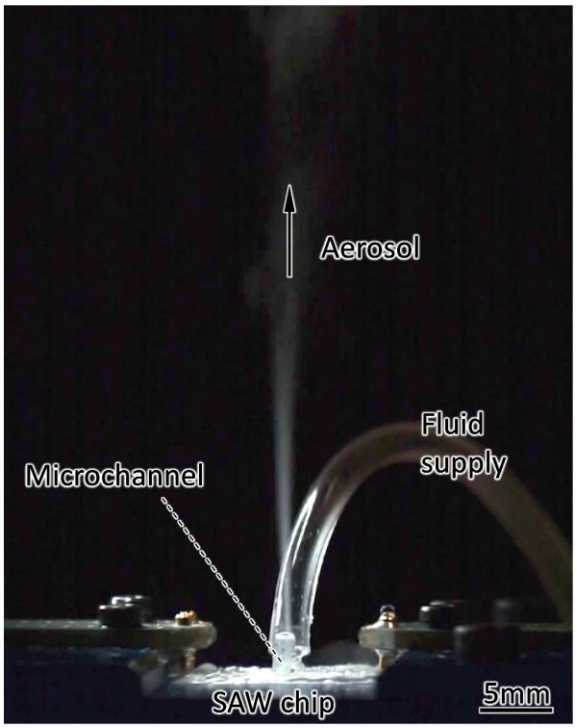

Fig. 1. Side view of a sSAW fluid atomization setup with on-chip SU-8 microchannels showing a vertical aerosol plume with small opening angle

This work was supported by the German Research Foundation (DFG Grant WI 4140/2-1) and the Federal Ministry of Education and Research (BMBF InnoProfile-Transfer 03IPT610A).

Collins, D. J., Manor, O., Winkler, A., Schmidt, H., Friend, J. R., and Yeo, L. Y. (2012). *Atomization off thin water films generated by high-frequency substrate wave vibrations*, Physical Review E 86, 1.

Nemani, K. V., Moodie, K. L., Brennick, J. B., Su, A., and Gimi, B. (2013). *In vitro and in vivo evaluation of SU-8 biocompatibility*, Mater. Sci. Eng. C-Mater. Biol. Appl. 33, 4453.

Qi, A. S., Friend, J. R., Yeo, L. Y., Morton, D. A. V., McIntosh, M. P., and Spiccia, L. (2009). *Miniature inhalation therapy platform using surface acoustic wave microfluidic atomization*, Lab on a Chip 9, 2184.

Rajapaksa, A., Qi, A. S., Yeo, L. Y., Coppel, R., and Friend, J. R. (2014). *Enabling practical surface acoustic wave nebulizer drug delivery via amplitude modulation*, Lab on a Chip 14, 1858.

On site air filter test system

I. Kulmala[1], T. Kalliohaka[1], A. Taipale[1] and H. Salmela[1]
[1]VTT Ltd, PO Box 1300, 33100 Tampere, Finland

Keywords: Air filter, on site measurement, indoor air, building protection.

One of the main purposes of supply air filtration is to reduce outdoor pollutants from entering indoors. Especially fine particles are considered harmful due to their adverse health effects. For example, long-term exposure to PM 2.5 is associated with an increase in the long-term risk of cardiopulmonary mortality by 6–13% per 10 µg/m3 of PM 2.5 (Beelen *et al.*, 2008).

The key performance indicators of the air filters are filtration efficiency, pressure drop and dust holding capacity. According to filter standards, these properties are currently measured in laboratory conditions using artificial test dust for challenging the filters (ASHRAE 52.2, EN 779). These methods, however, are not equivalent to the actual performance of air filters in real operating conditions which usually differ significantly from those in laboratory, especially with respect to dust concentration and particle size distribution.

In order to study the filter performance more accurately, a real-time test system was developed at VTT. The system consists of sampling tubes, a micromanometer, particle detectors and a valve system controlled by a laptop computer. The system is automated and it measures and stores pressure drop of supply air filters, particle concentrations upstream and downstream of the filters, as well as particle concentrations in the HVAC system's exhaust air. The measurement system was installed in two different test sites in Finland and in China with new type of high efficiency filters.

Long term tests proved that the concept is successful, and with the aid of the system detailed knowledge about the filter performance could be achieved. In addition to filtration efficiency, indoor/outdoor particle concentrations gave indication of the buildings protective capability against outdoor contaminants. With the aid of the system the effect of enhanced supply air filtration on the improvement of indoor air quality could be clearly demonstrated.

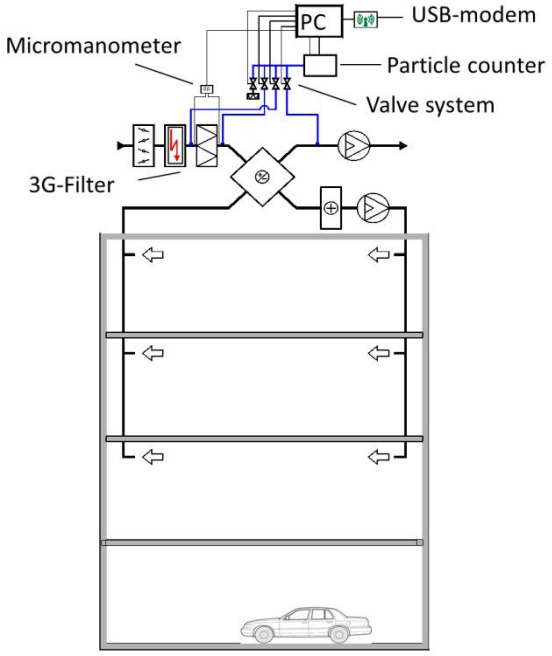

Figure 1. Principle of the on-site filter test system.

The research leading to these results has received funding from the European Union's Seventh Framework Programme under grant agreement n° 313077 within the EDEN Project (End-user driven DEmo for cbrNe)..

ASHRAE 52.2-201. Method of Testing General Ventilation Air-Cleaning Devices for Removal Efficiency by Particle Size

Beelen R et al (2008). Long-term effects of traffic-related air pollution on mortality in a Dutch cohort (NLCS-AIR Study).Environmental Health Perspectives, 116:196–203.

EN779:2012. Particulate air filters for general ventilation. Determination of the filtration performance.

On the correlation of spectral emission and nanoparticle yield in a spark discharge generator

A. Kohut[1], G. Galbács[2], L. Ludvigsson[3], B.O. Meuller[3], M.E. Messing[3], K. Deppert[3], and Zs. Geretovszky[1]

[1]Department of Optics and Quantum Electronics, University of Szeged, H-6720 Szeged, Hungary
[2]Department of Inorganic and Analytical Chemistry, University of Szeged, H-6720 Szeged, Hungary
[3]Solid State Physics, Lund University, SE-22100, Lund, Sweden

Keywords: nanoparticle, spark discharge, spectroscopy

Nanoparticle generation by spark discharge is a simple and versatile technique for producing metal and semiconductor nanoparticles (NPs) in the gas phase. In the conventional setup, the discharge is fed by a bipolar, capacitor charging circuit producing repetitive sparks between two electrodes. Thermal evaporation and sputtering erode the electrode material which will lead to NP formation in the surrounding, flowing gas.

In the present work, we report on a correlation found between the emission spectroscopic signal of the electrode material and the total number concentration of the produced NPs. The spectroscopic measurements were carried out on a spark discharge nanoparticle generator (SDG), parallel with a simultaneous on-line nanoparticle characterization. The effect of experimental parameters (i.e. charging current, electrode distance, gas environment) on the spark plasma and the nano aerosol was investigated.

A high sensitivity spectroscopy setup consisted of an Echelle spectrograph equipped with an intensified CCD camera as detector was added to the SDG. The emitted light of the plasma was spatially integrated over a ca. 5 mm dia. circular area and collected in a direction perpendicular to the axis of the electrodes. The setup allowed for spectral data collection in the 300-800 nm wavelength and 100 ns-50 µs temporal ranges, with a corresponding resolution of 0.1 nm and 50 ns, respectively. Each spectrum was measured on separate sparks and few hundred spectra were averaged at each experimental setting. The mobility diameter of the produced NP agglomerates was measured by an on-line Differential Mobility Analyzer.

Various species of both the gas (N^{3+}, N^{2+}, N^{+}, N, or Ar^{2+}, Ar^{+}, Ar) and the electrode material (Cu, or Au, Au^{+}) were identified. The emission of copper and gold atoms becomes detectable ~0.5-1 µs after the onset of breakdown and they emit 2-2.5 times longer than the characteristic duration of the oscillating voltage/current signal in N_2, and even 5-7 times longer in Ar.

We found that the total particle concentration of the agglomerated NPs – defined as the area under the mobility size distribution curve – correlates with the temporally integrated emission intensity of spectral lines characteristic of the electrode material. This correlation is exemplified for copper and gold on Figure 1 and 2, respectively.

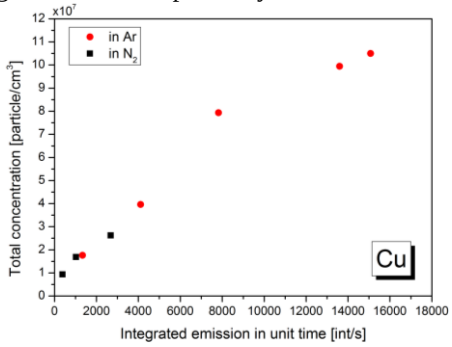

Figure 1. Total NP concentration as a function of integrated emission of Cu I 521.80 nm spectral line in N_2 and Ar gases.

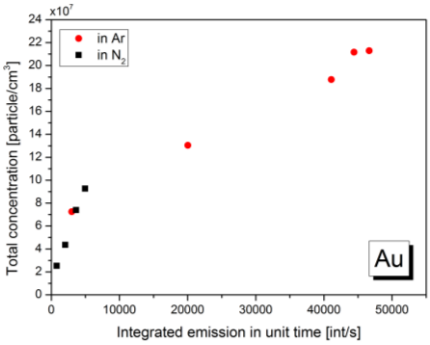

Figure 2. Total NP concentration as a function of integrated emission of Au I 479.26 nm spectral line in N_2 and Ar gases.

In our view, these findings, together with the correlation found between the mode of the mobility size distribution of the NPs and the time position of maximum intensity of spectral lines (Kohut *et al.*, 2013) allows for the optical monitoring of the NP generation process.

This project has received funding from the European Union´s Seventh Framework Program (FP7/2007-2013) under grant agreement no. 280765 (BUONAPART-E).

Kohut, A., Metzinger, A., Galbács, G., Ludvigsson, L., Meuller, B. O., Messing, M. E., Márton, Zs., Deppert, K., and Geretovszky, Zs. (2013). *European Aerosol Conference*, Prague, #B148J.

On the importance of particle density in ELPI data post-treatment

A. Charvet[1, 2], S. Bau[3], D. Bémer[3] and D. Thomas[1, 2]

[1] Université de Lorraine, Laboratoire Réactions et Génie des Procédés, UMR 7274, F-54000, Nancy, France
[2] CNRS, Laboratoire Réactions et Génie des Procédés, UMR 7274, F-54000, Nancy, France
[3] Institut National de Recherche et Sécurité (INRS), F-54519, Vandœuvre-lès-Nancy, France

Keywords: ELPI, intercomparison, particle density.

Different devices for the measurement of airborne particle number size distribution (APS, SMPS, ELPI …) are classically implemented for online workplace and/or environmental aerosol characterization. Though several intercomparison studies have already been carried out, comparing data obtained from these instruments based on different measurement principles remains uncertain.

The difficulty is all the more important when using the ELPI, which involves particle density to be provided by the user for data analysis. Among the previous published studies, Ristimäki et al. (2002) or more recently Price et al. (2014) adjusted particle effective density to obtain an overlapping of number size distributions stemming from SMPS and ELPI. The case of the use of an ELPI alone remains unresolved, however.

The aim of this study is to compare number and mass concentrations obtained by different reference devices (SMPS, TEOM) with ELPI data. Specific attention will be paid to the importance of particle density in ELPI data post-treatment.

Tested aerosols are Zn/Al agglomerates generated by thermal metal spraying (Bémer *et al.*, 2010). Number and mass concentrations obtained with a SMPS and a TEOM, respectively, were compared to calculated concentrations obtained with an ELPI. The data post-treatment was performed assuming different particle densities: the mobility-dependent effective density as determined by a tandem DMA/APM (Charvet et al., 2014), the standard density (ρ_0 = 1 g/cm^3), the raw material density ($\rho_{Zn/Al}$ = 5.7 g/cm^3) and an average effective density, as defined by:

$$\bar{\rho}_e = \frac{\sum_{d_p} C_N(d_p) \cdot \rho_e(d_p)}{\sum_{d_p} C_N(d_p)}$$

Results highlight a good agreement between SMPS and ELPI number and mass concentrations when effective density and average effective density are considered (cf. figure 1). On the contrary, considering raw material density induces an overestimation of the number concentration by a factor close to 30. Besides, the good agreement also observed when considering the standard density could be explained by the fortuitous combination of the Zn/Al aerosol size distribution and its effective density.

Indeed, the aerosol considered in this study has a modal mobility-equivalent diameter close to 100 nm and consequently the average particle effective density is close to unity.

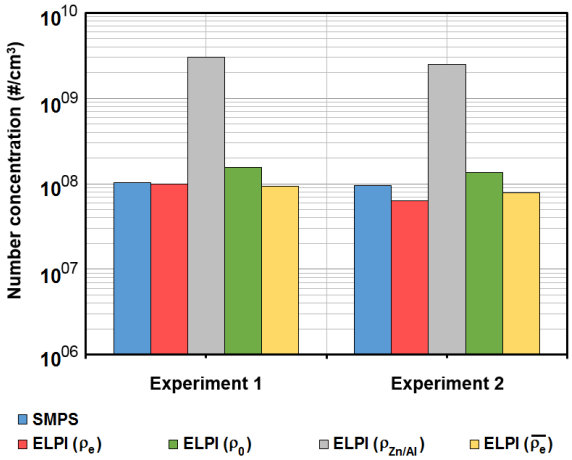

Figure 1. Comparison of SMPS and ELPI number concentrations according to particle density choice

Theoretical calculations of ELPI currents were further performed for different simulated particle number size distributions. When the distribution is centered at 200 nm and considering a unit standard density, number concentration is overestimated comparatively to the SMPS, by a factor 3.5. These results highlight that considering the standard density in calculations is not a universal approach and induces a strong discrepancy on the number concentrations measured by the ELPI.

Bémer, D., Régnier, R., Subra, I., Sutter, B., Lecler, M.T. & Morele, Y. (2010) *Ann. Occup. Hyg.*, 54, 607-614.

Charvet, A., Bau, S., Bémer, D & Thomas, D. (2014) *J. Nanopart. Res.*, 16, 2418.

Price, H.D., Stahlmecke, B., Arthur, R., Kaminski, H., Lindermann, J., Daüber, E., Asbach, C., Kuhlbusch, T.A.J, Bérubé, K.A & Jones, T.P. (2014) *J. Aerosol Sci.*, 76, 48-55.

Ristimaki, J., Virtanen, A., Marjamäki, M., Rostedt, A., & Keskinen J. (2002) *J. Aerosol Sci.*, 33, 1541-1557.

Online characterization of wood combustion emissions and their atmospheric aging

O. Sippula[1], P. Tiitta[1], M. Kortelainen[1], P. Yli-Pirilä[2], H. Czech[3], C. Radischat[3], J. Tissari[1], A. Leskinen[2,4], A. Hartikainen[1], H. Koponen[1], J. Leskinen[1], T. Torvela[1], M. Ihalainen[1], H. Lamberg[1], J. Grigonyte[1], L. Hao[2], T. Streibel[3], J. Orasche[3], A. Virtanen[2], K. Lehtinen[2,4], R. Zimmerman[3], J. Jokiniemi[1]

[1]Department of Environmental Sciences, Univ. of Eastern Finland, P.O. Box 1627, FI-70211 Kuopio, Finland
[2]Dept. of Applied Physics, Univ. of Eastern Finland, Kuopio, Finland
[3]Joint Mass Spectrometry Centre, Cooperation Group Comprehensive Molecular Analytics, University of Rostock, Institut für Chemie Dr.-Lorenz-Weg 1, 18059 Rostock / Helmholtz Zentrum München, Germany
[4]Finnish Meteorological Institute, Kuopio Unit, P.O. Box 1627, 70211, Kuopio, Finland

Keywords: combustion, biomass, mass spectrometry

Residential wood combustion has been identified in several European countries as a major source of fine particle emissions. In addition, wood combustion may generate high organic gaseous emissions that induce adverse health effects and are precursors for secondary aerosol formation. These emissions are especially high from batch-wise operated wood combustion appliances and there is a clear need to develop effective emission reduction methods for these appliances. To achieve this goal, detailed online information on the emission formation and chemical composition is required from this highly dynamic process.

The emissions of a modern wood-log fired masonry heater and a modern pellet boiler were measured with several online mass spectrometers in the HICE wood combustion campaign, in Kuopio 2013. First, the soot particle aerosol mass spectrometer (SP-HR-ToF-AMS, Aerodyne), equipped with a laser vaporizer, was used to analyse particle chemical composition, including refractory black carbon (rBC), particulate organic matter (POM) and its oxidation state, metals, and inorganic ions. Second, a high resolution proton transfer mass spectrometer (HR-PTR-ToF-MS, Ionicon) was used to analyse the composition of volatile organic compounds. Third, two photo-ionization mass spectrometers were used for measuring volatile and semivolatile organics; a resonance enhanced multiphoton ionization mass spectrometer (REMPI-ToF-MS) and a Single photon ionization mass spectometer (SPI-ToF-MS) (Zimmermann, 2013). In addition, filter and adsorbent samples were collected for offline chemical analyses and aerosol particle size distributions and morphologies were determined (Leskinen et al., 2014).

The masonry heater was operated with birch, spruce and beech logs, and each experiment with 6 consecutive batches. Sampling for aerosol instruments was carried out with a combination of a porous tube diluter and an ejector diluter. In addition, samples were taken to an environmental aging chamber to study the secondary formation and decomposition of emission components in the atmosphere.

The particle mass was mainly composed of black carbon (rBC, soot) and POM and their concentrations varied largely within the period of one batch. The rBC emissions were peaking mainly during the period of the highest combustion rate of the batch, while the highest POM was observed during ignition of the batches (Figure 1). The increase in the combustion chamber temperature clearly decreased both POM and gaseous organics, while the same was not observed for rBC. POM and gaseous organics generally contained high contents of oxygenated species, but their composition changed depending on the combustion phase. Interestingly, the CO emission behaved differently from soot and organics and the peaks were located mainly at the end of the each batch, and in the char burnout phase. During the CO peaks also the partitioning of organic species between gas and particulate phase changed substantially. Finally, the chamber experiments were used to derive secondary emission factors for POM and various organic species.

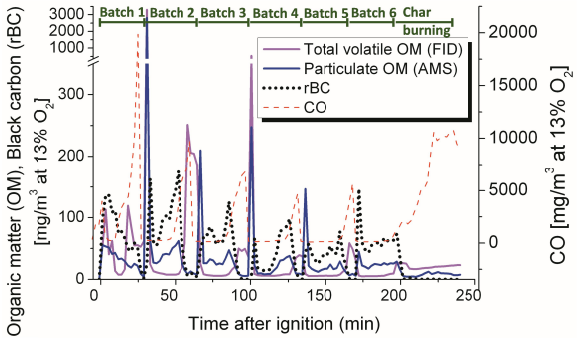

Figure 1. Emission time trends from birch log wood combustion, including organic matter (OM), soot (rBC) and carbon monoxide (CO).

Zimmermann, R. (2013). *Anal. Bioanal. Chem.*, 405, 6901-6905.

Leskinen, J., Ihalainen, M., Torvela, T. *et al* (2014). *Environ. Sci. Technol.*, 48, 13298-13306.

Support by the Academy of Finland (Grant: 258315, 259946), the strategic funding of the University of Eastern Finland and the Helmholtz Virtual Institute of Complex Molecular Systems in Environmental Health (HICE) is gratefully acknowledged.

Optimization of silver particle number size distributions from a nucleation furnace by modification of heat shields and injection nozzles

J. Rosahl[1], A. Nowak[1], A.Kuntze[1], M.Hildebrandt[1], I.-C. Masthoff[2], G. Garnweitner[2] and V. Ebert[1, 3]

[1]Physikalisch-Technische Bundesanstalt Braunschweig, 38116, Braunschweig, Germany
[2]Insitute for Particle Technology, Technische Universität Braunschweig, 38108, Braunschweig, Germany
[3]Center of Smart Interfaces, Technische Universität Darmstadt, 64287, Darmstadt, Germany

Keywords: formation, homogenous nucleation, aerosol generation, silver, particle number size distribution

With the implementation of the EURO 5 and EURO 6 legislation, the European Union (EU) established for the first time a number limit of engine exhaust particles emitted by light vans and passenger cars, which are powered by diesel or even gasoline engines. Therefore, a metrological basis for the measurement of particle number concentration of mostly nano-scaled pollutants is required. Within the work package 1 (WP1; *Automotive particle emission metrics*) of the EMRP project ENV02 (PartEmission[1]) metrological criteria like SI traceability, temperature stability and "soot likeness" were investigated and implemented at several national metrological institute in Europe. (Andres *et al.*, 2014).

One well-suited reference aerosol is silver from a nucleation furnace. PTB, the national metrological institute of Germany, is using this reference aerosol to establish a calibration service for Engine exhaust condensation particle counters (EECPC). For that purpose a tube furnace is used to generate silver aerosol. Compared to Scheibel and Porstendörfer (1983) a larger tube furnace is used to provide nucleated particles at larger particle sizes up to 100 nm based on homogenous nucleation.

To influence the shape and the width of the particle number size distributions (PNSD) several process modifications were investigated. The modification consists of heat shields combined with a nozzle at the inlet and a hopper at the outlet of the tube furnace. Additionally, several disks at the heat shields were mounted to adjust the heat in the middle of the tube furnace and to provide a more uniform temperature profile over the entire tube length. Also, a faster temperature drop was achieved with the disk for both heat shields in the furnace.

Using different nozzle sizes (1 mm up to 4 mm) it is possible to adjust the maximum of PNSD towards larger diameters and to generate a higher particle number concentration (Figure 1). Without a heat shield an unwanted bimodal size distribution was observed in the longer tube. Including both heat shields smaller silver particles were generated and the PNSD showed a sharper peak in a lower size range. With only the inlet heat shield at the beginning of the tube a higher particle number concentration was generated and again a bimodal size distribution in the larger size range was observed.

Finally, we investigated with the presented setup a more flexible use of the common tube furnace and managed to adjust the number particle size of homogenously nucleated silver particles by up to a factor of 3.

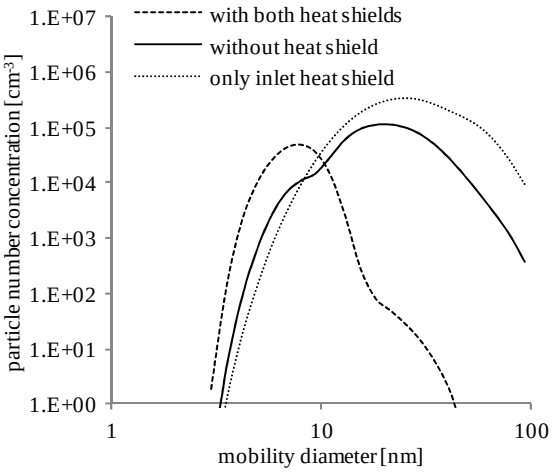

Figure 2: Influence of the heat shields at 1200 °C furnace temperature for PNSD.

Andres, H., Lüönd, F., Schlatter, J., Auderset, K., Jordan-Gerkens, A., Nowak, A., Ebert, V., Buhr, E., Klein, T., Tuch, T., Wiedensohler, A., Mamakos, A., Riccobono, F., Discherl, K., Högström, R., Yli-Ojanperä, J. and Quincex, P. (2014). EPJ Web of Conferences 77, 00020, *Measuring soot particles from automotive exhaust emissions*

Scheibel, H. G. and Porstendörfer, J. (1983). *J. Aerosol Science, 2, 113-126, Generation of monodisperse AG- and NaCl aerosols with particle diameters between 2 and 300 nm*

[1] The project is part of the European Metrology Research Programme (EMRP), which is jointly funded by the EMRP participating countries and the European Union.

Optimization of ultrafine particles filtration in granular beds

L. Wingert[1, 2, 3], D. Bémer[1], S. Pacault[2, 3], A. Charvet[2, 3], N. Bardin-Monnier[2, 3], D. Thomas[2, 3]

[1] Institut National de Recherche et Sécurité (INRS), F-54519, Vandœuvre-lès-Nancy, France
[2] Université de Lorraine, Laboratoire Réactions et Génie des Procédés, UMR 7274, F-54000, Nancy, France
[3] CNRS, Laboratoire Réactions et Génie des Procédés, UMR 7274, F-54000, Nancy, France

Keywords: granular bed filtration, optimization, performance

Ultrafine particles are generated by many manufacturing processes: surface processing and coating (thermal spraying ...), machining (drilling, grinding ...), combustion (fire, blast furnaces ...), fragmentation of raw materials (crushing, sieving, demolition ...), welding and cutting of metals etc... Among these, metal coating processes are based on spraying fine metal particles melted by a heat source (flame or electrical arc) using a carrier gas. This technique is a major source of ultrafine metal particles generation (zinc, aluminum, tin and alloys).

The development of suitable protection systems therefore appears crucial in order to protect persons and the environment. The most efficient and widely used de-dusting methods for separating the particles from the carrier fluid are currently fibrous media. These pleated fiber filters are initially very efficient but generate a strong increase in pressure drop because of a quick and sometimes irreversible clogging as well as an extra cost resulting from their replacement.

Granular beds also exhibit interesting performance, in terms of ultrafine particle collection efficiency, and a higher resistance to mechanical and thermal stresses comparatively to fibrous filters. Nevertheless, Bémer et al. (2013) highlighted that ultrafine particles deposit is essentially located in the first layers of the granular bed. Thus, only a small depth is useful thereby reducing both operation time of granular beds between each unclogging and the process yield. In other recent studies, a special attention is notably devoted to moving granular bed filters (Chen et al., 2009; El-Hedok et al., 2011).

Our optimization approach is quite different and consists in increasing the time between two unclogging operations, i.e. in reducing the pressure drop increase while maintaining a high collection efficiency. Experiments were achieved using a three-stage column, each composed of a given diameter stainless steel beads. Performances of an optimized column filled with bead diameters equal to 1 mm in the first stage, 0.8 mm in the second and 0.5 mm in the third are compared to those of a conventional granular bed (with beads diameter of 0.5 mm in the 3 stages). So, as collection efficiency is a decreasing function of the collector size, this optimized configuration permits to firstly clog the downstream layers of the granular bed, i.e. the third stage.

These two kinds of granular bed are clogged with Zn/Al nanostructured particles (generated by metal thermal spraying). The efficiency and pressure drop temporal evolutions were monitored (cf. figure 1).

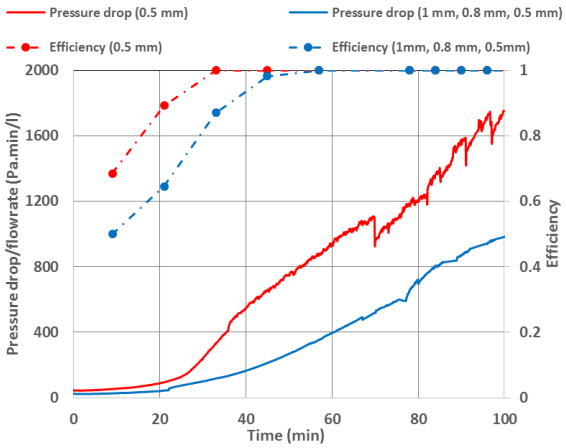

Figure 1. Efficiency and pressure drop evolution of optimized and conventional granular beds.

Although there is a 20% decrease of the initial efficiency for the optimized bed compared to the conventional one, this gap is rapidly reduced during the clogging process (13% after 30 min and 0% after 40min). At the same time, results highlight a lower pressure drop increase of the optimized granular bed. Indeed, the pressure drop reached after 40 min is 70% lower than in case of the conventional bed.

According to these results, the optimization of the granular bed filtration by means of a collector diameter gradient seems quite promising. This approach could allow extending the operation time between two unclogging operations. Others improvements, such as finding the optimal combination of collector diameters, are yet needed to enhance performances of this granular bed.

Bémer, D., Subra, I., Morele, A., Charvet, A. & Thomas, D. (2013). *J. Aerosol Science*, 63, 25-37.

Chen, Y.S., Hsiau, S.S., Lai, S.C., Chyou, Y.P., Li, H.Y. & Hsu, C.J. (2009). *J. Hazard. Mater.* 171, 987-994.

El-Hedok, I.A., Whitmer, L. & Brown, R.C. (2011). *Powder Technol.*, 214, 69-76.

Oxygen deficient tin dioxide made by flame spray synthesis

M. Stanzel[1], P. Herre[1] and W. Peukert[1,2]

[1]Institute of Particle Technology, Friedrich-Alexander-University Erlangen-Nuremberg, Cauerstr. 4, 91058 Erlangen, Germany
[2]Interdisciplinary Center for Engineering of Advanced Materials (EAM), Friedrich-Alexander-University Erlangen-Nuremberg, Nägelsbachstr. 49b, 91052 Erlangen, Germany

Keywords: flame spray pyrolysis, tin oxide, zinc oxide, morphology, nanoparticles

Tin dioxide nanoparticles (NPs) as a wide band gap semiconductor and as binary zinc-tin-oxide NPs, are economic and promising basic materials for the application in printable electronic devices. Deposited *in situ* in the spray flame of a pyrolysis process on temperature resistant wafers they can be used in solar cells, transistors or sensors. (Kilian et al, 2014). Moreover, the morphological, optical and electronic properties of the powders can be adjusted depending on composition, synthesis route and oxygen content.

To cover the high demand of low cost nanoparticulate materials an energy efficient and solvent free synthesis method with scalable production rates, i.e. a flame spray process, is required. Particle size, shape, optical band gap and defect states of the particles can be controlled by the precursor composition and the process parameters. In this work, the synthesis of binary Zn-Sn-O and pure SnO_2, as well as the influence of process parameters and precursor composition are investigated.

A liquid precursor of mixtures of zinc- and tin acetylacetonate in 2-methoxyethanol is dispersed by a nozzle into the spray flame. In the flame, pyrolysis reactions lead to high supersaturations and therefore to particle nucleation with subsequent growth, agglomeration and sintering. The reactor set-up (Siriwong et al., 2009) allows to produce Sn-Zn-O and SnO_{2-x} with mean primary particles in the size range of 5 nm up to 10 nm. These particles are then collected with a membrane filter. To control phase and oxidation level of the tin oxide particles precursor and process parameter variation will be investigated.

The change in primary particle size is characterized with BET, XRD and TEM. A HRTEM-image for pure SnO_{2-x}, see figure 1, shows single-crystalline and sintered particles with sizes smaller than 10 nm. Phase changes can be determined from SAED (Selected Area Electron Diffraction) and XRD pattern. Also a steadily increasing Zn content in the precursor influences particle size and morphology. EDX and ICP-OES proof the precise composition of the binary system and indicate oxygen deficiency in the tin oxide powders. The latter one can be affected by varying the process parameters. To reduce the flame temperature also various amounts of water were added to the precursor solution. The optical band gap differs from the one of pure SnO_2 and can be influenced by adjusting e.g. precursor flow, dispersion gas flow and concentration. PL measurements provide insight into the defect states of the binary Sn-Zn-O and reveal a change in the luminescence behaviour upon doping with Sn.

The aerosol synthesis will be presented, the properties of the Sn doped zinc oxide particles, regarding morphology, composition and electronical properties, as well as the impact of process parameters on pure SnO_{2-x} will be discussed in detail.

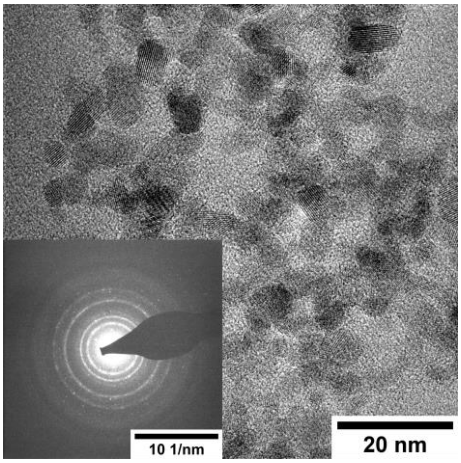

Figure 1. HRTEM-image and SAED pattern of pure tin oxide synthesized at a dispersion gas stagnation point pressure drop of Δp=1.5bar.

This work was supported by the German Research Council (DFG) and the Cluster of Excellence "Engineering of Advanced Materials" (EAM).

Kilian D., Engel S., Borsdorf B., Gao Y., Kögler A.F., Kobler S., Seeger T., Will S., Leipertz A., Peukert W. (2014). *Journal of Aerosol Science, 69*, 82-97.

Siriwong, C. Wetchakun, K., Wisitoraat, A., & Phanichpant, S. (2009). in *Proc. of IEEE Sensors 2009 Conference*, 118-123.

Particle based Functional Materials from the Gas Phase

Martin Seipenbusch[1,2]

[1]Department of Chemical Engineering, Karlsruhe Institute of Technology, Karlsruhe, Germany. Current Address: Department of Energy-, Process- and Bioengineering, University of Stuttgart, Stuttgart, Germany
[2]Seipenbusch particle engineering, technical business consulting, Kuppenheim, Germany

Keywords: nanotechnology, particle engineering, catalysis, CVD.

The development of functionally optimized materials for applications such as catalysts, sensors or electronics can greatly benefit from aerosol methods. A major advantage of these methods is their high precision and the wide range of possibilities in structure formation. The other important feature of aerosol technology is the availability of on-line methods for structural characterization. In combination with suitable methods for the assessment of the functional properties a direct correlation between structure and function is possible which enables rapid optimization.

For the structuring of particle based materials we have developed a process based on the combination of chemical vapor synthesis (CVS) and chemical vapor deposition (CVD) (Binder, Heel, & Kasper, 2007; Faust, Enders, Bruns, et al., 2013; Faust, Enders, Gao, et al., 2013). Examples for structures generated with this method are presented in Fig. 1 which shows electron microscopic images (TEM) of precious metal islands on an oxide support (Pt on Al_2O_3) and a core-shell structure of two oxides (MoOx on SiO_2).

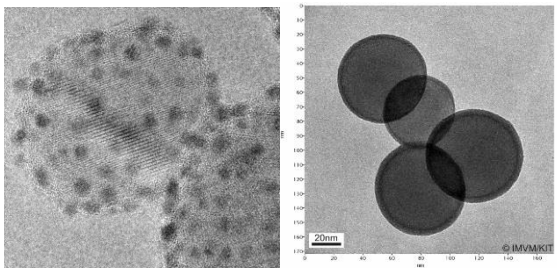

Figure 1: Structures generated by CVS/CVD. Left: Pt on Al_2O_3, right: MoOx coating on SiO_2.

In both cases the precision of the structuring methodology allows a high degree of control. For precious metal islands the particle size, the width of the size distribution and the number density of islands on the support surface can be controlled independently of each other, which is a unique feature of CVS/CVD. Additionally, the nature of the support can be varied in chemical composition, size but also surface roughness which enables the generation of a wide array of structures. For the core shell structures coating thickness can be controlled from Angstroms up to tens of nm.

For the characterization of the generated structures new analysis tools had to be developed in addition to the existing ones. One of these is a highly sensitive method for the on-line determination of the coating thickness from the CVD-process (Seipenbusch, Heel, Weber, & Kasper, 2002; Weis, Seipenbusch, & Kasper, 2015) enabling real time process control.

Finally, methods for the evaluation of the functional properties of the generated structures are necessary to correlate function and structure.

The presentation will present the methods and show their potential in combination for the development of a catalyst for automotive exhaust treatment.

Acknowledgements

This work was supported by Jointlab IP[3], a collaboration between BASF and KIT.

References

Binder, A., Heel, A., & Kasper, G. (2007). *Chemical Vapor Deposition*, *13*(1), 48–54. doi:10.1002/cvde.200606543

Faust, M., Enders, M., Bruns, M., Bräse, S., Gao, K., & Seipenbusch, M. (2013). *Surface and Coatings Technology*, *230*, 284–289. doi:10.1016/j.surfcoat.2013.06.088

Faust, M., Enders, M., Gao, K., Reichenbach, L., Muller, T., Gerlinger, W., … Seipenbusch, M. (2013). *Chemical Vapor Deposition*, *19*(7-8-9), 274–283. doi:10.1002/cvde.201207038

Seipenbusch, B. M., Heel, A., Weber, A. P., & Kasper, G. (2002). *Chem. Eng. Technol.*, *25*, 77–82.

Weis, F., Seipenbusch, M., & Kasper, G. (2015). *Journal of Nanoparticle Research, Accepted for Publication*.

Particle depletion in an enclosure with turbulent natural convection

J. Kalilainen[1], A. Dehbi[1], T. Lind [1]and A. Auvinen [2]

[1] Paul Scherrer Institut, CH-5232 Villigen PSI, Switzerland
[2] VTT Technical Research Centre of Finland, P.O.box 1000, BI7, FI02044 VTT Espoo, Finland
Keywords: deposition, enclosure, turbulence, natural convection.

In this study, depletion rates of supermicron particles from the atmosphere of an air filled cubic differentially heated cavity (DHC) with two vertical isothermal walls, was investigated. The temperature difference between the isothermal walls induces a turbulent natural convective flow to the cavity with Rayleigh number approximately Ra = 10^9. Flow and temperature field in experimental DHC facility DIANA were determined using thermocouple and Particle Image Velocimetry (PIV) measurements. The experimental results were used to validate a Large Eddy Simulation (LES) with experimentally measured thermal boundary conditions (BC) at the horizontal cavity walls.

Next, the deposition of airborne particles in the DHC was investigated both experimentally and numerically using spherical monodisperse SiO_2 particles with diameters d_p = 1 µm and 2.5 µm and density ρ_p = 2 g/cc. In the experimental work, the change in particle mass- and number concentration in different points inside the cavity was monitored using Tapered Element Oscillating Microbalance (TEOM) and laser intensity measurements, respectively. The measurement results were compared against Lagrangian Particle Tracking (LPT) simulations data, obtained using the validated LES. The particle tracking calculations were performed using a Continuous Random Walk model (CRW) (Dehbi, 2008), which was validated against pure LES LPT results.

Table 1. The time constants, obtained from the measurement data and simulation results.

d_p	1 µm	2.5 µm
Avg. τ, TEOM [s]	5219 ± 188	1697 ± 86
Avg. τ, laser int. [s]	4965 ± 64	1796 ± 79
WT-CRW τ [s]	4885	1505
IDEAL-CRW τ [s]	6361	1860
Theor. Stirred τ [s]	10210	1784

At the beginning of the measurement and particle tracking simulation, the particles were uniformly distributed in the cavity atmosphere. The particle depletion rates were obtained from the experimental results by fitting an exponential curve to the mass and number concentration *C* as a function of time *t*:

$$C = C_0 e^{-t/\tau},$$

where C_0 is the initial mass concentration or laser intensity and τ is the time constant of the deposition. The experiments indicated almost uniform depletion rates in most of the measurement points. The average time constants form the measurements are shown in Table 1. The time constant form the WT-CRW LPT simulations (Table 1) with experimental BCs was in good agreement with the measurements. However, results with 1 µ particles differed form theoretical stirred settling (Table 1, Fig.1), where particles are kept uniformly distributed in a cubic volume and deposit only through gravitational settling onto the enclosure floor (Hinds, 1999). With 2.5 µ particle the results coincided with the stirred settling theory. Second LPT simulation using adiabatic BC in horizontal cavity walls (IDEAL-CRW) was conducted and validated against the Direct Numerical Simulation (DNS) data by Puragliesi (2010). IDEAL-CRW with smaller level of turbulence resulted in slower particle depletion (Fig. 1), indicating that in the DHC setup the increased turbulence level is partly responsible for the faster particle depletion. The stirred settling model, on the other hand, turns out to be too simplistic to properly describe the dynamics of small particles in DHC.

Simulations conducted with smaller particles having a diameter d_p = 0.5 µm are ongoing, and results will be shown at the meeting.

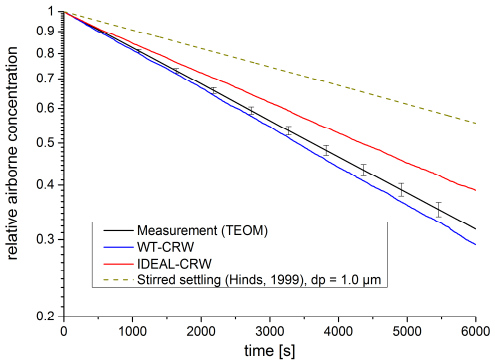

Figure 1. Depletion of d_p = 1 µm particles from the cavity atmosphere.

Dehbi, A. (2008). *Int. J. Multiphase Flow*, 34, 819-828.

Hinds, W. C. (1999). Aerosol Technology. 2nd edition, John Wiley & Sons, Inc..

Puragliesi, R. (2010). *Numerical Investigation of Particle-Laden Thermally Driven Turbulent Flows in Enclosure*. Ph.D. thesis, No: 4600, EPFL, Lausanne.

Particle Number Portable Emission Measurement System

T. Reinisch[1], A.Bergmann[1], G. Brunnhofer[1], A. Mamakos[1], M. Fierz[2]

[1]AVL List GmbH, 8020, Graz, Austria
[2] Naneos, 5210, Windisch, Switzerland

Keywords: particle number, portable, diffusion charger, automotive

Controlling the emission from light-duty diesel and gasoline engine passenger cars is expected to face significant challenges as a result of the reduction of pollutant thresholds at Euro 6, followed by the introduction of Real Driving Emission (RDE) legislation and the World-harmonized Light-duty vehicle Test Procedure (WLTP, GTR Number 15) [1].

The term real driving emissions (RDE) has been deployed to refer to efforts to reduce the discrepancies between laboratory testing and real world scenarios. A considerable body of evidence attests to the fact that laboratory test procedures, particularly type approval, represent a "best" case scenario and that a range of emissions are considerably higher in real life than according to the results of laboratory tests.

Various options for implementation of RDE have been considered by the European union: the use of on the road vehicle testing with so called Portable Emission Measurement Systems (PEMS) in combination with post processing of the results to evaluate NO_x, NO_2, CO and CO_2 emissions has already been introduced, for Particle Number (PN) emissions it is very likely that PEMS will be required.

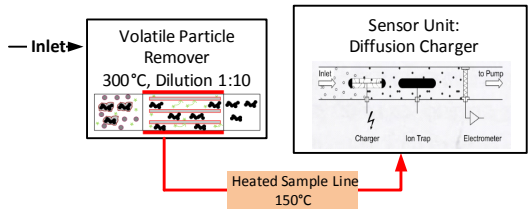

Figure 1: Setup of device

We present in this work a PEMS system for PN, which was provided to the Joint Research Centre (JRC) for the first evaluation exercise [2]. The results show that particle number counting with a diffusion charger (DC) as sensing principle and appropriate exhaust gas preconditioning results in very good correlation to a PMP conform system usually equipped with condensation particle counter (CPC) as core sensor. These tests have been performed on a chassis dyno. Additionally, the robustness of DC compared to CPCs (e.g. shock resistance, no tricky handling of a working fluid) constitutes them as more suitable core sensors for portable emission measurement systems.

The used PN PEMS setup contains components similar to the PMP conform systems and is shown in figure 1. The exhaust is heated up to 300 to 400°C in the dilution cell which is located close to the tail pipe. Alternatively, the temperature can be reduced to about 200 to 300°C by using a catalytic stripper [3]. This is comparable to the volatile particle remover (VPR). Right after that hot section the aerosol is cold diluted to minimize thermophoretic losses. The dilution ratio of 1:10 is enough for a DC because of the measurement principle [4]. Via a heated sample line the exhaust is sucked to the sensor unit which includes the all necessary components to regulate the aerosol flow through the system (e.g. pump, valves, sensor and electronic elements).

DCs and their measurement principle have been described a lot in the past. Details can be looked up in [5]. In short the measured value is the amount of charges on particles that pass a Faraday cage in a certain time. A change of the particle concentration causes a change in the electric field of the Faraday cage that is induced by charges on the particle deposited on the surface. This can be detected with a sensitive electrometer [4].

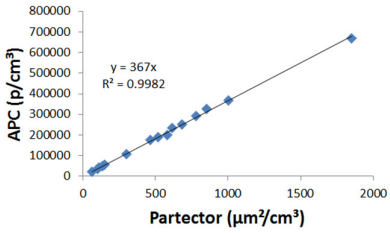

Figure 2: Correlation between the PN-PEMS and a PMP conform system (AVL Particle Counter) during a test run on a chassis dyno at the Joint Research Centre (JRC)

During the tests at the JRC a very good correlation to the PMP system has been ascertained. High transient emissions could be resolved as well as high and low particle number concentration [Fig.2].

[1] M. André, R. Joumard, R. Vidon, P. Tassel, P. Perret, (2006) *Atmospheric Environment*, Vol.40, 31, 5944-5953, doi:10.1016/j.atmosenv.2005.12.057

[2] F. Riccobono. M. Weiss, B. Giechaskiel, P. Bonnel, *PEMS 2014 International Conference & Workshop,* 3-4 April 2014

[3] J. Swanson, D. Kittelson, B. Giechaskiel, A. Bergmann, et al., *SAE 2013 World Congress & Exhibition,* doi:10.4271/2013-01-1570

[4] M.Fierz, D.Meier, P. Steigmeier and H.Burtscher (2014) *Aerosol Science and Technology*, 48, 350-357.

[5] H. Burtscher, (2005), *J. Aerosol Sci.,* Vol.36, 7, 896-932, doi:10.1016/j.jaerosci.2004.12.001

Patterns of airborne pollen and fungal spore concentrations and their mass fraction in Hyytiälä, Finland

H. E. Manninen[1,2*], S.-L. Sihto-Nissilä[1], J. A. Huffman[3,4], J. Bäck[5], A.-M. Pessi[6], V. Hiltunen[1], P. P. Aalto[1], P. J. Hidalgo[7], P. Hari[5], A. Saarto[6], M. Kulmala[1], and T. Petäjä[1]

[1]Department of Physics, University of Helsinki, Finland
[2]Department of Forest Ecology, University of Helsinki, Finland
[3]Department of Chemistry and Biochemistry, University of Denver, Colorado, USA
[4]Max Planck Institute for Chemistry, Mainz, Germany
[5]Department of Biology, University of Turku, Finland

Keywords: Primary Biological Aerosol Particles, Boreal forest, PM.

Pollen grains and fungal spores are two main classes of primary biological aerosol particles (PBAP) in the atmosphere. They have been observed to be efficient ice nuclei, thus having possible effects on weather and climate. We studied annual variation of airborne pollen and fungal spore concentrations in a boreal forest in Finland during 2003-2004. The pollen grains were categorized into 15 genera and fungal spores into 26 genera, in total representing a majority of higher plant pollen and fungi genera observed in the boreal environment.

PBAP were collected throughout the pollen season from March to September (October) using a Hirst-type volumetric spore trap (Burkard Manufacturing Co. Ltd. The Burkard samples were examined by light microscopy. The pollen and spore count was normalised for the counted surface area and the number was reported as pollen grains per volume of air (m-3). The measurements were performed at SMEAR II (Station for Measuring Forest Ecosystem-Atmosphere Relations II) station located in Hyytiälä, Southern Finland (61°51'N, 24°17'E, 181 asl). Coniferous and mixed coniferous-deciduous forests account for over 65% of the region surrounding Hyytiälä within a 50-km scale radius.

The highest concentrations of pollen were observed in late spring and early summer, while first pollen observations in February-March were long-range transported from central Europe or Baltic countries. Airborne fungal spores were present during the whole growing season (number concentration in the range 10^4-10^5 m-3), with the highest peak occurring in August-September. The observed annual pattern of fungal spores was similar to that of fluorescent aerosol particles measured in 2010 at the same location (Schumacher et al., 2013). Although the annual pattern was similar in both years studied, the concentration levels were significantly different between 2003 and 2004.

Fungal spores constituted the largest fraction of observed PBAP numbers (~99%), whereas pollen showed a higher relative mass fraction (~97%) of PBAP. We estimated the contribution of pollen and spores to be about 65% of the observed total particle mass during the growing season (average pollen and spore mass 5.9 and 0.4 μg m-3, respectively, in respect to total PM mass 9.9 μg m-3), but the effect on total particle number was negligible.

Further, the relationships between pollen and spore concentrations and basic meteorological parameters were characterized. Most of the spore plume observations were observed on rainless days with only moderate temperature and wind speeds, but during intense rain episodes increased number concentration of spores was detected. The relationship between pollen grains and meteorological variables showed no clear dependence when looking at daily means.

This study focuses on species-specific information on pollen and spore concentrations, providing long-term field measurement data of biological aerosol concentrations on seasonal scales (Manninen et al., 2014), which may be used to constrain the bioaerosol concentrations in the global aerosol models. On an annual scale and show the high relative importance of PBAP to coarse atmospheric particles (appox. 65% by mass). Atmospheric quantities of PBAP have been poorly constrained, and the high fraction of biological particles discussed here suggests that biological material may be important for complex atmospheric processes such as the formation and evolution of ice clouds and precipitation.

Acknowledgements: H. E. M. acknowledges support by the Finnish Cultural Foundation. This research is supported by the EU FP7 project PEGASOS (project no. 265148), the EU FP7 ERC-Advanced 'ATMNUCLE' grant no. 227463, the BAECC project funded by U.S. Department of Energy, and the Academy of Finland Centre of Excellence program (project no. 1118615).

Manninen, H. E. (2014). Patterns in airborne pollen and other primary biological aerosol particles (PBAP), and their contribution to aerosol mass and number in a boreal forest. *Boreal Env. Res.* 19 (suppl. B): 383–405.

Schumacher, C. J. et al. (2013). Atmos. Chem. Phys., 13, 11987-1200.

Performance test of HR-ELPI+ inversion calculation in laboratory and in various applications

S. Saari[1], A. Arffman[1], H. Wihersaari[1], A. Rönkkö[1] and J. Keskinen[1]

[1]Department of Physics, Tampere University of Technology, Korkeakoulunkatu 3, 33720, Tampere, Finland

Keywords: performance test, HR-ELPI+, inversion, intercomparison.

The electrical low pressure impactor (ELPI) has been used over twenty years in various applications including engine exhaust, combustion emission, atmospheric aerosol and air quality studies (Keskinen et al., 1992). The ELPI can measure airborne particle size distribution and concentration in real-time. The resolution of the particle size distribution has been limited to the number of impactor stages when traditional impactor cut diameter concept is used. The particle size resolution can be enhanced using inversion calculation that is based on the kernel functions of the instrument. In this study, the performance of a new commercial inversion calculation based ELPI, High Resolution ELPI+ (HR-ELPI+, Dekati Ltd.) was tested in laboratory and in various applications.

Operating principle of the HR-ELPI+ is the same as ELPI+ operation added with data inversion software. The particles are first charged into a known charge level in a corona charger after which they are size classified in a 14-stage impactor with electrically insulated impactor stages. Each impactor stage is connected to an electrometer that measures the current signal produced by the charged particles as they are collected on the impactor stage. The primary particle collection efficiencies and the amount of diffusion and image charge deposition have been determined for each impactor stage allowing determination of impactor Kernel functions (Järvinen et al., 2014).

The data inversion calculation method used in the HR-ELPI+ is based on the Kernel functions and iterative calculation routine resulting in determination of particle size distribution with enhanced resolution. The inversion calculation runs in real-time and is simple to use and do not require any adjustments nor optimizations from the user of the instrument, contrary to the previous ELPI inversion calculation routines (Lemmetty et al., 2006).

Experimental set-up consisted of parallel test aerosol measurements with the HR-ELPI+ and other reference instruments. The reference instruments were Engine Exhaust Particle Sizer 3090 (EEPS™, TSI Inc.), two Scanning Mobility Particle Sizer Spectrometer: nanoSMPS (TSI Inc.) and longSMPS (TSI Inc.) and high-resolution low-pressure cascade impactor (HRLPI, Arffman et al., 2014). The aim of this study is to provide information on accuracy of particle size distribution and concentration output of the instruments in various conditions.

In the laboratory, different test aerosols with single mode, two modes and three modes were generated and measured by the instruments. Performance of the HR-ELPI+, EEPS and HRLPI was tested in a transient measurement, where the emissions of a modern passenger car diesel engine were measured over the US06 cycle.

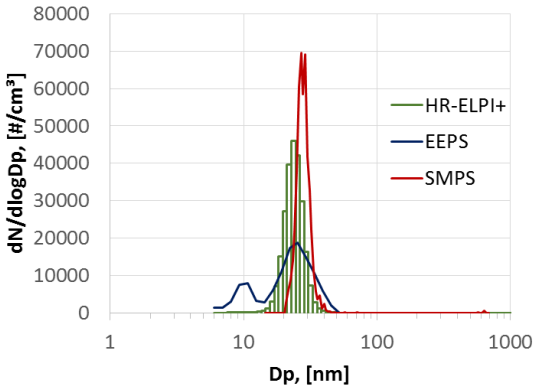

Fig. 1: Size distribution outputs of HR-ELPI+, EEPS, SMPS in laboratory test.

The results showed reasonable particle size distribution output of HR-ELPI+ inversion both in the laboratory and in the field test. An example of particle size distributions is shown in Fig. 1. The results provide information on the real particle size resolution and behaviour of HR-ELPI+ inversion calculation in various conditions and help user to analyse the data.

This work was supported by the Doctoral School of Tampere University of Technology.

Arffman, A., Yli-Ojanperä, J., Kalliokoski, J., Harra, J., Pirjola, L., Karjalainen, P., ... & Keskinen, J. (2014). J. Aerosol Sci., 78, 97-109.

Järvinen, A., Aitomaa, M., Rostedt, A., Keskinen, J. & Yli-Ojanperä, J. (2014). *J. Aerosol Sci.* 69, pp. 150-159.

Keskinen, J., Pietarinen, K., and ja Lehtimäaki, M. (1992). *J. Aerosol Sci.* 23:353–360.

Lemmetty, M., Marjamäki, M and Keskinen, J. (2006). *Aerosol Sci. Tech*., 39(7), 583-595.

Portable emission measurement system (PEMS) for tailpipe and exhaust plume aerosols

A. Järvinen[1], A. Rostedt[1], H. Wihersaari[1], M. Olin[1], J. Yli-Ojanperä[1,2], T. Rönkkö[1] and J. Keskinen[1]

[1]Aerosol Physics Laboratory, Department of Physics, Tampere University of Technology, 33720, Tampere, Finland
[2]Electrical Engineering and Energy Technology, Faculty of Technology, University of Vaasa, 65200, Vaasa, Finland

Keywords: PEMS, emission, vehicle.

Vehicle emission measurements have been traditionally conducted in laboratory conditions. Emission laboratories require large investments and measurement procedures are not always representing real world driving situations (Weiss *et al*. 2012). In recent years, portable emission measurement systems (PEMS) have been developed in order to enable the measurements of gaseous and particulate emissions of vehicles in real-world driving conditions (e.g. Johnson *et al*. 2009). The particle measurement capabilities have been rather limited or fixed to certain technologies.

We have developed a highly versatile PEMS which allows different exhaust sampling and dilution options. The PEMS works as a platform for a wide variety of aerosol and gas sensing instruments typically used in laboratory conditions. The main module of the PEMS provides filtered air needed in exhaust sampling and dilution. Modified CO_2 sensors (GMM111 and GMM112, Vaisala Oyj) for raw exhaust, diluted exhaust sample and dilution air are used to determine the dilution ratio (DR, see e.g. Giechaskiel *et al.* (2004)). The main unit also contains two outputs for heating the dilution air and the diluted sample (evaporation chamber). An inverter (PP 2004, Dometic WAECO International GmbH) is installed in the main unit to provide 230 VAC for the measurement instruments. The energy needed is stored in a 2.4 kWh lithium iron phosphate battery. The exhaust measurement system is designed to be easily installed into vehicles equipped with a towing hook and requires no modifications to the car itself. The diluters are installed into a rail attached to the towing hook. The basic dilution setup consists of two sequential diluters: the first is either a porous type or an ejector type (both with heating option) and the second one is an ejector type diluter. The diluted sample is led inside the vehicle by flexible tubing and connected to the instruments. In addition to the direct tailpipe sampling, the PEMS system allows also the measurements from the exhaust plume.

The PEMS has been tested by measuring particle emissions from a 2001 Opel Astra passenger car with 1.7 dm^3 turbocharged diesel engine. The vehicle was equipped only with a diesel oxidation catalyst. The PEMS was installed into the cargo compartment. The particle size distribution was measured by an Engine Exhaust Particle Sizer (EEPS, TSI Inc.) and number concentration by a Condensation Particle Counter (CPC 3776, TSI Inc.), both after two stage ejector type dilution.

The CO_2 measurements were used to calculate DR for which a value of 130 was obtained. This value was used to correct measurements to tailpipe conditions. The measured size distribution consisted of two modes, one at 10 nm size (nucleation mode) and the other at 60 nm particle size (soot mode), see Figure 1. When heating was applied to the first dilution stage, the 10 nm concentration of nucleation mode particles decreased significantly. This effect demonstrates that the ability to control dilution conditions is an important factor in a research grade PEMS.

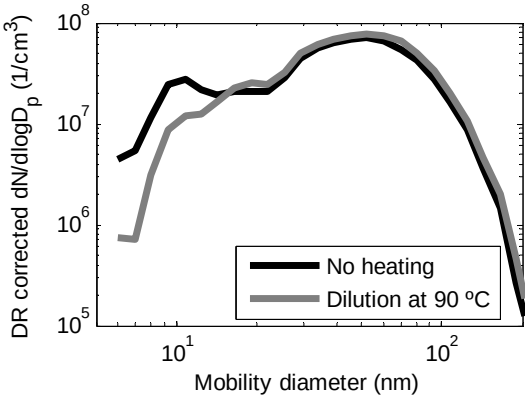

Figure 1. Particle size distributions using first dilution stage without heating and with heating to 90 °C.

This work was funded by Tekes, the Finnish Funding Agency for Innovation, through CLEEN Ltd. as a part of MMEA program.

Giechaskiel, B., Ntziachristos, L., Samaras, Z. (2004). *Meas. Sci. Technol.*, 15, 2199-2206.

Johnson, K.C., Durbin, T.D., Cocker, III, D.R., Miller, W.J., Bishnu, D.K., Maldonado, H., Moynahan, N., Ensfield, C., Laroo, C.A. (2009). *Atmos. Environ*., 43, 2877–2883.

Weiss, M., Bonnel, P., Kühlwein, J., Provenza, A., Lambrecht, U., Alessandrini, S., Carriero, M., Colombo, R., Forni, F., Lanappe, G., Le Lijour, P., Manfredi, U., Montigny, F., Sculati, M. (2012). *Atmos. Environ*., 62, 657-665.

Portable ice nuclei counter SPIN: Key specifications, principle of operation and the first experiments

K.Korhonen[1], A.Virtanen[1] and M.Komppula[2]

[1]University of Eastern Finland, Department of Applied Physics. P.O. box 1627, FI-70211 Kuopio, Finland
[2]Finnish Meteorological Institute, Atmospheric Research Centre of Eastern Finland, P.O. box 1627, FI-70211 Kuopio, Finland

Keywords: Ice nucleation, Ice nuclei counter, Diffusion chamber, SPIN.

INTRODUCTION

This abstract presents the key specifications of a recently developed portable ice nuclei (IN) counter instrument SPIN (**SP**ectrometer **I**ce **N**uclei), its principle of operation, first experiments and plans of ice nucleation experiments in the near future. The instrument, manufactured by Droplet Measurement Technologies (DMT), is the first commercially available IN counter and it uses continuous flow diffusion chamber (CFDC) technique. Currently five SPIN units have been manufactured so far, and our unit (number 5) will be used in experiments on both laboratory-produced and ambient aerosols.

THE INSTRUMENT

The SPIN is a portable IN counter where the icing conditions are created using the CFDC technique (Stetzer et al., 2008), where the aerosol flow is exposed to water vapour in temperatures below the freezing point. All parts of the instrument are fitted in one rack. Both walls of the IN chamber have independent refrigeration systems and thus the walls can be set to different temperatures. The temperature difference creates a diffusional vapour flux across the ice-coated chamber and saturation conditions can be regulated via adjusting the difference. Sample temperature can then be regulated via either cooling or heating the both walls simultaneously, while keeping this difference constant.

When the particles exit the IN chamber they are observed via using an optical 4-channel detector, where they are illuminated by linearly polarized laser beam of 500 mW in power and 670 nm in wavelength. The channels include size detection via scattered signal strength, two channels for parallel polarization (P1 for backscattering and P2 for forward scattering) and one for perpendicular (S1, backscattering). The polarization data is needed for separating the ice crystals from liquid water droplets, because the scattered light has a different polarization pattern depending on shape of the particle, i.e. spherical liquid droplets versus non-spherical ice crystals.

EXPERIMENT AND DEVELOPMENT PROGRAMME

The development of portable IN counters is relatively new and the published knowledge about the performance of these instruments is still limited (Chou et al., 2011). Therefore our experiment programme consists of starting the measurements using particles that have well-documented IN capabilities, such as different mineral clay particles (Arizona Test Dust, Kaolinite, Illite and so on). Once validation experiments have been carried out the aim is to extend the research on various aerosol types, such as secondary organic aerosols (SOA) and real-life ambient aerosols in field campaigns.

In addition to currently ongoing testing and experimental studying we participate to development of the SPIN instruments and data analysis procedures, in co-operation with DMT and other SPIN research groups. This co-operation includes e.g. intercomparison experiments between earlier SPIN units and other IN counter instruments. The refrigeration systems of all SPIN instruments are currently undergoing a major upgrade where the temperature control is enhanced and refrigeration system improved.

ACKNOWLEDGEMENTS

This work has been supported by Academy of Finland , Finnish Center of Excellence (decision no 272041) and North-Savo Council - European Regional Development Fund's (project no A32350).

REFERENCES

Chou C., Stetzer O., Weingartner E., Juranyi Z., Kanji Z.A. and Lohmann U.: Ice nuclei properties within a Saharan dust event at the Jungfraujoch in the Swiss Alps. *Atmos. Chem. Phys.* 11, 4725-4738, 2011.

Stetzer O., Baschek B., Lüönd F. and Lohmann U.: The Zurich Ice Nucleation Chamber (ZINC) – A new instrument to investigate atmospheric ice nucleation. *Aerosol Science and Technology* 42, 64-74, doi: 10.1080/02786820701787944, 2008.

Possible release of metallic nanoparticles along their life cycle

B. Stahlmecke[1], H. Kaminski[1], U. Sager[1], C. Asbach[1], M. Stein[2], E. Hontañon[2], E. Kruis[2], M. Stadlbauer[3] and T.A.J. Kuhlbusch[1]

[1]Institut für Energie- und Umwelttechnik, Bliersheimer Straße 58-60, 47229, Duisburg, Germany
[2]Nanostrukturtechnik, University of Duisburg-Essen, Bismarckstraße 81, 47057, Duisburg, Germany
[3]RE-Technologie Erz und Eisen, ThyssenKrupp Steel Europe AG, Kaiser-Wilhelmstr. 100, 47166, Duisburg, Germany

Keywords: Workplace Aerosol, Particle Release, Copper Nanoparticles, Life Cycle Analysis.

The possible exposure to nanoparticles has been under intense investigation for more than ten years. Starting with workplace exposure measurements in the carbon black industry in 1998 the topic has evolved and workplace measurements have been conducted in many different settings (Kuhlbusch et al., 2011). General concepts on how to best assess a possible exposure to airborne nanomaterials in workplace settings have been conceived and are currently on the edge of standardisation (Asbach et al, 2015). Beyond workplace exposure measurements the complete life cycle of nanomaterials is nowadays under investigation and measurements on release as a prerequisite of exposure become more and more important.

Within the EU funded BUONAPART-E project novel techniques for the mass production of metallic nanoparticles by spark and arc discharges are being developed and scenarios for their use are tested. Alongside, a possible release of and exposure to the produced particles during their life cycle are studied exemplarily. In this work we present results of several measurements obtained on the case study of copper nanoparticles during production and use.

The copper nanoparticles are produced in a closed vessel by an arc-based process. They are deposited on inert filter media which are periodically cleaned by a blast of nitrogen. Particles are then collected at the bottom of the filter unit and are manually bagged. Workplace measurements were conducted during production, bagging and the cleaning operations of the production unit in order to assess a possible release of the nanoparticles. Background concentrations of particles are accounted for by a second set of measurement instruments to distinguish between process based emissions and the laboratory particles background.

Figure 1 shows as an example the time series of the particle concentration measured during operation of a single production unit for copper nanoparticles. A pronounced peak occurs when the welding generators are switched on. During the production phase no enhanced particle concentration has been identified which is not surprising, since the whole process takes place in a closed vessel. During maintenance work the particle concentration is slightly enhanced, indicating a minor release of particles.

The copper particles are intended to be used as an additive in a cooling agent. For this purpose they have to be suspended in a liquid. Thus, a possible release during the mixing phase of the particles into the liquid is also investigated.

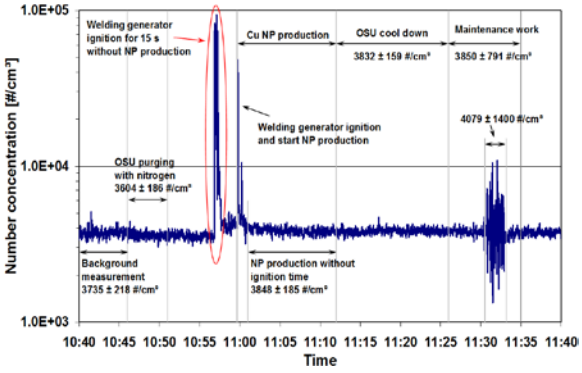

Figure 1. Time series of airborne particle concentration near a copper nanoparticle production unit during production and maintenance work.

Furthermore, due to a possible pyrophoricity of the as-produced particles, investigations on possible self-ignition and flammability were conducted to obtain a complete picture of possible threads stemming from these metallic nanoparticles.

The presentation will focus on the safety and life cycle analysis procedure used in BUONAPART-E. While focussing on safety, release and exposure measurements some general information on toxicity and possibly environmental implications will be included.

The research leading to these results has received funding from the European Research Council under the European Union's Seventh Framework Programme (FP/2007-2013) / ERC Grant Agreement n.280765.

Kuhlbusch, T.A.J., et al.. (2011). *Particle and Fibre Toxicology*, 8, 22, 1-18.

Asbach, C, et al. (2015) *Measurement and Monitoring Strategy for Assessing Workplace Exposure to Airborne Nanomaterials* in *Safety of Nanomaterials along their Lifecycle – Release, Exposure and Human Hazards*, Florida, US, CRC Press.

Quasi-online non-invasive structural study of spark generated aerosol nanoparticles using X-ray scattering technique

Xiaoai Guo[1], Moritz Wagner[1], Alexander Gutsche[1], Jörg Meyer[1], Martin Seipenbusch[2], Hermann Nirschl[1]

[1]Institute for Mechanical Process Engineering and Mechanics, Karlsruhe Institute of Technology, Strasse am Forum 8, 76131 Karlsruhe, Germany. Email: xiaoai.guo@kit.edu
[2]Institute for Chemical Process Engineering, University of Stuttgart, 70199 Stuttgart, Germany.

Keywords: nanoparticles, morphology, spark discharge, small- and wide-angle X-ray scattering

Spark discharge has recently been used as a chemistry-free synthesis method to generate aerosol nanoparticles (NPs) using a wide range of electrode materials (Meuller *et al.*, 2012; Pfeiffer *et al.*, 2014). The utilization of multiple parallel electrical discharge generators allows for the scale-up of nanoparticle and nanostructure production (Stein *et al.*, 2013; Hontanon *et al.*, 2013). Quick acquisition of the structural information on the synthesized NPs, e.g. crystalline properties and particle morphology, helps to optimize the synthesis process and thus improve the product quality.

In this work, a new quasi-online monitoring setup is reported for non-invasive structural study of spark generated aerosol NPs. As shown in Fig.1, a spark was generated between two electrodes fixed inside a low frequency (below 100 Hz) generator at atmospheric pressure. The vaporized electrode material was mixed with inert carrier gas (N_2) and metal aerosol NPs were formed downstream of the plasma region. Monometallic and bimetallic aerosol NPs were produced from the electrodes of the same material or different materials, respectively. The generated NPs were analysed with a newly developed small- and wide-angle X-ray scattering (SAXS/WAXS) laboratory camera with a detection angle up to 90° (Guo *et al.*, 2015), which is equipped with a conventional X-ray source and a special X-ray Göbel mirror, greatly reducing the measuring time.

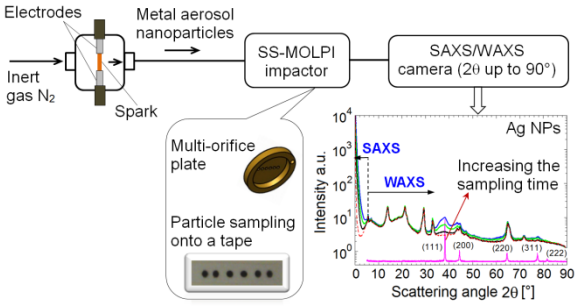

Figure 1. Experimental setup for synthesis and quasi-online monitoring of aerosol NPs.

To overcome the insufficient particle number concentration of aerosols leaving the spark discharge generator during the SAXS/WAXS measurement, a specially designed single-stage multi-orifice low-pressure impactor (SS-MOLPI) has been utilized for concentrating and sampling the aerosol particles onto an adhesive substrate for SAXS/WAXS analysis. The entire sampling and analysis process takes a few minutes and provides a wealth of structural information on the primary particle size, fractal dimension, surface properties, oxidation state, and crystalline properties. Fig.2 shows that the scattering signals of Ni NPs increase linearly with the sampling time and that the corresponding SAXS data at different sampling times deliver identical structural and morphological information, implying that the generator worked stably and produced NPs with the constant properties. Results of various generated metal aerosol NPs are studied and discussed in detail. Therefore, this technique is very interesting for structural study and quality control of NPs.

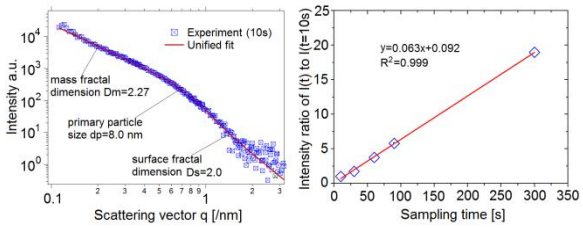

Figure 2. Results of spark generated Ni NPs at different sampling times between 10 s and 300 s.

The research leading to these results received funding from the European Union Seventh Framework Programme (FP7/2007-2013) under Grant Agreement No. 280765 (BUONAPART-E), as well as the support from the German Research Foundation (DFG Ni 414/13-1 and DFG Ni 414/22-1).

Guo, X., Gao, K., Gutsche, A., Seipenbusch, M., & Nirschl, H. (2015). *Powder Technol.*, 272, 23-33.

Hontanon, E., Palomares, J.M., Stein, M., Guo, X., Engeln, R., Nirschl, H., & Kruis, F.E. (2013). *J. Nanopart. Res.*, 15, 1957.

Meuller, B.O., Messing, M.E., Engberg, D.L.J., Jansson, A.M., Johansson, L.I.M., Norlen, S.M., Tureson, N., & Deppert, K. (2012). *Aerosol Sci. Technol.*, 46, 1256-1270.

Pfeiffer, T.V., Feng, J., & Schmidt-Ott, A. (2014). *Adv. Powder Technol.*, 25, 56–70.

Stein, M., Kiesler, D., & Kruis, F.E. (2013a). *J. Nanopart. Res.*, 15, 1400.

Relationship of Gas Precursors and Water-soluble Ionic Species in Airborne Particulate Matter in Southern Taiwan

Jiun-Horng Tsai[1], Li-Peng Chang

[1] Department of Environmental Engineering & Research Center for Climate Change and Environmental Quality, National Cheng-Kung University, Tainan 701, Taiwan, R.O.C.

Keywords: inorganic gas precursor, ionic species, ammonium, sulfate.

Fine particulate matter characteristics are important because of their visible light scattering ability affecting visibility, their adverse impact on human health, and their role in global climate change (Đorđević *et al.* 2012). The airborne particulate matter (PM) concentration in southern Taiwan does exceed the air quality standard during cold seasons. Secondary PM is critical in the high concentration events. This study investigated the relationship between inorganic gas precursors, including HCl, HONO, HNO_3, SO_2 and NH_3 gases, and water-soluble ionic species in PM in southern Taiwan.

Inorganic gases were sampled by annular denuder system and analyzed by ion chromatography. A Micro Orifice Uniform Deposition Impactor (MOUDI) and a Nano-MOUDI were conducted to determine the size-segregated mass distributions of ambient PM. Field sampling work were conducted in winter and summer, respectively.

The results showed that average PM concentrations in winter (130 μg/m^3) were much higher than those in summer. Ammonium, nitrate, sulfate and chloride were the dominant water-soluble ionic species in PM which contributed 35-45% of PM mass. Table 1 presents the particulate matter and water soluble ionic mass concentrations in summer and winter at the field sampling site in southern Taiwan.

Table 1. Particulate matter and water soluble ionic mass concentrations (μg/m^3)

Season	PM	Na^+	NH_4^+	K^+
Summer	38±19	2.0±0.6	3.9±3.5	0.5±0.2
Winter	132±42	2.9±1.0	11±5.8	1.3±0.7
Average	102±57	2.6±1.0	8.8±6.1	1.1±0.7

Season	Ca^{2+}	Cl^-	NO_3^-	SO_4^{2-}
Summer	1.2±0.5	2.0±0.9	5.8±3.6	8.4±8.0
Winter	2.9±1.6	4.0±3.1	20±11	18±7.2
Average	2.4±1.6	3.4±2.7	16±11	15±8.7

More than 85% of PM mass concentration was in the size range of 0.1-3.2 μm. High concentrations of ammonia and SO_2 were observed in the gas precursors. Average concentration of ammonia was 31.5 μg/m^3 in wintertime which was 1.3 times of that in summer time. Average concentration of SO_2 in winter time was 4.2 times higher than that in summer. Table 2 shows the precursor gas concentrations in particular matter. The molar ratio ($[NH_4^+]/[SO_4^{2-}]$) was higher than two. The values of molar ratio are 2.9 ± 1.1 in summer and 3.3 ± 1.2 in winter, respectively.

Table 2. Precursor gas concentrations (μg/m^3) in the atmosphere in southern Taiwan

Season	HCl	HNO_2	HNO_3	SO_2
Summer	2.8±3.0	2.4±1.5	1.4±1.3	4.9±5.5
Winter	2.0±1.9	5.0±2.5	2.8±2.9	21±11
Average	2.2±2.3	4.1±2.5	2.4±2.6	16±12

Season	NH_3	NO_2	NO
Summer	23±14	14±7.5	2.7±1.7
Winter	31±16	55±14	8.4±9.0
Average	29±16	42±23	6.6±8.0

These data indicated that the airborne PM in southern Taiwan was always rich in ammonium (Seinfeld & Pandis, 2006). The excess ammonium could neutralize nitrate to form ammonium nitrate, after the more stable ammonium sulfate and ammonium bisulfate formation in the southern Taiwan atmosphere. The finding indicates the importance to control the emission of ammonium for PM attainment strategy in southern Taiwan.

This work was supported by the National Science Council, Executive Yuan, Taiwan (NSC 96-2211-E-006-004).

Đorđević, D., Mihajlidi-Zelić, A., Relić, D., Ignjatović, Lj., Huremović, J., Stortini, A.M., Gambaro, A. (2012). *Atmos Environ*, 46, 309-317.

Seinfeld, J.H., & Pandis, S.N. (2006). *Atmospheric chemistry and physics: from air pollution to climate change.* New York: John Wiley & Sons, Inc.

Relative roles of agglomeration, dispersion and deposition in aerosol dynamics taking place in a Gaussian plume

T. Anttila[1,2], and M. Dal Maso[1]

[1] Tampere University of Technology, Department of Physics, PO Box 527, FI-33101 Tampere, Finland
[2] Finnish Meteorological Institute, Research and Development, P.O. Box 503, FI-00101 Helsinki, Finland

Keywords: Aerosol Dynamics, Agglomeration, Deposition, Air quality.

Industrial accidents may lead to a release of a large number of nano-sized particles into the air. Such accidents may also form a serious health hazard as the plume formed disperses into the surrounding air. In order to estimate associated health risks, various numerical models have been developed to simulate the transport and physico-chemical properties of particulate pollutants (e.g. Stockie, 2011).

Our aim was to develop a numerical model which simulates the time evolution of a monodisperse aerosol population (with an initial diameter d_0), released from point-like source, that undergoes dispersion, deposition, and agglomeration of primary particles released by the source. Our starting point is so-called Gaussian puff model where it is assumed that aerosols are released instantaneously into the air.

The governing equation for the change in the particle number concentration N_c due to dispersion is the so-called advective-diffusion equation (see equation 2.2 in Stockie, 2011). By making several assumptions regarding advection and diffusion processes, analytical solution for $N_c = N_c(x, y, z, t)$ can be derived and expressed in the in the following form:

$$N_c = N_0 c_x c_y c_z \qquad (1)$$

where N_0 is the initial number of particles released onto the air, and $c_x = c_x(x, \sigma_x, U)$, $c_y = c_y(y, \sigma_y)$, $c_z = c_z(z, \sigma_z, W_{dep})$ where U is the wind velocity. The variables σ_x, σ_y and σ_z are,so-called dispersion coefficients which are calculated with a parameterization chosen by the user. Moreover, deposition velocity is calculated in a separate module. Regarding agglomeration, we have applied the parameterization of Lehtinen et al. (1996) to calculate the change in the average particle volume due to the process (eq. 3 in the aforementioned paper).

We considered two different model formulations: Eulerian and Lagrangian. Former approach is straightforward: equation 1 is used to calculate N_c at given coordinates and at a given time moment. However, agglomeration cannot be accounted for by this approach at the moment. In the Lagrangian formulation, the change in the particle number concentration due to the dispersion is calculated by differentiating eq. 1 with respect to time and the total change in N_c is calculated using the operator splitting technique where dispersion and agglomeration are treated separately.

The model has been applied to investigate the relative roles of roles of agglomeration, dispersion and deposition. Example simulation is shown in Figure 1 which illustrates that dispersion leads to such a rapid decrease in N_c that agglomeration does not grow particles effectively. Also, conducted sensitivity studies showed that the deposition, of which velocity was set equal to 0.01 m/s, did not affect N_c significantly in this case.

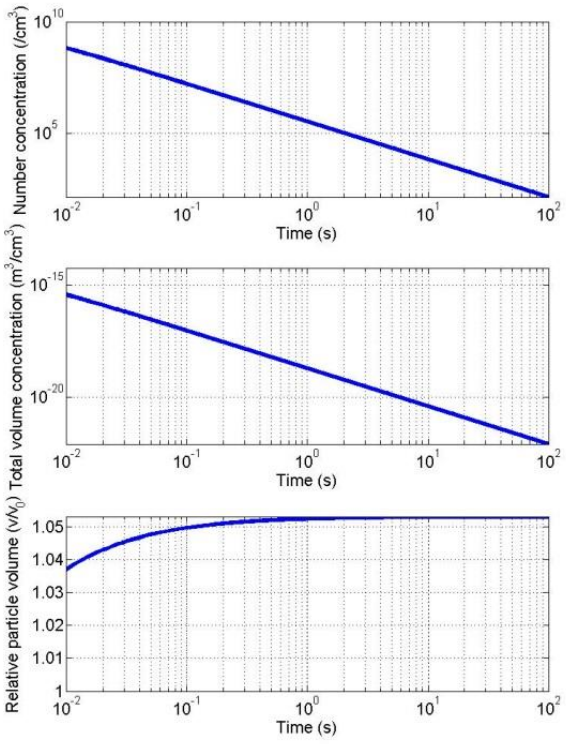

Figure 1. Time evolution of the particle number concentration (top), the total particle volume (middle), and the volume of a single particle relative to its initial value (bottom) in a simulation where $N_0 = 10^{10}$ cm^{-3}, $d_0 = 10$ nm, and $U = 5$ m/s.

References

Lehtinen, K. E. J., Windeler, R. S., & Friedlander, S. K. (1996), *J. Coll. Int. Sci*., 182 (2) , 606–608.
Stockie, J. M. (2011), *SIAM review*, 53(2), 349-372.

Robust films of graphene nanomaterials created by ultrasonic spraying

L.B. Modesto-López[1], M. Miettinen[2], T. Torvela[2], A. Lähde[2], and J. Jokiniemi[2,3]

[1]Department of Aerospace Engineering and Fluid Mechanics, University of Seville, 41092, Seville, Spain
[2]Department of Environmental Science, University of Eastern Finland, 70211, Kuopio, Finland
[3]VTT Fine Particles, P.O. Box 1000, 02044, VTT, Finland

Keywords: Graphene, Ultrasonic spraying, Film, Adhesion.

Graphene, a one-atom-thick layer of carbon atoms, has remarkable surface area, gas impermeability, thermal and electrical conductivities, and transparency (Novoselov et al., 2004). Generally, to maximize the benefit from its properties, graphene is layered onto substrates, e.g., energy storage devices and catalyst supports (Geim 2009). The mechanical robustness of graphene films is of paramount importance for many applications.

Spraying is effective for preparing layered materials on substrates allowing control of film thickness and composition. Particularly, ultrasonic spraying is advantageous in the break-up of agglomerates held in suspension and, simultaneously, in the deposition of relatively large-area films.

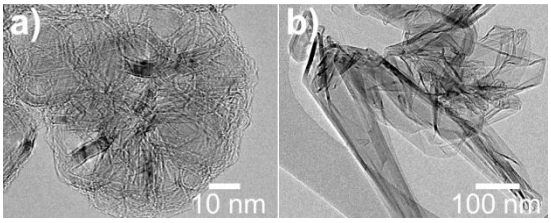

Figure 1. TEM images of a) a GNF and b) a MLG flake.

In this work, a graphene nanopowder (Miettinen et al., 2014) is dispersed in ethanol and N,N-dimethylformamide (DMF) by a series of ultrasonication-centrifugation steps to prepare sprayable suspensions. The nanopowder consists of graphene nanoflowers (GNFs, Fig. 1a) and multilayer graphene (MLG) flakes (Fig. 1b). GNF and MLG flake suspensions are ultrasonically sprayed onto glass and methacrylic acid copolymer (MA)-coated glass substrates. Poly(vinylidene fluoride) (PVDF) was added to the suspensions to enhance the structural robustness of films (Modesto-López et al., 2015). The suspension concentration, substrate temperature, nozzle ultrasonic frequency, spray distance, and spray time (t_s) are controlled to produce uniform films. Material spatial distribution on the substrate, film surface roughness and electrical conductivity are investigated. A scotch tape test is used to investigate the adhesion of the films to substrates.

Fig. 2 shows films from suspensions consisting of nearly 100 % GNFs sprayed on both substrates. The large-scale film morphology is similar in both cases. Strips of graphene nanomaterials are observed in some areas (inset of Fig. 2a). The inset of Fig. 2b shows deposited nanostructures with large-scale uniformity. Inspection of the images reveals thin lines of PVDF protruding from the GNF deposits, as in the white ovals of Fig. 2b. Both MLG and GNF films on MA-glass show a larger number of coated areas compared to their counterparts on glass, thus indicating that MA promotes nanomaterial deposition by improving the adhesion. The corresponding film height is observed in Figs. 2c and 2d. In both cases the films are compact, uniform, and have nearly the same height of ~ 700 nm. The large-scale uniformity of the films is also appreciated in the insets. In MLG, the thickness of the films increased on MA-glass compared to glass substrates. Conversely, in GNF films the thickness and uniformity appear to be independent of substrate type (Modesto-López et al., 2015).

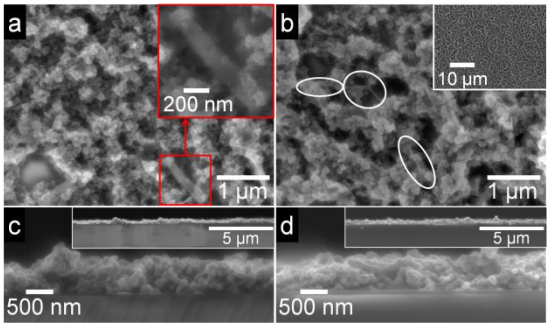

Figure 2. Top-view SEM images of GNF films sprayed (with 0.0005 wt% PVDF) for 14 min on a) glass and b) MA-glass. Their corresponding cross-sectional images on c) glass and d) MA-glass.

This work was supported by a TEKES grant, No. 1749/12. The UEF's strategic funding is also acknowledged.

Geim, A. K. (2009). *Science*, 324, 1530-1539.
Miettinen, M. et al. (2014). *J. Nanopart. Res.*, 16, 2168.
Modesto-López, L.B. et al. (2015). *Thin Solid Films*, in press.
Novoselov, K. S. et al. (2004). *Science*, 306, 666-669.

Role of lattice mismatch in heterogeneous nucleation of ice

O. H. Pakarinen[1] and H. Vehkamäki[1]

[1]Department of Physics, University of Helsinki, Finland

Keywords: Fundamentals of particle formation, ice nucleation, simulation, molecular dynamics

An accurate description of clouds in climate models requires solid knowledge about their properties, including their phase. Formation of ice clouds, in particular, is not well understood. Ice crystals may form either by homogeneous or heterogeneous ice nucleation. The latter process, where ice formation is initiated by an aerosol seed particle, is active at clearly higher temperatures than homogeneous nucleation. The effect is not thoroughly understood. Different nucleation modes (immersion-, contact- and deposition nucleation) are active in the atmosphere at different temperature and water supersaturation ranges. We are using parallel molecular dynamics (MD) simulations to study heterogeneous nucleation of ice, looking at kinetic and thermodynamic factors controlling nucleation at different conditions and in the presence of different surfaces with varying lattice match with ice, representing aerosol particles.

To capture the details of the rare stochastic events of ice nucleation, it is necessary to simulate relatively large systems over long time scales, and therefore classical interaction potentials are used. We utilize the TIP4P/2005 model for water (Abascal&Vega, 2005), as this rigid point charge all-atom model has been shown to reproduce the water phase diagram well and is widely used to study water-ice phase transitions, as well as a computationally cheaper monoatomic water model (Molinero&Moore, 2009). Unbiased MD is an ideal method to study physical pathways of ice formation from disordered water requiring collective molecular movement. We employ the DL_POLY 4 code (Todorov *et al.*, 2006) for parallel MD simulations, where a system including a surface immersed in water is cooled continuously below the melting point over tens of nanoseconds of simulation time and crystallization is followed. Also isothermal simulations are utilized, and we have investigated different nucleation modes including immersion-, contact- and deposition nucleation. We are simulating both ideal test systems with a suitable lattice match, surface corrugation, water-surface interactions, and realistic materials that are experimentally found to be active in heterogeneous nucleation.

Interaction with a flat surface induces layering in water, the first step towards ice nucleation. A surface with a good lattice match with hexagonal ice nucleates ice effectively at MD time scales (in the order of 100 nanoseconds) in immersion mode nucleation (see Fig. 1.), which is regarded as the most important nucleation mode for ice formation in clouds in the atmosphere. Deposition nucleation mode (i.e. formation of ice from the vapour phase, active at low temperatures in high-level clouds) leads to even more effective creation of hexagonal bilayers on moderately hydrophilic surfaces. This can be attributed to clearly larger diffusivity of water molecules in the building water layers, compared to bulk water in immersion nucleation.

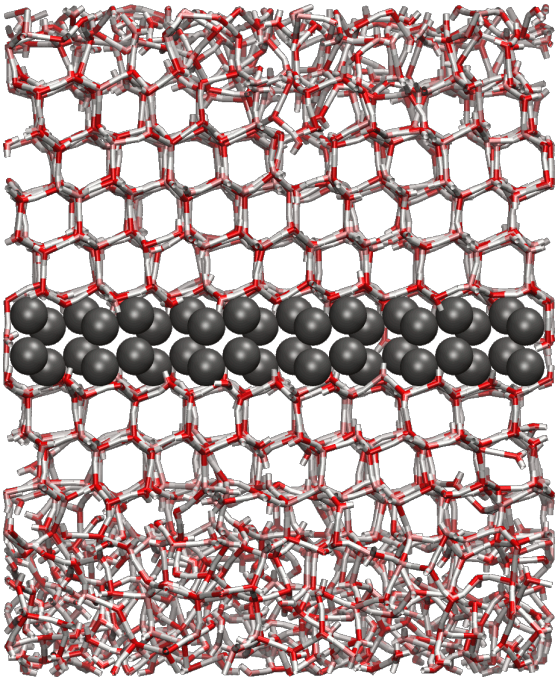

Figure 1. Surface with a good lattice match with hexagonal ice nucleates ice effectively in MD.

This work was supported by the Academy of Finland (CoE program grant no. 272041), by the Nordic Centre of Excellence CRAICC and by supercomputing resources at CSC - IT Center for Science.

Abascal, J. L. F. & Vega C. (2005) J. Chem. Phys. 123, 234505.

Molinero, V. & Moore E. B. (2009) J. Phys. Chem. B 113, 4008.

Todorov, I. T., Smith W., Trachenko K. & Dove M. T. (2006). J. Mater. Chem. 16, 1911-1918.

Role of Sulphur and Carbon Precursors on Catalyst Nanoparticle Growth and CNT Formation in a Continuous Gas Phase Process

C. Hoecker[1], F. Smail[2], M. Pick[2] and , A.M. Boies[1]

[1]Department of Engineering, University of Cambridge, Trumpington St, Cambridge CB2 1PX, United Kingdom
[2]Q Flo Ltd., Pennyfoot Street, Nottingham, NG1 1GF

Keywords: Carbon Nanotubes (CNTs), CVD, Ferrocene, Particle Formation.

Carbon nanotubes (CNTs) have been shown to possess significantly improved mechanical and electrical properties compared to existing materials. However, the quality of industrially produced bulk CNTs are limited in comparison. In this paper, we present an investigation into the role of sulphur and carbon containing precursors on the nucleation of catalyst nanoparticles for carbon nanotube synthesis in a continuous gas phase process. To date, few studies have examined the phenomena associated with the precursor breakdown, catalyst nucleation and growth within the reactor. These phenomena are critical to the quality and throughput of the CNT production, as the CNT diameter and chirality are strongly coupled to catalyst diameter.

CNT formation follows the thermal decomposition of sulphur and iron precursors, nucleation of iron catalyst nanoparticles, and decomposition of a carbon source in a horizontal tube furnace (see Figure 1). Conditions within the furnace are a temperature range of 300–1300°C and a (reducing) hydrogen atmosphere at atmospheric pressure. The nucleated iron nanoparticles act as a catalyst to form CNTs from decomposed carbon sources. The resulting CNTs agglomerate to form an annulus concentric within the reactor, which propagates down the reactor and is continuously wound out of the furnace as a fibre or film.

Studies along the axis of the reactor tube were carried out by means of a sample probe system and a scanning mobility particle size spectrometer. Samples of nanoparticles and CNTs were collected from different points along the tube axis and then analysed by means of SEM. The effect of different conditions (temperature, flow rate, background gas-atmosphere and tube diameter (ID 14 – 40 mm)) and carbon precursors on the decomposition, nucleation, agglomeration and formation processes of catalyst nanoparticles and CNTs were studied.

We will show that the decomposition of the iron precursor (e.g. ferrocene) and the sulphur precursor (e.g. thiophene) are independent of each other. Additionally we will show that there is a link between the different decomposition locations and temperatures in the reactor tube and the catalyst nanoparticle nucleation. In further studies the nature of the breakdown of the carbon precursor is studied by using different precursors.

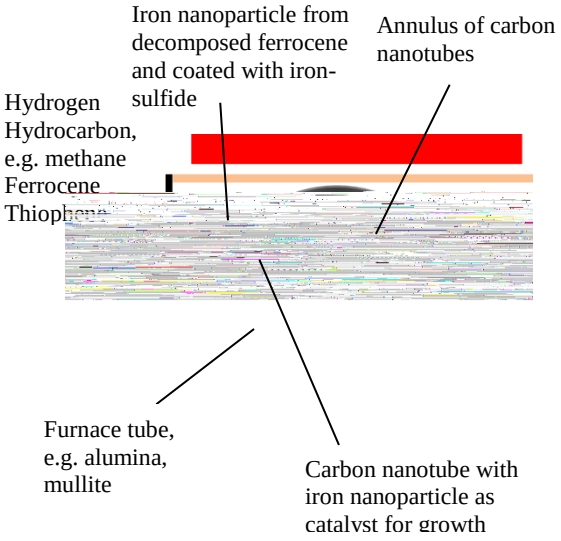

Figure 1: Ferrocene and thiophene are mixed with hydrogen and then injected into a tube furnace, in which an aerogel of CNTs forms that is then continuously wound out of the hot zone as a fiber or film.

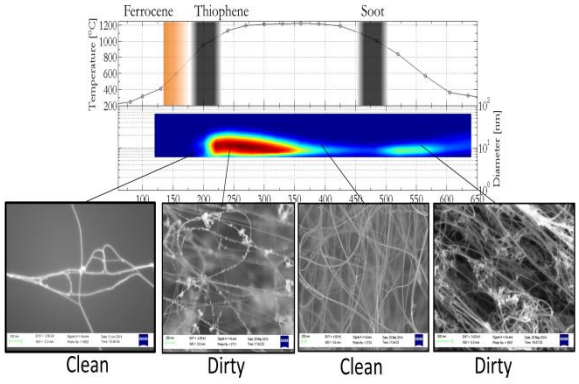

Figure 2: SEM images showing CNTs collected from different locations along the reactor tube corresponding to different reactions stages.

Li Y., Kinloch, I., Windle, A., (2004). Science 304, 276–278.

D. Conroy, A. Moisala et al. (2010). Chemical Engineering Science 65 (2010) 2965–2977

A. Moisala et al. (2005). Carbon 43, 2066-2074

Sampling of initial stages of gold particles formed during spark discharge

Linus Ludvigsson[1], Bengt O. Meuller[2] and Maria E. Messing[2]

[1]Solid State Physics, Lund University, SE-22100, Lund, Sweden

Keywords: Spark discharge, TEM, Proximity Sampling

The number of nanoparticle-based products on the market is expected to increase considerably during the coming decades. This forces the industry to have highly meticulous manufacturing of large amounts of nanoparticles using cheap and environmentally friendly methods. For production of metal and metal oxide nanoparticles spark discharge generation is a promising route to fulfill these demands, Tabrizi (2009). The scalability of the process makes it suitable for mass production due to its simple design solely by placing several units in parallel.

Before doing so, one first needs to optimize a single spark discharge generator unit. To optimize the spark discharge generator in a controlled way the first stage of nanoparticle formation needs to be understood. Matsoukas (1991) and others have done extensive investigations on generation of nanoparticles and large effort has been put into deriving models on how these particles actually are formed. However the fundamentals of metal nanoparticle formation during spark discharge is not as well investigated. To improve this understanding we have constructed a customized nanoparticle TEM sampler; see Figure 1.

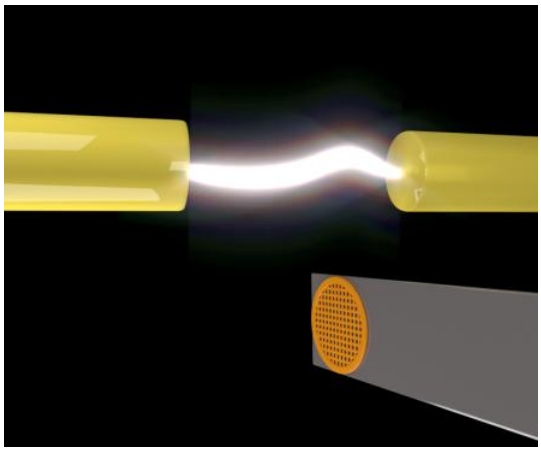

Figure 1 – Schematic of the sampling setup during production of gold nanoparticles

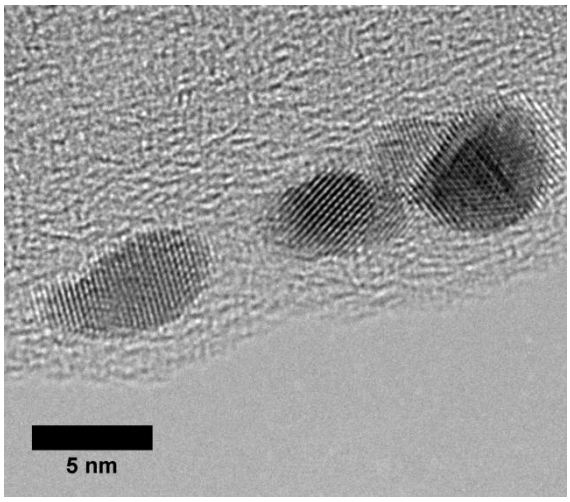

Figure 2 – Particles sampled at a flow of 0.5 lpm N_2 sampled 9 mm from the electrode gap

The constructed TEM sampler allows for collection of particles formed close to the very first moments of generation, only a few mm from the discharge. Our results show that single crystalline particles with diameters smaller than the primary particle size in the final agglomerated particles (3nm vs 5 nm) are possible to collect as seen in figure 2. A varied gas flow also shows an effect on the particle size, already 9 mm below the discharge. Understanding of these initial steps in particle formation is crucial in order to further optimize and realize mass production of metal nanoparticles in a cheap and environmentally friendly way.

Acknowledgements

This work was supported by the European Union's Seventh Framework Program (EU FP7) under Grant Agreement No. 280765 (BUONAPART-E).

References

Matsoukas, T., and S. K. Friedlander. (1991), *Journal of Colloid and Interface Science,* **146**, 495-506.

Tabrizi, N. S., M. Ullmann, V. A. Vons, U. Lafont, and A. Schmidt-Ott. (2009) *Journal of Nanoparticle Research,* **11**, 315-332.

Saturation vapour pressures from evaporation rates of organic aerosol particles

E. U. Emanuelsson[1], M. Tschiskale[1], M. Bilde[1]
[1]Department of Chemistry, Aarhus University, 8000 Aarhus, Denmark

Keywords: saturation vapour pressure, evaporation rate, flow tube, aerosol

Introduction

Atmospheric aerosol particles represent a mixture of organic and inorganic molecules, of which the organic typically constitute above 50% by mass (Zhang *et al.*, 2007). These organic molecules have both natural and anthropogenic sources. Isoprene is one of the major non-methane volatile organic compounds released into the atmosphere (Hallquist *et al.*, 2009).

Many approaches to modeling atmospheric aerosols result in under-prediction of organic aerosol mass. Saturation vapour pressure and the associated temperature dependence (enthalpy ΔH), are key parameters for improving predictive atmospheric models. Generally, the aerosol community lack experimentally determined values of these properties for atmospheric relevant organic aerosol compounds (Bilde *et al.*, 2015).

Methods

There are several techniques available to determine saturation vapour pressures. One is from measured evaporation rates of aerosol particles. This work presents the ARAGORN (AaRhus Atmospheric Gasphase OR Nanoparticle) - flow tube setup, where evaporation rates of organic aerosol particles are experimentally determined.

Sub-micron particles are generated by nebulization from aqueous solution, dried, and a mono disperse fraction of the aerosol is selected using a differential mobility analyser. The particles are then allowed to evaporate in the ARAGORN-flow tube that is the central part of the system. It is a 3.5 m long stainless steel pipe with an internal diameter of 0.026 m (Bilde *et al.*, 2003, Zardini *et al.*, 2010). Along its length, the flow tube has four ports that can be used for aerosol particle sampling, and measurements of temperature, relative humidity and pressure.

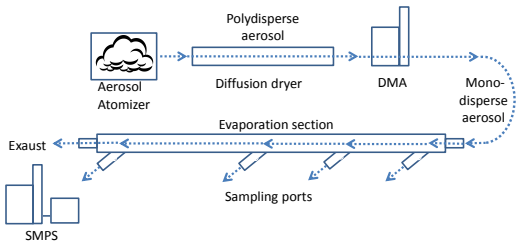

Figure 1. Schematic of the ARAGORN-flow tube setup, used for aerosol particle evaporation measurements under controlled conditions.

Changes in particle size as function of evaporation time are determined using a scanning mobility particle sizer system. Physical properties like air flows, temperatures, humidity and pressure are controlled and monitored on several places in the setup.

The saturation vapour pressures are then inferred from the experimental results in the MATLAB® program AU_VaPCaP (Aarhus University_Vapour Pressure Calculation Program).

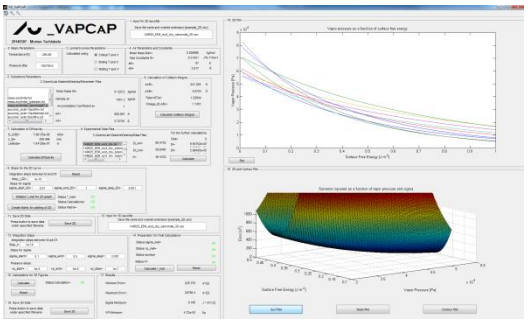

Figure 2. The interface of AU_VaPCaP for calculations of saturation vapour pressure from evaporation of aerosol particles.

Results

Saturation vapour pressures at several temperatures from the organic compound *meso*-erythritol will be presented. *meso*-Erythritol is a second generation oxidation product of isoprene. Following evaporation, this compound under certain conditions showed a bimodal size distribution for initial aerosol particle diameters < 60 nm. The issue of physical phase or phases, along with critical assumptions e.g. the accommodation coefficient, in the calculations of saturation vapour pressures of atmospheric relevant compounds will be discussed.

Zhang, Q. et al., (2007), *Geophysical Research Letters*, 34(13), L13801.
Hallquist, M., et. al., (2009) *Atmospheric Chemistry and Physics* 9, 5155-5236.
Bilde, M. et al., (2015), Accepted in *Chemical Reviews*
Bilde, M. et. al., (2003), *Environmental Science and Technology* 37(7), 1371-1378.
Zardini, A. A. et al., (2010), *Journal of Aerosol Science*, 41, 760-770.

Scalable One-Step Synthesis of Efficient Ultra-fine Manganese Oxide Catalysts for Water Oxidation

*Guanyu Li[1], Jeremy Hall[2], Noushin Nasiri[1], Mun Hon Cheah[3], and Antonio Tricoli[1]**

[1]Nanotechnology Research Laboratory, Research School of Engineering, the Australian National University, 2601, Canberra, Australia
[2]Research School of Chemistry, the Australian National University, 2601, Canberra, Australia
[3]Research School of Biology, the Australian National University, 2601, Canberra, Australia
Keywords: Flame Synthesis, Water Splitting, Nanocatalysts, Aerosols.

Synthesis of renewable fuels by processes that mimic natural photosynthesis has attracted considerable scientific and industrial interest. In particular, water splitting, inspired by photosystem II in green plants, is a promising process for direct production of hydrogen from sunlight.[1] Water splitting is usually described as a two-step reaction requiring first the production of dioxygen by oxidation of H_2O and thereafter the reduction of the hydrogen ions resulting in the formation of dihydrogen. The oxygen evolution reaction (OER) step is the most demanding. Its potential enhancement by heterogeneous catalysis has been intensively investigated. Among water oxidation catalysts both IrO_2 and RuO_2 were found to be highly active.[2] Recently a ruthenium complex with a turnover frequency of ca. 300 s^{-1}, close to that of the photosystem II oxygen evolution centre, has been reported.[3] However, Ru and Ir are relatively scarce and too expensive for large-scale H_2 production.

Among transition metal oxides, manganese oxides can serve as catalysts for both oxygen reduction reaction (ORR) and OER which play key role in energy conversion and storage technologies such as mental-air batteries, fuel cells and electrolysers.[4] Lately, manganese-based catalysts have increasingly been investigated as they have similar water-oxidation centres as in photosystem II, namely manganese-calcium cluster $Mn_4CaO_5(H_2O)_4$ supported by a protein environment. Calcium manganese oxides having short-range order structure and lamellar morphologies have been discussed as promising water oxidation catalysts.[5] Among others, manganese oxides are earth-abundant, inexpensive and environmentally friendly.[1]

Here, we present the one-step synthesis of high specific surface area Mn_xO_y nanoparticles by scalable spray flame synthesis[6] of combustible solutions (Figure 1). We demonstrate the facile tuning of the particle properties by adjusting the flame key parameters such as atomization conditions, high temperature residence time, and precursor feed rate. We discuss optimal conditions for the synthesis of Mn_3O_4, Mn_2O_3 and Mn_5O_8 leading to the achievement of high water oxidation efficiency by low-cost manganese oxide-based nanostructures.

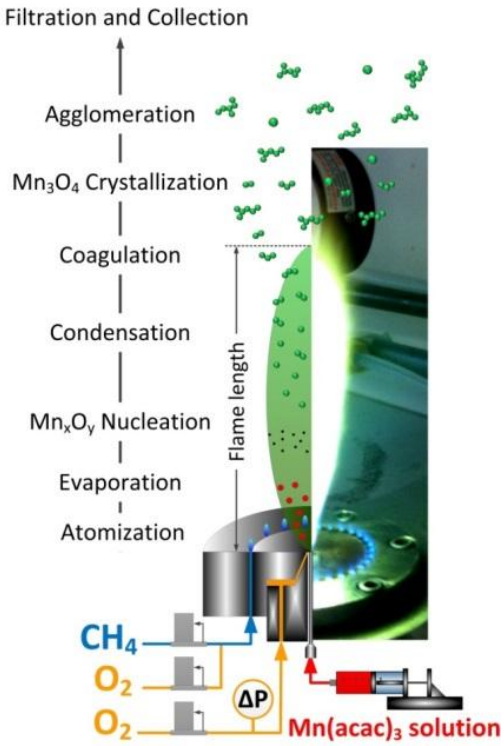

[1] M. Wiechen, M. M. Najafpour, S. I. Allakhverdiev, L. Spiccia, Energy & Environmental Science 2014, 7, 2203.
[2] N. D. Morris, M. Suzuki, T. E. Mallouk, The Journal of Physical Chemistry A 2004, 108, 9115; S. K. Das, P. K. Dutta, Microporous and mesoporous materials 1998, 22, 475.
[3] L. Duan, F. Bozoglian, S. Mandal, B. Stewart, T. Privalov, A. Llobet, L. Sun, Nat Chem 2012, 4, 418.
[4] K. Kinoshita, *Electrochemical oxygen technology*, Vol. 30, John Wiley & Sons, 1992.
[5] N. Birkner, S. Nayeri, B. Pashaei, M. M. Najafpour, W. H. Casey, A. Navrotsky, Proceedings of the National Academy of Sciences 2013, 110, 8801.
[6] J. Tikkanen, K. A. Gross, C. C. Berndt, V. Pitkanen, J. Keskinen, S. Raghu, M. Rajala, J. Karthikeyan, Surf. Coat. Tech 1997, 90, 210; L. Mädler, H. K. Kammler, R. Mueller, S. E. Pratsinis, J. Aerosol. Sci. 2002, 33, 369.

Scanning Supersaturation CPC applied as a nano-CCN counter for size-resolved analysis of the hygroscopicity and chemical composition of nanoparticles

Z. B. Wang[1], H. Su[1,*], X. Wang[1], N. Ma[2], A. Wiedensohler[2], U. Pöschl[1], Y. Cheng[1,*]

[1] Multiphase Chemistry Department, Max Planck Institute for Chemistry, 55020 Mainz, Germany
[2] Leibniz-Institute for Tropospheric Research, 04318 Leipzig, Germany

Keywords: nano-CCN counter, hygroscopicity, chemical composition, nanoparticle

Knowledge of the chemical composition and hygroscopicity is essential for understanding the formation and evolution of atmospheric aerosol particles. However, relatively little information is available for nanoparticles due to experimental difficulties. We present the design of a nano-cloud condensation nuclei (nano-CCN) counter for the purpose of measuring size-resolved hygroscopicity and interpreting chemical compositions of sub-10 nm particles. Advanced than the previous study (Kulmala et al., 2007), here we extend the use of counting efficiency spectra of condensation particle counter (CPC) and link it to the analysis of CCN activation spectra, which provides a theoretical basis for the modification of CPC to a nano-CCN counter. Since CCN hygroscopicity has been demonstrated as an effective parameter reflecting organic and inorganic mass fractions, the nano-CCN counter may thus provide size-resolved information on the chemical composition of sub-10 nm nanoparticles.

By using calibration aerosols, we show the importance of using activation fraction of aerosol samples to calibrate supersaturation distribution inside CPC and its use in further retrieval of aerosol hygroscopicities (Figure 1). Measurement procedures and data analysis methods are demonstrated through laboratory experiments with monodisperse particles of diameter down to 2.5 nm, where sodium chloride, ammonium sulfate, sucrose and tungsten oxide can be easily discriminated by different characteristic supersaturations of water droplet formation. This study improved and extended the understanding and application of CPC counting efficiency spectra. Though named nano-CCN counter, the design is not limited to the water-CPC, but also applies to CPCs of other working fluid (e.g. butanol). We suggest that a combination of scanning supersaturation CPCs with multiple working fluids may provide further insight into the chemical composition of nanoparticles and the role of organic and inorganic compounds in the initial steps of atmospheric new particle formation and growth.

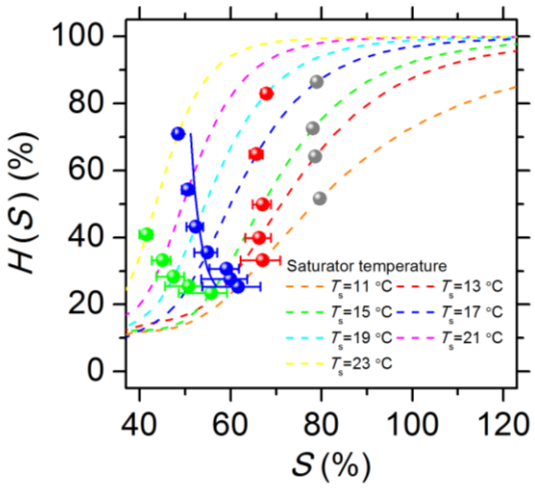

Figure 1. Calculated critical supersaturations (filled symbols) for 2.5 nm NaCl (green), AS (blue), Sucrose (red) and WOx (gray) aerosol particles based on the determined supersaturation distributions $H(S)$. The colored dash lines indicate the $H(S)$ inside the nano-CCNC at different saturator temperatures. Solid line represents the theoretical critical supersaturation for 2.5 nm AS particles.

This work was supported by the Max Planck Society and the Pan-European Gas-AeroSOls-climate interaction Study (PEGASOS No.265148). We also thank Johannes Schneider and Thomas Klimach for instrument support.

References

Kulmala, M., Mordas, G., Petäjä, T., Grönholm, T., Aalto, P. P., Vehkamäki, H., Hienola, A. I., Herrmann, E., Sipilä, M., Riipinen, I., Manninen, H. E., Hämeri, K., Stratmann, F., Bilde, M., Winkler, P. M., Birmili, W., and Wagner, P. E. (2007). *J. Aerosol Sci.*, 38, 289-304.

Wang, Z. B., Su, H., Wang, X., Ma, N., Wiedensohler, A., Pöschl, U., and Cheng, Y. (2014). *Atmos. Meas. Tech. Discuss.*, 7, 11137-11168.

Set-up for Bioaerosol Exposure on Photocatalytic Surfaces

M. Luhtalampi[1], J. Haapanen[2], S. Mustalahti[1], T. Humppi[1], and J.M. Mäkelä[2]

[1]Finnish Defence Research Agency, FDRA, Energetic and CBRN Technology Division, Ylöjärvi, Finland
[2]Tampere University of Technology, Department of Physics, Aerosol Physics Laboratory, Tampere,

Keywords: bioaerosol, exposure chamber, nanoparticle, TiO_2, photocatalytic surface.

Several ways exist to test the promising potential of the novel functional surfaces, such as e.g. self-cleaning, omniphobic, photocatalytic, anti-bacterial thin films, which have been fabricated using state-of-art processes in nanotechnology, e.g. nanoparticle coating and other surface modification techniques. Here, we focus on antibacterial property of photocatalytic surfaces.

The bioaerosol chamber was designed for testing different kinds of surfaces for example photocatalytic UV-active nanoparticle coated surface. *Bacillus atrophaeus* spores were used as biological agent. BA aerosol was generated by Hudson RCI nebulizer and introduced into a small scale test chamber. The aerosol generation process was monitored by Aerodynamic Particle Sizer, APS. The amount of CFU (colony forming unit) per litre air was determined by impinger. Also slit to agar collector was used to measure ACPLA (agent containing particles per litre air).

Test substrates were metal plates coated with two layers of paint and one layer of lacquer. Onto top of the lacquer TiO_2/Ag nanoparticles were generated using Liquid Flame Spray method (Tikkanen et al. 1997, Mäkelä et al., 2011). Lacquered surfaces without nanoparticles were used as reference. Also glass plates were used as reference.

Along with test substrates, nutrient agar Petridishes were positioned at the bottom of the chamber to counting the number of settled spores.

The bioaerosol was seen to be evenly distributed throughout the chamber bottom. Contact samples were taken of 1/3 of the plates immediately after contamination of the test plates. 1/3 of the plates were exposed to UV-radiation and the rest were kept in dark several hours and tested afterwards. Decontamination efficiency of UV active surface was estimated by comparing number of CFU/cm2 on UV-coated and reference samples.

Gravitational deposition of spores was measured by collecting the settled spores onto nutrient agar plates (NAP) and taking surface contact samples with Petrifilm Aerobic Count plates (3M, Espoo, Finland). Before the aerosol generation freshly prepared NAPs were placed on the bottom of the chamber. After spore generation NAPs were removed from the chamber and incubated at 37°C for 24 h. Surface contact samples from the chamber floor were taken with Petrifilms according to manufacturer's instruction. Colonies were enumerated after incubation in order to determine the surface spore loading in CFU/cm^2.

In the tests, clear reduction of number of spores was observed on nanocoated samples compared to reference samples without UV active nanomaterial coating. The results show that nanocoated and UV-radiated surfaces have evident killing effect on Bacillus atrophaeus spores. Note, that only UV or only nanocoating alone did not kill the spores.

The results indicate successful evenly distributed bioaerosol deposition onto the test surfaces. Also, the decontamination efficiency of the photocatalytic surfaces was verified.

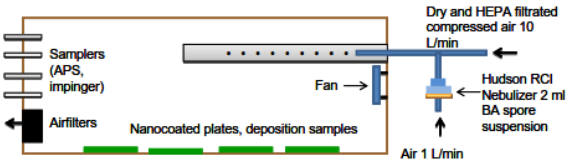

Figure 1. The test set-up. A schematic of the side view of the bioaerosol chamber.

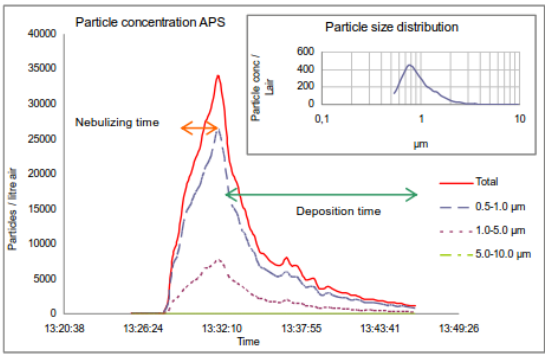

Figure 2. Data from Aerodynamic Particle Sizer.

Bacillus atrophaeus, strain number E-052737, Culture Collection, VTT, Finland.

Mäkelä J. M., Aromaa, M., Teisala, H., Tuominen, M., Stepien, M., Saarinen, J.J., Toivakka, M. , and Kuusipalo, J. (2011) Nanoparticle Deposition from Liquid Flame Spray Onto Moving Roll-to-roll Paperboard Material, *Aerosol Sci Technol.* 45(7): 827-837.

Tikkanen, J., Eerola, M., Pitkänen, V., & Rajala, M., (1997) Patent No. FI98832.

Short wavelength optical characterization of aerosol nanoparticles in a flow tube

Paulus S. Bauer[1], H. Amenitsch[2], H. Peterlik[1] and Paul M. Winkler[1]

[1] Faculty of Physics, University of Vienna, 1090 Vienna, Austria
[2] Institute of Inorganic Chemistry, Graz University of Technology, 8010 Graz, Austria

Keywords: nanoparticle formation, short wavelength, SAXS, flow tube.

Gas-to-particle conversion is known to dominate the aerosol number concentration in the global atmosphere (Kulmala *et al.*, 2004). The rigorous study of airborne particles in the size range from 1 nm to 50 nm is hence crucial for a better understanding of the underlying nanoparticle formation mechanisms. Conventional techniques are able to retrieve size information from electrical mobility analysis or use mass spectrometers to determine the chemical composition of nanoparticles. However, most techniques suffer from insufficient time resolution (Winkler *et al.*, 2012).

Noninvasive optical approaches provide size and structure information at time scales as low as milliseconds. To this end, wavelengths close to the size of the particles are needed. For the study of nanoparticles this implies radiation at wavelengths close to or below 1nm. Accordingly, x-rays (ca. 0.2 – 1 nm) can be considered appropriate for optical nanoparticle characterization.

Small Angle X-ray Scattering (SAXS) is commonly used in material science or in biochemical process analysis in order to acquire structural information from 1 nm to 50 nm. In aerosol science this approach promises in situ information on nucleation mode particles (Laksmono *et al.*, 2011). Here we report experiments conducted recently at the SAXS beamline at the Elettra synchrotron Triest. We have chosen this beamline due to high beam intensity and the available experience on aerosol studies in flow tubes (Jungnikl et al., 2011). We extended this approach to the study of newly formed biogenic particles from the ozonolysis of α-pinene. To provide a representative environment for aerosols a flow tube with a movable inlet for variable residence time was used. Figure 1 displays a sketch of the flow tube setup at the synchrotron. A Differential Mobility Particle Sizer (DMPS) and a Condensation Particle Counter (CPC) were run in parallel to allow direct comparison of the SAXS data to the conventional aerosol measurements. Figure 2 presents SAXS intensities of biogenic nanoparticles measured at different inlet positions, reflecting the particle evolution at different residence times.

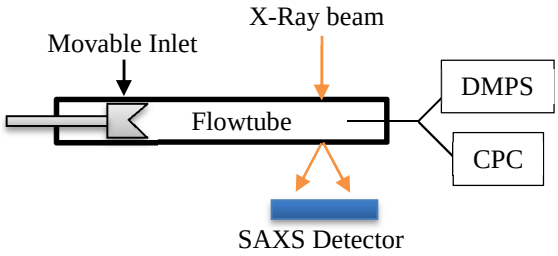

Figure 1. Sketch of the flow tube setup at the SAXS beamline at Elettra.

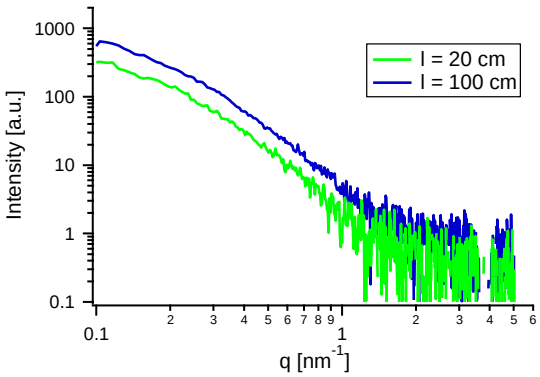

Figure 2. Scattering intensity of SAXS measurements at different inlet positions in the flow tube.

This work was supported by the European Research Council under the European Community's Seventh Framework Programme (FP7/2007-2013) / ERC grant agreement No. 616075.

Kulmala, M., et al. (2004). *J. Aerosol Sci.* 35, 143.
Winkler, P. M., et al. (2012). *Geophys. Res. Lett.* 39, L20815.
Laksmono, H. et al. (2011). *Phys. Chem. Chem. Phys.* 13, 5855.
Jungnikl, K., et al. (2011). *Aerosol Sci. Technol.* 45, 7, 805.

Similar DMA aerosol size measurements with Krypton and post-DBD neutralizers

R. Mathon, N. Jidenko and J.-P. Borra

Laboratoire de Physique des Gaz et des Plasmas (UMR 8578 CNRS –Univ. Paris Sud Orsay, F-91405)
Equipe Décharges Electriques et Aerosol, SUPELEC, F-91192 Gif-sur-Yvette Cedex, France

Keywords: electrical discharge, aerosol charging, electrical mobility, neutralization.

Aerosol size measurements based on electrostatic classification mainly rely on aerosol neutralization. The neutralization is achieved by diffusion of bipolar ions on particle surface. Ions are commonly produced by radioactive sources that are subjected to legal restrictions. The ions density in the neutralizer is in order of 10^{13} m^{-3}. Recent alternatives, based on X-ray sources (Modesto 2011) or electrical discharge, have been developed (Kwon et al. 2005).

We report here the charge distribution of monodispersed aerosol acquired after mixing of ions extracted from a Dielectric Barrier Discharges (DBD) by a dry clean air flow. Actually when aerosols are injected in the discharge ion properties (electrical mobility and density) are affected by both the chemical composition of the gas and the discharge destabilization due to the collection of particle on the dielectric surfaces (Jidenko 2014).

The DBD reactors are made of two planar electrodes both covered by a dielectric material that are separated by a gas gap spacing. The dielectric barrier prevents from arc formation and involves an alternative polarization of the system (typically a few kV at 50 Hz to 1 MHz and above 30 kHz for ion extraction). In air, at atmospheric pressure, the plasma occur as thin and brief filaments discharge (a few 10's of μm, a few 10's of ns) crossing the gap and homogeneously distributed over the electrode surfaces. Thus, DBD produce high transient ions density. The electro-hydrodynamic transport of ion is controlled by the electric field (due to the applied voltage, the ion space charge and the surface polarization), the convexion and the ion losses (recombination and diffusion to the wall). Post-discharge ions densities and mobilities have been investigated versus plasma and hydrodynamics parameters (Mathon et al. 2014). Ion currents in post-DBD reach few hundreds of pA for flow rates around 1 $L.min^{-1}$. In most cases, the net post-discharge ion current is positive. The measured aerosol charge distributions tend to Boltzmann distribution The mean charge per particles depends on the size and on the ratio of the product $(N_i^+.Z_i^+)/(N_i^-.Z_i^-)$ (Gunn et al.). We will show how this ratio can be controlled and the consequences on aerosol charge distribution. Once the operating conditions to reach similar aerosol neutralization than in classical radioactive neutralizer, size measurements on monodispersed and polydispersed aerosol are compared (cf. Fig. 1).

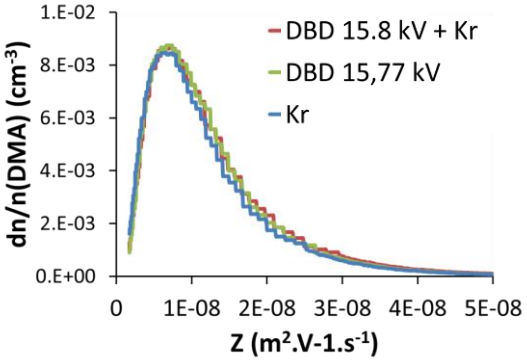

Fig. 1. Mobility distributions of 300 nm oil droplets at 10^7 cm^{-3} for post-DBD at 60 kHz 15.5 kV with 0.25 lpm aerosol and 0.25 lpm bipolar ion and Kr neutralizer

Similar mobility and thus size distribution are measured by both neutralizers. The concentrations are normalized due to the dilution factor of 2 for the DBD. Finally, the aim is to define the limit in terms of particle size range and maximal concentration that can be neutralized in post-DBD.

As a conclusion, post-DBD are can be used as neutralizer, more stable than corona ionizer without oxidation of metal electrodes inducing discharge evolution in time, with ions properties nearly independent of aerosol. Besides, most of the size distribution measurements are similar to those obtained with a radioactive neutralizer so that classical data inversion can be used. Nevertheless, oxidative species (ozone) and nanoparticle below 10 nm are extracted from the DBD. An alternative to this last drawback is under study.

Acknowledgments: The authors want to thank the Palas society for its financial support.

References

Gunn R., J. of Colloid Sci. (1955) **10-1**, 107-119

Jidenko N., Borra J-P Aerosol Technology (2014) Karlsruhe, Germany

Kwon S. B., Fujimoto T., Kuga Y., Sakurai H.and Seto T., JAST, , **vol. 39**, pp. 987-1001, 2005

Mathon R, N. Jidenko J-P Borra (2014) Gas Discharge Conference Orléans, France

Modesto-Lopez L. B. , Kettleson E. , M. Biswas P., Journal of electrostatics (2011) , **69 ,** 357-364

Pipa A.V., Hoder T.K., Schmidt J.M., Brandenburg R., Review of sci. instrument (2012) , **83**, 75111

Simulation of a condensing aerosol in homogeneous isotropic turbulence

A. Alshaarawi, A. Attili, and F. Bisetti

Clean Combustion Research Center, King Abdullah University of Science and Technology, Thuwal, 23955-6900, Saudi Arabia

Keywords: condensing aerosol, turbulent mixing, direct numerical simulation, homogeneous isotropic turbulence

The formation of aerosol particles in turbulent, spatially inhomogeneous flows is a fundamental process in nature and is relevant in many technological applications. These include cloud formation, the production of advanced powders, and soot formation.

We consider aerosol particles nucleating from a supersaturated vapor, where supersaturation is induced by the turbulent mixing of two streams (a saturated stream and a cold one). As the rates of nucleation and other aerosol dynamics are highly sensitive and nonlinear functions of the scalar fields, turbulence has a strong effect on aerosol dynamics. We perform and analyze a simulation of the formation and evolution of a condensing aerosol in homogeneous isotropic turbulence. The aerosol evolves due to the formation, growth, and coagulation of dibutyl phthalate (DBP) droplets. The homogeneous isotropic turbulence configuration is selected to identify the Reynolds number of the flow unequivocally, thereby facilitating parametric studies. Moreover, the flow field is characterized by well-defined length and time scales, e.g., the eddy turnover time (τ_{eddy}), which may be compared to the time scales of the processes responsible for the formation and growth of the aerosol.

A direct numerical simulation (DNS) is employed for the simulation of velocity, temperature (T), and vapor mass fraction (Y) fields. Velocity is linearly forced using the method of Rosales & Meneveau (2005) in order to achieve a statistically-stationary velocity field. The computational domain of size $L = 6.25\,\text{mm}$ is discretized into 134 million grid points (512^3). The Quadrature Method of Moments (QMOM) (McGraw, 1997) is used to describe the aerosol phase. The diffusion term is neglected due to the large Schmidt number of aerosol particles. The transport of the aerosol moments is simulated with a Lagrangian particles method (Attili & Bisetti, 2013) and the domain is populated with 1.3 billion Lagrangian particles (an average of ten particles per cell).

Nucleation is maximum on the cold side at $Z = 0.11$, where the mixture fraction Z is defined as a rescaled temperature $Z \equiv (T - T_c)/(T_h - T_c)$. On the other hand, the growth rate of particles peaks on the hot side at $Z = 0.76$. Thus, droplets nucleate on the cold side near the peak nucleation rate location first.

Turbulent mixing drives mixture fraction towards its mean value, i.e., $\langle Z \rangle = 0.4$. Unlike the scalar fields, the transport of droplets is characterized by a very large Schmidt number, i.e., droplets are convected along the pathlines, whereas the transport of the scalar fields (T and Y) includes diffusion processes. The resulting differential diffusion between droplet and the scalar fields causes a drift of the droplets in mixture fraction or composition space (Zhou *et al.*, 2014). This drift moves droplets from the location where they nucleate to the warmer regions of the flow where the growth rate of the droplets increases, and droplets grow in size. Nucleation is confined in the region $0 \leq Z \leq 0.3$, and so is number density as shown in Fig. 1. Although number density is mostly confined in the region of the flow where droplets nucleate, droplets that drift towards the warm and humid regions of the flow (larger values of mixture fraction) grow fastest creating peaks of volume fraction outside the nucleation zone.

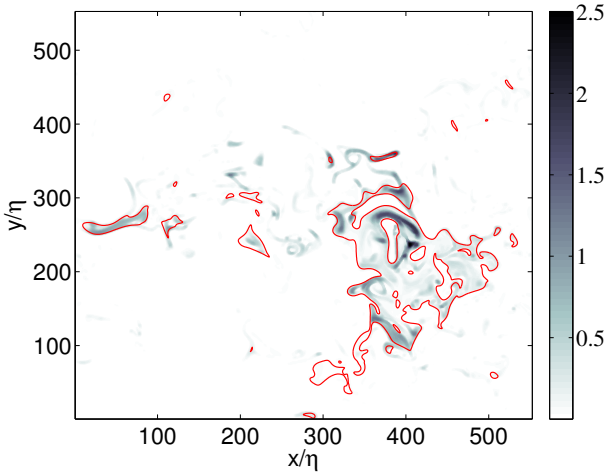

Figure 1: Isocontour for number density ($10^{11}/\text{cm}^3$) in a selected plane at $t = 0.3\tau_{\text{eddy}}$. The red isocontour marks mixture fraction $Z = 0.3$ and marks a region inside which the temperature is below 281 K.

Attili, A. and Bisetti, F. (2013) Application of a robust and efficient Lagrangian particle scheme to soot transport in turbulent flames. *Comput. Fluids*, 84: 164-175.

McGraw, R. (1997) Description of aerosol dynamics by the quadrature method of moments. *Aerosol Sci. Tech.*, 27(2):255-265.

Rosales, C. and Meneveau, C. (2005) Linear forcing in numerical simulations of isotropic turbulence: Physical space implementations and convergence properties. *Phys. Fluids* (9) 095106.

Zhou, K., Attili, A., Alshaarawi, A., and Bisetti, F. (2014) Simulation of aerosol nucleation and growth in a turbulent mixing layer. *Phys. Fluids* (26) 065106.

Small biomass boiler particle removal system

A. Laitinen, K. Janka and J. Keskinen
Department of Physics, Tampere University of Technology, P.O. Box 692, 33101 Tampere, Finland

Keywords: small scale, biomass combustion, particle removal, ESP.

Removal of particles from a small biomass boiler's flue gas stream is a very demanding task. In domestic use the available space for removal device is often very limited and the users are not specialist in the fields of burners or particle removal devices. Additionally, in small scale burners the collecting device must have very low investment and operation costs.

Electrostatic precipitators (ESPs) are widely used in industrial scale particle removal and there are now several devices available also for small scale energy production (Obernberger *et al*.,2011). One of the major advantages of ESP technology is that it produces only a very low pressure drop in the flue gas system. Major drawbacks are large size and that the dust build up on corona electrodes and high voltage insulators can cause reliability problems.

We have developed and tested a shielded corona charger construction that uses a small air flow to keep the corona electrodes clean. It consists of an outer shell made of electrically insulated ceramic material. Sharp needles are used as corona electrodes. Needles are connected to a metal rod that operates as a conductor rail inside the charger. The corona discharge is formed between the needles and the grounded wall structure of the flue gas duct. Particles are collected to the surfaces of the flue gas duct and removed by the boilers own cleaning system.

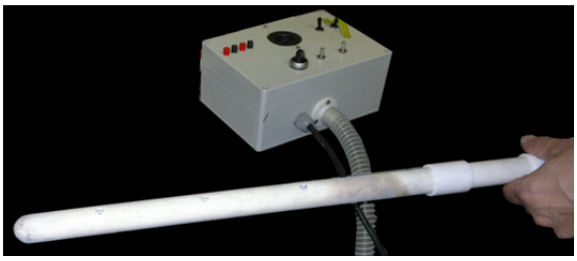

Figure 1. The charger and the external control/HV unit.

Simple implementation allows the system to be retrofitted in existing units and requires only the addition of small port for the charger. For testing the charger was be placed inside a commercial pellet boiler.

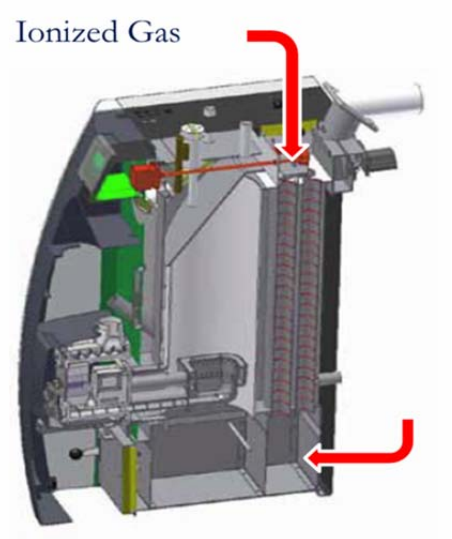

Figure 2. The charger can be located for example before heat exchanger or in the dust box. Particles are collected in the dust box and heat exchanger. Collected particles are further removed by the boilers own cleaning mechanism.

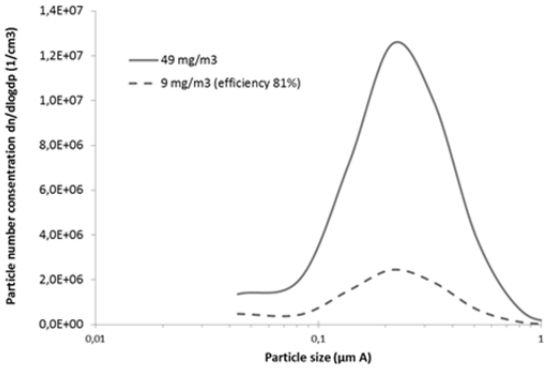

Figure 3. Flue gas particle number distributions measured from a wood pellet boiler. Measured particle mass was 49 mg/m^3 charger off-line and 9 mg/m^3 charger on-line.

Obernberger, I.,& Mandl, C. (Ed.) (2011). *Survey on the present state of particle precipitation devices for residential biomass combustion with a nominal capacity up to 50 kW in IEA Bioenergy Task32 member countries.* http://www.ieabcc.nl/

Spark-discharge technique for the production of nanoparticles with a tunable plasmon resonance to enhance photoelectrochemical reactions on semiconductors

M. Valenti[1], W. A. Smith[1], G. Biskos[1,2,3] and A. Schmidt-Ott[1]

[1]Faculty of Applied Sciences, Delft University of Technology, 2628 BL Delft, The Netherlands
[2]Faculty of Civil Engineering and Geosciences, Delft University of Technology, 2628 CN Delft, The Netherlands
[3]Energy Environment and Water Research Center, The Cyprus Institute, Nicosia 1645, Cyprus

Keywords: Spark discharge particle generator, Plasmonic nanoparticles.

There is significant evidence that the surface plasmon resonance (SPR) of nanoparticles (NPs) can enhance the rate of important photoelectrochemical (PEC) reactions (e.g. water splitting) on semiconductors (Linic et al., 2011.). There are three mechanisms by which plasmonic NPs can transfer energy to the semiconductor, enhancing its performance (Linic et al., 2011.): (1) direct electron/hole transfer from the NP to the semiconductor, (2) enhancement of the incident electric field (e.g. supplied by the sunlight) at the NP semiconductor interface and (3) light scattering.

Most studies found PEC enhancement only when the NPs' SPR absorb light at the same wavelengths as the semiconductor (Linic et al., 2011.). Therefore, it is of great importance to be able to tune the NP absorption peak, through their size and composition, in order to match the absorption of a specific semiconductor. This work introduces a methodology to optimize the PEC performance of NP-semiconductor composites by controlling the NPs' SPR absorption peak position and intensity. This is achieved by depositing well-defined aerosol plasmonic NPs on semiconductors. This way, the SPR absorption properties can be tuned by independently changing the material, size and concentration of the aerosol NPs, without compromising the NP's purity.

Methodology: The spark-discharge technique (Schwyn et al., 1998) is used as the source of aerosol plasmonic NPs (e.g. Au, Ag). The particles are sintered into spheres in a tube oven. Subsequently, they pass through a neutralizer and are size selected with a differential mobility analyzer (DMA). An electrostatic precipitator (EP) is used to deposit the particles on the semiconductor surface.

Results: Plasmonic NPs were electrostatically deposited on CuWO4 (promising semiconductor for PEC water splitting). The deposited NPs' material (Au) and size (~ 39 nm) were selected in order to enhance the absorption of the semiconductor (c.f. Figure 1, Valenti et al. 2015) near its band gap edge (~ 540 nm) where it exhibits the lowest PEC performance. It is found that the PEC water splitting performance of the semiconductor was significantly enhanced after NP functionalization (c.f. Figure 2, Valenti et al. 2015).

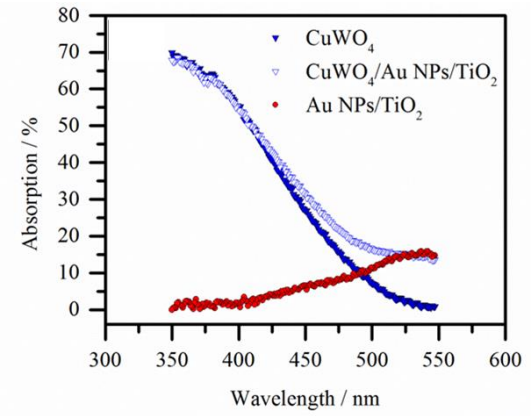

Figure 1. Absorption spectra of the semiconductor, composite and Au NPs.

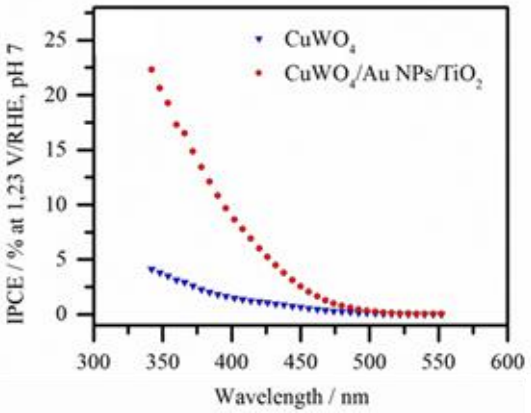

Figure 2. Incident photon to current conversion efficiency (IPCE) for a CuWO4 film before and after NP functionalization.

References

Linic, S., Christopher, P. & Ingram, D. B. (2011). *Nature mater*., 10, 911-921.

Schwyn, S., Garwin, E. & Schmidt-Ott, A. (1998). J. *Aerosol Sci*., 19(5), 639-642.

Valenti, M., Dolat, D., Biskos, G., Schmidt-Ott, A. & Smith, W. (2015). *J. Phys. Chem. C*., 119, 2096−2104.

Structural analysis of a new multi-layer graphene-carbon nanoflower composite

M. Miettinen[1], T. Torvela[1], C. Pfüller[1], J. Hokkinen[2], M. Ramsteiner[3], L. Modesto-Lopez[1], J. Jokiniemi[1] and A. Lähde[1]

[1]Department of Environmental Science, University of Eastern Finland, P.O. Box 1627, 70211, Kuopio, Finland
[2]VTT, P.O. Box 1000, 02044, VTT, Finland
[3]Paul-Drude-Institut für Festkörperelektronik, Hausvogteiplatz 5-7, 10117, Berlin, Germany

Keywords: CVS, multi-layer graphene, carbon nanoflower, structural analysis

INTRODUCTION

Different carbon nanomaterials have been synthesized eagerly during the past years because they may result in more efficient materials for, e.g., energy production and storage.

The features of the fabricated materials may affect the electrical, optical and mechanical properties. Therefore, it is important to examine the structure of the new materials to find out the most feasible application areas.

The synthesis of a multi-layer graphene-carbon nanoflower composite (MLG/CNF) (Fig. 1a) is previously reported (Miettinen et al., 2014). Here, structure of the composite was studied (Miettinen et al., 2015) using transmission electron microscopy and Raman spectroscopy.

METHODS

Aberration corrected high-resolution transmission electron microscope (TEM, JEOL JEM-2200FS) was used. The analyses were performed at electron acceleration voltage of 80 kV. Selected area diffraction analysis (SAED) was performed from the MLG sheets.

Raman spectroscopic analyses were done with two confocal setups, a Jobin-Yvon LabRAM HR Evolution equipped with a 405-nm SureLock solid state laser and a 632.8-nm He-Ne laser and a Jobin-Yvon LabRAM HR using the 482.5-nm line of a Coherent Kr^+-ion laser.

RESULTS AND CONCLUSIONS

Both SAED and Raman analyses verified that graphene layers in the MLG sheets were rotated to each other. A typical rotation angle in SAED analysis was 30 ± 2° (Fig. 1a insert) but also other rotation angles were detected. Raman analysis designated the rotation angle of 11-12° which may indicate that this is the predominant rotation angle in the composite.

Folded and free standing, unfolded edges were present in the sheets (Fig. 1b). The free standing edges were rough and no preferred chirality was found. Overlapping boundary interfaces were dominant between the graphene domains.

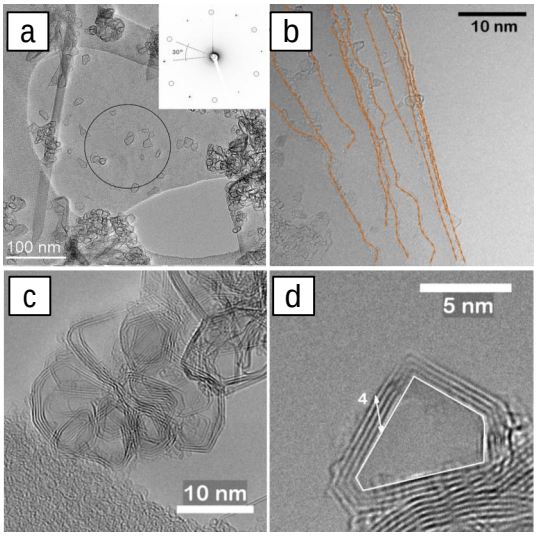

Figure 1. TEM images of the MLG/CNF composite with SAED pattern from the area marked with circle inserted (a), an edge of a MLG sheet (b), a CNF (c), and a higher magnification image of a cavity in a CNF (d).

Due to rotational faults the interlayer distance in the MLG sheets was increased ~12 % compared with graphite. The CNFs (Fig. 1c) contained nanosize (5-10 nm) cavities (Fig 1d).

Rough edges and overlapping boundary interfaces may degrade the electronic properties of the composite from the ideal values. However, the wrinkled network of the MLG sheets and the CNFs may increase, e.g., lithium-ion insertion capacity of the composite.

ACKNOWLEDGEMENTS

This work was supported by the strategic funding of the University of Eastern Finland (NAMBER) and by the funding from the Finnish Funding Agency for Technology and Innovation (TEKES) under ScaleG project (grant number 70014/13). This work made use of Aalto University Nanomicroscopy Center (Espoo, Finland) and Paul-Drude-Institut für Festkörperelektronik (Berlin, Germany) facilities.

REFERENCES

Miettinen, M., Hokkinen, J., Karhunen, T., et al. (2014). *J. Nanopart. Res.*, 16, 2168.

Miettinen, M., Torvela, T., Pfüller, C., et al. (2015) *Carbon*, 84, 214-224.

Structural and chemical characterization of soot particles

I. K. Ortega[1], B. Chazallon[1], Y. Carpentier[1], C. Irimiea[1], M. Ziskind[1], C. Pirim[1], F. X. Ouf[2], F. Salm[2], D. Delhaye[3], D. Gaffié[3], J. Yon[4], D. Ferry[5] and C. Focsa[1]

[1]Laboratoire de Physique des Lasers, Atomes et Molécules, Université Lille 1, 59655 Villeneuve d'Ascq, France
[2]Institut de Radioprotection et de Sûreté Nucléaire (IRSN), Gif-sur-Yvette, 91192, France
[3]Onera – The French Aerospace Lab, F-91123 Palaiseau, France
[4]CORIA, Université et INSA de Rouen, Av. de l'Université, 76801 Saint-Etienne du Rouvray, France
5 CINaM, Campus de Luminy, 13288, Marseille, France

Keywords: combustion aerosols, particle characterization, Raman spectroscopy, mass spectrometry.

Physico-chemical properties of soot particles play a key role in their impact in both human health and climate. The two main aims of this study are: i) find a good surrogate for airplane soot and ii) provide a systematic characterization of soot particles that can be used to interpret future ice nucleation studies planned in our group. In the present work, we have used three different techniques to characterize the structure and the surface chemical composition of soot samples, collected from three different sources in the frame of the MERMOSE project (http://mermose.onera.fr/): PowerJet (SNECMA/ Saturn) SaM146 turbofan (four engine regimes), CAST generator (propane fuel, four different global equivalence ratios), and Kerosene laboratory flame.

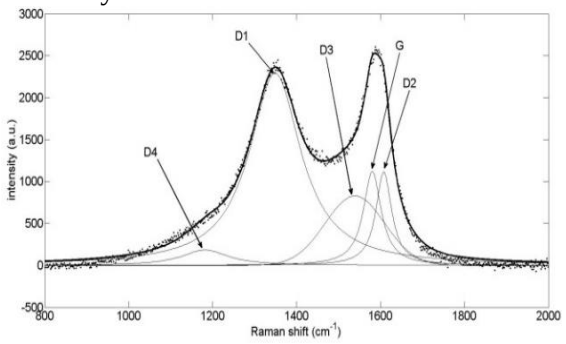

Figure 1. Example of band deconvolution of a Raman spectrum obtained from an airplane soot sample

To characterize the structure of the studied soot particles, we have used Raman microscopy. We studied the spectral parameters of the first-order Raman band of different soot samples using the five bands de-convolution approach described by Sadezky *et al.* (2005). This approach provides information about the amount of amorphous carbon and organization degrees of the samples.

To determine the surface chemical composition of the samples we use two different mass spectrometry techniques: Two-Step (Desorption/ Ionization) Laser Mass Spectrometry (L2MS) and Time of Fight Secondary Ion Mass Spectrometry (ToF-SIMS). In L2MS, the adsorbed phase is probed by nanosecond laser desorption (λ_d=532nm), then the ejected molecules are ionized with a second ns laser (λ_i=266nm) and further mass-separated by ToF-MS. While in ToF-SIMS the sample is bombarded with a Bi^{3+} ion beam and the secondary ions generated are detected by ToF-MS. Using laser desorption and ionization in L2MS technique leads to very low fragmentation of the compounds studied. L2MS is especially well suited for the study of poly-aromatic hydrocarbons (PAH) present in the soot surface thanks to the resonant enhanced multi-photon ionization (REMPI) of this compounds at 266 nm. ToF-SIMS is complementary to L2MS since it gives a more uniform response to various families of compounds, moreover the higher resolution achieved with this instrument allows a more precise identification of certain compounds. On the other hand, the fragmentation produced in this technique is higher than in L2MS.

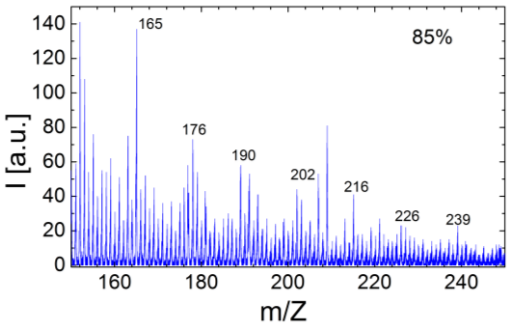

Figure 2. Example of ToF-SIM positive polarity mass spectra for an airplane soot sample

This work was supported by the French Civil aviation Authority (DGAC) through the MERMOSE project.

Sadezky, A., Muckenhuber, H., Grothe, H., Niessner, R., Pöschl, U. (2005). *Carbon*, 43, 1731-1742.

Studies of particle monolayer deposits re-suspension at low pressure in a wind-tunnel

A. Rondeau[1], A. Roynette[1], J.-C. Sabroux[1], F. Gensdarmes[1] and E. Chassefière[2]

[1] Institut de Radioprotection et de Sûreté Nucléaire (IRSN), PSN-RES, SCA, 91192, Gif-sur-Yvette, France
[2] Laboratoire Géosciences Paris Sud (GEOPS), UMR 8148, Université Paris Sud Orsay

Keywords: Re-suspension, ITER, Low pressure, Dust, Adhesion forces.

During normal operating conditions of the future ITER tokamak, a massive production of dust in its toroidal vacuum vessel is anticipated. This dust, originating from the erosion of the tokamak internal walls by the plasma, could be mobilized to some extent during a loss of vacuum accident (LOVA). For safety reasons, it is essential to quantify the re-suspended dust fraction that can be potentially mobilized during such an event. In the ITER tore, there will be principally tungsten particles deposited on tungsten surfaces, a system which is consequently the core of our studies. Here, we focus on the re-suspension of particle monolayer deposits by an airflow at 1000, 600 and 300 mbar in the IRSN BISE (*BlowIng facility for airborne releaSE*) wind tunnel.

The size distribution of the tungsten powder used is between 0.1 and 30 µm, as anticipated in ITER (see Rondeau *et al.*, 2015). The monolayer deposits were made on a tungsten surface of 16 cm^2 with a dedicated commercial device (Morphologi G3 Malvern). We measured, with an optical microscope, the particles size and number before and after submitting the deposit to an airflow during ten minutes in the BISE facility. For this purpose, we used an acquisition system together with an image processing. The particles are then ordered by size bin of 1 µm wide.

In figure 1, we present an example of experimental result of particle re-suspension in BISE at an absolute pressure of 300 mbar (Kn < 1). For each experiment, we measured the parameters entering the re-suspension mechanism, namely the pressure *P*, the airflow velocity *U*, the friction velocity *u**, the relative humidity *HR* and the temperature *T*. In addition, we calculated the re-suspended particle fraction given by the Rock'n Roll (R'nR) model correlated by Biasi *et al.* (2001).

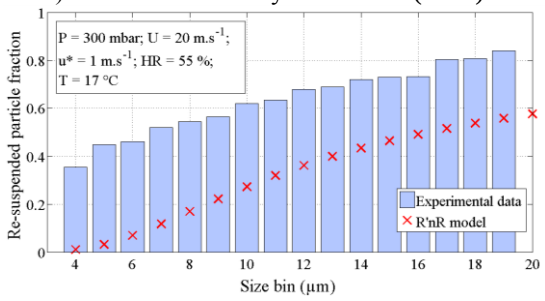

Figure 1. Histogram of the re-suspended particle fraction by size bin, as obtained experimentally and R'nR model predictions.

As we can see in figure 1, the predictions of the model are not in quantitative agreement with our experimental data. Indeed, the experimental fractions are higher than the predictions of the R'nR model.

This discrepancy is due to the adhesion forces implemented by Biasi *et al.* (2001) in the R'nR model. The adhesion forces corresponding to their specific systems (various particles on different surfaces) are not similar to tungsten particles deposited on a tungsten surface. Therefore, experimentally we measured by AFM (Atomic Force Microscopy), the adhesion forces of our particular system. The measurement technique is presented by Naphtali *et al.* (2014). In figure 2, we present an example of adhesion force measurements by AFM using a tungsten particle, stuck on the AFM cantilever tip, with an equivalent diameter, in projected surface, of 6.3 µm and deposited on the tungsten surface studied.

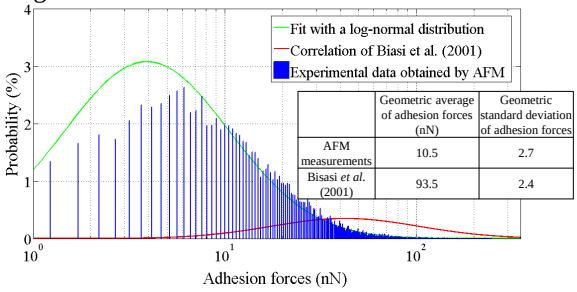

	Geometric average of adhesion forces (nN)	Geometric standard deviation of adhesion forces
AFM measurements	10.5	2.7
Biasi *et al.* (2001)	93.5	2.4

Figure 2. Comparison of adhesion forces as measured by AFM or calculated by the correlation of Biasi *et al.* (2001) (surface energy was set to 0.56 $J.m^{-2}$).

As we can see in figure 2, the adhesion forces measured by AFM are lower than those given by the correlation of Biasi *et al.* (2001). Thus, logically the lower the adhesion forces in the R'nR model, the higher the re-suspension fractions. This tendency is in qualitative agreement with our experimental data presented figure 1. A perspective of this work is to determine a correlation of adhesion forces, specific to ITER materials and surface properties.

Biasi, L. *et al.* (2001). *J. Aerosol Science*, 32, 1175-1200.

Naphtali *et al.* (2014). Nuclear Technology, 186, 45-59.

Rondeau, A. *et al.* (2015). *J. Nuclear Materials*, in press.

Study of Chemical Transformation of Exhaust Emissions from Biofuels and Diesel

F. Reyes[1], Y. Vazquez[1], P. Oyola[1], G. López[1], H. Timonen[2], M. Aurela[2], S. Saarikoski[2], R. Hillamo[2], R. Albarrán[3], A. Cadiz[3], Vasileios Papapostolou[4]

[1]Mario Molina Center Chile, Santiago de Chile, Chile
[2]Atmospheric Composition Research, Finnish Meteorological Institute, FI-00560, Helsinki, Finland
[3]Vehicle's Control and Certification (3CV), Maipú, Chile
[4]Harvard School of Public Health, Boston, Massachusetts, USA

Keywords: Direct Injection Technology, Multiport Injection engine, Particulate Matter, Aerosol Mass Spectrometry, Chemical Composition

Vehicle emissions are a major source of secondary aerosol pollution in the atmosphere. However, the formation of secondary aerosol from vehicle primary emissions is still not well understood. Gasoline Direct Injection technology (GDI) may contribute to higher particles emissions than Multiport Injection engine (MPI) that may be comparable to Diesel engine particle emissions.

A Photochemical Chamber (DPC), operated in a dynamic mode, was installed inside the test area at 3CV, Santiago, Chile, a center for light duty vehicle performance and emissions certification. The 14 m^3 cube-shape Teflon bag-style chamber was mounted on a wooden enclosure that carried 180 UVA 340nm lamps. The lamps were used to irradiate the fresh vehicle emissions inside the chamber. A Potential Aerosol Mass (PAM) chamber was installed side by side with the DPC. Primary vehicle emissions were introduced into the two chambers and photochemical transformation into secondary pollutants was initiated. Secondary aerosol (SA) formation was evaluated in both chambers. A Soot-Particle Aerosol Mass Spectrometer (SP-AMS), Multi-angle absorption photometer and a Differential Mobility Particle Size (DMPS) were used to measure aerosol composition and size distribution inside the chambers.

The 3CV chassis dynamometer and the New European Driving Cycle (NEDC) in a "hot start" condition were used to investigate the transformation of various ethanol and diesel fuel blends emissions into secondary pollutants inside the photochemical chambers. E0, E10, E85W fuels were tested with a Ford Focus Car (GDI), diesel fuel with a Kia Soul Euro V Car, and E100 with a Chevrolet Prisma Car (MPI).

Prior to the start of each experiment, the chamber was flushed with clean air. Room air was passed through a clean air system consisting of a particle pre-filter, a carbon scrubber to remove VOCs, a scrubber to remove acid gases and sulfur dioxide and an ultra particle air filter in series before introduced into the DPC chamber.

To estimate wall losses, after the DPC was filled with fresh emissions, a sample was drawn with the lamps remaining off. After approximately 1 hour, the UV lamps were turned on and photochemistry was initiated inside the DPC. the output of the DPC passed through the PAM chamber in order to complete the oxidation process of the sample.

Organics and ammonium nitrate were the major contributors in the SA formed. Mass concentrations of primary particles and gases showed high variability among different experiments. High NOx and particles concentrations were observed during experiments with the diesel and pure ethanol mixtures. A high variability in SA formation was observed that was proportional to the high amounts of precursors primary emissions concentrations.

The SA concentration formed in the DPC was approximately twice as high as the SA formed in the PAM chamber. However, the oxidation state reached in the PAM chamber was significantly higher. .

An in-depth data analysis of SP-AMS's results will allow to better understand the differences between secondary aerosol formed on PAM and DP chambers. In addition, comparison between fuel blends and GDI, MPI and Diesel engines will enhance our knowledge and understanding regarding vehicle emissions and their potential SA formation.

Acknowledgements

This work was funded by the Chilean Ministry of Environment and supported by the Chilean Ministry of Transportation and Telecommunication and the Academy of Finland (grant no 259016). We would like to thank the group at the Harvard School of Public Health for supporting and advising this study.

References:

Development and characterization of an exposure generation system to investigate the health effects of particles from fresh and aged traffic emissions. Air Quality Atmosphere & Health. 2013, Vol 6, Issue 2, pp 419-429 V. Papapostolou, J. E. Lawrence, S. T. Ferguson, J. M. Wolfson, E. A. Diaz, J. J. Godleski, P. Koutrakis

Introducing the concept of Potential Aerosol Mass (PAM). Atmos. Chem. Phys., 7, 5727-5744, 2007. E. Kang, M. J. Root, D. W. Toohey, and W. H. Brune

Study of corona discharge in high pressure helium under various temperature conditions

A.Bologa, K.Woletz, H.-R.Paur

[1]Karlsruhe Institute of Technology, D-76344 Eggenstein - Leopoldshafen, Germany

Keywords: corona discharge, high pressure, high temperature, helium

In electrostatic precipitation technology the efficiency of particles charging in corona discharge field depends on ionizer geometry, applied voltage, gas flow rate, pressure and temperature and particle mass and number concentration. The fundamental study of corona discharge phenomena, especially in high temperature high pressure (HT/HP) gases, opens the possibilities for development of compact and effective HT/HP electrostatic precipitators (ESP).

In the abstract are presented the results of the study of corona discharge in helium at gas pressure up to 2,2 MPa and temperature up to 500 °C. The experiments were carried out with a HP reactor with integrated corona charger. The charger consists of a grounded cylinder equipped with a heating element. The HV insulator is maintained at the upper part of the reactor. Two disk star-form high voltage (HV) electrodes are installed inside the cylinder and are connected to a HV unit. The electrode gap is 15 mm.

At room temperature and atmospheric pressure, the spark-over discharges take place in the electrode gap at low values of applied voltage. The corona current for negative polarity is higher than for positive polarity of applied voltage. The increase of gas pressure improves the stability of corona discharge at high corona currents. At constant gas pressure and voltage, the increase of temperature results in increase of corona current (Bologa, 2011).

The study of corona discharge at gas pressure of 2,0 MPa shows, that at constant voltage there is a difference in corona currents when the voltage is increased from 0 kV to spark-over discharge value ("direct" current voltage characteristic (CVC) and when voltage is decreased to 0 kV ("in-direct" CVC), Fig.1. One can observe the hysteresis phenomena, when the "in-direct" CVC is above the "direct" CVC (Fig.1,a) and vice-verse (Fig.1,b). At the "in-direct" CVC it is still possible to have the corona currents below the value of on-set corona voltage for the "direct" CVC. With time, the CVCs "move" to the right (Fig.1,b).To ensure constant corona current, it is necessary to apply higher voltages in comparison with previous experiments (Fig.1,a and b). The increase of temperature "moves" the CVC to the left.

It is observed, that at voltage ca. 15 kV there is an "inflection point", where the CVC-curve changes the angle of tilt. There is a divergence between the data above 15 kV and those which correspond to the Townsend equation used for CVC description at voltages below the "inflection point".

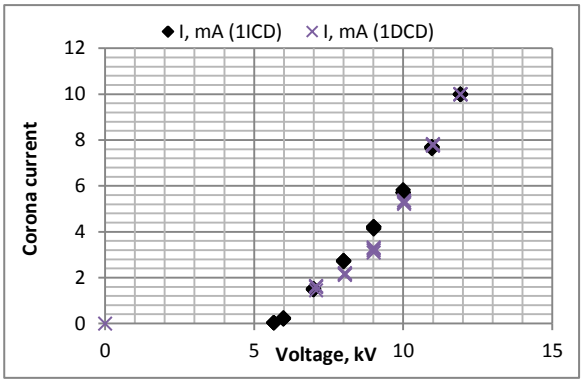

Figure 1,a

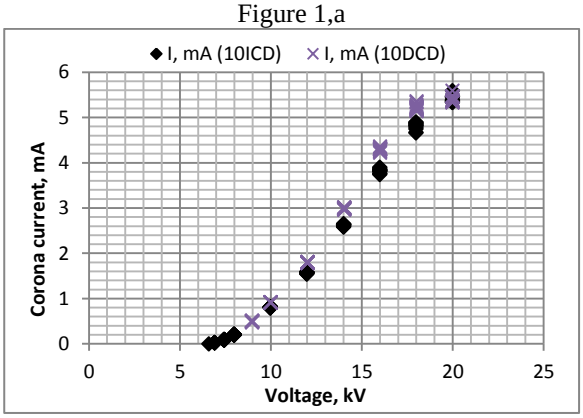

Figure 1, b

Figure 1. "Direct (DCD)" and "in-direct (ICD)" CVC after the 1st (a) and 10th measurement (b)

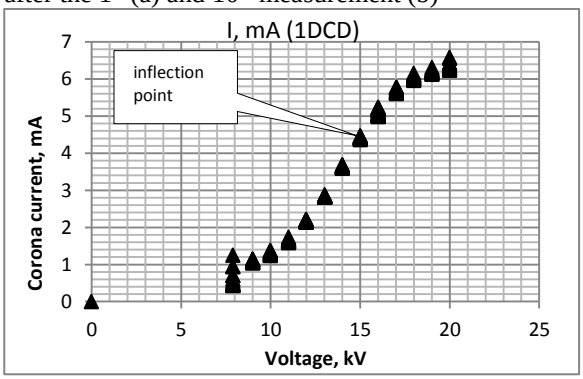

Figure 2 CVC with "inflection point"

Bologa, A. (2011). *Inter. J. on Plasma Environ. Science & Technology*, 5 (2), 110-116.

Acknowledgement: The authors thank Julian Broß for his able technical assistance. Project is funded by the Federal Ministry of Education and Research (BMBF), FKZ-Nr: 01DK13014

Study on nanoparticle scavenging and filter cakes in a waste incineration plant

Thaseem Thajudeen, Henning Förster, Christine Funk and Wolfgang Peukert

Institute of Particle Technology, Friedrich-Alexander-University, Erlangen, Germany.
Keywords: Filtration, Nanoparticle scavenging, Filter cake, Waste incineration plant.

Owing to their unique properties, nanoparticles are used ubiquitously and find applications in a wide variety of fields. This has resulted in an increased amount of nanoparticles being used in everyday life, which demands greater filtration efficiency to prevent untoward health problems. Very often products are treated at the end of their life cycles at waste incineration plants. Generation and possible release of sub-micron particles during incineration often makes the filtration of these particles a complex process. It is therefore quite important to understand how efficiently the current filtration systems perform in removing the new composition of sub-micron particles in a waste incineration plant.

The removal of nanoparticles generated in a waste incineration plant is by combination of two processes. The nanoparticles could collide and subsequently adhere to larger particles like fly ash (often with diameters above a few microns) which are then easily removed by the filters or they could be trapped directly by the filter medium. In this study we look at the efficacy of inter particle coagulation in aiding nanoparticle filtration as well as a systematic study on filtration by filter cakes in a pulse-jet cleaned filter media.

Inter-particle coagulation (Scavenging)

The rate of collision between particles depends on the collision kernel which is a function of the particle sizes and the operating parameters. With appropriate collision kernels, population balance (PB) equations can be solved to investigate the extent of coagulation (often termed as scavenging) between the nanoparticles and the fly ash particles (Lee and Wu, 2005). We have utilized the expressions developed by Dr. Hogan and co-workers where a non-dimensional collision kernel is linked to the mass and momentum transfer Knudsen numbers (Gopalakrishnan et al. 2011) that can also be modified to study the effect of singular potentials on scavenging even in the transition regimes.

For realistic operating conditions in an incineration plant, PB modelling was done using PARSIVAL for different mean sizes of the nanoparticles. Results suggested that for near complete scavenging of copper nanoparticles, with mean diameter of 15 nm, there should be an overabundance of fly ash particles (100 times higher particle number concentration than normal concentration in the incineration plant). This reinforces the need for testing the existing filter systems.

Filter Cakes

The nanoparticle filtration experiments were realised according to VDI 3926 in a modified test rig equipped with nanoparticle generation system and measurement probes upstream and downstream of the filter. (Peukert & Wadenpohl, 2009). A commercial needle felt currently used in a German incineration plant was used as the test filter medium.

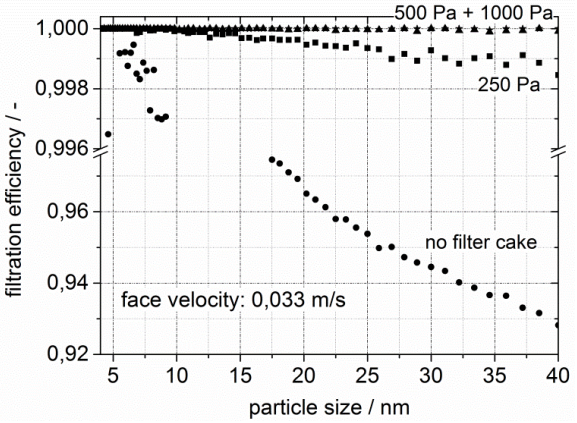

Figure 1. Influence of filter cake thickness and nanoparticle size on the filtration efficiency.

Alumina powder was used as model cake dust to form filter cake and after the cake build up experiments were done to ascertain the effects of filter cake thickness, the filtration velocity and the filtration temperature. Copper nanoparticles of mean diameter around 15 nm were generated and used to study the efficiency of the filter for various operating parameters. As shown in figure 1, the filtration efficiency strongly increased with the filter cake thickness and at a face velocity of 3.3 cm/s and at pressure drops higher than 500 Pa, the filtration efficiency attained a value close to 1. From further experiments, the lowest efficiencies were observed for a very thin filter cake with a pressure drop of only 80 Pa and a high face velocity of 10 cm/s. As expected, results also suggested better efficiency at higher temperatures due to the effect of diffusion.

This work was supported by BMBF Grant: 03X3578 D

Sang-Rin Lee and Chang-Yu Wu (2005). *Aerosol Science and Technology,39: 358-370.*

Gopalakrishnan, R., Thajudeen, T., & Hogan, C. J. (2011). *J. Chem. Phy. 135,054302*

Peukert, W., Wadenpohl, C. (2009). *Powder Technology 118, 136-148.*

Sub-3 nm particle detection with commercial TSI 3772 and Airmodus A20 condensation particle counters

J. Kangasluoma[1], M. Attoui[2], L. Ahonen[1], H. Vuollekoski[1], M. Kulmala[1] and T. Petäjä[1]

[1]Department of Physics, P.O. Box 64, 00014, University of Helsinki, Helsinki, Finland
[2]University Paris Est Creteil, University Paris-Diderot, LISA, UMR CNRS 7583, France

Keywords: CPC, calibration, nanoparticle

Recently several new condensation particle counters (CPCs) are developed for detection of sub 3 nm particles (Jiang, Chen, Kuang, Attoui, & McMurry, 2011; Sipila et al., 2009; Vanhanen et al., 2011; Wimmer et al., 2013). Improved particle activation is based on increasing the supersaturation and using pulse height analysis to the final droplet size to separate homogeneous nucleation of the working fluid from the heterogeneous nucleation onto particles. Alternatively diethylene glycol is used as the working liquid, allowing sub 3 nm particle detection. In this study we show how to achieve sub 3 nm particle detection by using conventional TSI 3772 and Airmodus A20 butanol CPCs.

The temperature difference of the saturator and the condenser were set to the maximum allowed by the CPC firmware: saturator temperatures to 50 and 50 ºC respectively, optics temperatures to 50 and 51 ºC respectively, and the condenser temperatures to 10 ºC. These operation temperatures yielded homogeneous background concentration of approximately 1-2 cm^{-3} in dry conditions. At saturator temperatures 46 and 47 ºC, respectively, the homogeneous background lowered to < 1 per minute. For a comparison the TSI ultrafine 3776 CPC was operated with similar background conditions and factory settings. In these conditions the CPCs were calibrated by using high resolution Herrmann type DMA, with negative tungsten oxide and bisulfate, and positive tetraheptylammonium bromide and tetrapropylammonium iodide as test aerosol.

Figure 1 shows the measured sub 3 nm detection efficiencies for the CPCs. d50 diamter for the CPCs is approximately 3 nm. The conventional compare well to the ultrafine which is at factory settings, altough the diffusional losses are much bigger, making the slope less steep. By increasing the saturator from 46 or 47 to 50 ºC do not yield a significant improvement in the performance.

The results show that the conventional CPCs can be also used as a detector in a DMPS system down to 2 nm, especially in high concentration places. Other applications like combination of many CPCs with different d50 diameters would benefit from a CPC with low d50 diameter. Elsewhere these boosted CPCs could be used as any other ultrafine CPC to monitor concentrations of small nanoparticles, especially if an ultrafine CPC is not available.

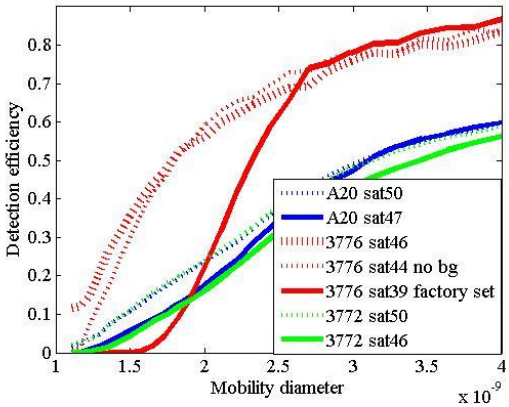

Figure 1. Detection efficiencies for the tuned 3772 and A20, and comparison to 3776 with negative tungsten oxide particles.

Jiang, J. et. al. (2011). *Aerosol Science and Technology*, *45*(4), 510-521. doi: Doi 10.1080/02786826.2010.547538

Sipila, M., et. al. (2009). *Aerosol Science and Technology*, *43*(2), 126-135. doi: Doi 10.1080/02786820802506227

Vanhanen, J. et al. (2011). *Aerosol Science and Technology*, *45*(4), 533-542. doi: Doi 10.1080/02786826.2010.547889

Wimmer, D. (2013). *Atmospheric Measurement Techniques*, *6*(7), 1793-1804. doi: DOI 10.5194/amt-6-1793-2013

Suitability of two mini-CAST generators as laboratory surrogate sources for black carbon mass measurements in the aircraft engine exhaust

L. Durdina[1, 2, 3], P. Lobo[3], E. Black[3], M.B. Trueblood[3], D.E. Hagen[3], P.Whitefield[3] and J. Wang[1, 2]

[1]Laboratory for Advanced Analytical Technologies, Empa, CH-8600, Dübendorf, Switzerland
[2]Institue of Environmental Engineering, ETH Zürich, CH-8093, Zürich, Switzerland
[3]Center of Excellence for Aerospace Particulate Emissions Reduction Research, Missouri University of Science and Technology, MO 65409, Rolla, USA

Keywords: black carbon, elemental carbon, soot, aircraft emissions

The miniature combustion aerosol standard (mini-CAST, Jing Ltd.) generators produce soot with a wide range of particle properties and mass concentrations. Mini-CASTs generate particles with elemental carbon (EC) to total carbon (TC) ratios from 0.1 to 0.9. The high EC/TC conditions have been used as laboratory surrogates for real-world primary soot emissions from internal combustion engines.

Mini-CAST exhaust with EC/TC fraction higher than 0.8 determined by the carbon burn-off method NIOSH 5040 has been used as the reference standard for non-volatile PM (nvPM) aircraft engine exhaust mass measurements (SAE, 2013). The two instruments that meet the specifications for measurement of aircraft engine nvPM mass emissions are AVL Micro-Soot Sensor (MSS) and Artium Laser-Induced Incandescence (LII) LII-300. The MSS measures the equivalent black carbon (BC) concentration based on the photoacoustic principle and the LII measures the refractory BC volume fraction. Recent inter-comparisons have shown that despite the same calibration standard, these instruments can measure up to 40% different BC mass concentration in the aircraft engine exhaust (Durdina et al., 2014). To investigate what soot properties drive these differences, we measured chemical, physical and morphological properties of soot generated by two mini-CAST burners over a wide range of operating conditions.

The two mini-CASTs were the 6203C and 5201C. Seven operating conditions for each unit were set by adjusting the burn air, propane, and mixing nitrogen flow rates. The exhaust sample was diluted with clean air and measured unconditioned and conditioned by a catalytic stripper. An instrumentation suite was used to determine BC mass concentration (two MSSs and one LII), EC and organic carbon (OC) mass concentrations, particle effective density, particle size distributions, particle morphology and microstructure.

The two BC mass measurement technologies agreed within 10% at near-stoichiometric conditions of the mini-CAST 5201C and fuel-lean conditions of the mini-CAST 6203C but not necessarily at the conditions with the highest EC/TC. Increasing OC fraction caused the LII to underestimate the BC mass compared to the NIOSH 5040 EC mass. The MSS data strongly correlated with the EC mass across all the test points in the study (R^2 = 0.851, Fig.1). Catalytic stripper increased the EC/TC ratio and improved the agreement of the MSS and LII, however the LII correlation with the EC across all the test points remained weak (R^2 = 0.137). Particle effective density increased with fuel/air equivalence ratio for both the mini-CASTs. The effective density changed due the use of the catalytic stripper and the mixing nitrogen.

Characteristics of the two mini-CASTs strongly differed. Defining the calibration standard only by the EC/TC ratio for aircraft nvPM mass instrument calibrations may not be sufficient. These results will help to lower the uncertainty of the BC mass measurement in the future certification of aircraft engine emissions.

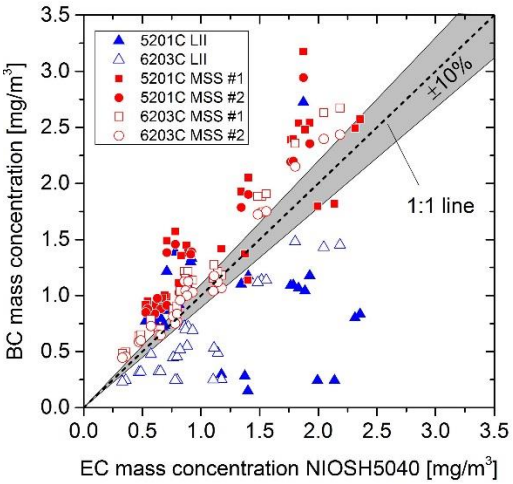

Figure 1. Comparison of the BC and EC mass concentrations for all the test points.

SAE. Procedure for the Continuous Sampling and Measurement of Non-Volatile Particle Emissions from Aircraft Turbine Engines: Aerospace Information Report AIR6241, 2013.

Durdina, L. et al. Determination of PM mass emissions from an aircraft turbine engine using particle effective density. In *Atmospheric Environment* 99, pp. 500-507.

Surface properties for atmospheric surfactant aqueous solutions and their variation with environmental parameters observed directly with synchrotron XPS

N.L. Prisle[1], G. Öhrwall[2], J. Werner[3], V. Ekholm[3], M.-M. Walz[3], and O. Björneholm[2]

[1]Department of Physics, University of Helsinki, P.O. Box 64, 00014 University of Helsinki, Finland
[2]MAX-lab University of Lund, Box 118, 22100, Lund, Sweden
[3]Department of Physics and Astronomy, Uppsala University, P.O. Box 516, S-751 20 Uppsala, Sweden

Keywords: aqueous aerosol, surface chemistry, surfactants, synchrotron XPS.
Presenting author email: nonne.prisle@helsinki.fi

Surface active compounds (surfactants) are ubiquitous in atmospheric organic aerosols. Commonly found atmospheric surfactants are dicarboxylic acids and long-chain carboxylic (fatty) acids, and salts of their carboxylate anions. Studies of their cloud droplet activation thermodynamics have revealed that the influence of surfactant properties on organic aerosol cloud condensation nucleus (CCN) activity for especially the stronger surfactants is governed by significant bulk-to-surface partitioning (Prisle *et al.*, 2010, and references therein). In general, due to the very large surface areas of sub-micron atmospheric aerosol particles, surface compositions and properties can be expected to pose a disproportionally large influence on aerosol processes and their impacts in the atmosphere (Prisle *et al.*, 2012). Furthermore, these surfaces may differ significantly from their associated bulk phases (Prisle *et al.*, 2011). It is therefore of great interest to directly probe the compositions and properties of atmospherically relevant aqueous surfaces directly on the molecular level.

Using synchrotron-based X-ray Photo-electron Spectroscopy (XPS) on a liquid micro-jet, we have successfully made direct observations of the surface chemical environment in aqueous solutions comprising different atmospheric organic surfactants (dicarboxylic acids, fatty acids, and their ionic forms). All experiments were performed at the Swedish national synchrotron facility MAX IV Laboratory, Lund University, at the soft X-ray beamline I411 (Bergersen *et al.*, 2007). XPS is a highly chemically sensitive and surface specific spectroscopic technique (Winter and Faubel, 2006) and this way ideal for studying the adsorption of surfactants in the aqueous surface region. We have obtained unique insights into how the composition of the surface differs from that of the bulk, in terms of organic enrichment and chemical speciation, and how these quantities are affected by important environmental parameters such as aqueous concentration, added salts, and pH of the bulk aqueous phase.

Consistent with our recent work (Prisle *et al.*, 2012; Werner *et al.*, 2014; Öhrwall *et al.*, 2015), we observe that in aqueous mixtures with inorganic salts containing ammonium cations, organic surfactant carboxylate functional groups are protonated in the surface region to yield the corresponding carboxylic acids, to an extent which is much greater than expected from the respective bulk solution concentrations and Brønsted acid and base strengths involved. This strongly enhanced protonation is intricately connected to organic surface activity and occurs specifically in the aqueous surface region. With increasing ionic strength, salting out in general pushes more of the carboxylate anions to the aqueous surface region, but only in ammonium solutions does increasing the amount of ions significantly affect the abundance of acid in the surface. As the abundances of inorganic aerosol species vary greatly between different types of ambient environments, this means that the organic-inorganic mixing state may affect aqueous aerosol surface properties in highly environment-specific ways.

Surface protonation significantly changes the surface composition with respect to the corresponding bulk solute and occurs without any accompanying significant changes in aqueous bulk phase properties, in particular the solution pH. By measuring surface titration curves for aqueous surfactant solutions using XPS, we have derived "effective acid constants" for surface adsorbed surfactants analogous to the traditional Henderson-Hasselbalch equation. These indicate a significantly more acidic environment in the surface, compared to the associated bulk phase. Future work will be directed at gaining more insight into the quantification and underlying mechanisms of such aqueous surface-specific acidity, as well as the implications of such changes for atmospheric aerosol processes, e.g. cloud activation and organic aerosol formation, which are central to their impacts on atmospheric processes and climate.

This work was supported by the NordForsk researcher network project NICITA, the Knut and Alice Wallenberg Foundation, the Swedish Research Council, and the Finnish Centre of Excellence in Atmospheric Science: From Molecular and Biological processes to the Global Climate (272041). N.L. Prisle is grateful for the personal funding received from the Carlsberg Foundation and the Finnish Academy of Sciences (257411).

Prisle, N. L., *et al.* (2010) Atmos. Chem. Phys. **10**, 5663-5683.
Prisle, N. L., *et al.* (2012) Atmos. Chem. Phys. **12**, 12227-12242.
Prisle, N. L., *et al.* (2011) Atmos. Chem. Phys. **11**, 4073-4083.
Winter, B. and Faubel, M. (2006) Chem. Rev. **106**, 1176-1211.
Bergersen, H., *et al.* (2007) J. Phys. Cond. Matt.**19**, 326-101.
Werner, J., *et al.* (2014), Phys. Chem. Chem. Phys., DOI: 10.1039/c4cp02776k.
Öhrwall, G., *et al.* (2015), J. Phys. Chem. B, *in press.*

Synthesis of catalytic materials from controlled deposition of electrosprayed inks

J.L. Castillo, B. Martinez-Vazquez and P.L. Garcia-Ybarra

Dept. Fisica Matematica y de Fluidos, Facultad de Ciencias, UNED, Senda del Rey 9, Madrid 28040, Spain

Keywords: Electrosprays, Aerosol deposition, Material synthesis, Catalytic materials

Synthesis of catalytic materials via aerosols offers many practical benefits. Catalytic processes require the availability of materials with a large effective surface area to provide the active sites for the surface reactions to take place. The use of nanoparticles partially covered with the catalyst as building blocks for these materials has several advantages. On the one hand, they contain small amounts of the precious catalyst. On the other hand, the dynamics of nanoparticle arrival to the collector can be used to control the porosity and surface roughness of the resulting granular material (Castillo *et al*, 2014). In a previous work, highly porous materials with very low catalyst loadings were prepared in this way resulting in extremely efficient 5 cm^2 fuel fell electrodes (Martin *et al*, 2013).

Now, a scaling-up process has been implemented to elaborate ultra-low platinum loading electrodes of market size (25 cm^2 active area electrodes) for proton exchange membrane fuel cell (PEMFC). Catalyst inks were prepared by ultrasonic stirring solutions of Pt/C nanopowders (Pt 10 wt.% and Pt 20% on Vulcan XC-72R) with ethanol (96% v/v, Panreac) as solvent and Nafion® (Aldrich) as ionomer. The electrohydrodynamic atomization of the ink was performed at a constant flow rate (Q) in a bipolar configuration with the electrospray working in steady cone-jet mode (Martin *et al*, 2012). The evaporation of the ethanol in the spray promotes the dispersion of charged solid particles that are collected on a plate facing the electrospray needle. This electrodynamically assisted deposition leads to granular materials with a fractal structure on the small scale (up to a cut-off size) whereas, on the large scale, they are continuous media with a controllable mean density and averaged constant porosity. For given geometric configuration and ink composition, the flow rate (Q) and working voltages (needle voltage V_n and plate voltage, V_p) determine the deposit morphology and its fractal cut-off size.

The resulting granular materials are catalytic layers with open and porous structure. Electrodes with 0.01 mg_{Pt} cm^{-2}, 0.02 mg_{Pt} cm^{-2} and 0.04 mg_{Pt} cm^{-2} Pt loadings were prepared. The homogeneity of the catalytic layers was tested by getting Energy Dispersive X-ray (EDX) spectra at different locations on the surface of the layer. The horizontal EDX scanning confirms the rather even distribution (in weight percentage) of the different elements on the surface of the deposited layer.

A membrane electrode assembly (MEA) is formed by two such electrodes on each side of a Nafion electrolytic membrane. The performance of these MEAs in single fuel cells has been assessed under different working conditions of pressure, temperature and humidity (Martinez-Vazquez *et al*, 2015). The maximum catalyst utilization (fuel cell power per gram of platinum in the MEA) delivered by a fuel cell with these electrodes, under optimal conditions, reaches the interval 30-35 kW g_{Pt}^{-1}.

The results confirm that the scale up of the electrospray technique is quite straightforward. This accomplishment opens the possibility of using this methodology for other commercial applications where larger active areas may be required.

Work supported by research funding agencies in Spain: Ministerio de Economia y Competitividad (grant ENE2011-26868, and Program Consolider-Ingenio 2012 grant CSD2010-00011), and also by Comunidad de Madrid (Proyect HYSYCOMB, S2009ENE-1597).

Castillo, J. L., Martin, S., Rodriguez-Perez, D., Perea, A. & Garcia-Ybarra, P. L. (2014) *KONA Powder and Particle J*., 31, 214-233.

Martin, S., Perea, A., Garcia-Ybarra, P. L. & Castillo, J. L. (2012) *J. Aerosol Sci.*, 46, 53-65.

Martin, S., Martinez-Vazquez, B., Garcia-Ybarra, P. L. & Castillo. J. L. (2013) *J. Power Sources*, 229, 179-184.

Martinez-Vazquez, B., Sanchez, D.G., Castillo, J.L., Friedrich, K.A. & Garcia-Ybarra, P.L. (2015) Scaling-up and characterization of ultralow-loading MEAs made-up by electrospray. *Int J Hydrogen Energy*, in press.

Testing a Near Field/Far Field model for prediction of particulate matter emissions in a paint factory

A.J. Koivisto[1], A.C.Ø. Jensen[1], M. Levin[1,2], K.I. Kling[1], M. Dal Maso[3], S.H. Nielsen[1], K.A. Jensen[1] and I.K. Koponen[1]

[1]National Research Centre for the Working Environment, Lersø Parkallé 105, Copenhagen DK-2100, Denmark
[2]Department of Micro- and Nanotechnology, Technical University of Denmark, DK-2800, Lyngby, Denmark
[3]Department of Physics, Tampere University of Technology, Tampere, Finland

Keywords: exposure assessment; exposure modeling; NF/FF model; dustiness

A Near Field/Far Field (NF/FF) model is a well-accepted tool for precautionary exposure assessment but its capability to estimate particulate matter (PM) concentrations is not well studied. Major uncertainties are related to a) characterization of PM source emission rates and b) air flow between the NF and FF volumes (Q_{NF}) *i.e*. dispersion of the particles. One way to characterize PM emission source strength is by using the material dustiness index which is scaled to correspond to industrial use by using modifying factors, such as handling energy factors (H_i). In this study we investigate how well the NF/FF model predicts PM concentration levels in a paint factory when the source was characterized using powders dustiness.

A near field (NF) and far field (FF) concentrations were measured in a paint factory during pouring of paint pigments/fillers from 25 kg and 500 kg bags (Koivisto *et al*., 2015). The pigments/fillers dustiness indices were characterized by using the down-scaled EN15051 dustiness drum in particle number and mass (Schneider & Jensen, 2008). Dustiness indices were used to calculate the dusts emission rates by taking into account modifying factors (Fransman *et al*., 2011). The measured concentrations were compared with concentrations predicted with a NF/FF model (*e.g*. Koivisto *et al*., 2015).

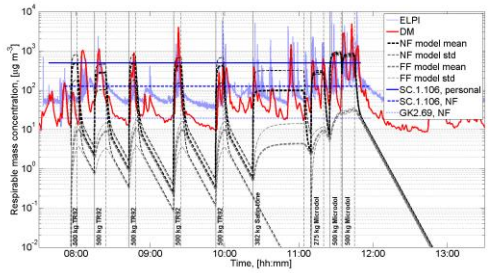

Figure 1. The NF respirable mass concentrations calculated from particle measurements using the electrical low pressure impactor (ELPI) and optical particle sizer (DM) and assuming spherical particles with mean density of 1.7 g cm^{-3}, and gravimetric samplers, and modelled NF and FF respirable mass concentrations using the NF/FF model.

Work environment, processes, measurements and the NF/FF model parameterization are by Koivisto *et al*. (2015). For each pouring were calculated an average respirable mass concentration from the DM measurements. The H_i was adjusted so that the modelled NF respirable mass concentration was similar as measured by the DM (Figure 1). It was found that depending on Q_{NF}, H_i was from 6 to 49 times higher than expected values. The modelled NF particle number concentration was approximately 2 times the measured number concentration.

This study shows that the emissions and modifying factors need to be studied in well controlled environments to understand factors affecting on the powder emissions scaling from dustiness measurements to industrial scale. A better understanding is needed in:

- Handling energy factors (H_i) for different processes
- NF and FF air flow (Q_{NF})
- Localized control efficiencies
- Sampling of NF and FF concentrations
- Composition of the measured mass concentration, i.e. fraction of the process particles, condensates, and background particles.

The research leading to these results has received funding from the European Community's Seventh Framework Programme (FP7/2007-2013) under NanoValid (grant agreement N°263147) and a grant from the Danish Centre for Nanosafety (grant agreement N°20110092173/3) by the Danish Working Environment Research Fund.

Koivisto, A.J., Jensen, A.C.Ø., Levin, M., Kling, K.I., Dal Maso, M., Nielsen, S.H., Jensen, K.A., & Koponen, I.K. (2015) *Environ. Sci.: Processes Impacts*, 17, 62-73.

Schneider & Jensen, (2008). *Ann. Occup. Hyg.*, 52, 23–34.

Fransman, W., Van Tongeren, M., Cherrie, J.W., Tischer, M., Schneider, T., Schinkel, J., Kromhout, H., Warren, N., Goede, H., & Tielemans, E. (2011) *Ann. Occup. Hyg.*, 55, 957–979.

The critical velocity of rebound determined for sub-micron silver particles

Heino Kuuluvainen, Anssi Arffman, Juha Harra, Ossi Vuorinen, Paxton Juuti,
Jaakko Yli-Ojanperä, Jyrki M. Mäkelä and Jorma Keskinen

Aerosol Physics Laboratory, Department of Physics, Tampere University of Technology, Tampere, Finland

Keywords: nanoparticle, bouncing, critical velocity, low pressure impactor

Particle rebound from a surface is a fundamental phenomenon in aerosol physics. Recently, it has been of interest in several fields of research, including atmospheric aerosols and aerosol synthesis. For instance, the amorphous solid state of biogenic SOA (secondary organic aerosol) particles was found by investigating the bounce behavior of the particles (Virtanen et al., 2012). The research of the particle–surface interaction in the field of engineered nanoparticles has been focused on the fragmentation and binding energy of agglomerates. However, one of the most important fundamental parameters in this respect, the critical velocity of rebound, has not previously been studied in a wide sub-micron size range.

A novel instrument, a variable nozzle area impactor is introduced to investigate the particle–surface interaction as a function of the particle impact velocity (Arffman et al., 2015). The impactor consists of a narrow slit with a small nozzle throat height, and the nozzle area can be varied by changing the slit length from 30 mm down to 3 mm. By decreasing the slit length, the impact velocity increases and a certain particle size chosen with a DMA can be scanned. The impactor stage and the filter stage placed downstream are connected to electrometers. After determining the critical slit length and the critical collection efficiency, the corresponding critical velocity can be calculated using computational fluid dynamics (CFD) simulations. In this study, the spherical silver particles were generated using furnace techniques and commercially available silver powder for different size ranges. The morphology of the particles was confirmed by electron microscopy and an effective density measurement. The effective density was also an important parameter in validating the model and simulations.

Finally, the critical velocity of rebound was determined for spherical silver aerosol particles in the size range of 20–1000 nm (Figure 1). The results show that the critical velocity of rebound decreases from 14 to 0.022 m/s as the particle size increases from 20 to 1000 nm. Furthermore, the critical velocity was found to be proportional to the power of –1.6 of the particle size, instead of the theoretical inverse proportionality. This result is in line with the previous studies for micron-sized particles (Wall et al., 1990). In the nanoparticle size range, the obtained critical velocity values are approximately 3 to 10 times greater than the recent literature values for silver particles (Rennecke & Weber, 2013). This discrepancy can most likely be explained by the different surface materials. All in all, our results give valuable information about the particle–surface interactions in the unexplored sub-micron size range.

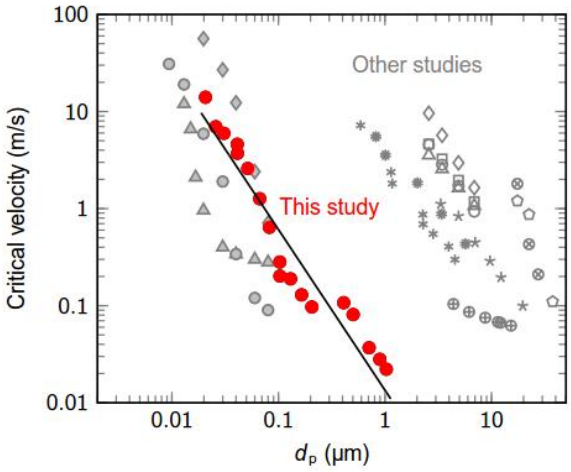

Figure 1. The critical velocity of rebound as a function of the particle size for spherical silver particles and an aluminium substrate. The results are seen in relation to other previous studies for a variety of different particle and surface materials.

The authors acknowledge the TUT's graduate school for financial support.

Arffman, A., Kuuluvainen, H., Harra, J., Vuorinen, O., Juuti, P., Yli-Ojanperä, J., Mäkelä, J. M. & Keskinen, J. (2015). The critical velocity of rebound determined for sub-micron silver particles with a variable nozzle area impactor. Submitted to *J. Aerosol Sci.*

Rennecke, S. & Weber, A. P. (2013). The critical velocity for nanoparticle rebound measured in a low pressure impactor. *J. Aerosol Sci.*, 58, 135–147.

Virtanen, A., Joutsensaari, J., Koop, T., Kannosto, J., Yli-Pirilä, P., Leskinen, J., Mäkelä, J. M., Holopainen, J. K., Pöschl, U., Kulmala, M., Worsnop, D. R. & Laaksonen, A. (2010). An amorphous solid state of biogenic secondary organic aerosol particles. *Nature*, 467, 824–827.

Wall, S., John, W., Wang, H.-C. & Goren, S. L. (1990). Measurements of kinetic energy loss for particles impacting surfaces. *Aerosol Sci. Technol.*, 58, 135–147.

The Development and Application of Unified Catalogues for Real-Time Multiband Fluorescence Signatures to Discriminate between Bioaerosol Classes

Mark Hernandez[3], Alina Handorean[3], Anne Perring[2], Greg Kok[1], Gary Granger[1], and Darrel Baumgartner[1]

[1]*Droplet Measurement Technologies, Boulder, Colorado, USA, 80302*
[2]*National Oceanic and Atmospheric Administration, Boulder Colorado, USA, 80303*
[3]*Dept. of Civil, Environmental and Architectural Engineering, University of Colorado, Boulder, USA, 80309*

Keywords: bioaerosol, on-line characterization, fluorescence

Rapid and accurate bioaerosol characterization is at the forefront of military and environmental surveys. Recent instrumentation and materials advances have led to the integration of lasers, UV flashlamps and high quality optical cavities, fitted with ultra-sensitive photon sensors that filter hi-fidelity signals into mobile electronic platforms (Pan et al, 2014). These are now available in prototype and commercial devices which can simultaneously report multiple optical properties, including multiple fluorescent spectra, in near real time. When gated for specific size ranges, these compound fluorescence instruments can be calibrated with particles engineered for this purpose (e.g. latex spheres), as well as airborne microbes of different origins. While a new generation of instruments has demonstrated the utility of leveraging particle fluorescence for PM characterization in laboratory (Saari, 2014) and field trials (Pohlker et al, 2012), the respective resolving power of various versions of these instruments—for discriminating between different classes of aerobiological particles—remains to be systematically catalogued. In this context, the optical recognition of whole cell microbial aerosols (and their fragments), is complex where considering master optical variables including nephelometric properties, and fluorescence spectra.

For certain microbial growth conditions, the cellular content and distribution of fluorescence varies widely across the microbial world, and specific fluorescent yields in whole cell microbial bioaerosols have been reported to have significant sensitivities to age, cultivation history, as well as environmental conditions (Saari, et al 2014). In addition to calibration practices, there as of yet exists no unified approach for challenging an emerging generation of fluorescence-based instruments and cataloguing the optical signatures associated with primary biological airborne particles (PBAPs) given their origins. While many PBAPs will produce fluorescence emissions, interpreting measurements for bioaerosol characterization (recognition) presents challenges that can be aided using referenced distributions of fluorescence emissions complimented with other optical properties.

We report here, selected optical properties of common models for bioaerosols, that were compiled from wideband bioaerosol sensor observations in a cohort of engineered chamber studies that were executed with aerosolized pure cultures of common airborne bacteria (12), fungi (35) and pollen grains (15) under reproducible conditions (RH and temp).

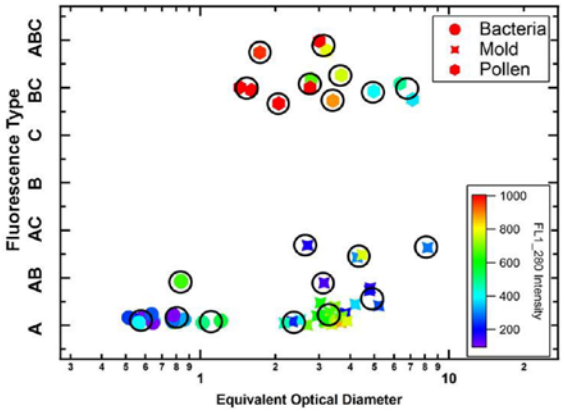

Figure 1. Grouping of selected optical scattering and fluorescence properties of common bacterial, fungal and pollen bioaerosols in controlled chamber studies.

Results suggest that three metrics—fluorescence type, fluorescence intensity, and nephelometric diameter—can resolve bioaerosol classes, as well as indicate physiological groupings in real time.

This work was supported by funding from the USA National Science Foundation, the State of Colorado, and Droplet Measurement Technologies.

Pan, Y, et al. (2014), Spectrally resolved fluorescence cross sections of aerosolized biological agents across 5 excitation wavelengths.., *Opt.Express*, *22*(7), 8165.

Pöhlker, C., J. A. Huffman, and Pöschl U. (2012), Autofluorescence of atmospheric bioaerosols fluorescent biomolecules and potential interferences, *Atmospheric Measurement Techniques*, *5*(1), 37.

Saari, et al (2014) Effects of fungal species, cultivation time, growth substrate, and air exposure velocity on the fluorescence properties of airborne fungal spore. *Indoor Air*, DOI:10.1111/ina.12166

The Effect of Inhaled Submicron Particles of a Nanocomposite Preparation in Mice with the Acute Respiratory Distress Syndrome

V.A. Vechkanov[1], A.S. Safatov[1*], L.N.Shishkina[1], S.L. Vedenchuk[1], E.I. Vereshchagin[2], A.V. Dushkin[3], L.P. Suntsova[3], N.A. Zhukova[4], T.G. Tolstikova[4]

[1]FBRI SRC VB "Vector", Koltsovo, Novosibirsk region, Russian Federation
[2]JSC "Biocomposite", Novosibirsk, Russian Federation
[3]ISSC&M SB RAS, Novosibirsk, Russian Federation
[4]RIOC SB RAS, Novosibirsk, Russian Federation
**Corresponding author: safatov@vector.nsc.ru*

Keywords: aerosol, nanocomposite, acute respiratory distress, mice.

The acute respiratory distress syndrome in humans results from toxic poisoning, viral pneumonia, etc. It requires surgical intervention to relieve changes in the lungs that can lead to a lethal outcome. This intervention can be the administration of effective antioxidants into the body.

The most effective way to deliver drugs to the lungs is the aerosol one. The experiments were carried out using laboratory animals, JCR mice weighing 23 - 25 g with artificially induced acute respiratory distress syndrome. The mice were primed with aerosolized solution of *E. coli 0127:B8* lipopolysaccharide at a dose of 5 mg/kg of body weight in combination with a preliminary intramuscular injection of lipopolysaccharide at a dose of 10 mg/kg.

The mechanochemically produced nanocomposite preparation of dihydroquercetin and arabinogalactan is characterized by high solubility, stability and bioavailability of the active ingredients due to the formation of 5-7 nm supramolecular complexes in the solution (Pribytkova *et al.*, 2011; Tolstikova *et al.*, 2011). The introduction of the submicron aerosol of nanocomposite solution (produced by highly stable aerosol generator with average particle size of 654 nm, geometrical standard deviation σ_g = 1.64, mass concentration of nanocomposite in aerosol of 0.3 mg/l, Vechkanov *et al.*, 2015) was carried out for 6 hours using an experimental device for exposure of mice shown schematically in Fig. 1, immediately after priming the animals (total inhaled dose of 17.3 mg/kg). Lethality was assessed after 24 hours. Three of 6 animals with induced acute respiratory distress syndrome died (50%). Therapy with aerosolized nanocomposite solution saved the lives of all 6 animals.

Thus, submicron aerosol of nanocomposite solution of dihydroquercetin and arabinogalactan showed promise when used to relieve the acute respiratory distress syndrome.

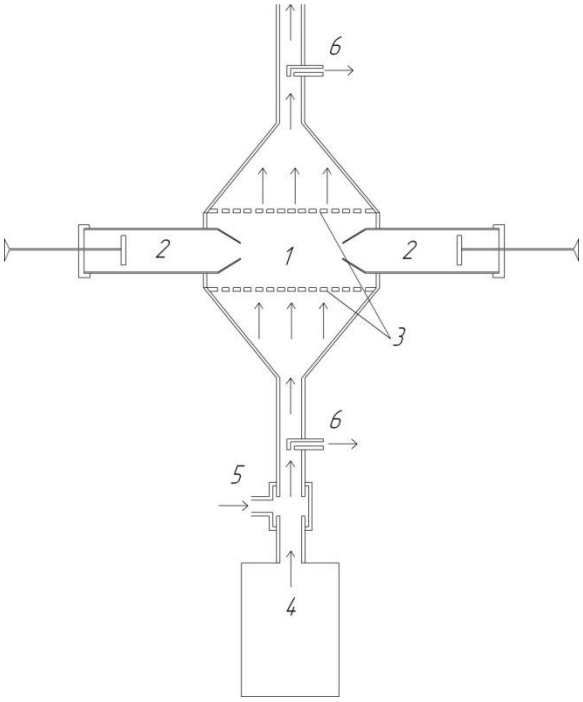

Fig. 1. Experimental device for exposure of mice. 1 – exposure chamber; 2 – decoy glass; 3 – rectifier; 4 – aerosol generator; 5 – diluting flow; 6 – control sampling points.

Acknowledgements

The work was supported by the Foundation for Assistance to Small Innovative Enterprises in Science and Technology, Government contract 10661p/19539 dated July 2, 2012.

References

Pribytkova, L.N., *et al.* (2011) *Chemistry of Natural Compounds*, **3**, 333-336.

Tolstikova, T.G., *et al.* (2011) Letters in Drug Design & Discovery, **8**, 201-204.

Vechkanov, V.A., *et al.* (2015) Russian Federation patent priority № 2014150336.

The MERMOSE project: Characterization of particulates emissions of a commercial aircraft engine

D. Delhaye[1], F.-X. Ouf[2], D. Ferry[3], C. Guin[1], S. Peillon[2], F. Salm[2], A. Crespin[1], I. Marhaba[3], D. Gaffie[1], O. Penanhoat[4], X. Vancassel[1], J.-J. Lecout[1], A. Vandestoc[1], E. Landais[1], C. Focsa[5], I.K. Ortega[5], J. Burguburu[4]

[1]*Onera – The French Aerospace Lab, F-91123 Palaiseau, France*
[2]*Institut de Radioprotection et de Sûreté Nucléaire (IRSN), BP 68, 91192 Gif-sur-Yvette Cedex, France*
[3]*Aix-Marseille Université, CNRS, CINaM UMR 7325, 13009, Marseille, France*
[4]*SNECMA/SAFRAN Group, Moissy Cramayel, 77550, France*
[5] *PhLAM, UMR CNRS 8523, Université de Lille 1, 59655 Villeneuve d'Ascq Cedex, France*

Keywords: Aircraft engine, combustion aerosol, size, composition, morphology.

Air transport is a continuously increasing commercial activity (Airbus, 2013; ICAO, 2013). Its environmental impacts on air quality and global warming (Lee *et al.*, 2010) are a main concern and request dedicated investigation.

In this framework, the French government funded several research projects in order to better understand the process that leads to the formation of condensation trails, to prevent and manage them. MERMOSE (http://mermose.onera.fr/en) is one of this projects dedicated to fill this gap. It aims to provide modern aircraft engine emission data and knowledge on emitted particles reactivity, mainly with water.

In 2014, a campaign coordinated by Onera has been performed behind a combustion chamber of the SaM146 aircraft engine. It follows a campaign conducted in 2013 behind a complete SaM146 engine at Snecma test bench (Delhaye *et al.*, 2014). During both campaigns Onera, IRSN, Snecma and CNRS research institutes (CINaM, PhLAM) made gas and particles measurements. On-line measurements and laboratory sampling were collected simultaneously for various engine thrust from 7% engine maximum take-off thrust to 100% including real cruise setting.

Sampling for laboratory characterizations have been obtained in order to feed a variety of instruments using different measurements techniques: microscopy (TEM) and chemical analysis (EC/OC ratio, XREDS, FTIR, laser and ionic desorption mass spectrometry, Raman spectroscopy). On-line monitoring of size distributions (SMPS+C, SMPS+E, DMS 500), mass (MAAP, Pegasor, filters) and number (CPC, Pegasor) concentrations and particle surface area density (NSAM) were also done.

The modal diameter of the particles ranges from 31 nm to 50 nm (figure 1), the particles denote a fractal morphology.

Emitted particles emission indices in terms of number and mass, size distributions and general properties determined during the combustor and the engine test campaigns will be compared. This will provide valuable information on the influence of combustion parameters on the emissions characteristics and the difference observed between emissions at the combustor exit and the engine exit.

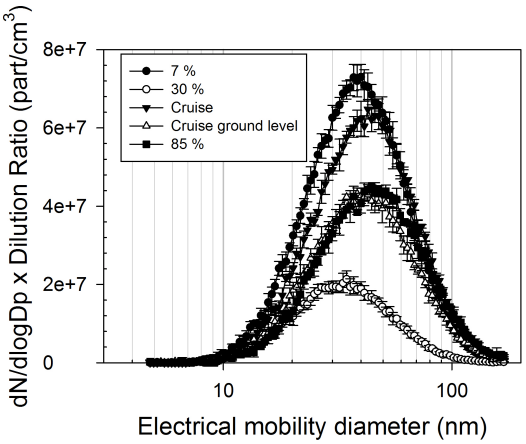

Figure 1. SMPS size distributions for various engine maximum thrusts behind a SaM146 aircraft engine representative tubular combustor.

Acknowledgements

This work was supported by the MERMOSE project for the characterization of emissions by aircraft engines and sponsored by DGAC (French Civil Aviation national funds).

References

Airbus, 2013, http://www.airbus.com/company/market/forecast/

ICAO, (2013), ICAO environmental report, aviation and climate change

ICAO, (2008). International Standards and Recommended practices, annex 16, volume II Aircraft engine emissions, 3rd edition.

Lee, D.S., G. Pitari, V. Grewe, K. Gierens, J.E. Penner, A. Petzold, M.J. Prather, U. Schumann, A. Bais, T. Berntsen, D. Iachetti, L.L. Lim, R. Sausen (2010). *Transport impacts on atmosphere and climate: Aviation. Atmospheric Environment*, **44**, 4678-4734.

Delhaye, D. F.-X. Ouf, D. Ferry, D. Gaffie, O. Penanhoat, S. Peillon, F. Salm, X. Vancassel, T. Cottard, C. Focsa, N. Harivel, B. Perez, E. Quinton (2014), International Aerosol Conference, Busan

Thermophoretic thin film deposition of self-assembled carbon nanotubes

J.L. de La Verpilliere and A.M. Boies

Department of Engineering, University of Cambridge, CB2 1PZ, Cambridge, UK

Keywords: carbon nanotubes, self-assembly, thermophoretic precipitator, thin film, nanomaterials

In order for the outstanding properties of individual carbon nanotubes (CNTs) to be transferred into commercial products, control of the nanomaterial's organisation at the nano, micro, and macro scales needs to be considered holistically when devising the manufacturing process. Gas-phase processes are continuous and inherently scalable, enabling *large scale* production volumes, while the power of self-assembly allows for a precise control of the final structure at the *microscale* and *nanoscale*. The present work proposes a novel illustration of this concept: so-called self-assembled CNT sea urchins are synthesized after a gas-phase process pioneered by Kim *et al.* (2010), and continuously deposited on a substrate using thermophoresis as the driving force. The resulting nanomaterial presents interesting properties in terms of nanostructure, porosity, electrical and thermal conductivity. Properties of the final material being largely influenced by particle deposition parameters, the design of the custom-made thermophoretic precipitator used in this study will also be discussed.

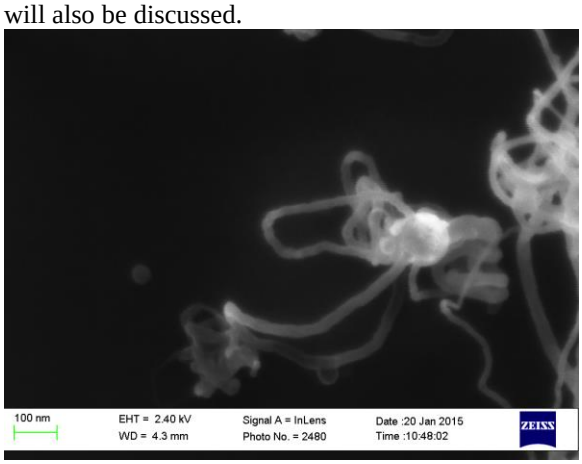

Figure 1. Scanning Electron Microscope (SEM) image of a CNT sea urchin consisting of a 100 nm diameter alumina and iron oxide composite core and ≈ 20 nm diameter radially grown CNTs.

An aqueous solution of aluminium nitrate $Al(NO_3)_3$ and iron nitrate $Fe(NO_3)_3$ is atomized in a flow of nitrogen using a collision nebulizer followed by a silica gel drier. Upon water droplet evaporation, both metallic salts precipitate, forming spherical composite nanoparticles with an aluminium-enriched surface consisting of small iron nitrate patches in an aluminium nitrate matrix. A first tube furnace is used to thermally decompose the metal nitrates in a reducing atmosphere, thus producing bimetallic Al-Fe nanoparticles. These nanoparticles form the core of the CNT sea urchins that are grown in a subsequent step, whereby a carbon source catalytically decomposes on the small iron patches at the surface of the particles in a second tube furnace, thus enabling CNTs to grow radially from the cores. An example of such self-assembled CNTs is displayed in figure 1. SEM, TEM, XRD, EELS, Raman spectroscopy, and TGA characterization of the as produced nanoparticles was performed in order to optimize the process to synthesize a high density of small diameter, long, straight CNTs on the surface of the cores.

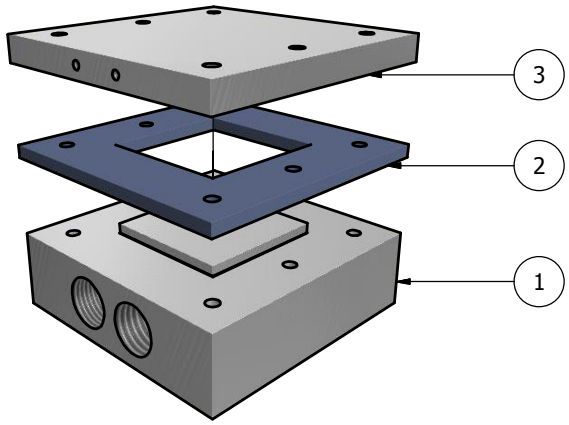

Figure 2. Sketch of the custom made precipitator: 1) cold plate, 2) insulating gasket, 3) hot plate.

A thermophoretic precipitator, shown on figure 2, allowing for high-efficiency controlled thin film deposition on a silicon wafer over a 5 cm^2 area was designed with the help of three dimensional simulations on COMSOL Multiphysics®. Theoretical and experimental deposition efficiencies and uniformities are compared. The model was us The thermophoretic precipitator was then used to deposit thin films of CNT sea urchins. Electrical conductivity of the resulting films was measured using the four points probe method, thermal conductivity and porosity were estimated using standard techniques.

Overall it is hoped that this work will contribute to the development of aerosol-based processes for the commercialization of nano-manufactured products.

Kim, S. H., Wang, C., & Zachariah, M. R. (2010). *Journal of Nanoparticle Research*, *13*(1), 139–146.

Titania–silver composite nanoparticles with interesting morphology

Juha Harra, Paxton Juuti, Janne Haapanen, Miika Sorvali and Jyrki M. Mäkelä

Aerosol Physics Laboratory, Department of Physics, Tampere University of Technology, Tampere, Finland

Keywords: aerosol synthesis, particle surface coatings, titanium dioxide, silver.

Metallodielectric composite nanostructures have found use in a multitude of applications due to their unique properties, such as, catalytic, electrical and optical. The optical properties of noble metal nanoparticles are particularly interesting because of the plasmon resonance of the conduction electrons, whose wavelength can be tuned with the particle size (Harra *et al.*, 2012), as well as, with the particle morphology. Different morphologies of the composite particles, for example, core–shell and decorated structure (Zdanowicz *et al.*, 2013, 2014), each produce individual optical responses. Thus, the ability to tailor the particle morphology has great advantages.

In this study, we explore the synthesis of titania–silver (TiO_2–Ag) composite nanoparticles via an evaporation–condensation method. First, aqueous suspension of Liquid Flame Spray (LFS) -generated (Haapanen *et al.*, 2015) titania nanopowder was sprayed with an atomizer aerosol generator into a nitrogen flow (Harra *et al.*, 2013). The aerosolized titania nanoparticles were sintered in a tube furnace from agglomerates to a spherical shape at a temperature of 1500 °C. This sintering step was followed by a particle size selection with a differential mobility analyzer. After that, the particles passed through a second tube furnace containing a small piece of bulk silver at the center. Here, we investigate the effect of the silver evaporation temperature to the mobility size of the sintered and size-selected titania particles using a scanning mobility particle sizer.

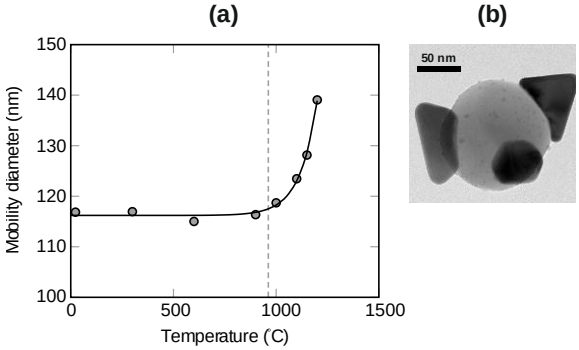

Figure 1. (a) The mobility diameter of the size-selected titania particles as a function of the silver evaporation temperature. The dashed line indicates the melting point of bulk silver (962 °C). (b) A TEM micrograph of a titania–silver composite nanoparticle synthesized at a temperature of 1200 °C. The size bar is 50 nm.

Figure 1(a) shows the mobility diameter of the titania particles as a function of the silver evaporation temperature. At lower temperatures, no change in the particle size is observed. However, when the evaporation temperature exceeds the melting point of bulk silver, we see an increase in the mobility size of the particles. This exponential particle growth as a function of the evaporation temperature suggests that some silver vapor has condensed onto the titania particles. At the maximum evaporation temperature of 1200 °C, the mobility diameter of the 120 nm titania particles increases approximately 20 nm.

A transmission electron microscope (TEM) image of a titania–silver composite nanoparticle synthesized using a silver evaporation temperature of 1200 °C is presented in Figure 1(b). The micrograph shows that three crystalline-looking silver structures (darker shade) have grown onto the spherical titania particle (lighter shade).

In summary, the amount of silver on titania nanoparticles was controlled with the evaporation temperature of the silver. The morphology of the resulting composite particles differs from the usual decorative dots obtained with similar methods. Thus, more study on the growth mechanism of the silver structures is required. Finally, we expect to achieve interesting optical responses from the produced nanomaterial, and the nanoparticles could be utilized, for example, in plasmonic and nonlinear optical applications.

J. Harra acknowledges the TUT's graduate school for financial support.

Haapanen, J., Aromaa, M., Teisala, H., Tuominen, M., Stepien, M., Saarinen, J. J., Heikkilä, M., Toivakka, M., Kuusipalo, J., & Mäkelä, J. M. (2015). *Mater. Chem. Phys.*, 149–150, 230–237.

Harra, J., Mäkitalo, J., Siikanen, R., Virkki, M., Genty, G., Kobayashi, T., Kauranen, M., & Mäkelä, J. M. (2012). *J. Nanopart. Res.*, 14, 870.

Harra, J., Nikkanen, J.-P., Aromaa, M., Suhonen, H., Honkanen, M., Salminen, T., Heinonen, S., Levänen., E., & Mäkelä, J. M. (2013). *Powder Technol.*, 243, 46–52.

Zdanowicz, M., Harra, J., Mäkelä, J. M., Heinonen, E., Ning, T., Kauranen, M., & Genty, G. (2013). *Appl. Phys. Lett.*, 103, 251907.

Zdanowicz, M., Harra, J., Mäkelä, J. M., Heinonen, E., Ning, T., Kauranen, M., & Genty, G. (2014). *Sci. Rep.*, 4, 5745.

Toward industrial scale incorporation of nanoparticles onto catalytic membrane by aerosol route

J. Feng[1], C. Denonville[2], X. Guo[3], M. Fontaine[2], H. Fjeld[4], A. S. Azar[2] and A. Schmidt-Ott[1]

[1]Department of Chemical Engineering, Delft University of Technology, 2628 BL, Delft, The Netherlands
[2]SINTEF Materials and chemistry, Oslo, Norway
[3]Karlsruher Institut für Technologie, Karlsruhe, Germany
[4]Protia AS, Oslo, Norway

Keywords: nanoparticle, spark ablation, catalysis.

Aerosol methods, including spark discharge and arc discharge, represent industrial scale routes to nanomaterials on account of their continuous nature. Recently, these methods have been used to prepare size, shape, composition and architecturally controlled nanostructures for a range of metallic materials (Pfeiffer *et al*., 2014; Byeon & Kim, 2012; Cole *et al*., 2010). Here we demonstrate a general method for the synthesis of metallic nanoparticles distributed on a ceramic membrane as catalysis. The membrane is designed to separate H_2 from the steam methane reforming process.

Our approach of covering membrane discs with Ni NPs of any size makes use of the fact that diffusional deposition of atomic cluster sized species is extremely efficient. For the coating method to approach the industrial scale, a new high frequency spark system is applied (Pfeiffer *et al*., 2014). TEM micrographs (Figure 1) of the deposited material show agglomerates of primary particles smaller than 4 nm in diameter. The deposited particles are still smaller, and being liquid-like at room temperature, they coalesce until they reach the primary particle size.

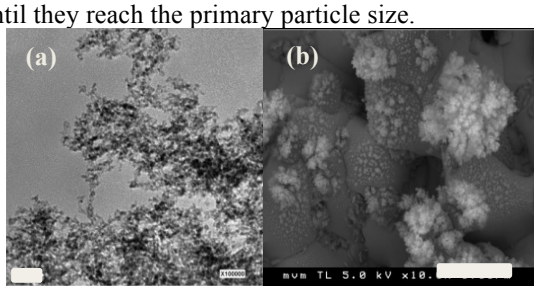

Figure 1. TEM and SEM of as-deposited Ni NPs, scale bar 20 nm (a) scale bar 3 µm (b)

Annealing to required reaction temperatures of 700 ℃ for 1 h (Figure 2 left column) and 900 ℃ for 100 h (Figure 2 right column) in H_2 atmosphere leads to coalescence of the primary particles to form larger units. The SEM studies revealed that at small coverages (10 min deposition in Figure 2a, b) the NPs can form a quasi-continuous pattern with characteristic dimensions in the range of a few tens of nanometers. At higher coverages (1000 min deposition in Figure 2e, f) the deposited material adopted a round shape. Thicker coverages coalesce to form larger particles. We conclude that at small coverages the structure of the substrate has a larger influence on the patterns of the deposited material after annealing. Figure 2 shows that the resulting particle size after heating treatment essentially depends on the deposited mass per unit area. The art is now to find the size dependence for optimum catalytic activity.

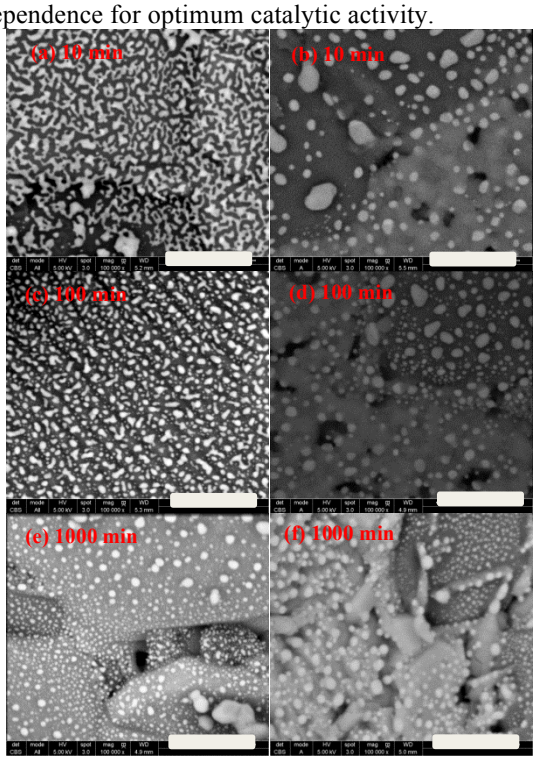

Figure 2. SEM micrographs of Ni NPs on ceramic discs exposed to 700 ℃ for 1 h (left column) and 900 ℃ for 100 h (right column) in H_2.

In summary, our trick to obtain high surface coverage that is independent on the roughness of membrane discs is to produce small enough particles at high yield, so that diffusional deposition is effective.

The research leading to these results has received funding from the European Union's Seventh Framework Program under Grant Agreement No. 280765 (BUONAPART-E).

Pfeiffer, T. V., Feng J. & Schmidt-Ott A. (2014). *Adv. Powder Technol.*, 25, 56-70.

Cole, J. J., Lin E.C., Barry, C.R. & Jacobs, H. O. (2010). *Small*, 6, 1117-1124.

Byeon, J., Kim, Y. (2012), *Nanoscale*, 4, 6726-6729.

Towards a Portable NanoParticle Sizing System

G. Lewis[1], S. Spielman[1], S. V. Hering[1], W. Mui[2] and R .C. Flagan[2]

[1]Aerosol Dynamics Inc., 935 Grayson St, Berkeley, CA 94710, USA
[2]Department of Chemical Engineering, California Institute of Technology, Pasadena, CA 91125, USA
Keywords: nanoparticle, condensation particle counter, mobility size separation, size distribution

Knowledge of nanoparticle size and concentration are important to industrial hygiene, for understanding worker exposures in traditional occupations, such as welding or transportation, and in the rapidly evolving nanomaterials industry. Globally, nanoparticles are formed through atmospheric nucleation processes, and can grow rapidly to form cloud condensation nuclei that affect the nature and extent of Earth's cloud cover. Both applications need small, portable monitors that can be worn, or operated at remote sites, or deployed on tethered balloons or unmanned aircraft.

Reported here is the preliminary development of technology that would make such a portable sensor feasible. Our instrument utilizes the opposed migration aerosol mobility size classifier (OMAC) developed at the California Institute of Technology, and the self-sustaining, laminar-flow water condensation particle counter developed by Aerosol Dynamics.

The opposed migration aerosol classifier provides particle size-selection based on electrical mobility in an inherently compact form. In contrast to the typical mobility systems, in which the electric field moves charged particles at right angles to the flow streamlines, the OMAC is configured to such that the particle motion is directly opposite the direction of the flow. This allows for larger particle (low mobility) size segregation in a smaller geometry. The critical dimensions are about 5% of the volume of the commercially available differential mobility columns that span the same size range (Flagan, 2004; Mui et al, 2013).

The self-sustaining water condensation counter counts individual particles as small as 5 nm through condensational enlargement and optical detection, much as done by benchtop instruments. The key difference is that it does not require a liquid reservoir. Referred to as MAGIC, for ***m***oderated ***a***erosol ***g***rowth with ***i***nternal water ***c***ycling, this new design incorporates a "moderator" stage that allows the water vapor to be recovered internally (Hering et al, 2014). Because it has no external water reservoirs, MAGIC performs equally well when tipped, jostled or inverted. Moreover, the water stored within the wick is sufficient to sustain operations for days to weeks, depending on prevailing humidity conditions. Shown in Figure 1, it is relatively small.

Figure 1. MAGIC self sustaining water condensation particle counter.

We have combined these two technologies to provide a OMAC-MAGIC sizing system. Figure 2 compares results from the OMAC-MAGIC to those from a collocated scanning mobility size spectrometer (SMPS) while sampling ambient air in Berkeley, CA. Both instruments captured the morning rush on the first day of operations (Jan 24th, a Friday), as well as the midday traffic on the following day (a Saturday). Linear regression of 12-min averaged data against that from the SMPS yield slopes of 1.11, 1.04 and 1.00 for particle number, surface area and geometric mean diameter, respectively. R^2 values were greater than 0.90, and the relative standard deviation was 9% in number, 5% in surface area and 2% in particle diameter.

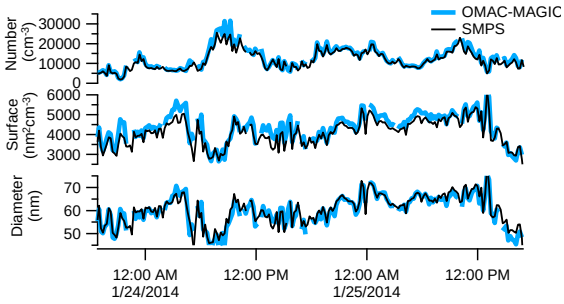

Figure 2. Number concentration, surface area, and mean particle diameter time lines for ambient aerosol obtained with collocated OMAC-MAGIC and SMPS.

This work was supported by the U.S. Department of Health and Human Services, National Institute of Occupational Safety and Health, grant OH-010515.

Flagan, R. C. 2004. Opposed Migration Aerosol Classifier, *Aerosol Science and Technology*, 38:890-899.

Hering, S. V., Speilman, S. R., Lewis, G. L. (2014). Moderated, water-based condensational growth of particles in a laminar flow. *Aerosol Science and Technology* 48:401-408.

Mui, W. D.A. Thomas, A. J. Downard, J. L. Beauchamp, J. H. Seinfeld and R. C. Flagan (2013), Continuous Flow Ion Mobility Mass Spectrometry with a Radial Opposed Migration Ion and Aerosol Classifier (ROMIAC)*Anal. Chem.* 85 6319-6326.

Towards standardized measurements of atmospheric aerosol particle number concentration

J. Vanhanen[1]

[1]Airmodus Ltd., Pietari Kalmin katu 1 F 1, 00560, Helsinki, Finland

Keywords: Standardization, number concentration, fine particles, CPC

Regulatory measurements of atmospheric aerosol particle concentration are to this date all based on measuring the mass of the particles. Ultrafine particles (diameter below 100nm) have insignificant contribution to the total mass of particles. The growing awareness of the importance of the ultrafine particles has raised a question of measurement metric of atmospheric particle concentration. Instead of mass, aerosol number concentration should be measured. Technology for particle number concentration measurement has been available commercially from 1980 (McMurry, 2000). Condensation particle counters grow particles using condensation of a working fluid (e.g. n-butanol) to increase the particles size up to optically detectable sizes, and then counts them individually by using laser particle counting method.

In order to measure particle number concentration of atmospheric aerosol in accurate and reproducible manner a standardized method is needed. This method is being developed by CEN / TC 264 / WG 32. The scope of the work is to describe standard method for determining the particle number concentration in ambient air in the range up to about 10^7 cm^{-3} for averaging times equal to or larger than 1 min. The size range of the measurement is from 7 nm up to a few micrometres in particle diameter.

The standard method describes both particle sampling and counting. The counter should have 50% lower cut-off limit of 7 ± 1 nm and use n-butanol as a working fluid. Detection efficiency should exceed 90% at < 14 nm and the upper limit should be above 1000 nm ± 100 nm. The CPC should be able to measure concentrations between lower limit of 10-100 cm-3 up to upper limit of at least 10 000 cm-3 with a slope of 1 ± 0.05. The dynamic range should be at least 3 orders of magnitude and the response time should be below 5 s.

The sampling in the standard method takes into account the relative humidity of the sample, diffusion losses for 7nm particles and the particle concentration of the sample. The relative humidity should be kept lower than 40%. Three cases should be considered with respect to the temperature conditions: 1. if the room temperature is higher than 22°C no aerosol dryer is needed if the ambient dew point never exceeds 10°C, 2. if the dew point is between 10°C and the room temperature, the instrument flow shall be dried, 3. in case that the dew point temperature is above the room temperature, the sample flow shall be dried before entering the room. The total losses for 7nm particles in the total sampling system should be less than 30%. Dilution should be used if without dilution the CPC would be in the photometric measurement mode.

The standard describes a list of test and measurement procedures that should be taken into account while performing standardized measurements. They include all the important parameters that will affect the total accuracy and reproducibility of the measurement. The standard includes variety of quality assurance and quality control procedures to ensure high quality measurements. Also some informative information about the data reporting is given based on the EUSAAR project.

McMurry, P. H. (2000). *Aerosol Science and Technology*, 33, 297-322.

Transformation of diesel vehicle exhaust, pellet boiler exhaust, and their mixture in an environmental chamber

A. Leskinen[1,2], P. Yli-Pirilä[2], L. Hao[2], J. Kim[2], T. Torvela[3], E. Asmi[4], D. Brus[4], J. Grigonyte[3], A. Jaatinen[2], E. Kari[2], A. Kortelainen[2], K. Kuuspalo[3], H. Lamberg[3], J. Leskinen[3], U. Makkonen[4], P. Miettinen[2], I. Nuutinen[3], T. Raatikainen[4], O. Sippula[3], H. Hakola[4], J. Jokiniemi[3], A. Virtanen[2], M. Komppula[1], K.E.J. Lehtinen[1,2]

[1]Finnish Meteorological Institute, P.O.Box 1627, FI-70211 Kuopio, Finland
[2]Department of Applied Physics, University of Eastern Finland, P.O.Box 1627, FI-70211 Kuopio, Finland
[3]Department of Environmental Science, University of Eastern Finland, P.O.Box 1627, FI-70211 Kuopio, Finland
[4]Finnish Meteorological Institute, P.O.Box 503, FI-00101 Helsinki, Finland

Keywords: diesel, pellet boiler, exhaust, aging, environmental chamber

Aerosols are known to induce both health and climate effects, which are connected to the aerosol physicochemical properties. In the atmosphere, the aerosol properties change in transformation processes, which can be studied, e.g., in environmental chambers.

Diluted exhausts of a diesel vehicle, a pellet boiler burning softwood pellets, and their mixture was injected into a 29 m^3 environmental chamber. In some experiments also ozone, nitrous acid, acting as a hydroxyl radical (OH) precursor, and/or alphapinene was injected. The mixture was aged for 4 hours under UV irradiation. During the aging the size, number concentration, hygroscopic growth factor (HGF), chemical composition, morphology, optical properties, and mixing state of the particles, as well as concentration of nitrogen oxides, sulfur dioxide, ozone, selected ions, and volatile organic compounds in the gas phase were monitored.

The mobility and projected area equivalent diameters of the particles from both sources, both separately and in the mixture, increased from 80–90 to 120–130 nm during aging. Meanwhile, the number concentration decreased, but aerosol volume increased by 10–30 %.

The initial mass concentration was 45 (pellet) or 35 µg/m^3 (diesel). The concentration of particulate organics increased from 4 to 12 µg/m^3 (pellet) or remained at 2 µg/m^3 (diesel). The initial NO concentrations were 16–46 ppb (pellet) and 81–143 ppb (diesel). The increase in organics originates from secondary organic aerosol (SOA) formation, which is known to be more intense, when nitrogen monoxide (NO) concentration is lower (Ng *et al.*, 2007).

The concentration of particulate nitrate increased from 1 to 8 µg/m^3 (pellet) or was very low (diesel). The increase was faster when OH was present (Figure 1). The HGF for 100 nm particles was initially and remained at 1.55–1.60 (pellet), indicating very hygroscopic particles, or remained at 1.01–1.03 (diesel), indicating hydrophobic particles. A small decrease in the fractal dimension of pellet burner exhaust particles was seen.

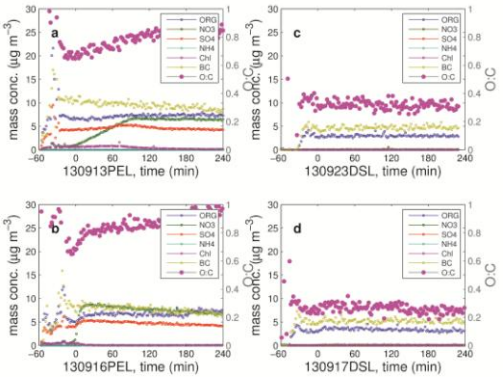

Figure 1. The chemical composition of aerosol from pellet boiler (a,b) and diesel engine (c,d) in the absence (a,c) and presence (b,d) of OH precursors.

The evolution of the mixed aerosol was a combination of the separate emissions. Both more and less hygroscopic fractions were seen, and the particles from each source could be separated from the electron micrographs. The HGF of the less hygroscopic fraction increased to 1.05, while that of the more hygroscopic fraction decreased from 1.60 to 1.45 or as low as 1.35 when alphapinene was present. The increase in particulate organics was less than (the expected) 50 % of that observed in the pellet boiler exhaust experiment, indicating that the high NO concentration of the diesel exhaust might inhibit the SOA formation.

In conclusion, the diesel vehicle exhaust is quite passive during aging while the pellet boiler exhaust produces SOA and particulate nitrate. In the mixture the particles are externally mixed, whereas the gas phases mixed and affected, e.g., the SOA formation potential of the individual emissions.

The infrastructure used in this work has been supported financially by the ERDF, Tekes, and the strategic funding of UEF (Sustainable Bioenergy, Climate Change and Health).

Ng, N. L., Kroll, J. H., Chan, A. W. H., Chhabra, P. S., Flagan, J. H., & Seinfeld, J. H. (2007). *Atmos. Chem. Phys.*, 7, 3909-3922.

Transient particulate emissions of a modern diesel passenger car under real-world driving conditions

H. Wihersaari[1], P.Karjalainen[1], L. Pirjola[2], A. Malinen[2], J. Keskinen[1] and T. Rönkkö[1]

[1] Department of Physics, Tampere University of Technology, P.O. Box 692, Tampere FI-33101, Finland
[2]Department of Technology, Metropolia University of Applied Sciences, P. O. Box 4021, FI-00180 Helsinki, Finland

Keywords: transient emissions, exhaust particles, diesel, engine braking

Particulate mass has been proven to impose a health risk. As legislation has brought more stringent emission limits, measuring particulate mass emissions have come down to the limit of detection. Positive loading caused by condensing hydrocarbons on the weighted filter is a problem in the sensitive measurement. As a solution, the emitted number concentration has been adopted as a part of regulated components in vehicle exhaust in Europe. The emissions factors of light-duty vehicles are determined by measuring the emissions over the New European Driving Cycle (NEDC) and averaging them over the distance travelled.

We measured the size distribution and number concentration of the exhaust particles of a modern Euro 5 -compliant diesel passenger car under transient real-world driving conditions. The aim was to compare the particulate emissions produced with three different lubricant oils. Measurements were conducted in two phases: a laboratory and an on-road campaign.

In the laboratory campaign, the car was driven on a chassis dynamometer. Transient cycles such as NEDC, US06 and custom cycles were driven in addition to three steady driving conditions. The sample was taken from the tailpipe with a porous tube –type diluter followed by an ageing chamber and an ejector –type diluter. Particle number concentration and size distributions were measured with an UCPC, ELPI and EEPS. A thermodenuder operated at 265 °C was used to distinguish dry particles.

The on-road campaign was conducted in a remote location by chasing the test vehicle with a mobile emission laboratory (Pirjola et al., 2004). Steady speeds and custom transient cycles similar to those used by Karjalainen et al. (2014) were driven. The distance between the vehicles was kept at 10 meters and the sample was taken from the exhaust plume at the front bumper of the emission laboratory, at a height of 0.7 meters from the ground.

The diesel particulate filter was observed to remove practically all particles from the engine exhaust. Therefore, the aftertreatment system was removed or bypassed during some measurements in order to determine the effect of lubricant on the particulate emissions.

During acceleration and steady speeds the car was found to emit a unimodal soot mode. Under transient driving conditions with the aftertreatment system bypassed, the vehicle emitted particles even when not fuelled. The worst emission factor was roughly 20-fold compared to the current particle number limit in Europe. The size distributions of particles emitted during engine braking at the chassis dynamometer were bimodal. The two modes were located at 10-20 nm and at 100 nm, see Figure 1. Thermodenuded samples indicate that the larger mode consists of non-volatile particles and the smaller mode has a non-volatile core with volatile material condensed on the surface.

Particles of this size may penetrate into the lungs and impose a health risk. The emissions with the aftertreatment system bypassed resemble diesel passenger cars (Euro 4 or worse emission level) or cars with malfunctioning aftertreatment systems.

Previous studies (Rönkkö et al., 2014; Karjalainen et al., 2014) have reported similar results for HD diesel vehicles and GDI passenger cars, but this is the first study reporting particulate emission during engine braking for a diesel passenger car.

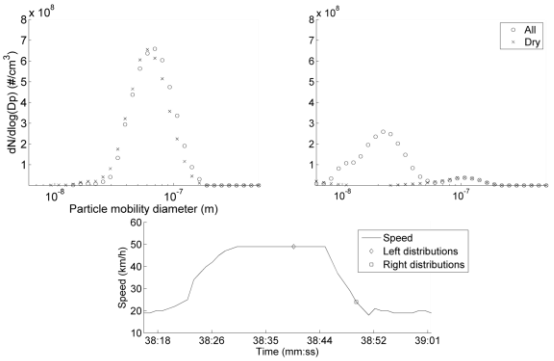

Figure 1: Change in particle size distribution during a transient driving cycle

The study was part of the TREAM project funded by Ecocat Oy, Neste Oil Oyj, AGCO Power Oy, Ab Nanol Technologies oy and Tekes (the Finnish Funding Agency for Innovation).

Karjalainen, P. *et al.* (2014). Atmospheric Environment, 97, 262-270.

Pirjola, L. *et al.* (2004). Atmospheric Environment, 40, 867-879.

Rönkkö T. *et al.* (2014). Environmental Science & Technology, 48, 2043-2050.

Types of Aerosol Formed by Condensation

Charles Clement

15 Witan Way, Wantage, Oxon OX12 9EU, U.K.
Keywords: condensation, nucleation, aerosol formation
Presenting author email: charles.clement@btinternet.com

Aerosols are widely formed in the atmosphere and in industry by a variety of processes and it is important to answer two questions about each process: does the condensation occur on existing aerosol? ; what are the characteristics of the size distribution of the new aerosol? These characteristics can strongly affect the climate via number of cloud condensation nuclei formed and can create potential health hazards. For example, ultrafine particles in the workplace can be highly injurious to health (Vincent and Clement 2000). Here we classify the different physical processes and expected size distributions and point out theoretical problems in their calculation.

Type 1. Gas-to-Particle Conversion

Condensable molecules are formed by photochemical reactions homogeneously in the atmosphere. In the upper troposphere the rapid production of sulphuric acid aerosol, and its possible suppression by existing aerosol, have been comprehensively investigated (Clement *et al* 2006). Its size distribution quickly becomes specified by coagulation, making the nucleation process irrelevant. At the surface, observations in Finland and elsewhere reveal a now familiar "banana-shaped" growth in new aerosol size distributions with time which shows the initial nucleation to be cut off by condensation on the aerosol produced. Nucleation may be suppressed altogether by enough existing aerosol. The common features of this type of aerosol formation are spatial homogeneity and a distribution growing with a single peak. Ultrafine particles disappear quite rapidly.

Type 2. Vapour Cooling at Constant Pressure.

In this case there are two main subtypes corresponding to cooling by gas or cooling at solid or liquid surfaces. Cooling by radiation is also possible, e.g. at the top of radiatively thick ground mists, but it will not be discussed here.

2A. Cooling by Gas Mixing

This occurs when plumes enter the atmosphere, for example from volcanoes or industry. The cooling process involves both heat and mass transfer, in particular heat conduction and vapour diffusion, and also motion of both existing aerosol and newly created particles. Differences in these motions means that there is no spatial homogeneity and nucleation is often highly localised. As indicated in calculations of aerosol formation in a volcanic plume (Clement and Mather (2005) and in laboratory experiments in mixing (Buckle and Mawella 1987), suppression of nucleation by existing aerosol may not occur and more than a single aerosol may be formed. Altogether, condensation can result in an aerosol with a very wide size distribution with significant numbers of ultrafine particles. Significant hazards can arise from any processes involving potentially toxic materials at high temperatures. Aerosol emissions from steel plants have caused large adverse health effects in the past and similar problems may exist today.

Although, basic equations for the calculation of aerosol formation by mixing have been formulated, there are major difficulties in their implementation. One problem is the lack of experimental data on nucleation rates of materials at high temperatures. Where aerosol motion is also involved, especially in turbulent flows, adequate theory does not exist.

2B Cooling at Surfaces

Aerosol formation can occur from both diffusion to a colder surface and vapour evaporation into a cold flow. Atmospheric examples exist and this is a common problem in industrial situations such as flows in pipes. Again, motion of aerosol must be included in the theory, particularly in and out of thermal boundary layers where nucleation is likely to occur. Examples exist where new aerosol formation is not inhibited by large amounts of existing aerosol, so that two or more aerosols can be formed. Only limited theory exists on the subject, but it is possible to predict that nucleation probability increases with increase in pipe velocity.

Type 3. Cooling by Pressure Drop.

Clouds are formed by upward motion in the atmosphere and aerosols are often formed locally in high pressure jets. If this occurs into an empty space, there is spatial homogeneity and nucleation is followed by aerosol growth, resulting in a highly peaked aerosol size distribution with no small particles or droplets. As the space usually contains a gas, entrainment and mixing can occur and experiments with a free turbulent jet were performed by Lesniewski and Friedlander (1998) showing that an additional aerosol could be formed at high vapour concentrations. For atmospheric clouds formed by rising air, the wide size distributions observed in them still require a full satisfactory explanation.

Buckle, E.R. and Mawella, K.J.A. (1987) *J. Aerosol Science*, 18, 139-146.

Clement, C. F., Pirjola, L., Twohy, C.H., Ford, I.J., and Kulmala, M. (2006) *J. Aerosol Science*, 37, 1717-1729.

Clement, C.F. and Mather, T.A. (2005) Abstracts of the European Aerosol Conference ed. W. Maenhaut p178

Lesniewski, T.H. and Friedlander, S.K. (1998) *Proc.Math. Phys. & Eng. Sci*. 454, 2477-2504..

Vincent, J.H. and Clement, C.F. (2000) Phil. Trans. R. Soc. Lond. A **358** 2673-2682**.** 454, 2477-2504.

Urban air quality measurements in Beijing, China, using a PPS-M sensor

M. Dal Maso[1], J. Gao[2], A. Järvinen[1], and T. Rönkkö[1]

[1]Department of Physics, Tampere University of Technology, P.O. Box 692, 33101, Tampere, Finland
[2]Chinese Research Academy of Environmental Sciences, Beijing, China

Keywords: atmospheric aerosols, measurement, urban aerosol, haze

Concern regarding the harmful health effect of airborne particles has increased the demand for observations and data on the concentrations of harmful aerosol particles. Current methods for observations of the number concentration of harmful particles have yet to become affordable enough to allow the construction of dense measurement stations that would provide data on the high spatial resolution required for effective measures to lower population exposures. A promising, economically affordable and operationally robust method for harmful aerosol measurements are diffusion charging-based aerosol sensors, such as the Pegasor PPS-M (Lanki et al., 2011).

The aim of this study was to deploy the PPS-M instrument in a highly-polluted urban setting over a longer time period to evaluate the instruments response in varying aerosol loadings. Because the response of the PPS-M depends on the size distribution of the ambient aerosol, we compared the PPS-M data with data from a MSP Wide Range Particle Spectrometer (WPS).

In addition to studying the PPS-M data, we also performed measurements in which the PPS-M was set up to operate with variable trap voltages applied. The instrument trap voltage is known to affect the particle size-dependent response function, and therefore our aim was to investigate the differences in the PPS signal with different PPS-M trap voltages, and explore the possibilities of using this information to gain insight in on the size distribution using only the PPS-M instrument.

Based on these aims, this study will a) describe PPS-M measurements and the analysis of the data in the polluted Beijing megacity oover a period of XX months; b) present a general overview of the types of aerosol size distrubutions and their variation observed at the site of observation; c) show the response of the PPS-M instrument to ambient aerosol number, mass and surface area concentrations.

The PPS-M was installed at the roof of a building at the Chinese Research Academy of Environmental Sciences, situated in the city of Beijing, China, but somewhat outside the city center. The station is also equipped with a range of other aerosol measurement devices along with trace gas and meteorology instrumentation.

The PPS-M instrument was collecting data from February to December; starting from October, the instrument was modified to use variable trap voltages. PPS_M data coverage in the first period is around 85%. The data coverage for simultaneous WPS and PPS-M is ca. 40%.

Analysis of the size distribution data showed that the aerosol size distribution was highly variable in the Beijing air. k-means clustering of the normalized size distribution data showed that at times, the aerosol was loaded with fresh nanosized particles, while at times the aerosol was clearly dominated by the accumulation size. The variability in the size distribution was also reflected in the PPS-M response, which varied with the aerosol size distribution.

Based on the WPS size distribution, we applied the response model developed by Rosted et al, (2014) to the data (see Fig. 1). Using the data with variable trap voltages, we were able to develop a calibration expression for total particulate volume and number using only PPS-M data.

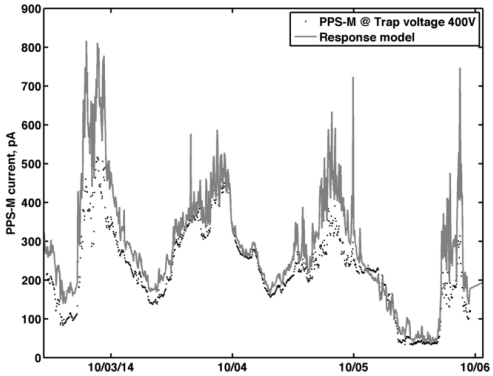

Figure 1: Example time series of observed PPS-M data and calculated response model data at CRAES, Beijing, in 2014

Acknowledgements: The research presented here has been supported by the CLEEN MMEA project.

Lanki, T., Tikkanen, J., Janka, K., Taimisto, P., and Lehtim€aki, M. (2011). An electrical sensor for long-term monitoring of ultrafine particles in work- places. J. Phys.: Conf. Ser., 304:012013.

Rostedt, A., Arffman, A., Janka, K., Yli-Ojanperä, J., Keskinen, J., Characterization and Response Model of the PPS-M Aerosol Sensor, Aerosol Sci. Tech. 48, 10, 1022-1030, 2014

Verification of particle mass classification using the centrifugal particle mass analyser at small particle sizes

J.S Olfert[1], J.P.R. Symonds[2],

[1]Department of Mechanical Engineering, University of Alberta, T6G 2G8, Edmonton, Canada
[2]Cambustion Ltd, CB1 8DH, Cambridge, United Kingdom

Keywords: particle mass classifier, low particle mass

The Centrifugal Particle Mass Analyser (CPMA) is an instrument that classifies particles by their mass-charge ratio (Olfert and Collings, 2005). The particles are classified between two concentric cylindrical rotating electrodes where they experience centrifugal and electrostatic forces. In the CPMA the inner cylinder rotates slightly faster than the other cylinder, which increases the transfer efficiency. The Aerosol Particle Mass (APM) analyser is a similar instrument but where the cylinders rotate at the same rotational speed (Ehara et al, 1996).

Previous experiments have shown that the APM systematically measures particles masses that are lower than the expected mass for DMA-classified particles below 50 nm (Tajima et al, 2013). The purpose of this presentation is to investigate the accuracy of the CPMA at low particle masses.

Experimentally determining the accuracy of the CPMA is difficult. Theoretically, the CPMA has an uncertainty of ~3% (Symonds et al., 2013). The uncertainty in particle mass of PSL spheres is on the order of ~10% (depending on size). The uncertainty in diameter from a differential mobility analyser (DMA) is ~ 3% (Kinney et al., 1991), which gives an uncertainty in mass of ~9%. (All uncertainties given with 95% confidence.)

The accuracy of the CPMA was tested by measuring particles of PSL or Santovac that were classified by a DMA. The Santovac particles were generated via electrospray. This experiment cannot determine the accuracy of the CPMA because the uncertainty of the PSL or DMA is greater than the expected uncertainty in the CPMA. However, these experiments can verify that the CPMA accuracy is within the accuracy of the DMA or PSL spheres.

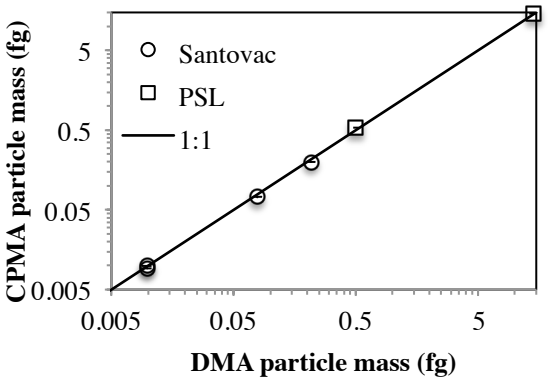

Figure 1. Comparison of particle mass measured by CPMA and DMA.

Figure 1 shows the mass of particles measured with the CPMA versus the expected mass of particles classified by the DMA. Figure 2 shows the ratio of particle masses (m) measured by CPMA to DMA as a function of the particle size selected by the DMA. The error bars represent the standard deviation of the CPMA measurements (typically 4 measurements at each point). These error bars show that the CPMA is quite repeatable. The dashed lines represent the limits of the DMA uncertainty in terms of mass (~9%). The measurements fall within these limits, suggesting the uncertainty of the CPMA is within the uncertainty of the DMA (although it cannot be said by how much). Furthermore, there is no apparent systematic error in either of the instruments down to 25 nm.

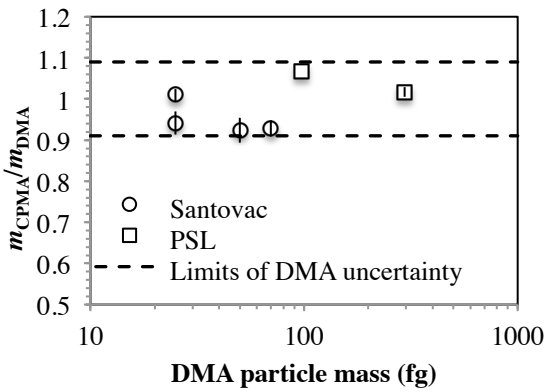

Figure 2. Comparison of particle mass measured by CPMA and DMA.

This work was supported by Cambustion Ltd.

Ehara, K., Hagwood, C., & Coakley, K. J. (1996). *J. Aero. Sci.* 27, 217– 234.

Kinney, P.D., David, Y.H., Bryner, N.P., & Mulholland, G.W. (1991). *J. Res. Nat. Inst. of Std. and Tech.,* 96, 147–176.

Olfert, J. S. and Collings, N. (2005). *J. Aero. Sci.* 36, 1338–1352 .

Symonds, J.P.R., Reavell, K. StJ., Olfert, J.S. (2013). *Aero. Sci & Tech.* 47, i-iv.

Tajima, N., Sakurai, H., Fukushima, N. and Ehara, K. (2013). *Aero. Sci & Tech.* 47, 1152-1162.

Volatility of wood-burning SOA precursors: a chance for mitigating SOA production

A. Keller[1], J. C. Corbin[2], A. A. Mensah[3], B. Sierau[3], H. Burtscher[1]

[1]Institute of Aerosol and Sensor Technology, University of Applied Sciences Northwestern Switzerland, 5210, Windisch, Switzerland
[2]Laboratory for Atmospheric Chemistry, Paul Scherrer Institute, Villigen, Switzerland
[3]Institute for Atmospheric and Climate Science, ETH Zurich, 8092 Zurich, Switzerland

Keywords: SOA (Second. Organic Aerosols), Wood Combustion, Emissions, Measurement (characterization), Abatement strategies.

Wood burning (WB) is a major contributor to pollution by carbonaceous particulate matter. At certain locations in Western Europe, it surpasses many-fold the contribution from fossil fuel (Szidat *et al.*, 2007).

Ambient measurements establish organic carbon (OC) as the largest carbonaceous fraction from WB emissions. In turn, the secondary organic aerosol (SOA) produced by atmospheric aging may amount to more than 50% of the atmospheric OC related to this type of combustion (Lanz *et al.*, 2007). This makes wood burning SOA one of the most important atmospheric pollutants.

We have previously shown that it is possible to simulate atmospheric aging within seconds by means of the micro smog chamber (MSC), a continuous-flow reactor-tube (Keller & Burtscher, 2012). Aging is essential to fully capture the potential impact of the emissions, which is by far not reflected by gravimetric sampling, the current legal standard.

Using our setup, we have studied the emissions of different combustion appliances from small (7kW) batch-operated logwood stoves to medium size (up to 450kW) automatic installations. We will show results from positive matrix factorization analysis of on-line data collected by means of an Aerodyne Aerosol Mass Spectrometer, as well as size distribution measurements and filter based thermo-optical characterization of emissions with and without aging. Our results give us insight into the processes producing SOA precursors. We will discuss these results and show that the least-volatile organic gaseous carbon fraction is the main source of SOA for these appliances.

Finally, we will discuss measurements performed on appliances equipped with a combination of a flue gas cooling system and an electrostatic precipitator (ESP) for filtering raw gas emissions. We will show that gas-to-particle phase partitioning can be exploited to reduce the potential for SOA production to levels which are only achievable by larger installations with a very efficient combustion (Figure 1). On the other hand, the emission factor of non-methane hydrocarbons remains practically unaffected by the ESP, confirming that only a small subset of these substances is responsible for most of the SOA production.

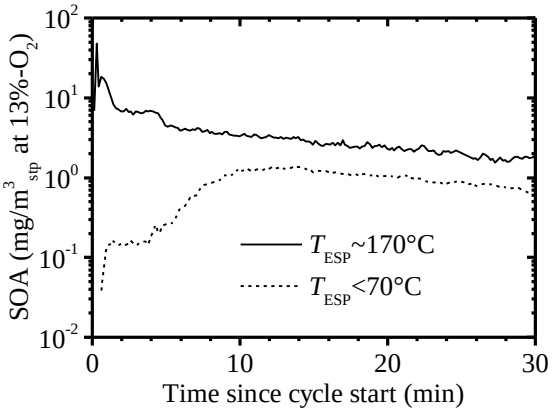

Figure 1. Real-time determination of the secondary organic aerosol production potential during warm start cycles of a 7kW logwood stove equipped with an electrostatic precipitator (ESP). The lines represent different flue gas temperatures measured at the exit of the ESP.

This research was supported by the Swiss Federal Office for Energy (SFOE), the Swiss Federal Office for the Environment (FOEN) and the OPTIWARES project of the Competence Center Environment and Sustainability (CCES) from the ETH Zurich, the Competence Center Energy and Mobility (CCEM).

Keller, A. and Burtscher, H. (2012) *Aerosol Sci.* 49, 9-20.

Lanz, V. A., Alfarra, M. R., Baltensperger, U., Buchmann, B., Hueglin, C. and Prévôt, A. S. H. (2007). *Atmos. Chem. Phys.* 7, 1503-1522.

Szidat, S., Prévôt, A., Sandradewi, J., Alfarra, M., Synal, H.-A., Wacker, L., and Baltensperger, U. (2007). *Geophys. Res. Lett.* 34, L05820.